US Army Corps of Engineers

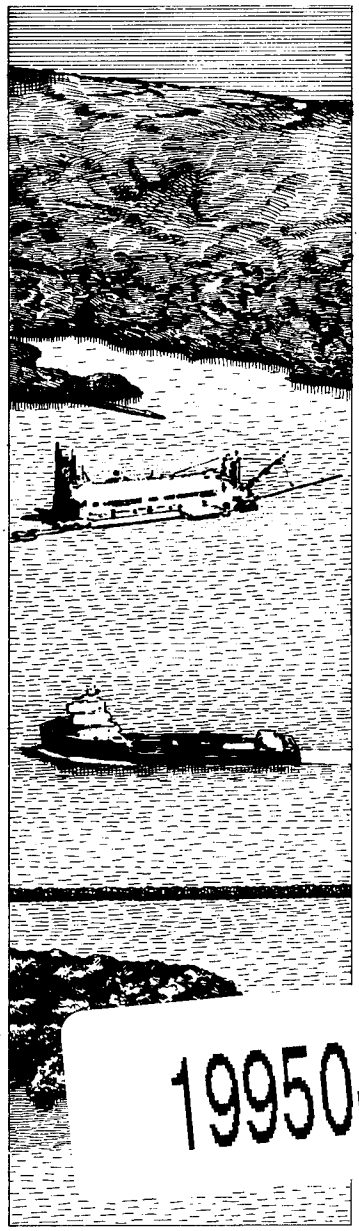

DREDGING RESEARCH PROGRAM

TECHNICAL REPORT DRP-95-4

INFLUENCE OF DOMAIN SIZE AND GRID STRUCTURE ON THE RESPONSE CHARACTERISTICS OF A HURRICANE STORM SURGE MODEL

by

C. A. Blain, J. J. Westerink

Department of Civil Engineering and Geological Sciences
University of Notre Dame
Notre Dame, Indiana 46556

R. A. Luettich, Jr.

University of North Carolina at Chapel Hill
Institute of Marine Sciences
Morehead City, North Carolina 28557

Norman W. Scheffner

DEPARTMENT OF THE ARMY
Waterways Experiment Station, Corps of Engineers
3909 Halls Ferry Road, Vicksburg, Mississippi 39180-6199

DTIC
ELECTE
APR 2 6 1995
S C D

19950425 100

DTIC QUALITY INSPECTED 5

March 1995

Final Report

Approved For Public Release; Distribution Is Unlimited

Prepared for DEPARTMENT OF THE ARMY
U.S. Army Corps of Engineers
Washington, DC 20314-1000

Under Work Unit 32466

The Dredging Research Program (DRP) is a seven-year program of the US Army Corps of Engineers. DRP research is managed in these five technical areas:

Area 1 - Analysis of Dredged Material Placed in Open Waters

Area 2 - Material Properties Related to Navigation and Dredging

Area 3 - Dredge Plant Equipment and Systems Processes

Area 4 - Vessel Positioning, Survey Controls, and Dredge Monitoring Systems

Area 5 - Management of Dredging Projects

The contents of this report are not to be used for advertising, publication, or promotional purposes. Citation of trade names does not constitute an official endorsement or approval of the use of such commercial products.

PRINTED ON RECYCLED PAPER

US Army Corps
of Engineers
Waterways Experiment
Station

Dredging Research Program Report Summary

Influence of Domain Size and Grid Structure on the Response Characteristics of a Hurricane Storm Surge Model (TR DRP-95-4)

ISSUE: Dredged material disposal sites located in open water are classified as either dispersive or nondispersive depending on whether local water velocities are strong enough to erode and transport dredged material from the deposited mound. The Corps needs the capability to predict stability of the mound and long-term migration patterns of eroded material to (1) identify acceptable disposal-site locations, and (2) provide a quantitative approach for gaining site-designation approval.

RESEARCH: The overall work-unit objective is development of a systematic approach for predicting the dispersion characteristics of a specific open-water disposal site. This objective includes the following goals:

- Identify realistic wind-, wave-, tide-, and storm-generated velocity boundary conditions.
- Develop numerical models capable of simulating dispersion characteristics of dredged-material mounds for periods of time in excess of one year.
- Provide site-designation technology to field engineers as a tool in site identification and designation.

One of the areas of interest concerns the effect of tropical storm surges on disposal site stability. This report presents results of studies undertaken to investigate the influence of numerical model grid domain size and grid structure on the accuracy of numerical simulations of hurricane surge in the coastal region.

SUMMARY: The numerical model ADCIRC-2DDI was used to develop a relationship among computational domain size, boundary condition specification, and the resulting physics associated with hurricane storm surge generation. Results of the study are guidelines which can be used to select a numerical domain and subsequently construct an appropriate computational grid.

AVAILABILITY OF REPORT: The report is available through the Interlibrary Loan Service from the U.S. Army Engineer Waterways Experiment Station (WES) Library, telephone (601) 634-2355. National Technical Information Service (NTIS) numbers may be requested from WES librarians.

To purchase a copy of the report, call NTIS at (703) 487-4780.

About the Authors: Ms. C. A. Blain and Dr. J. J. Westerink are with the Department of Civil Engineering and Geological Sciences of the University of Notre Dame; Dr. R. A. Luettich, Jr., the Institute of Marine Sciences, University of North Carolina at Chapel Hill; and Dr. Norman W. Scheffner, the Coastal Engineering Research Center, WES. For further information about the DRP, contact Mr. E. Clark McNair, Jr., Manager, DRP, at (601)634-2070.
Point of Contact: Dr. Scheffner, Principal Investigator for the work unit.

Please reproduce this page locally, as needed.

Dredging Research Program

Technical Report DRP-95-4
March 1995

Influence of Domain Size and Grid Structure on the Response Characteristics of a Hurricane Storm Surge Model

by C. A. Blain, J. J. Westerink

Department of Civil Engineering and Geological Sciences
University of Notre Dame
Notre Dame, IN 46556

R. A. Luettich, Jr.

University of North Carolina at Chapel Hill
Institue of Maine Sciences
Morehead City, NC 28557

Norman W. Scheffner

U.S. Army Corps of Engineers
Waterways Experiment Station
3909 Halls Ferry Road
Vicksburg, MS 39180-6199

Final report

Approved for public release; distribution is unlimited

Accesion For
NTIS CRA&I ☑
DTIC TAB ☐
Unannounced ☐
Justification
By
Distribution /
Availability Codes
Dist | Avail and / or Special
A-1

Prepared for U.S. Army Corps of Engineers
Washington, DC 20314-1000

Under Work Unit 32466

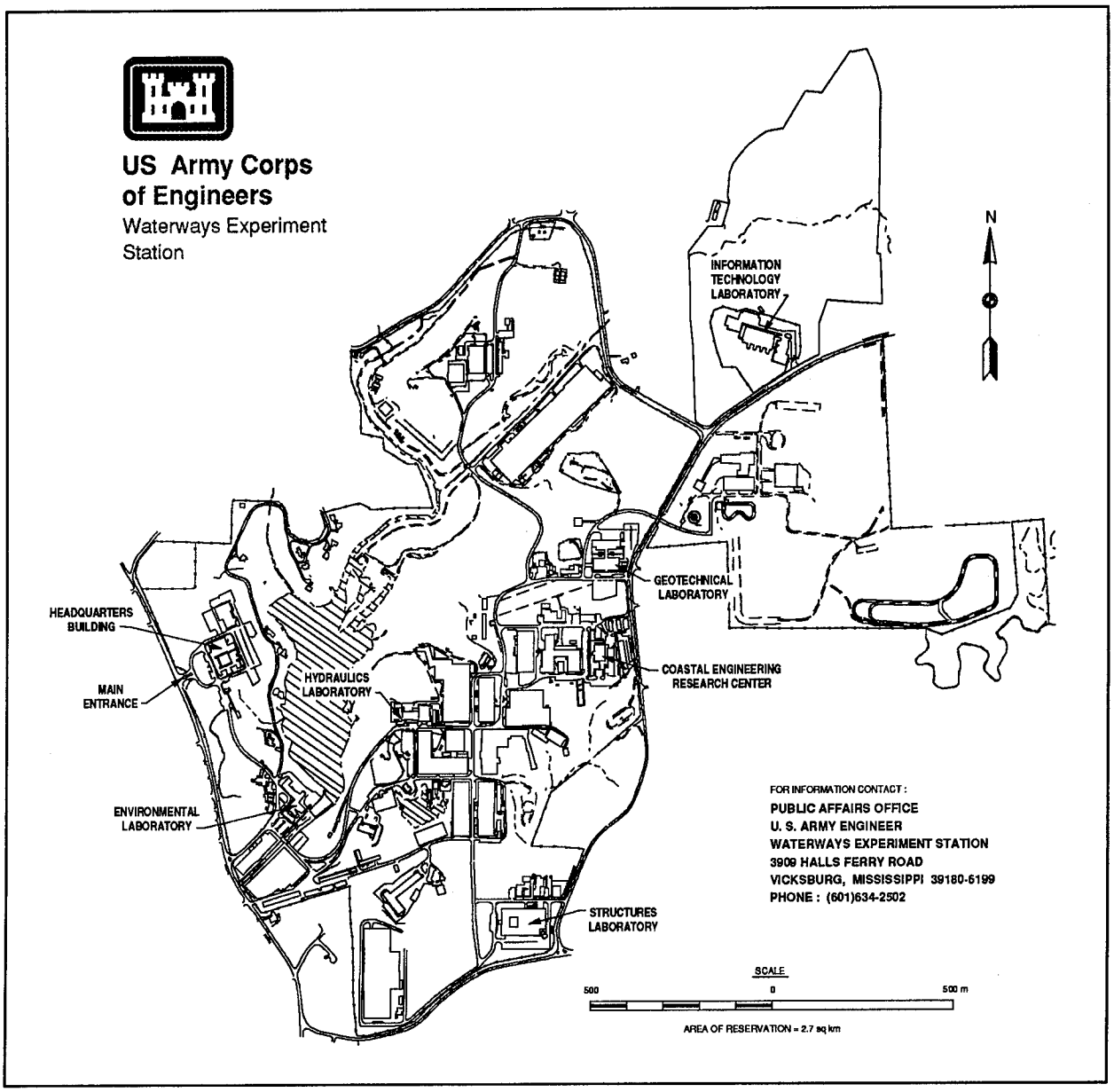

Waterways Experiment Station Cataloging-in-Publication Data

Influence of domain size and grid structure on the response characteristics of a hurricane storm surge model / by C.A. Blain ... [et al.] ; prepared for U.S. Army Corps of Engineers.

174 p. : ill. ; 28 cm. — (Technical report ; DRP-95-4)

Includes bibliographical references.

1. Storm surges —Mathematical models. 2. Ocean waves — Mathematical models. 3. Numerical grid generation (Numerical analysis) 4. Finite element method. I. Blain, C. A. II. United States. Army. Corps of Engineers. III. U.S. Army Engineer Waterways Experiment Station. IV. Dredging Research Program. V. Series: Technical report (U.S. Army Engineer Waterways Experiment Station) ; DRP-95-4.

TA7 W34 no.DRP-95-4

Contents

Preface xii

Summary xiv

1—Introduction 1

2—Hydrodynamic Model 5

Model Selection 5
ADCIRC-2DDI Model Description 9
Summary 19

3—Meteorological Forcing 21

Hurricane Forcing and Modeling Approaches 21
HURWIN Wind Model 23
Hurricanes of Record 27
Synthetic Hurricanes 29
Summary 31

4—Domain Size Sensitivity 33

Hydrodynamic Domain Descriptions 34
Comparison of Storm Surge Predictions Using Three Domain Sizes . . . 38
Comparison Between Observed and Computed Storm Surge Elevations Over the East Coast Domain 55
Conclusions 64

5—Influence of Grid Structure 66

Grid Descriptions 67
Error Analysis 69
Discussion of Results 75
Conclusions 97

6—Application of Domain Size and Gridding Strategy 111

Domain and Grid Construction 112
Storm Surge Simulations 115
Discussion of Convergence Analysis 117
Conclusions 143

7—Concluding Remarks 145

References 149

SF 298

List of Figures

Figure 1. Track of Hurricane Kate through the western North Atlantic Ocean and Gulf of Mexico (18:00 GMT 15 November 1985 to 18:00 GMT 23 November 1985) shown at 6-hr intervals 28

Figure 2. Track of Hurricane Camille through the western Caribbean Sea and Gulf of Mexico (18:00 GMT 14 August 1969 to 18:00 GMT 22 August 1969) shown at 6-hr intervals 30

Figure 3. Two synthetic hurricane tracks, one perpendicular (Path 1) and one parallel to the coastline (Path 3) 31

Figure 4. Boundaries of the (a) Florida Coast domain, (b) Gulf of Mexico domain, and (c) east coast domain 35

Figure 5. Bathymetry contours for the Florida coast domain 36

Figure 6. Florida coast domain discretization 36

Figure 7. Bathymetry contours for the Gulf of Mexico domain 37

Figure 8. Gulf of Mexico domain discretization 37

Figure 9. Bathymetry contours for the east coast domain 38

Figure 10. East coast domain discretization 38

Figure 11. Elevation station locations along the Florida coast and on the continental shelf with respect to the Florida coast domain 40

Figure 12. Additional elevation stations located within the Gulf of Mexico domain 40

Figure 13. Computed storm surge from Hurricane Kate using (a) a still-water boundary condition, and (b) an inverted barometer boundary condition at St. Marks, FL 41

Figure 14. Computed storm surge from Hurricane Kate using (a) a still-water boundary condition, and (b) an inverted barometer boundary condition at Shell Point, FL 42

Figure 15. Computed storm surge from Hurricane Kate using (a) a still-water boundary condition, and (b) an inverted barometer boundary condition at Turkey Point, FL 43

Figure 16. Computed storm surge from Hurricane Kate using (a) a still-water boundary condition, and (b) an inverted barometer boundary condition at Carrabelle, FL 44

Figure 17. Computed storm surge from Hurricane Kate using (a) a still-water boundary condition, and (b) an inverted barometer boundary condition at Apalachicola, FL 45

Figure 18. Computed storm surge from Hurricane Kate using (a) a still-water boundary condition, and (b) an inverted barometer boundary condition at Panama City, FL 46

Figure 19. Computed storm surge from Hurricane Kate using (a) a still-water boundary condition, and (b) an inverted barometer boundary condition at Alligator Bayou, FL 47

Figure 20. Computed storm surge from Hurricane Kate using (a) a still-water boundary condition, and (b) an inverted barometer boundary condition at Destin, FL 48

Figure 21. Computed storm surge from Hurricane Kate using (a) a still-water boundary condition, and (b) an inverted barometer boundary condition at Pensacola, FL 49

Figure 22. Computed storm surge from Hurricane Kate using (a) a still-water boundary condition, and (b) an inverted barometer boundary condition at Station T6.3 50

Figure 23. Storm surge elevations (in cm)) in the northeast Gulf of Mexico due to Hurricane Kate on (a) 20:00 GMT 20 November 1985, (b) 6:00 GMT 21 November 1985, and (c) 18:00 GMT 21 November 1985 52

Figure 24. Computed storm surge from Hurricane Kate using an inverted barometer boundary condition at Station T8.5 53

Figure 25. Comparison of storm surge computed over the east coast domain using both still-water boundary condition and an inverted barometer boundary condition at Apalachicola, FL . . . 54

Figure 26. Comparison of computed and measured tidal elevations over the east coast domain at Key West, FL 57

Figure 27. Comparison of computed and measured tidal elevations over the east coast domain at Cedar Key, FL 57

Figure 28. Comparison of computed and measured tidal elevations over the east coast domain at St. Marks, FL 58

Figure 29. Comparison of computed and measured tidal elevations over the east coast domain at Alligator Bayou, FL 58

Figure 30. Comparison of computed and measured tidal elevations over the east coast domain at Southwest Pass, LA 59

Figure 31. Comparison of computed and measured tidal elevations over the east coast domain at the outer Florida shelf station 59

Figure 32. Comparison of computed and measured storm surge elevations for Hurricane Kate over the east coast domain at St. Marks, FL 60

Figure 33. Comparison of computed and measured storm surge elevations for Hurricane Kate over the east coast domain at Shell Point, FL 60

Figure 34. Comparison of computed and measured storm surge elevations for Hurricane Kate over the east coast domain at Turkey Point, FL 61

Figure 35. Comparison of computed and measured storm surge elevations for Hurricane Kate over the east coast domain at Carrabelle, FL 61

Figure 36. Comparison of computed and measured storm surge elevations for Hurricane Kate over the east coast domain at Apalachicola, FL 62

Figure 37. Comparison of computed and measured storm surge elevations for Hurricane Kate over the east coast domain at Panama City, FL 62

Figure 38. Comparison of computed and measured storm surge elevations for Hurricane Kate over the east coast domain at Destin, FL 63

Figure 39. Comparison of computed and measured storm surge elevations for Hurricane Kate over the east coast domain at Pensacola, FL 63

Figure 40. Bathymetry profile for the rectangular domain used in the study of grid structure relative to storm surge predictions 68

Figure 41. Enlargements of the (a) 50-km, (b) 25-km, and (c) 12.5-km uniform discretizations for grids G01, G02, and G03, respectively 70

Figure 42. Enlargements of the variably graded discretizations for grids (a) VG01, (b) VG02, and (c) VG03, respectively 71

Figure 43. Sinusoidally varying coastlines (a) C1, (b) C2, and (c) C3, having resolutions of 5, 9, and 17 points per wavelength, respectively 72

Figure 44. Maximum storm surge elevations over the domain and the depth at the location of maximum surge computed over grid VG03 for (a) Hurricane H011 and (b) Hurricane H012 forcing 76

Figure 45. Maximum over- and underprediction errors of the storm surge generated by Hurricane H011 as computed over grids (a) G01, (b) G02, (c) VG01, (d) VG02, and (e) VG03 78

Figure 46. Maximum over- and underprediction errors of the storm surge generated by Hurricane H012 as computed over grids (a) G01,

(b) G02, (c) VG01, (d) VG02, and (e) VG03 82

Figure 47. Maximum over- and underprediction errors of the storm surge generated by Hurricane H013 as computed over grids (a) G01, (b) G02, (c) VG01, (d) VG02, and (e) VG03 85

Figure 48. Maximum over- and underprediction errors of the storm surge generated by Hurricane H031 as computed over grids (a) G01, (b) G02, (c) VG01, (d) VG02, and (e) VG03 88

Figure 49. Maximum over- and underprediction errors of the storm surge generated by Hurricane H011 as computed over grids (a) G01_C1, and (b) G02_C1 94

Figure 50. Maximum over- and underprediction errors of the storm surge generated by Hurricane H011 as computed over grids (a) G03_C1, and (b) G02_C1 when compared to grids G03_C3 and G02_C2, respectively 96

Figure 51. Maximum over- and underprediction errors of the storm surge generated by Hurricane H011 as computed over grids (a) G01_C1, (b) G02_C2, (c) VG01_C3, (d) VG02_C3, and (e) VG03_C3 98

Figure 52. Maximum over- and underprediction errors of the storm surge generated by Hurricane H012 as computed over grids (a) G01_C1, (b) G02_C2, (c) VG01_C3, (d) VG02_C3, and (e) VG03_C3 101

Figure 53. Maximum over- and underprediction errors of the storm surge generated by Hurricane H013 as computed over grids (a) G01_C1, (b) G02_C2, (c) VG01_C3, (d) VG02_C3, and (e) VG03_C3 104

Figure 54. Maximum over- and underprediction errors of the storm surge generated by Hurricane H031 as computed over grids (a) G01_C1, (b) G02_C2, (c) VG01_C3, (d) VG02_C3, and (e) VG03_C3 107

Figure 55. Region of coastline detail surrounding Biloxi, MS, which has been added to the east coast domain used throughout Chapter 4 113

Figure 56. Distribution of nodal spacing, in kilometers, over grid SG01 114

Figure 57. Coastline detail and discretization for grid SG01 in the northeast Gulf of Mexico 115

Figure 58. Distribution of nodal spacing in kilometers over grid SG01 in the northeast Gulf of Mexico 116

Figure 59. Storm surge elevation stations located throughout the northeast Gulf of Mexico 118

Figure 60. Additional storm surge elevation stations, shown as solid squares, in and around the Gulf of Mexico 119

Figure 61. Seven storm surge elevation stations, shown as solid squares, along the eastern United States coastline 119

Figure 62. Maximum over- and underprediction errors in the storm surge generated by Hurricane Camille as computed over grid SG01 120

Figure 63. Contours of the absolute overprediction (reds) and underprediction (blues) errors in the storm surge computed over grid SG01 121

Figure 64. Enlargement of the resolution provided by grid SG01 in the landfall region of Hurricane Camille 124

Figure 65. Storm surge hydrograph comparing computations over grids SG01 and CG01 at Alligator Bayou, FL 125

Figure 66. Storm surge hydrograph comparing computations over grids SG01 and CG01 at Pensacola, FL 125

Figure 67. Storm surge hydrograph comparing computations over grids SG01 and CG01 at Biloxi, MS 126

Figure 68. Storm surge hydrograph comparing computations over grids SG01 and CG01 at Bay St. Louis, MS 126

Figure 69. Storm surge hydrograph comparing computations over grids SG01 and CG01 at Cat Island, MS 127

Figure 70. Storm surge hydrograph comparing computations over grids SG01 and CG01 at Station C.6 127

Figure 71. Storm surge hydrograph comparing computations over grids SG01 and CG01 at Station C.9 128

Figure 72. Storm surge hydrograph comparing computations over grids SG01 and CG01 at Station C.13 128

Figure 73. Storm surge hydrograph comparing computations over grids SG01 and CG01 at Station S.8 129

Figure 74. Storm surge hydrograph comparing computations over grids SG01 and CG01 at Station S.9 129

Figure 75. Storm surge hydrograph comparing computations over grids SG01 and CG01 at Station SB.7 130

Figure 76. Storm surge hydrograph comparing computations over grids SG01 and CG01 at Station SB.8 130

Figure 77. Storm surge hydrograph comparing computations over grids SG01 and CG01 at the GOM (Gulf of Mexico) Pelagic station 131

Figure 78. Maximum over- and underprediction errors in the storm surge generated by Hurricane Kate as computed over grid SG01 132

Figure 79. Contours of the absolute overprediction (reds) and underprediction (blues) errors in the storm surge computed over grid SG01 133

Figure 80. Enlargement of the resolution provided by grid SG01 in the landfall region of Hurricane Kate 136

Figure 81. Storm surge hydrograph comparing computations over grids SG01 and CG01 at Alligator Bayou, FL 137

Figure 82. Storm surge hydrograph comparing computations over grids SG01 and CG01 at Destin, FL 137

Figure 83. Storm surge hydrograph comparing computations over grids SG01 and CG01 at Panama City, FL 138

Figure 84. Storm surge hydrograph comparing computations over grids SG01 and CG01 at Apalachicola, FL 138

Figure 85. Storm surge hydrograph comparing computations over grids SG01 and CG01 at Carrabelle, FL 139

Figure 86. Storm surge hydrograph comparing computations over grids SG01 and CG01 at Shell Point, FL 139

Figure 87. Storm surge hydrograph comparing computations over grids SG01 and CG01 at Cedar Key, FL 140

Figure 88. Storm surge hydrograph comparing computations over grids SG01 and CG01 at Station S.1 140

Figure 89. Storm surge hydrograph comparing computations over grids SG01 and CG01 at Station S.2 141

Figure 90. Storm surge hydrograph comparing computations over grids SG01 and CG01 at Station S.3 141

Figure 91. Storm surge hydrograph comparing computations over grids SG01 and CG01 at the outer Florida Shelf Station 142

Figure 92. Storm surge hydrograph comparing computations over grids SG01 and CG01 at Station SB.1 142

Figure 93. Storm surge hydrograph comparing computations over grids SG01 and CG01 at Station SB.3 143

List of Tables

Table 1. Characteristics of Synthetic Hurricanes 31

Table 2. Characteristics of Model Domains 35

Table 3. Tidal Potential Constants Used for Storm Surge Simulations 55
Table 4. Characteristics of Rectangular Grid Discretizations 72
Table 5. Definitions of Grid Comparisons 73
Table 6. Characteristics of Synthetic Hurricanes 74
Table 7. Maximum Errors Over Grid Series 1 for Hurricane H011 91
Table 8. Maximum Errors Over Grid Series 1 for Hurricane H012 92
Table 9. Maximum Errors Over Grid Series 1 for Hurricane H013 92
Table 10. Maximum Errors Over Grid Series 1 for Hurricane H031 92
Table 11. Maximum Errors Over Grid Series 2 for Hurricane H011 95
Table 12. Maximum Errors Over Grid Series 3 for Hurricane H011 97
Table 13. Maximum Errors Over Grid Series 4 for Hurricane H011 . . . 109
Table 14. Maximum Errors Over Grid Series 4 for Hurricane H012 . . . 110
Table 15. Maximum Errors Over Grid Series 4 for Hurricane H013 . . . 110
Table 16. Maximum Errors Over Grid Series 4 for Hurricane H031 . . . 110

Preface

The work described in this report was authorized and funded under Work Unit No. 32466, "Numerical Simulation Techniques for Evaluating Long-Term Fate and Stability of Dredged Material Disposed in Open Water," of Technical Area 1 (TA1), Analysis of Dredged Material Placed in Open Water, of the Dredging Research Program (DRP), sponsored by Headquarters, U.S. Army Corps of Engineers (HQUSACE). Messrs. Robert Campbell and Glenn Drummond were DRP Chief and TA1 Technical Monitors from HQUSACE, respectively. Mr. E. Clark McNair, Jr., (CERC), was DRP Program Manager (PM) and Dr. Lyndell Z. Hales was Assistant PM. Dr. Billy H. Johnson, WES, Hydraulics Laboratory, was the Technical Manager of DRP TA1 and Dr. Norman W. Scheffner, Coastal Processes Branch (CPB), RD, CERC, is the Principal Investigator of Work Unit No. 32466. The numerical modeling goals, concepts, and methodologies were developed by Drs. Norman W. Scheffner, Joannes J. Westerink, and Richard A. Luettich, Jr. Development and implementation of the model were completed by Drs. Westerink and Luettich.

This study was performed and the report prepared over the period 1 September 1992 through 3 June 1994. Dr. Scheffner was under the administrative supervision of Dr. James R. Houston, Director, CERC; Mr. Charles C. Calhoun, Jr., Assistant Director, CERC; Mr. H. Lee Butler, Chief, RD, CERC; and Mr. Bruce A. Ebersole, Chief, CPB, RD, CERC.

At the time of publication of this report, Director of WES was Dr. Robert W. Whalin. Commander was COL Bruce K. Howard, EN.

The contents of this report are not to be used for advertising, publication, or promotional purposes. Citation of trade names does not constitute an official endorsement or approval of the use of such commercial products.

Summary

This report details two convergence studies undertaken to investigate the influence of model domain size and grid structure on the prediction of hurricane storm surge in the coastal region. The result of these studies is a series of guidelines which direct selection of a domain size and construction of the grid discretization.

The domain size sensitivity study conducted establishes a relationship between domain size, boundary condition specification, and the resulting physics associated with hurricane storm surge generation. Storm surge response along the Florida shelf in the Gulf of Mexico due to Hurricane Kate is examined over three domains using two different open ocean boundary forcing functions. The computed storm surge response indicates that a small domain situated primarily on the continental shelf is inadequate since cross-shelf boundaries are in regions of significant storm surge generation where surge and, therefore, boundary conditions are not known a priori. A second domain including the entire Gulf of Mexico basin captures the primary storm surge well but may not correctly model resonant modes. The dependence of these modes on interactions with contiguous basins makes accurate setup by the boundary condition specification difficult. The primary storm surge response as well as resonant modes excited by the storm are best represented using the largest domain which encompasses the western North Atlantic Ocean, the Caribbean Sea, and the Gulf of Mexico. This domain with deep Atlantic Ocean boundaries facilitates simple boundary condition specification and minimizes the influence of boundary conditions on storm surge generation in the coastal region. Basin resonant modes and basin-to-basin interactions are also captured.

The influence of grid structure on hurricane storm surge computations is established by comparing storm surge elevations computed over 14 grid discretizations subject to 4 synthetic hurricane forcings. An error analysis indicates that accurate predictions of storm surge result when significant refinement of shoreline geometry and nearshore regions is provided, along with resolution to one half the spatial scale of the storm over deep waters. Grid discretization requirements are best met using a graded grid structure which yields low uniform prediction errors. The guidelines set forth for the specification of a domain size and gird structure are applied relative to the meteorological forcing from Hurricanes Kate and Camille. The convergence analysis reinforces

the necessity of using a large domain which has high levels of resolution in near-shore regions and areas of complex coastal geometry for accurate prediction of primary storm surge. In addition, easily implemented techniques for assessing grid performance relative to accurate storm surge prediction are presented.

1 Introduction

Numerical modeling has become an important tool for assessing the hydrodynamics of continental margin waters. It is important to recognize that the computed response of these waters is controlled by the various components which make up a model, including: the governing equations, the boundary conditions, the forcing functions, the numerics, grid structure, and the computational domain itself. The more that is understood about a numerical model and how its components influence computations, the more successful the model will be in representing hydrodynamic processes within shallow waters. The research presented herein focuses on the numerical modeling of storm surge generation and propagation over the continental shelf and in coastal regions due to the passage of a hurricane. In particular, the domain size and grid structure associated with the numerical model are examined in terms of their impact on computed storm surge response. Results from the studies undertaken provide guidelines for selection of a domain size and construction of a grid discretization that are applicable to the numerical prediction of storm surge.

Storm surge is a long-period wave caused by extreme wind and pressure forcing. The period, wavelength, and amplitude characteristics of the storm surge depend on geometric properties of the water body as well as characteristics of the meteorological forcing (Dendrou, Moore, and Myers 1985). Water heights associated with the storm surge are superimposed on water levels generated by tidal forcings. At times when peak tidal and surge elevations coincide, water heights can become extreme, producing dangerous conditions in coastal areas.

The impact of hurricane storm surge is well-documented throughout history. In recent memory, two particularly destructive storms occurred during the hurricane season of 1992, Hurricane Andrew in Florida and Hurricane Iniki in Hawaii. Apart from the number of lives lost during these hurricanes, the costs due to material damage and disruption to local economies totalled into the billions of dollars. The devastation wrought by these storms reinforces the seriousness of coastal flooding in seaside communities caused by hurricane storm surge.

Information regarding probable storm surge elevations generated by hurricane wind and pressure fields is desirable in a variety of applications. The

National Weather Service (NWS) issues warnings when hurricanes threaten U.S. shorelines. In defining the hurricane warning areas, the NWS considers the range of expected peak surge heights which have been extracted from numerical storm surge model predictions (Jelesnianski 1979, Jelesnianski and Taylor 1973, Jarvinen and Lawrence 1985). Furthermore, statistical databases of storm surge response along the eastern U.S. and Gulf of Mexico coasts are created using water elevations computed by numerical storm surge model hindcasts of historical hurricanes (Scheffner et al. 1994). In another application, design criteria for offshore oil structures are formulated with the aid of storm surge elevation and velocity fields generated by numerical model calculations. Storm surge models are also used to develop coastal protection systems and to investigate the fate of disposed dredged material within the coastal environment. The success of each of these endeavors rests upon accurate prediction of the storm surge response due to hurricane forcing and consequently on the formulation of an accurate numerical storm surge model.

Three important considerations in the numerical modeling of storm surge are the adequacy of the grid resolution, the specification of boundary conditions, and the representation of resonant modes and surge forerunner (Reid 1990). The primary objective of the research presented is to address these issues in the context of two sensitivity studies examining the influence of domain size and grid structure on the numerical computation of hurricane storm surge. Findings from this work form a set of guidelines which address domain size selection and grid construction for storm surge model applications.

As noted by Jarvinen and Lawrence (1985), the initial design and location of the basin domain are critical steps in the formulation of a storm surge model. Judicious location of a domain minimizes the effect of boundary condition specification and allows the proper set of resonant modes. Storm surge modeling efforts to date have primarily used domains which are limited to the continental shelf region. Little effort has been made towards assessing the appropriateness of such a domain in storm surge models or understanding the effects of model domain size on accurate storm surge prediction. Through a comprehensive investigation of domain size sensitivity in storm surge models to boundary condition specification and primary surge and surge forerunner generation, a domain size which accurately captures the storm surge response is established.

Since numerical models perform calculations at discrete points, the resolution provided by the domain discretization significantly influences computed storm surge elevations. An examination of the relationships among grid spacing, coastline variation and resolution, hurricane forcing, and errors in the computed storm surge provide insight into the selection of an optimal grid structure. An appropriate grid structure uses the least number of discrete points to produce storm surge predictions having minimal, uniform errors throughout the domain. In the process of studying the influence of grid resolution, a simple yet effective method of assessing numerical errors associated with the grid discretization is implemented.

Prior to the study of domain size and grid structure, a hydrodynamic model used for storm surge computations is selected in Chapter 2. During the course of development, storm surges and their associated forerunners encompass a large range of spatial scales. An acceptable numerical storm surge model must represent the dissipative processes acting on all scales of motion, so that energy in the system is not artificially excited, and/or trapped within the system, and/or aliased in nonphysical ways. Furthermore, an appropriate storm surge model incorporates complex coastal geometries, accounts for rapidly varying bathymetry in the continental slope and shelf regions, and permits reasonable boundary condition specification.

A finite-element- (FE)-based numerical model with its inherent grid flexibility is selected as the ideal formulation for a storm surge model. The FE-based storm surge model ADCIRC-2DDI, the depth-integrated portion of a system of two- and three-dimensional codes named ADCIRC (ADvance CIRCulation model for shelves, coasts, and estuaries) developed by Luettich, Westerink, and Scheffner (1992) is utilized. ADCIRC-2DDI implements the generalized wave-continuity equation (GWCE) and momentum balance equations. Accuracy of the equations used within ADCIRC-2DDI is well-documented with respect to the solution of various shallow-water problems (Foreman 1988; Lynch et al. 1988; Walters 1988; Werner and Lynch 1989; Walters and Werner 1989; Gray 1989; Lynch and Werner 1991; Luettich, Westerink, and Scheffner 1992). In addition, the finite element formulation of ADCIRC-2DDI leads to easy incorporation of coastline detail and allows nodal densities which range over three to four orders of magnitude. The wide variation in nodal density permits significant resolution of shoreline detail as well as high levels of refinement near coastal areas and in regions of shallow bathymetry and rapid bathymetric change. Moreover, the discrete problem remains well within computational limits despite the large variation in nodal density.

Aside from the numerical storm surge model, careful consideration is given in Chapter 3 to the specification of wind stress and pressure forcing at the water surface. Wind stress and pressure forcing are what drive the numerical storm surge model. As such, storm surge predictions are often limited by the accuracy of the specified wind stress and pressure fields (Hubbert, Leslie, and Manton 1990; Dendrou, Moore, and Myers 1985; Flather 1984). A numerical model of the dynamics of the planetary boundary layer, which takes advantage of available meteorological data from historical storms, is chosen to compute the wind stress and pressure forcing (Cardone, Greenwood, and Greenwood 1992). This physically based wind model offers a more realistic representation of hurricane winds than more common empirical models.

Upon establishing an acceptable framework for the numerical storm surge model, the domain size sensitivity study is conducted in Chapter 4. For this study, Hurricane Kate (November 1985), which made landfall on the Florida shelf in the Gulf of Mexico, is applied over three domains. Each domain extends out from the landfall point of the hurricane and covers successively larger regions. The first domain is a relatively small coastal domain which extends mainly over the continental shelf in regions of shallow water. The

second domain covers the entire Gulf of Mexico basin. The final domain extends well into the deep western North Atlantic Ocean. Storm surge computations over these three domains are compared to determine the most appropriate domain size for accurate representation of the storm surge response. Verification of the storm surge predictions computed over the domain selected as most appropriate with respect to boundary condition specification and accurate generation of primary surge and resonant modes is achieved through a comparison to measured storm surge elevations.

An examination of grid structure and its influence on storm surge computations in Chapter 5 proceeds by considering idealized domains and hurricane forcings. The effects of grid spacing, coastline variability, and coastline resolution, as well as the role of various hurricane forcing parameters on storm surge generation are determined separately using this simplified problem. A discussion of errors in the storm surge predictions computed using four hurricane forcings over fourteen grid discretizations, two coastline representations, and three discrete resolutions of the coastline highlights important aspects of the grid discretization necessary for accurate storm surge computations. Namely, representation of shoreline geometry and refinement in near coastal regions dramatically influences computed storm surge response. In addition, discretization requirements over the deep ocean vary significantly from the degree of refinement needed in coastal areas. Incorporation of observations regarding the effects of grid resolution leads to the selection of a graded grid structure appropriate for storm surge computations. Furthermore, the error analysis techniques implemented in the study of grid structure provide a practical means for evaluating the performance of a storm surge model in relation to its grid discretization.

In Chapter 6, an application of the guidelines set forth for selection of a domain size and grid structure are implemented in the context of modeling the storm surge generated by historical hurricanes Kate (November 1985) and Camille (August 1969). Use of a large domain having deep ocean boundaries in conjunction with a graded grid structure which provides significant refinement of shoreline detail and extensive resolution in coastal areas is validated by these applications. Furthermore, these applications establish a procedure by which storm surge model predictions can be evaluated relative to the grid discretization and a basis for further grid refinement is provided.

A final statement in Chapter 7 summarizes the major conclusions of this research and reiterates the implications of this work on the formulation of numerical storm surge models. Also mentioned are several issues relating to the numerical prediction of storm surge which are to be considered in future work.

2 Hydrodynamic Model

The purpose of a hydrodynamic model is to characterize the important flow features of surface waters driven by tides, wind, and atmospheric pressure gradients. Complex circulation patterns on the continental shelf and in coastal regions necessitate the use of a numerical hydrodynamic model. The numerical hydrodynamic model computes spatial and temporal distributions of velocity and sea surface elevation from which circulation patterns can be inferred.

The success of the investigation into the characteristics of storm surge response in the coastal ocean depends in part on the selection of an appropriate hydrodynamic model. An optimal model is one that captures the physics of the storm surge response, yet remains computationally feasible. In this chapter, the criteria used in selecting a hydrodynamic model are outlined. In particular, appropriate governing equations are set forth as well as stipulations naming accuracy, efficiency, and grid flexibility as necessary characteristics of a numerical solution algorithm. An overview and evaluation of current modeling strategies is presented in light of these model selection criteria. Subsequently, a hydrodynamic model is chosen and a description of the model follows. Highlights and important features of the governing equations and the numerical solution algorithm implemented within the selected hydrodynamic model are also presented.

Model Selection

Criteria for selection

The theoretical basis of a hydrodynamic model is found in the principles of mass and momentum conservation. For vertically well-mixed surface waters experiencing tidal and atmospheric forcing, the flow physics are described by the shallow-water equations, a depth-integrated form of the conservation laws (Le Mehaute 1976). The shallow-water equations have been used successfully by engineers and researchers for years to predict tidal and wind-forced circulations (e.g. Johns and Ali 1980; Gray and Kinnmark 1983; Flather 1984; Kowalik 1984; LeProvost and Vincent 1986; Murty, Flather, and Henry 1986; Dube, Sinba, and Roy 1986; Baptista, Westerink, and Turner 1989; Westerink,

Stolzenbach, and Connor 1989; Westerink et al. 1992a; Chen, Shaffer, and Kim 1993; Westerink et al. 1994a; Luettich and Westerink, in preparation).

Modeling storm surge response due to hurricane wind and pressure forcing in the coastal ocean is the primary focus of this work. In the shallow waters of the continental shelf, the large magnitude of hurricane wind forcing produces a boundary layer at the sea surface which extends essentially throughout the entire water column. As a result, variations in the velocity over the ocean depth are assumed negligible, making the depth-averaged shallow-water equations an appropriate framework for the hydrodynamic model.

Obviously, the hydrodynamic model formulation and solution strategy must be accurate. Wavelength and phase propagation characteristics, mass conservation properties, and performance for test cases and field applications are all used in the evaluation of model accuracy.

Efficiency of the numerical solution algorithm is the second consideration in model selection. The storm surge simulations conducted herein occur over several domain sizes including a very large domain which covers both continental shelf and coastal regions as well as portions of the deep ocean. The time frame for these simulations ranges from days to months, when tidal forcing is included. The feasibility of a model which utilizes large domains and extended simulation periods depends upon the efficiency of the numerical solution algorithm. Efficiency within a numerical algorithm is achieved through a minimization of the number of degrees of freedom and the number of operations per degree of freedom at each time-step.

Lastly, both efficiency and accuracy of the hydrodynamic model formulation are enmeshed with the grid flexibility characteristics inherent in the numerical solution algorithm. Maximum grid flexibility allows minimization of the number of degrees of freedom while simultaneously providing the localized resolution needed for accuracy of model predictions.

The selection criteria for the hydrodynamic model are summarized as follows: the governing equations are to be based on the shallow-water equations and the numerical solution algorithm must be highly efficient, accurate, and maintain a significant level of grid flexibility.

Current modeling approaches

The search for accurate and efficient solution algorithms for the shallow-water equations has led to a variety of equation formulations and the use of several numerical solution techniques. Two prevalent numerical discretization strategies are the finite difference and finite element methods. Finite difference methods discretize derivative operators within the model equations using point difference expressions (Lapidus and Pinder 1982). Finite element techniques approximate the solution to model equations through the use of interpolation functions (Celia and Gray 1992). A review of some finite element

solution techniques for the shallow-water equations is given by Lee and Froehlich (1986). Westerink and Gray (1991), in their recent review, note increasing similarities between finite-difference-based and finite-element-based models, especially with regard to the accurate propagation of short wavelengths, grid flexibility, and complex boundary representation.

Early finite difference solutions of the shallow-water equations were quite accurate owing in part to the implementation of a staggered grid approach which successfully avoids the introduction of artificial short waves (Westerink and Gray 1991). In contrast, early finite element schemes were plagued by spurious oscillations or numerical noise due to the introduction of $2 \cdot \Delta x$ wavelengths, a consequence of folded dispersion characteristics (Lynch 1983). Note that $2 \cdot \Delta x$ wavelengths are the smallest wavelengths captured by a mesh of minimum spacing Δx. Finite element algorithms included excessive damping mechanisms to counter the generation of spurious modes but, as a result, produced inaccurate solutions (Gray 1982). It wasn't until Lynch and Gray (1979) introduced the wave continuity equation (WCE) formulation for the shallow-water equations that the viability of finite element approaches improved.

The WCE formulation simply involves rearrangement of the shallow-water equations prior to spatial discretization. Solutions using the WCE successfully suppress short wavelengths without resorting to nonphysical dissipation. An understanding of the origin and behavior of spurious oscillations in finite element formulations (i.e., Walters and Carey (1983)) coupled with extensive numerical testing of the WCE formulation (i.e., Kinnmark and Gray (1984, 1985); Luettich, Westerink, and Scheffner (1992); Westerink et al. (1992b); Kolar (1994a,b)) has resulted in very accurate WCE-based finite element solutions (i.e., Lynch and Gray (1979); Foreman 1983).

In addition to accuracy, efficiency of a numerical algorithm must also be considered. Representation of complex circulation patterns by a hydrodynamic model often requires highly refined grids having very small nodal spacings. As a consequence, the stability criteria for various time-stepping schemes dictate use of a very small time interval for computations. The practicality of using small time-steps for long-period simulations depends on the efficiency of the numerical solution algorithm. Implicit time-stepping schemes are generally more stable and allow larger time-steps, but they result in time-dependent matrices which require reassembly and re-solution at every time-step. This procedure is computationally intensive. Many finite difference models overcome this problem by implementing the alternating direction implicit (ADI) solution algorithm, which reduces a two-dimensional problem to a sequence of one-dimensional problems, thus significantly reducing the computational effort (Leendertse 1987). The ADI approach, however, cannot be applied to unstructured grid algorithms such as the finite element solution strategies.

In contrast to the standard primitive shallow-water equation finite element formulation, a WCE-based finite element formulation leads to decoupled elevation and velocity solutions and sparse, symmetric matrices (Lynch and Gray

1979). Solutions for elevation are time-independent due to a reformulation of the WCE by Kinnmark (1984) into a GWCE. Matrices resulting from an application of the finite element method to the momentum equations remain time-dependent. In the solution procedure, this time dependence is overcome by lumping the matrices, which causes only a slight degradation in accuracy. As a consequence, velocities are computed by solving a trivial diagonal system of equations (Lynch and Gray 1979).

One final consideration in selecting a numerical solution algorithm is grid flexibility. The finite difference method is not readily amenable to providing high levels of refinement in localized areas. The restrictions on acceptable grid skewness and maximum cell-to-cell size ratios (i.e., Heath, Johnson, and Kim (1990); Celia and Gray 1992) often result in finite difference grids which are overrefined, causing an unnecessary computational burden. To represent detailed coastline features, coordinate transformation techniques have been developed in the context of finite difference schemes, but these methods still do not allow for increased resolution in localized areas.

In contrast, the advantage of the finite element method lies in its tremendous grid flexibility in representing the complexity of coastline detail and providing varying degrees of resolution throughout the model domain. In particular, finite element schemes based on triangular elements provide optimal flexibility in achieving local refinement (Luettich, Westerink, and Scheffner 1992). With the ever-increasing size and complexity of shallow-water problems, the degree of grid flexibility in the discretization strategy directly affects the efficiency and accuracy of the hydrodynamic model.

Selected hydrodynamic model

A careful evaluation of the accuracy, efficiency, and grid flexibility characteristics of current numerical solution algorithms for the shallow-water equations in the previous section has led to selection of a GWCE finite-element-based formulation of the shallow-water equations. One hydrodynamic model implementing a GWCE finite-element formulation is ADCIRC-2DDI, the depth-integrated portion of a system of two- and three-dimensional codes developed by Luettich, Westerink, and Scheffner (1992) and Westerink et al. (1992b). All tidal and storm surge simulations conducted within utilize the ADCIRC-2DDI model.

The efficiency and accuracy of ADCIRC-2DDI are well understood due to extensive numerical testing and analysis of the model code. The algorithms that comprise ADCIRC-2DDI effectively minimize the required number of degrees of freedom for a desired level of accuracy, show good stability characteristics, generate no spurious artificial modes, have a minimum inherent artificial numerical damping, efficiently separate the partial differential equations into systems of algebraic equations with time-independent matrices, and are capable of running months to years of simulation while providing detailed computations of the circulation patterns within a water body (Luettich,

Westerink, and Scheffner 1992). An investigation into the mass conservation properties of the GWCE formulation by Kolar et al. (1994b) provides an understanding of the mass balance characteristics of the ADCIRC-2DDI model. In addition, Westerink et al. (1994a) confirm the accuracy of the boundary condition formulation within ADCIRC-2DDI.

The ADCIRC-2DDI hydrodynamic model produces computations which are in agreement with two established benchmark problems, the quarter annular test case (Gray 1982) and the North Sea/English Channel system (Gray 1989). The ADCIRC-2DDI model has also been applied to a number of field studies with excellent results (Westerink, Stolzenbach, and Connor 1989; Westerink et al. 1992a,b; Westerink, Luettich, and Muccino 1994; Kolar et al. 1994a,b). Detailed documentation (Luettich, Westerink, and Scheffner 1992) as well as an instructive commentary regarding appropriate modeling strategies for use with ADCIRC-2DDI (Westerink et al. 1992b) facilitates application of the ADCIRC-2DDI model.

ADCIRC-2DDI Model Description

Governing equations

The generalized wave continuity equation formulation in ADCIRC-2DDI is based on the well-known shallow-water equations (Le Mehaute 1976; Kinnmark 1984). The primitive form of the shallow-water equations is derived by averaging the conservation laws of mass and momentum over the time scale of turbulent fluctuations and the ocean depth. Turbulent fluctuations at the microscale present in all hydrodynamic flows are characterized by spatial and temporal variations in the velocity and pressure fields and are a mechanism for momentum transfer. An application of time averaging to the conservation laws provides a means to parameterize these microscale fluctuations in terms of macroscale quantities. The scale for time averaging is selected to be long enough to capture a statistically significant sample of the turbulent fluctuations and yet short enough so that macroscopic variations of the average quantity are not included (Gray et al. 1993). Within the shallow-water equations, turbulent fluctuations are represented in an average way through the momentum diffusion terms.

Depth averaging of the conservation laws reduces a three-dimensional problem to a two-dimensional one, leaving as unknowns the surface water elevation ζ and the depth-averaged lateral velocities U and V. For flows having small vertical velocity gradients (e.g. well-mixed systems) or environments where lateral flows are quite large in comparison to vertical velocities (e.g. nearly horizontal flow), an application of the shallow-water equations is accepted practice.

Derivation of the shallow-water equations from the time and depth-averaged conservation laws involves assumptions of incompressibility and hydrostatic conditions as well as the Boussinesq approximation. In practice,

incompressibility of a fluid implies that density variations seen while moving with the fluid are negligible (i.e., $\frac{D\rho}{Dt} = 0$). Furthermore, the Boussinesq approximation specifies density as a constant value ($\rho = \rho_o$) except when gradients of density are considered. In flows appropriate for two-dimensional depth-averaged equations, the vertical acceleration is assumed negligible. Consequently, the momentum equation over the vertical reduces to a balance between pressure and gravitational forces. This is commonly referred to as the hydrostatic assumption. Other simplifications implicit within the shallow-water equations include the neglect of changes in the position of the ocean floor with respect to time and the exclusion of mass exchanges with the environment (i.e., evaporation, precipitation, overland flow, and groundwater interactions).

For a Cartesian coordinate system, conservative forms of the shallow-water equations are written as follows:

$$\frac{\partial \zeta}{\partial t} + \frac{\partial UH}{\partial x} + \frac{\partial VH}{\partial y} = 0 \tag{1}$$

$$\frac{\partial UH}{\partial t} + \frac{\partial UUH}{\partial x} + \frac{\partial UVH}{\partial y} - fVH = -H\frac{\partial}{\partial x}\left[\frac{p_s}{\rho_o} + g(\zeta - \alpha\eta)\right] + M_x + D_x + B_x + \frac{\tau_{sx}}{\rho_o} - \frac{\tau_{bx}}{\rho_o} \tag{2}$$

$$\frac{\partial VH}{\partial t} + \frac{\partial VUH}{\partial x} + \frac{\partial VVH}{\partial y} + fUH = -H\frac{\partial}{\partial y}\left[\frac{p_s}{\rho_o} + g(\zeta - \alpha\eta)\right] + M_y + D_y + B_y + \frac{\tau_{sy}}{\rho_o} - \frac{\tau_{by}}{\rho_o} \tag{3}$$

where

ζ = free surface elevation relative to the geoid

t = time

U = depth-averaged horizontal velocity

H = water column depth, $\zeta + h$

h = bathymetric depth

x = Cartesian coordinate direction

V = depth-averaged horizontal velocity

y = Cartesian coordinate direction

f = Coriolis parameter

p_s = atmospheric pressure at the free surface

ρ_o = reference density of water

g = acceleration due to gravity

α = earth elasticity factor

η = Newtonian equilibrium tide potential

M_x = depth-integrated horizontal momentum diffusion

D_x = depth-integrated horizontal momentum dispersion term

B_x = depth-integrated baroclinic forcing

τ_{sx} = applied free surface stress

τ_{bx} = applied bottom stress

M_y = depth-integrated horizontal momentum diffusion

D_y = depth-integrated horizontal momentum dispersion term

B_y = depth-integrated baroclinic forcing

τ_{sy} = applied free surface stress

τ_{by} = applied bottom stress

Further justification regarding the appropriateness of these equations in modeling the flow of tidal and atmospheric forces is provided by Blumberg and Mellor (1987); Westerink, Stolzenbach, and Connor (1989); and Luettich et al. (1992).

In operator notation, a relationship between the conservative and nonconservative momentum equations is given (Kolar et al. 1994b):

$$\mathrm{M}^{NC} = \frac{1}{H}(\mathrm{M}^{C} - \nu C) \tag{4}$$

where

M^{NC} = nonconservative momentum equations

M^{C} = conservative momentum equations (Equations 2 and 3)

ν = horizontal velocity vector

C = primitive continuity equation (Equation 1)

Substitution of Equations 1-3 into Equation 4 leads to a reformulation of the momentum equations into a primitive, nonconservative form:

$$\frac{\partial U}{\partial t} + U\frac{\partial U}{\partial x} + V\frac{\partial U}{\partial y} - fV = \frac{\partial}{\partial x}\left[\frac{p_s}{\rho_0} + g(\zeta - \alpha\eta)\right] + \frac{1}{H}\left[\mathrm{M}_x + D_x + B_x + \frac{\tau_{sx}}{\rho_o} - \frac{\tau_{bx}}{\rho_o}\right] \tag{5}$$

$$\frac{\partial V}{\partial t} + U\frac{\partial V}{\partial x} + V\frac{\partial v}{\partial y} + fU = -\frac{\partial}{\partial y}\left[\frac{p_s}{\rho_o} + g(\zeta - \alpha\eta)\right] + \frac{1}{H}\left[\mathrm{M}_y + D_y + B_y + \frac{\tau_{sy}}{\rho_o} - \frac{\tau_{by}}{\rho_o}\right] \tag{6}$$

A rigorous derivation of Equations 1-6 is presented by Kolar et al. (1994b) and will not be repeated here.

The implementation of a standard quadratic parameterization for bottom stress and the neglect of baroclinic and lateral diffusion/ dispersion terms leads to a modified form of the primitive, nonconservative shallow-water equations:

$$\frac{\partial \zeta}{\partial t} + \frac{\partial UH}{\partial x} + \frac{\partial VH}{\partial y} = 0 \tag{7}$$

$$\frac{\partial U}{\partial t} + U\frac{\partial U}{\partial x} + V\frac{\partial U}{\partial y} - fV = -\frac{\partial}{\partial x}\left[\frac{p_s}{\rho_o} + g(\zeta - \alpha\eta)\right] + \frac{\tau_{sx}}{\rho_o H} - \tau_* U \tag{8}$$

$$\frac{\partial V}{\partial t} + U\frac{\partial V}{\partial x} + V\frac{\partial V}{\partial y} + fU = -\frac{\partial}{\partial y}\left[\frac{p_s}{\rho_o} + g(\zeta - \alpha\eta)\right] + \frac{\tau_{sy}}{\rho_o H} - \tau_* V \tag{9}$$

with τ_* given by the expression $C_f (U^2 + V^2)^{1/2} / H$ for C_f equal to the bottom friction coefficient.

Recall that one of the objectives of the ADCIRC-2DDI hydrodynamic model is to consider very large domain problems. The use of large domains coupled with the recognition that tidal forcings are a global phenomenon necessitates the inclusion of effects caused by the curvature of the Earth's surface. Thus, the shallow-water equations (Equations 7-9) are recast into spherical coordinates (Flather 1988, Kolar et al. 1994a):

$$\frac{\partial \zeta}{\partial t} + \frac{1}{R\cos\phi}\left[\frac{\partial UH}{\partial \lambda} + \frac{\partial (VH\cos\phi)}{\partial \phi}\right] = 0 \tag{10}$$

$$\frac{\partial U}{\partial t} + \frac{U}{R\cos\phi}\frac{\partial U}{\partial \lambda} + \frac{V}{R}\frac{\partial U}{\partial \phi} - \left[\frac{\tan\phi U}{R} + f\right]V = -\frac{1}{R\cos\phi}\frac{\partial}{\partial \lambda}\left[\frac{p_s}{\rho_0} + g(\zeta - \eta)\right] + \frac{\tau_{s\lambda}}{\rho_0 H} - \tau_* U \tag{11}$$

$$\frac{\partial V}{\partial t} + \frac{U}{R\cos\phi}\frac{\partial V}{\partial \lambda} + \frac{V}{R}\frac{\partial V}{\partial \phi} + \left[\frac{\tan\phi U}{R} + f\right]U = -\frac{1}{R}\frac{\partial}{\partial \phi}\left[\frac{p_s}{\rho_0} + g(\zeta - \eta)\right] + \frac{\tau_{s\phi}}{\rho_0 H} - \tau_* V \tag{12}$$

where

R = radius of the Earth

λ, ϕ = degrees longitude (east of Greenwich positive) and degrees latitude (north of the equator positive)

$f = 2\Omega sin\phi$

Ω = angular speed of the Earth

$\tau_{s\lambda}$, $\tau_{s\phi}$ = applied free surface stresses

A practical expression for the Newtonian equilibrium tide potential is given by Reid (1990) as:

$$\eta(\lambda,\phi,t) = \sum_{n,j} C_{jn} f_{jn}(t_0) L_j(\phi) \cos[2\pi(t - t_0)/T_{jn} + j\lambda + v_{jn}(t_0)] \tag{13}$$

where

t = time relative to t_0

t_0 = reference time

C_{jn} = constant characterizing amplitude of tidal constituent n of species j

f_{jn} = time-dependent nodal factor

L_j =

T_{jn} = period of constituent n of species j

v_{jn} = time-dependent astronomical argument

j = 0, 1, 2 = tidal species (j = 0, declinational; j = 1, diurnal; j = 2, semidiurnal

Values for C_{jn} are presented by Reid (1990). The value for the Earth elasticity factor is often taken as 0.69 for all tidal constituents (Schwiderski 1980, Hendershott 1981) although its value has been shown to be slightly constituent-dependent, ranging between 0.693 and 0.736 (Wahr 1981, Woodworth 1990).

The Earth's curvature must be accounted for not only in the governing equations but also in the finite element discretization (Kolar et al. 1994a). The

finite element method, as briefly mentioned in the section titled "Current Modeling Approaches," approximates a solution using interpolating functions. These interpolating functions are defined over elements and these elements are most often cast within the framework of a Cartesian coordinate system. In order to conveniently implement the finite element method, the governing equations in spherical coordinates are projected onto a planar surface using cartographic projection techniques. The mapping of spherical equations (Equations 10-12) to a rectilinear coordinate system is accomplished using a Carte Parallelogramatique Projection (CP) (Pearson 1990):

$$x' = R(\lambda - \lambda_o)\cos\phi_o \tag{14}$$

$$y' = R\phi \tag{15}$$

where (λ_0, ϕ_0) is the center point of the projection. An application of the CP projection to Equations 10-12 yields shallow-water equations in primitive, nonconservative form expressed in the CP coordinate system:

$$\frac{\partial\zeta}{\partial t} + \frac{\cos\phi_0}{\cos\phi}\frac{\partial(UH)}{\partial x'} + \frac{1}{\cos\phi}\frac{\partial(VH\cos\phi)}{\partial y'} = 0 \tag{16}$$

$$\begin{aligned}\frac{\partial U}{\partial t} + \frac{\cos\phi_o}{\cos\phi}U\frac{\partial U}{\partial x'} + V\frac{\partial U}{\partial y'} - \left[\frac{\tan\phi}{R}U + f\right]V \\ = -\frac{\cos\phi_0}{\cos\phi}\frac{\partial}{\partial x'}\left[\frac{p_s}{\rho_0} + g(\zeta - \eta)\right] + \frac{\tau_{s\lambda}}{\rho_0 H} - \tau_* U\end{aligned} \tag{17}$$

$$\begin{aligned}\frac{\partial V}{\partial t} + \frac{\cos\phi_0}{\cos\phi}U\frac{\partial V}{\partial x'} + V\frac{\partial V}{\partial y'} + (\frac{\tan\phi}{R}U + f)U \\ = -\frac{\partial}{\partial y'}\left[\frac{p_s}{\rho_0} + g\,(\zeta + \eta)\right] + \frac{\tau_{s\phi}}{\rho_0 H} - \tau_* V\end{aligned} \tag{18}$$

As discussed in the section titled "Current Modeling Approaches," utilizing the finite element method to resolve the spatial dependence of the shallow-water equations in their primitive form leads to inaccurate solutions with severe artificial, near $2 \cdot \Delta x$ modes (Gray 1982; Lynch 1983; Westerink, Stolzenbach, and Connor 1989). A reformulation of the primitive equations into a GWCE form gives highly accurate, noise-free, finite-element-based solutions to the shallow-water equations (Lynch and Gray 1979, Kinnmark 1984). The high accuracy of GWCE-based FE solutions is a result of their excellent numerical amplitude and phase propagation characteristics. In fact, Fourier analysis indicates that in constant-depth water, using linear interpolation, a linear tidal wave resolved with 25 nodes per wavelength is more than adequately resolved over the range of Courant numbers, $C = \sqrt{gh}\,\Delta t/\Delta x$, less than or equal to one (Luettich, Westerink, and Scheffner 1992). Furthermore, the monotonic dispersion behavior of GWCE-based FE solutions avoids generating artificial, near $2 \cdot \Delta x$ modes, which have plagued the primitive FE-based solutions, in both interior and boundary equations (Platzman 1981; Foreman 1983; Westerink et al., in preparation (b)). Note that the monotonic dispersion behavior of GWCE-based FE solutions is very similar to that associated with staggered finite difference solutions to the primitive shallow-water equations (Westerink and Gray 1991). GWCE-based FE solutions to the shallow-water equations allow for extremely flexible spatial discretizations which result in a highly effective minimization of the discrete size of any problem (Le Provost and Vincent 1986; Foreman 1988; Vincent and Le Provost 1988; Westerink, Luettich, and Muccino 1994; Westerink et al., in preparation (a); Luettich and Westerink, in preparation).

Derivation of the GWCE is presented concisely by the operator notation invoked by Kinnmark (1984) and Kolar (1992):

$$GWCE = \frac{dC}{dt} + \tau_o\, C - \nabla \cdot \mathrm{M}^c \tag{19}$$

where *GWCE* is the generalized wave continuity equation and τ_o is a non-physical constant in time and space which controls the balance between primitive and wave equation formulations (Lynch and Gray 1979; Kinnmark 1984; Luettich, Westerink, and Scheffner 1992; Kolar et al. 1994b). Substituting continuity Equation 16 and the conservative forms of momentum Equations 17 and 18 into Equation 19, the *GWCE* in the CP coordinate system is:

$$
\frac{\partial^2 \zeta}{\partial t^2} + \tau_0 \frac{\partial \zeta}{\partial t} + \frac{\cos\phi_0}{\cos\phi} \frac{\partial}{\partial x'} \left[U \frac{\partial \zeta}{\partial t} - \frac{\cos\phi_0}{\cos\phi} UH \frac{\partial U}{\partial x'} - VH \frac{\partial U}{\partial y'} + \left[\frac{\tan\phi}{R} U + f \right] VH \right.
$$

$$
\left. - H \frac{\cos\phi_0}{\cos\phi} \frac{\partial}{\partial x'} \left(\frac{p_s}{\rho_0} + g\,(\zeta - \alpha\eta) \right) - (\tau_* - \tau_0) UH + \frac{\tau_{s\lambda}}{\rho_0} \right]
$$

$$
+ \frac{\partial}{\partial y'} \left[V \frac{\partial \zeta}{\partial t} - \frac{\cos\phi_0}{\cos\phi} UH \frac{\partial V}{\partial x'} - VH \frac{\partial V}{\partial y'} - \left[\frac{\tan\phi}{R} U - f \right] UH \right.
$$

$$
\left. - H \frac{\partial}{\partial y'} \left(\frac{p_s}{\rho_0} + g(\zeta - \alpha\eta) \right) - (\tau_* - \tau_0) VH + \frac{\tau_{s\phi}}{\rho_0} \right]
$$

$$
- \frac{\partial}{\partial t} \left[\frac{\tan\phi}{R} VH \right] - \tau_0 \left[\frac{\tan\phi}{R} VH \right] = 0 \qquad (20)
$$

The advective terms in the GWCE, written in nonconservative form, improve global and local mass conservation (Kolar et al. 1994b) as well as numerical stability, especially for advection dominant flows (Westerink et al. 1992b). The ADCIRC-2DDI hydrodynamic model solves the GWCE, Equation 20, in conjunction with the primitive momentum equations in nonconservative form, Equations 17 and 18.

Numerical solution

The numerical discretization of the GWCE equation (Equation 20) and momentum Equations 17 and 18 is implemented in three stages. First, the symmetrical weak weighted residual (SWWR) statements for Equations 17, 18, and 20 are developed. This procedure is based on a standard Galerkin finite element formulation (Becker, Carey, and Oden 1981; Celia and Gray 1992). One consequence of the SWWR form is that the order of the derivatives in the governing equations is reduced, leading to a requirement of only C_o functional continuity (i.e., only interpolating functions themselves, not their derivatives, need be continuous between discrete points). Next, the stable and accurate time discretization strategies of Kinnmark (1984) and Werner and Lynch (1989) are implemented. A variably weighted three-time-level implicit scheme is applied to most linear terms in the GWCE. The nonlinear Coriolis, atmospheric pressure, and tidal potential terms are all treated explicitly. Alternatively, convective terms within the GWCE are evaluated at two known time levels. This time discretization strategy results in a linear algebraic system of equations associated with the GWCE, which is solved for unknown elevations. For the momentum equations, a Crank- Nicolson two-time-level implicit

scheme is used for all terms except the bottom friction and convective terms, which are treated explicitly.

The final step in the numerical discretization scheme is approximation of the spatial domain using the finite element method. Variables are expanded using a C_o interpolation basis over three-node, linear triangular elements. Elemental equations are summed over the global domain and inter-element C_o functional continuity is enforced. Details of the finite element implementation on a term-by-term basis is presented by Luettich, Westerink, and Scheffner (1992) and Westerink et al. (1992b). It is noted that shoreline wetting and/or drying is not currently included in the ADCIRC-2DDI code.

The fully discretized model equations are written in matrix notation (Luettich, Westerink, and Scheffner 1992):

$$\mathrm{M}^{GWCE}\zeta^{k+1} = P^{GWCE} \tag{21}$$

$$\mathrm{M}^{\lambda\lambda ME}U^{k+1} + \mathrm{M}^{\lambda\phi ME}V^{k+1} = P^{\lambda ME} \tag{22}$$

$$\mathrm{M}^{\phi\lambda ME}\ U^{k+1} + \mathrm{M}^{\phi\phi ME}V^{k+1} = P^{\phi ME} \tag{23}$$

where

M^{GWCE} = banded, time-independent mass matrix in the GWCE equation

ζ^{k+1} = vector of unknown surface elevations at time level $k + 1$

P^{GWCE} = load vector of known forcings in the GWCE equation

$M^{\lambda\lambda ME}$, $M^{\lambda\phi ME}$, $M^{\phi\lambda ME}$, $M^{\phi\phi ME}$ = time-dependent, lumped mass matrices in the λ, ϕ directions

U^{k+1}, V^{K+1} = vectors of unknown velocity components at the $k + 1$ time level

$P^{\lambda ME}$, $P^{\phi ME}$ = load vectors of known forcings for the momentum equations

Elevation boundary conditions are enforced within the load vector P^{GWCE} of the GWCE equation (Equation 21) and zero normal velocity boundary conditions are enforced in the momentum equations (Equations 22 and 23). Westerink et al. (in preparation (b)) have shown that solutions to the GWCE equation are insensitive to this standard boundary condition formulation.

The decoupled discrete GWCE and momentum equations (Equations 21-23) lead to a sequential solution procedure. The GWCE equation (Equation 21) is solved at each time-step for the surface water elevations, ζ^{k+1}. The GWCE mass matrix M^{GWCE} is time independent, so it is assembled and decomposed only once. The banded structure of this matrix is not utilized by the iterative preconditioned conjugate gradient matrix solver used for computations performed in this work (Press et al. 1986; Kincaid and Cheney 1991). The preconditioned conjugate gradient solver is selected because of its efficiency at minimizing the memory requirements of ADCIRC-2DDI for larger problems. The load vector P^{GWCE} is updated at each time-step with newly computed surface water elevations and velocities from the previous time-step.

Upon solving the GWCE for surface water elevations, the computed elevations are substituted into momentum Equations 22 and 23 prior to solution for the velocity components U^{k+1} and V^{k+1}. The time-dependent mass matrices in the momentum equations ($M^{\lambda\lambda ME}$, $M^{\lambda\phi ME}$, $M^{\phi\lambda ME}$, $M^{\phi\phi ME}$) are lumped to yield diagonal matrices which require trivial solution. The lumping procedure applied here does not introduce significant errors as shown by Lynch and Gray (1979).

The numerical solution algorithm just described for the ADCIRC-2DDI model is implemented in fully vectorized form. A consequence of this solution procedure is a highly efficient code in terms of central processing unit requirements per node. This efficiency is largely due to the fact that GWCE-based FE solutions to the shallow-water equations allow for extremely flexible spatial discretizations which result in a highly effective minimization of the discrete size of any problem (Le Provost and Vincent 1986; Foreman 1988; Vincent and Le Provost 1988; Westerink et al. 1992a,b; Westerink, Luettich, and Muccino 1994).

Summary

Numerical formulation of the hydrodynamic model is critical to the success of any storm surge modeling application. The depth-averaged shallow-water equations are designated as an appropriate theoretical framework for the hydrodynamic model. Additional requirements of accuracy, efficiency, and grid flexibility are imposed on the numerical solution technique. A brief review of current hydrodynamic modeling approaches is presented in terms of the model selection criteria set forth. From the assessment of available numerical solution techniques for the shallow-water equations, a GWCE-based finite element approach is chosen as the optimal solution strategy. The GWCE-based finite element equations are implemented within the hydrodynamic model ADCIRC-2DDI.

ADCIRC-2DDI has demonstrated the desired characteristics of accuracy, efficiency, and a high degree of grid flexibility in numerous numerical tests, analyses, and field applications. Thus, the ADCIRC-2DDI hydrodynamic model is adopted for all storm surge simulations presented in this work.

Details of the governing equations, their limitations, advantages, and numerical solution are discussed.

The ADCIRC-2DDI hydrodynamic model provides a sound tool with which to study the characteristics of the computed storm surge response and to address convergence issues related to storm surge modeling. When using the ADCIRC-2DDI model, storm surge generation is simulated over large domains for lengthy time periods with striking efficiency and accuracy.

3 Meteorological Forcing

Storm surge development can be attributed to several mechanisms (Dendrou, Moore, and Myers 1985; Reid 1990) each of which is caused primarily by some combination of wind and pressure forcing. Furthermore, it is well-known that storm surge models are highly sensitive to the representation of wind forcing (i.e., Chen, Shaffer, and Kim 1993; Hubbert, Leslie, and Manton 1990; Dendrou, Moore, and Myers 1985; Flather 1984). Thus, realistic storm surge generation by a numerical model depends upon accurate specification of wind and pressure fields. Though measured values of wind speeds and pressures can be used, this data is almost always scarce and too limited in scope. More commonly, either an empirical or conservation-based model is used to generate wind and pressure fields associated with a hurricane.

This chapter begins by offering a physical description of the wind and pressure forces within a hurricane and their role in storm surge generation. The current state of hurricane models is briefly mentioned and selection of a wind model is made. The chosen wind model is then described in terms of its governing equations, numerical implementation, and interface with the hydrodynamic model ADCIRC-2DDI.

Two hurricanes of record (Kate (1985) and Camille (1969)) are applied as meteorological forcing for the storm surge computations in this work. For each of these hurricanes, the path, wind speed, eye pressure, and other important parameters are presented. A series of synthetic hurricanes used in the investigation of grid structure influence on storm surge generation are also described.

Hurricane Forcing and Modeling Approaches

A hurricane is a rotating cyclone in the tropical ocean having considerable size and intensity. More specifically, a hurricane is classified by wind speeds of 33 m/s (74 mph) or greater and is characterized by a low pressure center. The region of low pressure at the eye of the storm produces a rise in sea surface elevation named an inverted barometer effect. Outwards from the eye, pressures gradually increase towards the storm's edge.

Hurricane wind fields are characterized by high winds blowing spirally around the low pressure center of the storm. In the Northern Hemisphere, hurricane wind fields orient in a counterclockwise direction due to the Coriolis forcing, which accounts for rotation of the Earth. Relatively low wind speeds are experienced at the hurricane eye but rapidly increase out to a radius ranging anywhere from 15 km to 85 km (8.1-45.8 N miles), a distance often termed the radius to maximum wind. Wind speeds diminish beyond the radius to maximum wind out to the storm's periphery.

Hurricane winds exert a shearing stress at the ocean surface. Drag forces associated with the wind shear work both to maintain a sloping water surface against the shoreline and drive surface water in the direction of the wind, the latter being the primary mechanism for storm surge generation. Further details regarding the formation, life cycle, and impact of a hurricane are given by Dunn and Miller (1964), Stubbs (1966), and Simpson and Riehl (1981).

Recent numerical models of the hurricane itself are based on three-dimensional primitive conservation equations which are solved over a multiply-nested movable grid (Powell 1982; Bender, Tuleya, and Kurihara 1984; Jones 1987; Kurihara et al. 1990). These models are computationally intensive and fairly complex. Hydrodynamic modelers have traditionally sought simpler ways of estimating the wind and pressure forcing generated by a hurricane. In many storm surge modeling studies parameterizations or empirical models are used to represent wind and pressure forcing (e.g. Johns and Ali 1980; Johns et al. 1983a,b; Flather 1984; Jarvinen and Lawrence 1985; Shaffer, Jelenianski, and Chen 1986; Wang 1987; Westerink, Stolzenbach, and Connor 1989; Hearn and Holloway 1990). Murty, Flather, and Henry (1986) review many of the currently used empirical cyclone models and offer some inter-comparisons. The most complex empirical model reviewed by Murty, Flather, and Henry (1986) is the Standard Project Hurricane (SPH) model (Cialone 1991) used by Westerink, Stolzenbach, and Connor (1989), among others. Westerink, Stolzenbach, and Connor (1989) report severe overpredictions of hurricane winds coming off the land when using the SPH model. To obtain satisfactory results, an exponential decay factor was applied within the SPH model to winds computed near land.

To improve the quality of the specified meteorological forcing, a hurricane model which accounts for the basic physical and dynamical characteristics of a tropical cyclone is sought. Chen, Shaffer, and Kim (1993) suggest initially computing a pressure field and then using this pressure field to calculate geostrophic winds. One model adopting such an approach is the HURWIN wind model of Cardone, Greenwood, and Greenwood (1992). The HURWIN model uses the conservation of momentum as a foundation and is selected here to compute the meteorological forcing for the hydrodynamic model, ADCIRC-2DDI. Though specification of the wind and pressure forcing is important to the success of storm surge model predictions, any further review of hurricane models or testing of the HURWIN wind model is beyond the scope of this work.

HURWIN Wind Model

Governing equations

The HURWIN wind model is part of the Coastal Modeling System at the U.S. Army Corps of Engineers Waterways Experiment Station and is based on the vortex model of Chow (1971) modified by Cardone, Greenwood, and Greenwood (1992). The HURWIN wind model is a diagnostic model and thus is not a predictive tool. As a result, the HURWIN model utilizes data available from a specific storm to produce a time history of surface wind speeds and pressures over a rectangular grid.

Within the HURWIN model, the total pressure p_s which has been depth-averaged over the planetary boundary layer, is prescribed to be a sum of the pressure associated with the tropical cyclone p_c which is translating with the storm at a speed V_c and a large-scale background pressure $\overline{p}$:

$$p_s = p_c + \overline{p} \tag{24}$$

The well-known exponential pressure law which follows is used to represent a tropical cyclone having a circularly symmetric pressure field situated at the low pressure center of the storm:

$$p_c = p_{eye} + \Delta p e^{-(R/r)} \tag{25}$$

where

p_{eye} = pressure at the eye of the storm

$\nabla p = \overline{p} - p_{eye}$ = the pressure anomaly

R = scale radius, often assumed equivalent to the radius to maximum wind

r = radial distance outwards from the eye of the storm

The background (or far field) pressure can be specified in terms of a corresponding geostrophic flow as:

$$f\hat{k} \times V_g = -(\frac{1}{\rho}\nabla\overline{p}) \tag{26}$$

where $f\hat{k}$ is the Coriolis parameter in the vertical direction and V_g is the constant geostrophic velocity.

The HURWIN wind model determines wind speeds by solving the equations of horizontal motion which have been vertically averaged through the depth of the Planetary Boundary Layer (PBL). The two-dimensional equation of horizontal motion is expressed in coordinates fixed to the Earth:

$$\frac{dV_w}{dt} + f\hat{k} \times V_w = -(\frac{1}{\rho}\nabla p_s) + \nabla \cdot K_H \nabla V_w + (-\frac{C_{WD}}{d})|V_w|V_w \qquad (27)$$

where

$\frac{d}{dt}$ = total time derivative, given as $\frac{\partial}{\partial t} + V_w \cdot \nabla$

$\frac{\partial}{\partial t}$ = local time change relative to fixed coordinates

∇ = two-dimensional del operator

V_w = vertically averaged horizontal wind velocity vector

ρ_{air} = mean air density

K_H = horizontal eddy viscosity coefficient relative to the atmosphere

C_{WD} = surface wind drag coefficient

d = depth of the planetary boundary layer (PBL)

In the derivation of Equation 27, the vertical advection of momentum is assumed to be small compared to horizontal momentum advection and is thus neglected. Additionally, the shear stress at the top of the PBL is taken to be zero.

Substituting the pressure relationships in Equations 24 and 26 into Equation 27, the integrated wind field within the PBL can be obtained from:

$$\frac{dV_w}{dt} + f\hat{k} \times (V_w - V_g) = -(\frac{1}{\rho}\nabla p_c) + \nabla \cdot K_H \nabla V_w + (-\frac{C_{WD}}{d})|V|V \qquad (28)$$

The equations actually solved in the HURWIN wind model are derived by transforming Equation 28 to a moving Cartesian coordinate system whose origin is located at the low pressure center of the storm.

By neglecting acceleration and horizontal diffusion of momentum at the edges of the computational domain, boundary conditions at these points are written as a balance between the Coriolis, pressure gradient, and surface frictional forces.

The theoretical basis of the hurricane wind model, HURWIN, is only briefly outlined here. A more extensive and detailed description is given by Cardone, Greenwood, and Greenwood (1992).

Numerical solution strategy

The numerical discretization of the governing equations in the HURWIN wind model is based on a finite difference formulation, the details of which are given by Chow (1971). Resolution of the hurricane is critical to representing its interaction with the environment (Kurihara et al. 1990). To best represent the dynamics of the hurricane and maintain a computationally feasible problem, the discretized equations are solved over a nested grid system consisting of five rectangular grids each having uniform mesh spacing. Mesh spacing doubles for each successively larger grid (e.g., for an innermost grid spacing of 5 km (2.7 miles), remaining grids in the nested system have mesh sizes of 10 km (5.4 miles), 20 km (10.8 miles), 40 km (21.6 miles), and 80 km (43.2 N miles)). The maximum areal extent of the nested grid system corresponds to the areal coverage of the largest grid. The grid structure implemented within the HURWIN model is centered at the eye of the storm and moves with the storm throughout the domain. This solution strategy provides maximum resolution near the eye of the storm where wind speeds and pressure gradients vary most rapidly.

The HURWIN model computations are based on the concept that a tropical storm generally changes structure relatively slowly. As such, the structure of a hurricane travelling over open water is well-represented by parameters specified at intervals of 6 to 24 hr. These representative states or "snapshots" form a portion of the input to the HURWIN wind model. Parameters specified at 6-hr snapshot intervals include: pressure at the eye of the storm, far field or background pressure, radius to maximum wind, storm track direction, speed of the storm, surface geostrophic wind velocity, direction of the surface geostrophic wind, and mesh spacing of the innermost grid. The innermost nested grid spacing is set at 5 km for all HURWIN model simulations conducted herein. Additional hurricane parameters not enumerated above are specified according to average values as suggested by Cardone, Greenwood, and Greenwood (1992) and remain the same for all hurricanes considered.

Although the hurricane structure typically changes slowly, storm position can change relatively quickly. Differences in the time scale between changes in storm structure and position are accommodated by specifying the location of the storm center at every hour. This hourly input to the HURWIN model includes the latitude and longitude of the storm center and the relative

weightings of the hourly storm position between the previously discussed 6-hr snapshots describing hurricane parameter specifications.

The 6-hr snapshots detailing hurricane structure and the hourly data specifying storm position, both of which are required for operation of the HURWIN wind model, are obtained from widely available meteorological data appropriate to specific historical hurricanes.

The parameters input into the HURWIN model at 6-hr intervals which describe the hurricane wind field structure are used to compute pressure gradient and surface wind fields under steady state assumptions. An hourly time history of the surface wind field is then obtained through a weighted linear interpolation between successive 6-hr computed wind fields.

Despite the more realistic theoretical basis of the HURWIN model, several limitations arise in the model's ability to represent hurricane wind fields. The most prominent shortcoming relates to the lack of dissipation in the wind field of a hurricane making landfall. As a hurricane approaches land it generally slows and winds dissipate. Consequently, winds on the right side of the hurricane are somewhat reduced from full strength as they encounter the land. As the winds rotate over the land, their speed is further diminished by frictional forces resulting from the roughness of the topography. Consequently, winds on the left side of the hurricane coming off the land are significantly less in magnitude than winds coming onto land from the right side of the hurricane. The version of the HURWIN wind model used herein does not represent the processes associated with a landfalling hurricane. Thus, excessive winds near the land boundary are computed by the HURWIN model and may lead to large negative surge in coastal regions on the left side of the hurricane and overprediction of the peak surge on the right side of the hurricane.

Note that the HURWIN model does accommodate terrains of varying roughness. However, the incorporation of surface roughness variations within the HURWIN model does not account for asymmetry in the winds of a landfalling hurricane. Within the HURWIN model, the winds over land can be reduced by a constant factor but, as the winds come off the land into the open ocean, wind speeds uniformly increase in accordance with the reduced frictional coefficient specified over the open ocean. This instantaneous, uniform increase and subsequent decrease of the wind speed initiated by the specification of surface roughness is not physically realistic. The complex processes which dissipate winds in a landfalling hurricane are critical to generation of storm surge at the shoreline, and yet, are not addressed by the version of the HURWIN model implemented. For consistency, all surface roughness parameters specified within the HURWIN wind model pertain to the open ocean.

Interface with ADCIRC-2DDI

Output from the HURWIN model has been modified so that computed wind and pressure fields directly interface with the ADCIRC-2DDI hydrodynamic

model. The pressure field computed by a HURWIN model simulation is more conveniently expressed in terms of an equivalent height of water $p_s/\rho_0 g$. Furthermore, wind speeds generated by the HURWIN model are converted to surface wind stresses using a relationship proposed by Garratt (1977):

$$\frac{\tau\phi}{\rho_o} = C_D \frac{\rho_{air}}{\rho_0} |W| W_\phi \tag{29}$$

and

$$\frac{\tau_\lambda}{\rho_o} = C_D \frac{\rho_{air}}{\rho 0} |W| W_\lambda \tag{30}$$

where

τ_ϕ, τ_λ = wind stresses in the ϕ and λ directions, respectively

ρ_{air}/ρ_0 = 0.001293 = ratio of air density to average density of seawater (Pickard and Emery 1982)

C_D = frictional drag coefficient computed as $0.001\ (0.75 + 0.067|W|)$

$|W|$ = magnitude of the wind velocity

W_ϕ, W_λ = components of the wind velocity vector in the $_\phi$ and λ directions, respectively

The wind stress relationship of Garratt (1977) has been used successfully by others, including Cooper and Thompson (1989); Westerink, Stolzenbach, and Connor (1989); and Hearn and Holloway (1990).

Through a bilinear interpolation, both wind stresses and $P/(\rho_w g)$ values are transferred directly from the HURWIN model nested rectangular grids onto the finite element computational grid used by the ADCIRC-2DDI model. The hourly time series of spatial wind stress and $P_s/\rho_0 g$ fields associated with a specified hurricane serve as the meteorological forcing for the ADCIRC-2DDI hydrodynamic model in all storm surge simulations presented herein. Within the ADCIRC-2DDI model, linear interpolation between hourly wind and pressure forcings yields meteorological forcing appropriate at each time-step interval.

Hurricanes of Record

Hurricane Kate

Hurricane Kate is one of the historical storms selected as the meteorological forcing for the hydrodynamic model. The track of Hurricane Kate through the western North Atlantic Ocean and the Gulf of Mexico is shown at 6-hr increments in Figure 1. Beginning in the deep western North Atlantic Ocean, Hurricane Kate was recognized as a tropical storm at 18:00 Greenwich mean time (GMT) 15 November 1985, and was upgraded 24 hr later to a hurricane. As Kate moved northeastward through the Gulf of Mexico, a minimum pressure of 953 mb and a maximum sustained wind speed of approximately 54 m/s^{-1} (104.9 knots) were recorded 26.5 hr prior to landfall. At 22:30 GMT 21 November 1985, Hurricane Kate made landfall near Panama City, FL. The tracking of Hurricane Kate then continued through 18:00 GMT 23 November 1985 until the winds had significantly dissipated and Kate was classified as an extratropical storm. Extensive meteorological analysis of Hurricane Kate as well as measured storm surge hydrographs at 10 stations along the Florida coast in the vicinity of Panama City are reported by Garcia and Hegge (1987).

Simulation of Hurricane Kate using the HURWIN wind model begins at 18:00 GMT 15 November 1985 and ends 8 days later at 18:00 GMT 23 November 1985, a duration of 193 hr. During this period the forward speed of Hurricane Kate ranges from 1.5 m/s^{-1} (2.9 knots) to 13.4 m/s^{-1} (26.0 knots) and the radius to maximum wind varies between 80 km (43.2 miles) and 17 km (9.2 miles). A constant background pressure of 1,013 mb is assumed. All of the parameters pertaining to Hurricane Kate and used within a HURWIN model simulation are obtained from the HURDAT tape (Jarvinen, Neumann, and Davis 1984; 1993).

Hurricane Camille

Hurricane Camille is the second historical storm used as meteorological forcing in this study of storm surge generation. The track of Hurricane Camille through the western Caribbean Sea and the Gulf of Mexico is shown at 6-hr increments in Figure 2. As of 3 August 1969, Camille was tracked as a tropical cyclone having low pressures over the Cape Verde Islands in the eastern Atlantic Ocean. During the period covering 12-14 August 1969, Hurricane Camille began its formation in the western Caribbean Sea. After Camille passed over Cuba and was well into the Gulf of Mexico, a minimum pressure of 905 mb and a maximum sustained wind speed of about 62 m/s^{-1} (120.4 knots) were recorded at 0:00 GMT 17 August 1969. During the same period, water heights of 7.5 m (24.6 ft) above mean sea level were recorded at New Orleans, LA. On 18 August 1969, Hurricane Camille made landfall near Biloxi, MS. The tracking of Hurricane Camille then continued through 12:00 GMT 22 August 1969 until the winds had significantly dissipated.

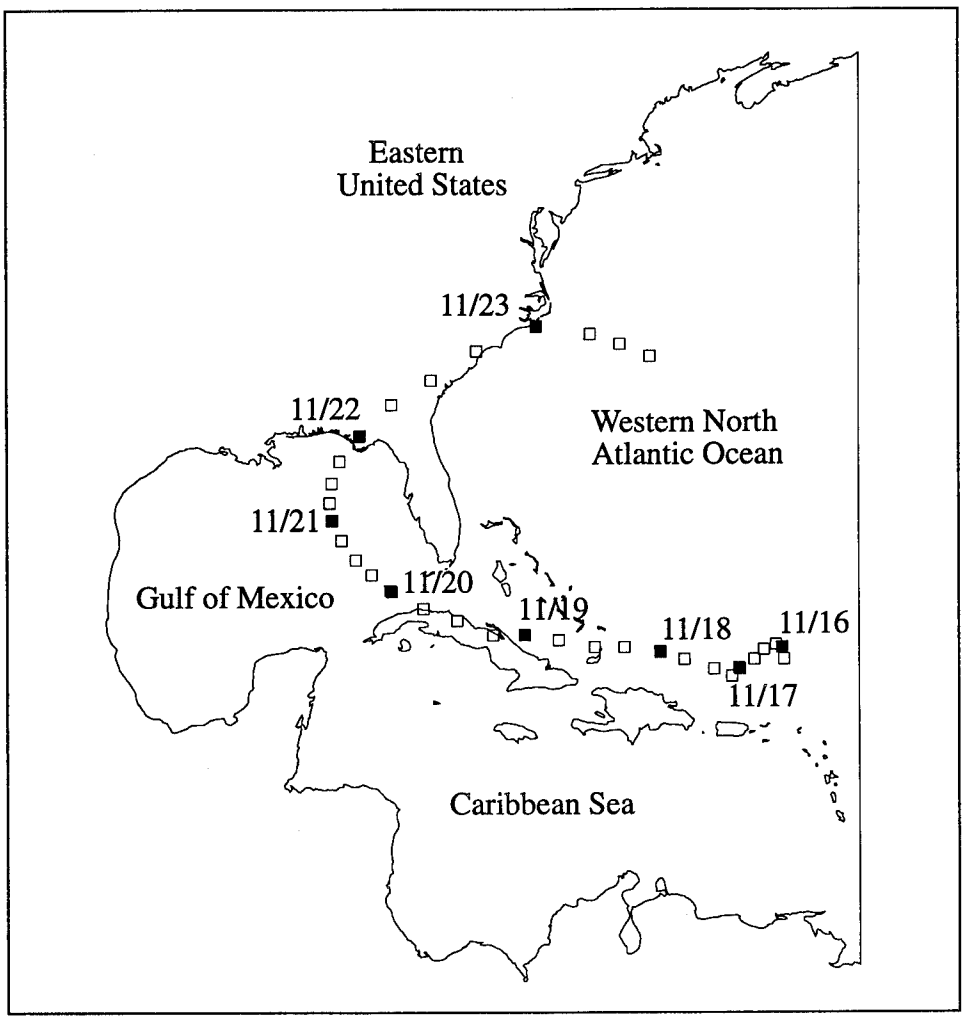

Figure 1. Track of Hurricane Kate through the western North Atlantic Ocean and Gulf of Mexico (18:00 GMT 15 November 1985 to 18:00 GMT 23 November 1985) shown at 6-hr intervals

Extensive meteorological analysis of the formation of Hurricane Camille, photos of the storm track, recorded parameters, and tidal heights were compiled by Simpson and Riehl (1981).

Simulations of Hurricane Camille using the HURWIN wind model began at 18:00 GMT 14 August 1969 and ended 7-3/4 days later at 12:00 GMT 22 August 1969, a duration of 187 hr. During this period the forward speed of Hurricane Camille ranged from 3.1 m/s^{-1} to 20.6 m/s^{-1} (6.0 to 40.0 knots) and the radius to maximum wind varied between 80 km and 17 km (43.2 and 9.2 n.m.). Throughout the simulation, a constant background pressure of 1,013 mb is assumed. All of the parameters pertaining to Hurricane Camille and used within the HURWIN model are obtained from the HURDAT tape (Jarvinen, Neumann, and Davis 1984; 1993).

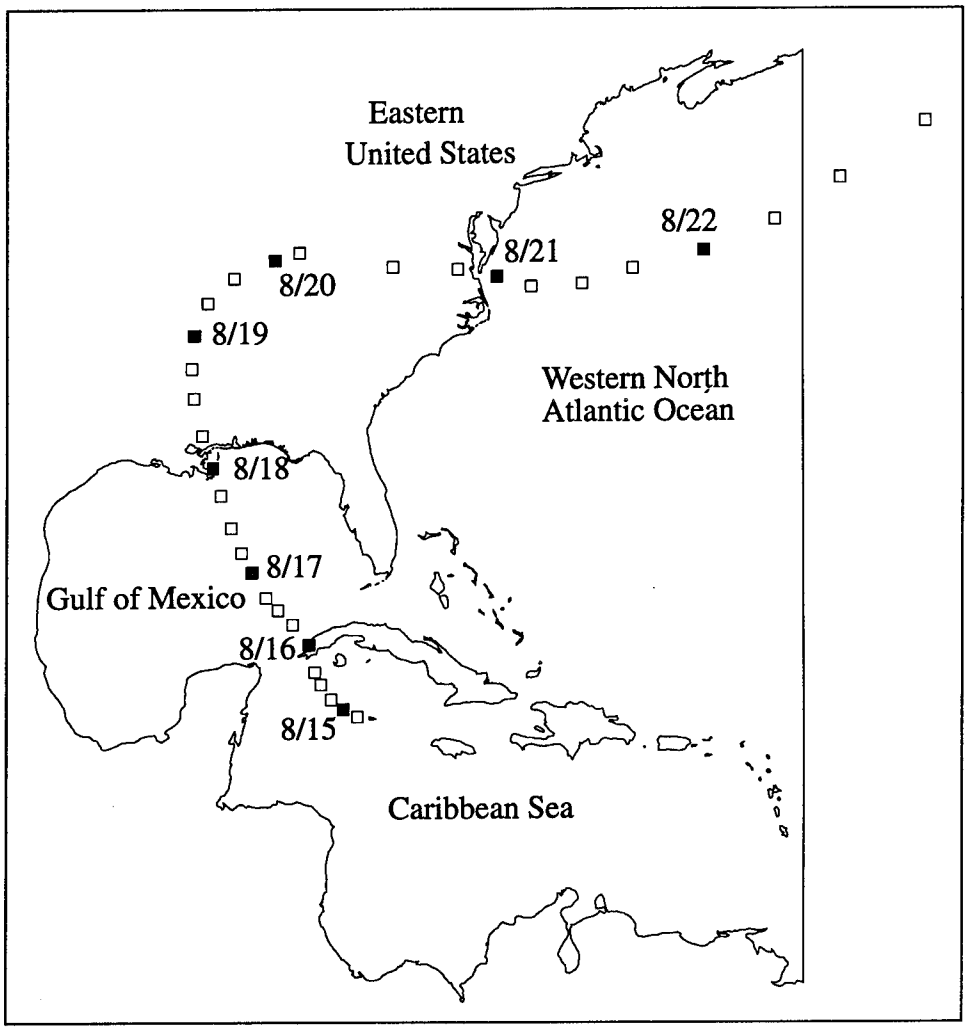

Figure 2. Track of Hurricane Camille through the western Caribbean Sea and Gulf of Mexico (18:00 GMT 14 August 1969 to 18:00 GMT 22 August 1969) shown at 6-hr intervals

Synthetic Hurricanes

A series of four synthetic hurricanes are created as meteorological forcing for the grid sensitivity study which investigates the relationships between grid structure, storm surge generation, and selected hurricane parameters. The synthetic hurricanes are constructed such that characteristics relating to path, spatial scale, and forward velocity are isolated for study.

Two different hurricane paths are considered, one perpendicular (Path 1) and one parallel (Path 3) to the coastline as shown in Figure 3. Along Path 3, the eye of the hurricane comes within 60 km (32.4 n.m.) of the shoreline. Two constant spatial scales R_{max} of 30 km (16.2 n.m.) and 60 km (32.4 n.m.) and two constant storm velocities of 15 km/hr (8.1 knots) and 25 km/hr

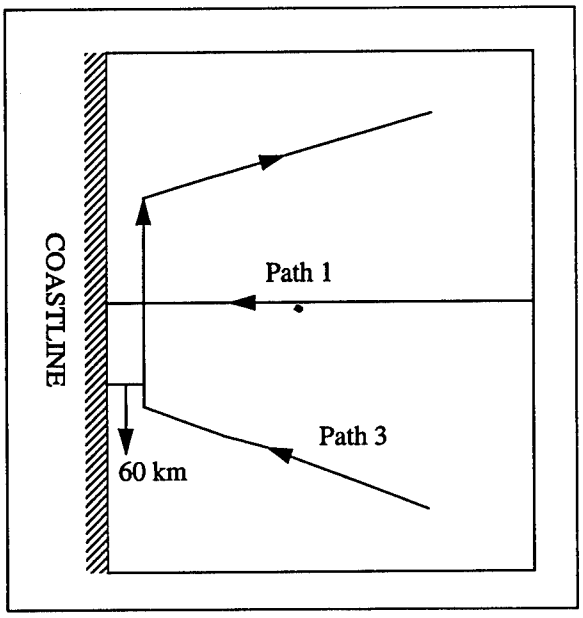

Figure 3. Two synthetic hurricane tracks, one perpendicular (Path 1) and one parallel to the coastline (Path 3)

(13.5 knots) are specified as parameters for the synthetic hurricanes. Each synthetic hurricane has a constant pressure deficit of 80 mb and no background surface winds are applied. Hurricane parameters are selected based on averages of the parameters associated with six historical hurricanes (Kate, Eloise, Elena, Hugo, Danny, and Camille) and the hurricane parameters utilized in the work of Bungpapong, Reid, and Whitaker (1985).

Table 1 summarizes the four synthetic hurricanes and their respective parameters. Hurricane names include three numbers which identify the parameter set associated with each hurricane. The first number refers to the specified pressure deficit (0 for a pressure deficit of 80 mb). The second number reflects the path specification (1 for Path 1, which is in a direction perpendicular to the coastline or 3 for Path 3, which has a segment parallel to the coastline). The third number of the hurricane name designates the combination of spatial scale and velocity which applies to the hurricane (i.e., 1 refers to a spatial scale of 30 km (16.2 miles) and a velocity of 15 km/hr (8.1 knots)).

Table 1
Characteristics of Synthetic Hurricanes

Hurricane Name	R_{max} (km)	Velocity (km/hr)	Hurricane Path (relative to the coast)	Simulation Period (days)	Time of Landfall (hr)
H011	30	15	Perpendicular	8.75	192
H012	60	15	Perpendicular	8.75	192
H013	30	25	Perpendicular	6.00	126
H031	30	25	Parallel	20.50	----

Summary

Hurricane wind and pressure fields are the primary mechanisms by which storm surge is generated in coastal regions. Consequently, meteorological forcing is the driving force for a storm surge hydrodynamic model. Realistic specification of hurricane wind and pressure forcing is a prerequisite for accurate representation of the storm surge response by the hydrodynamic model. Commonly, empirical hurricane models are used but a physically based conservation law model of the planetary boundary layer is more appealing and perhaps more accurate in representing hurricane wind and pressure fields. The HURWIN wind model of Cardone, Greenwood, and Greenwood (1992) is just such a model and is selected to compute the meteorological forcings for the storm surge simulations herein.

The theoretical basis and solution strategy of the HURWIN wind model are presented. Input parameters required by the HURWIN model to generate wind and pressure fields from specific historical hurricanes are readily obtained from available meteorological databases, simplifying implementation of the HURWIN wind model. The interface between HURWIN wind model computations and the wind and pressure forcing required by the hydrodynamic model ADCIRC-2DDI is discussed. Limitations in HURWIN's representation of a landfalling hurricane cause computed hurricane wind fields which are excessively high near land and in turn severely affect the accuracy of computed storm surge at the coastline. The effects of overpredicted winds near land are in fact manifest in the storm surge hydrographs presented in subsequent chapters.

Meteorological forcing throughout this work is obtained either from one of the historical hurricanes, Kate (November 1985) or Camille (August 1969), or from one of four synthetic hurricanes created to isolate the influence of the hurricane path, speed, and spatial scale on storm surge generation. Details regarding the characteristics defining each synthetic storm are provided.

4 Domain Size Sensitivity

A major shortcoming in coastal ocean modeling work is the lack of adequate studies to prove convergence with regard to grid structure, grid spacing, and domain size. In many studies it is unclear whether the computed water body response is significantly aliased due to inadequate grid resolution or is overwhelmed by the imposed boundary conditions and their interactions with the selected domain. Only recently have there been efforts to establish the level to which the computed physics have converged by doing systematic grid convergence studies for tidal, wind-driven, and large-scale baroclinic circulation (Johns et al. 1983a,b; Le Provost and Vincent 1986; Bennett and Campbell 1987; Dietrich, Roache, and Marietta 1990; Piacsek and Allard 1993; Dietrich 1993; Westerink, Luettich, and Muccino 1994; Luettich and Westerink, in preparation). None of these studies, however, specifically addresses the domain size and its effect on storm surge computations.

The primary focus of this chapter is to investigate the influence of domain size on hurricane storm surge response. Domain size affects both boundary condition specification and the computed storm surge response. Jarvinen and Lawrence (1985) specifically note that the initial design and location of the basin domain is a critical step in the construction of a storm surge model. Judicious selection of a domain size results in a computed storm surge response that captures the peak surge as well as possibly excited resonant frequencies documented by Bunpapong, Reid, and Whitaker (1985).

Storm surge modeling efforts to date have primarily used domains which are either limited to the continental shelf or cover the shelf and portions of the continental slope (e.g. Flather 1984; Dendrou, Moore, and Myers 1985; Jarvinen and Lawrence 1985; Dube, Sinha, and Roy 1986; Lardner and Cekirge 1988; Al-Rabeh, Eunay, and Cekirge 1990; Hearn and Holloway 1990; Hubbert, Leslie, and Manton 1990; Signorini and Miller 1992). Appreciable development of hurricane storm surge occurs on the continental shelf, precluding accurate specification of the open ocean boundary condition in shelf regions. Nested domains are often implemented to improve elevation specifications at the open ocean boundary of shelf domains (e.g. Flather 1984; Dendrou, Moore, and Myers 1985; Hubbert, Leslie, and Manton 1990; Al-Rabeh, Eunay, and Cekirge 1990). In the nested domain approach, computations over a large regional domain are interpolated onto the open ocean boundary of a smaller shelf domain. This interpolation from a coarsely

discretized domain to a typically highly resolved domain introduces numerical noise at inter-domain boundaries (i.e., Flather 1984; Hubbert, Leslie, and Manton 1990) causing a misrepresentation of the dynamics of storm surge generation at the open ocean boundary of the smaller domain. An extensive examination of the storm surge response computed over a shelf domain is included as part of the comprehensive study investigating the influence of domain size on storm surge computations.

For this domain size sensitivity study, an actual hurricane which made landfall on the Florida shelf in the Gulf of Mexico is applied over three domains. Each domain is of a different size fanning out from the point of hurricane landfall and covering successively larger regions. The first domain is a relatively small coastal domain which extends mainly over the continental shelf. The second domain covers the entire Gulf of Mexico basin. The final domain extends well into the deep Atlantic Ocean. Two different elevation boundary conditions are considered in the simulations, a still-water condition and a condition which incorporates the atmospheric pressure component of the meteorological forcing. Comparisons are made between storm surge elevations computed over all three domains using both boundary conditions to determine the influence of domain size and the sensitivity to boundary condition specification on storm surge response. Furthermore, computed storm surge elevations are compared to measured water levels from a historical hurricane. Results of this domain size sensitivity study provide criteria for domain size selection with regard to the accurate generation and propagation of hurricane storm surge.

Hydrodynamic Domain Descriptions

Three hydrodynamic domains of widely varied sizes are considered in this investigation. The domain sizes are selected to clearly demonstrate the relationship between the domain and open boundary elevation specification. The two smaller domains are constructed to correspond with domains used in recent storm surge modeling efforts. Hurricane Kate is the meteorological forcing used for the domain size comparison simulations. Thus, all domains used here expand outward from the landfall region of Hurricane Kate near Panama City, FL, and cover increasingly larger areas. Relative sizes of the three domains considered are shown in Figure 4 and the exact areal extent of each domain, as well as other characteristics pertinent to the domains and their discretizations, are summarized in Table 2.

The smallest domain considered is the Florida coast domain pictured in Figure 4a. The Florida coast domain is a semicircular basin similar to the one used by the National Weather Service at Pensacola Bay in conjunction with the SLOSH storm surge model (Jelesnianski 1979; Jarvinen and Lawrence 1985; Shaffer, Jelesnianski, and Chen 1986; Jelesnianski, Chen, and Shaffer 1992; Chen, Shaffer, and Kim 1993). The Florida coast domain extends radially outward into the Gulf of Mexico from the shoreline surrounding Panama City,

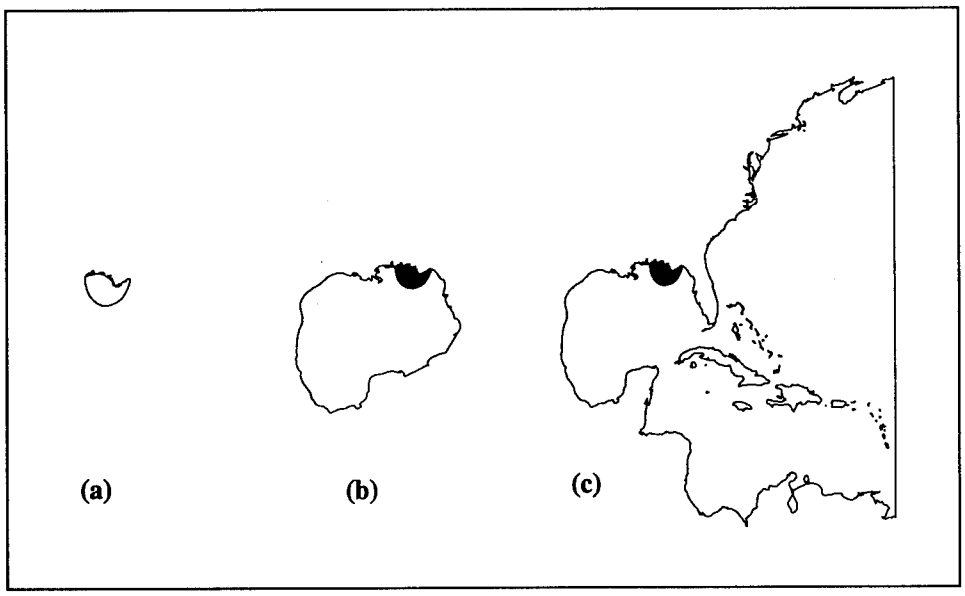

Figure 4. Boundaries of the (a) Florida Coast domain, (b) Gulf of Mexico domain, and (c) east coast domain

Table 2
Characteristics of Model Domains

Domain Name	Area (km^2)	Max Depth (m)	Discretization		Grid Size (km)	
			Nodes	Elements	Max	Min
Florida coast	5.07×10^4	1,094	1,451	2,326	32.5	0.5
Gulf of Mexico	1.41×10^6	3,781	6,325	11,441	50.0	0.5
East coast	8.35×10^6	7,765	22,711	41,709	98.3	0.5

FL, with a radius of approximately 175 km (109 miles). The outer arc of the semicircular basin forms the open ocean boundary of the domain. Bathymetric data for the Florida coast domain shown in Figure 5 are obtained from the topographic database ETOPO5 from the National Center for Atmospheric Research and supplemented by the National Oceanic and Atmospheric Administration (NOAA) Digital U.S. Coastal Hydrography sounding database (distributed by NOAA National Geophysical and Solar-Terrestrial Data Center in Boulder, CO) along the Florida shelf and coast. A minimum depth of 3 m (10 ft) is imposed throughout the Florida coast domain to eliminate complete drying in computational elements along the shoreline and in embayments. A maximum depth of nearly 1,100 m (3,600 ft) is recorded at the outer limit of the Florida coast domain, but as is seen in Figure 5, much of the Florida coast domain lies on the continental shelf at depths less than 130 m (426 ft).

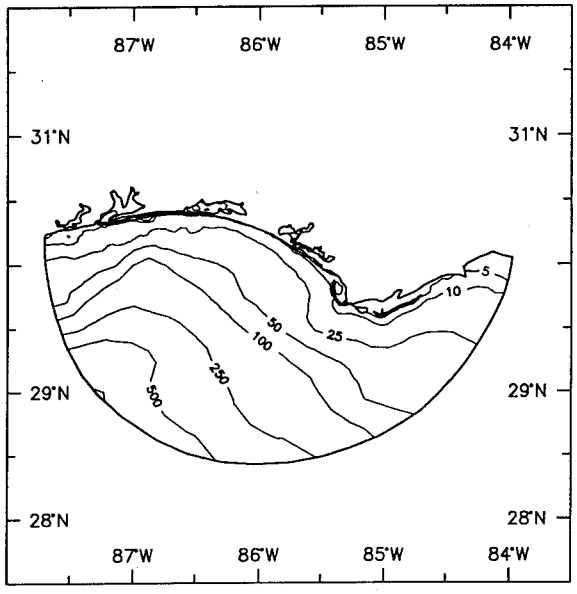

Figure 5. Bathymetry contours for the Florida coast domain

Discretization of the Florida coast domain, shown in Figure 6, is achieved using 1,451 nodes and 2,326 elements. The computational grid for the Florida coast domain is extremely detailed along the shoreline and has considerable refinement in the near coastal region resulting in a minimum node-to-node spacing of approximately 0.5 km (0.3 mile). Maximum node-to-node spacing of 32.5 km (20.2 statute miles) is found in the deeper regions of the Florida coast domain.

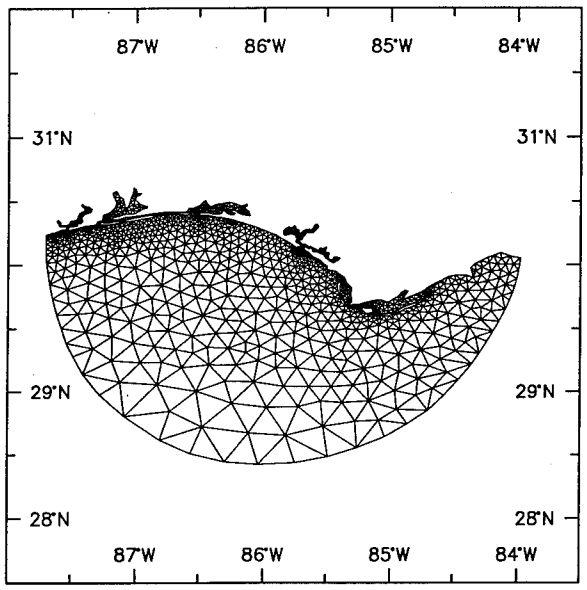

Figure 6. Florida coast domain discretization

The second domain considered, the Gulf of Mexico domain shown in Figure 4b, includes the entire Gulf of Mexico and is similar to domains used by several other investigators for storm surge modeling studies within the Gulf of Mexico (e.g. Bunpapong, Reid, and Whitaker 1985; Westerink et al. 1992a). The Gulf of Mexico domain is comprised of the Florida coast domain and all surrounding regions in the Gulf of Mexico. One open ocean boundary is located across the Strait of Florida (approximately from Cape Sable, Florida, to Havana, Cuba) and another is located across the Yucatan Channel (approximately from Cancun, Mexico, to Cabo San Antonio, Cuba). Bathymetry in the Gulf of Mexico domain, depicted in Figure 7, is again taken from the ETOPO5 database and in regions along the Florida coast and shelf it is supplemented by the NOAA Digital U.S. Coastal Hydrography sounding database. In the portions of the Gulf of Mexico domain which correspond to the Florida coast domain, the topography is identical to that specified for the Florida coast domain. The range of depths in the Gulf of Mexico domain vary between a minimum of 3 m (10 ft) and a maximum just under 3,800 m (12,500 ft).

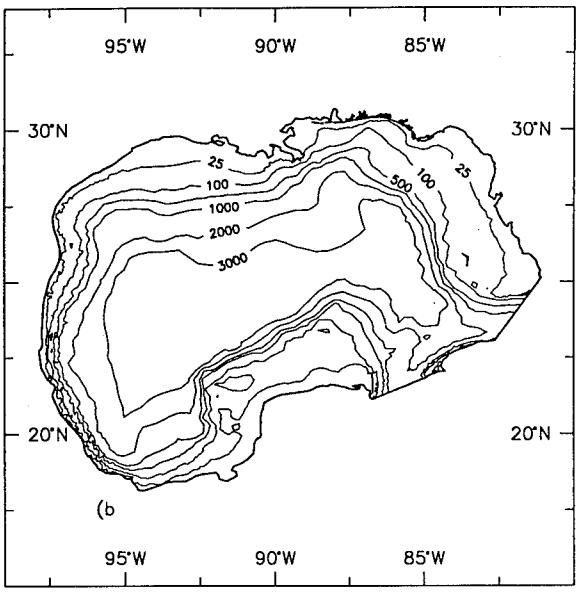

Figure 7. Bathymetry contours for the Gulf of Mexico domain

The discretization of the Gulf of Mexico domain is presented in Figure 8 and is comprised of 6,325 nodes and 11,441 elements. In the region encompassing the Florida coast domain, the discretization of the Gulf of Mexico domain is the same as that in the Florida coast domain. Nodal spacings within the Gulf of Mexico domain discretization range from a minimum of 0.5 km (0.3 statute miles) along the shoreline and in the coastal region of western Florida to a maximum of 50 km (31.1 statute miles) in the deepest waters of the Gulf of Mexico.

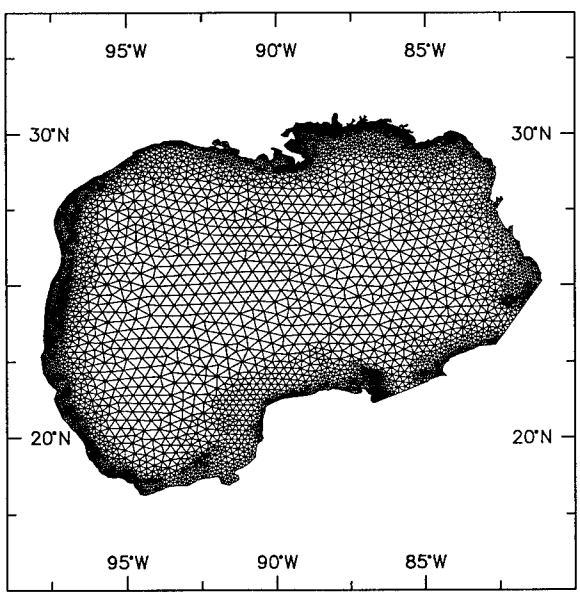

Figure 8. Gulf of Mexico domain discretization

The final and largest domain studied, shown in Figure 4c, is the east coast domain, which has been previously used by Westerink, Luettich, and Muccino (1994) to study tides in the western North Atlantic. The east coast domain encompasses the western North Atlantic Ocean, the Caribbean Sea, and the Gulf of Mexico and has been constructed such that both the Gulf of Mexico and Florida coast domains are contained within the east coast domain. A single deep Atlantic Ocean boundary within the east coast domain extends from Glace Bay, Nova Scotia, to the vicinity of Corocora Island in eastern Venezuela along the 60 °W meridian. All other boundaries are defined by the eastern coastlines of North, Central, and South America. Topography within the domain, depicted in Figure 9, includes the continental shelf, whose depths range from an imposed minimum between 3 m and 7 m (10 ft and 426 ft) to 130 m (426 ft) at the shelf break, the continental slope which has a typical depth range of 130 m to 3,000 m (426 ft to 9,800 ft), and the continental rise and deep ocean where depths increase upwards from 3,000 m to almost 8,000 m (9,800 ft to 26,000 ft). Depths within the Gulf of Mexico region are the same as those specified for the Gulf of Mexico domain.

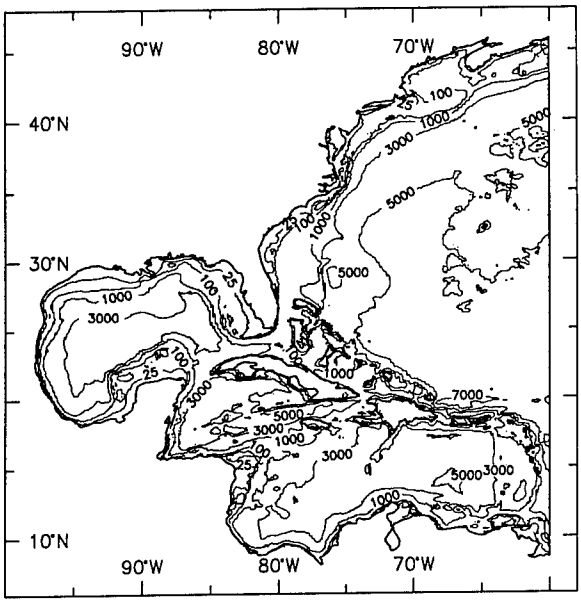

Figure 9. Bathymetry contours for the east coast domain

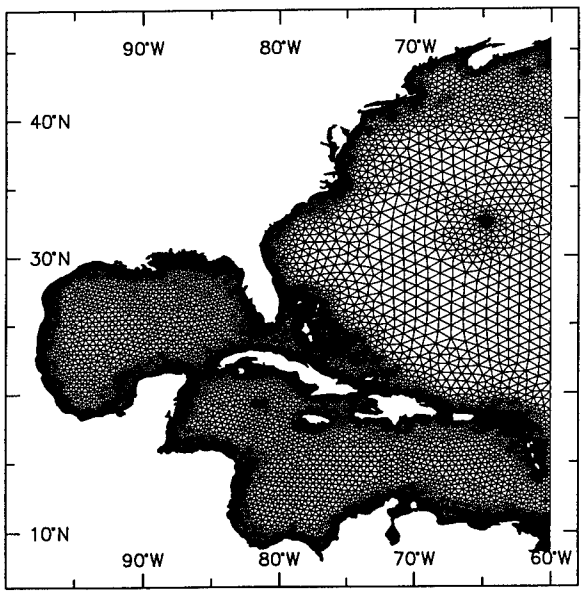

Figure 10. East coast domain discretization

Bathymetry in regions outside the Gulf of Mexico is obtained from the ETOP05 database.

The discretization of the east coast domain, shown in Figure 10, contains 22,711 nodes and 41,709 elements, reasonable numbers considering the level of refinement and the areal extent of the domain. The discretization of the Gulf of Mexico domain is exactly incorporated into the east coast domain discretization. The inclusion of deep Atlantic ocean regions within the east coast domain extends the range of grid spacings contained within the east coast domain discretization. Minimum node-to-node spacing is approximately 0.5 km (0.3 statute miles) along the Florida shoreline, while in the deep Atlantic Ocean, spacing increases to about 98 km (60.1 miles) or approximately 1.4 °. A large computational domain such as the east coast domain is manageable because of an optimal gridding strategy and the flexibility inherent in the finite element method.

Comparison of Storm Surge Predictions Using Three Domain Sizes

Simulations were conducted to investigate the influence of domain size and boundary condition specification on the storm surge and resonant mode generation associated with Hurricane Kate. Domain size is considered using the three previously described domains. Boundary condition specification is examined

by comparing a still-water boundary condition where water elevation is set equal to mean sea level with a boundary condition that partially accounts for meteorological forcing at the open ocean boundary by imposing an inverted barometer effect. An inverted barometer $p_s/\rho_0 g$ is simply the height to which seawater will rise due to pure static pressure forcing. For this series of simulations, wind stress and pressure forcing from Hurricane Kate are applied at the boundary and on the interior of the domain, while tidal forcing is neglected both on the interior and at the open ocean boundaries.

Model parameters are identical for all simulations so that results for different domains using each boundary condition can be compared. The convective and finite amplitude terms are not included in the governing equations for these simulations due to instabilities caused by near drying elements. Consequently, the only nonlinear term included in the governing equations is bottom friction. The bottom friction coefficient is constant and equal to 0.003 over all domains. The GWCE parameter τ_0, which represents the balance between the primitive continuity and wave equation portion of the GWCE, is defined equal to 0.001 (Kolar et al. 1994b).

Simulations are spun up from homogeneous initial conditions using a 1-day ramp in time. Application of the hyperbolic ramp function reduces the excitation of nonphysical short wavelength frequencies. An identical ramp function of 1 day is applied to the wind and pressure forcing as well as the inverted barometer boundary condition when used. Actual simulations began at 12:00 GMT 15 November 1985 and ran over 8.25 days (including a 1-day ramp-up period). During the first 6 hr of the simulation, the initial hurricane wind and pressure forcings were held stationary. Thereafter, storm surge computations used the time-varying wind and pressure fields. A time-step of 45 sec is used throughout the simulation period. No calibration or tuning of parameters is performed in either the weather model or in the hydrodynamic model.

As part of this domain size study, 118 elevation stations were placed throughout the three domains. Ten elevation stations were concentrated on the Florida coast extending from St. Marks, Florida, to the Mississippi Sound. Other stations were placed along the Gulf of Mexico coastline, at the open ocean boundaries of each domain, and on tracks parallel to the path of Hurricane Kate. Samplings of these elevation stations are shown in Figures 11 and 12.

Storm surge response at nine of the stations along the Florida coast (St. Marks, Shell Point, Turkey Point, Carrabelle, Apalachicola, Panama City, Alligator Bayou, Destin, and Pensacola) and Station T6.3 on the continental shelf, is shown in Figures 13-22. The computed storm surge hydrographs in Figures 13a-22a were obtained using a still-water boundary condition and in Figures 13b-22b using an inverted barometer boundary condition. The storm surge profiles at St. Marks, Shell Point, Turkey Point, Carrabelle, and Apalachicola (Figures 13-17) are representative of conditions on the right-hand side of the hurricane. Storm surge elevations at Alligator Bayou, Destin, and

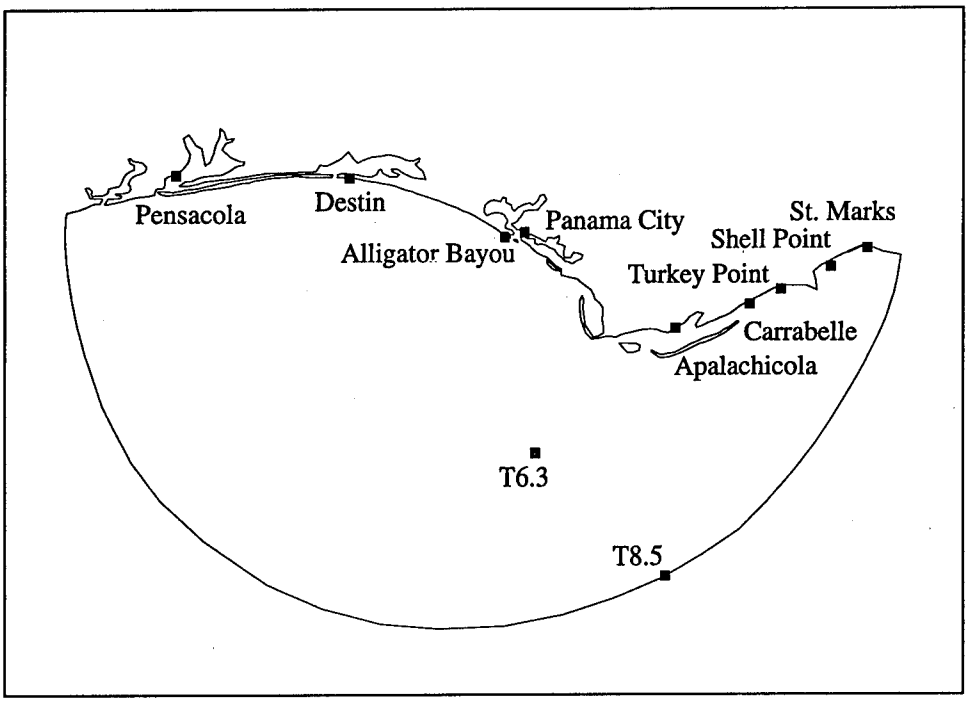

Figure 11. Elevation station locations along the Florida coast and on the continental shelf with respect to the Florida coast domain

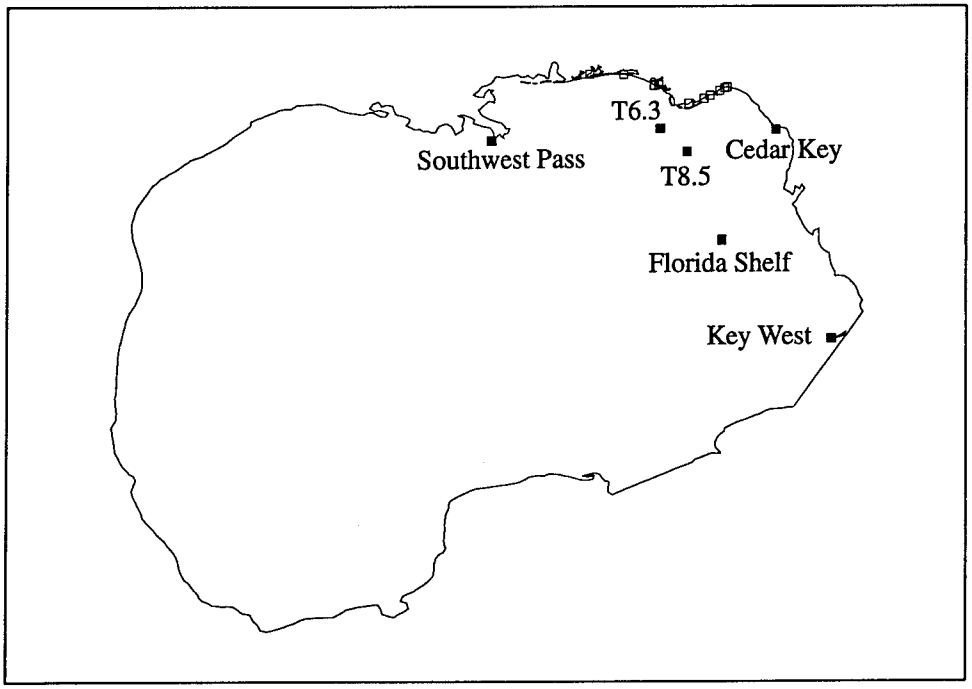

Figure 12. Additional elevation stations located within the Gulf of Mexico domain

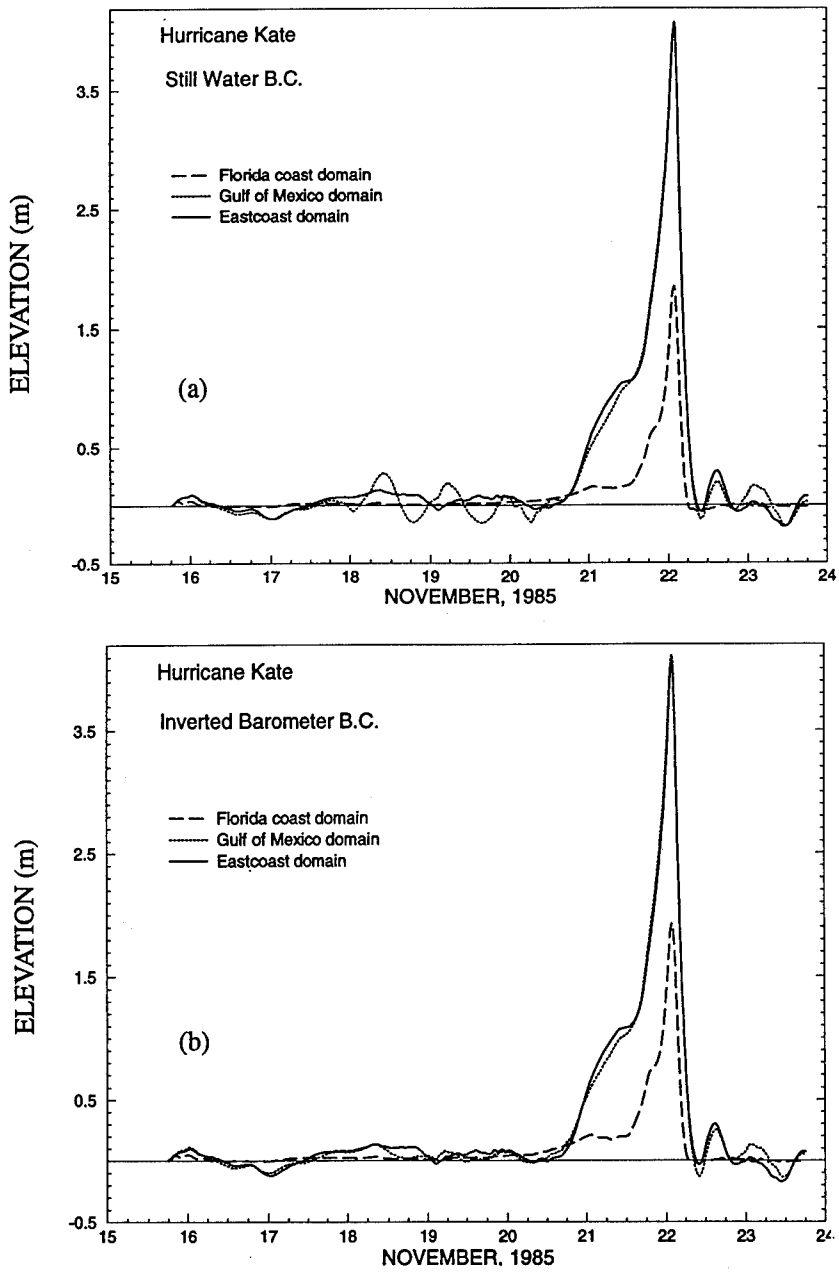

Figure 13. Computed storm surge from Hurricane Kate using (a) a still-water boundary condition, and (b) an inverted barometer boundary condition at St. Marks, FL

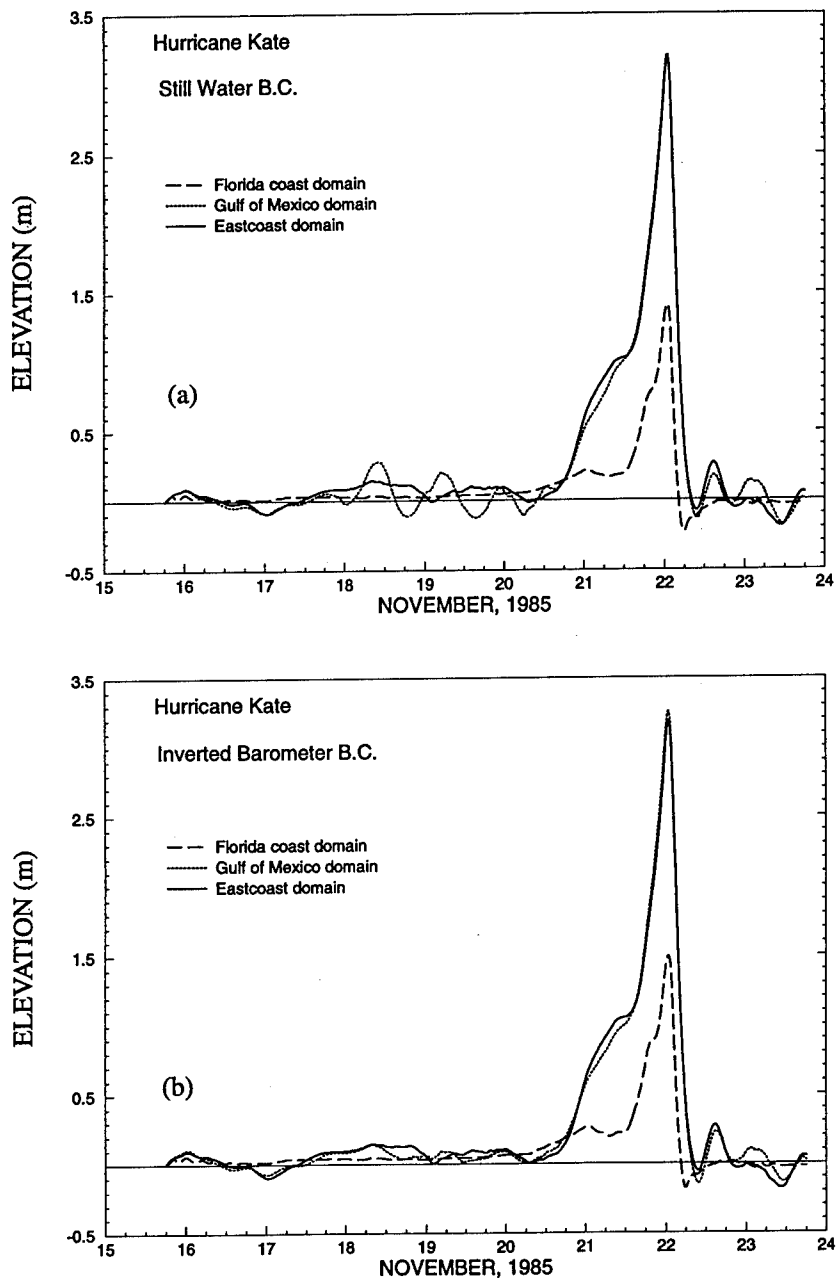

Figure 14. Computed storm surge from Hurricane Kate using (a) a still-water boundary condition, and (b) an inverted barometer boundary condition at Shell Point, FL

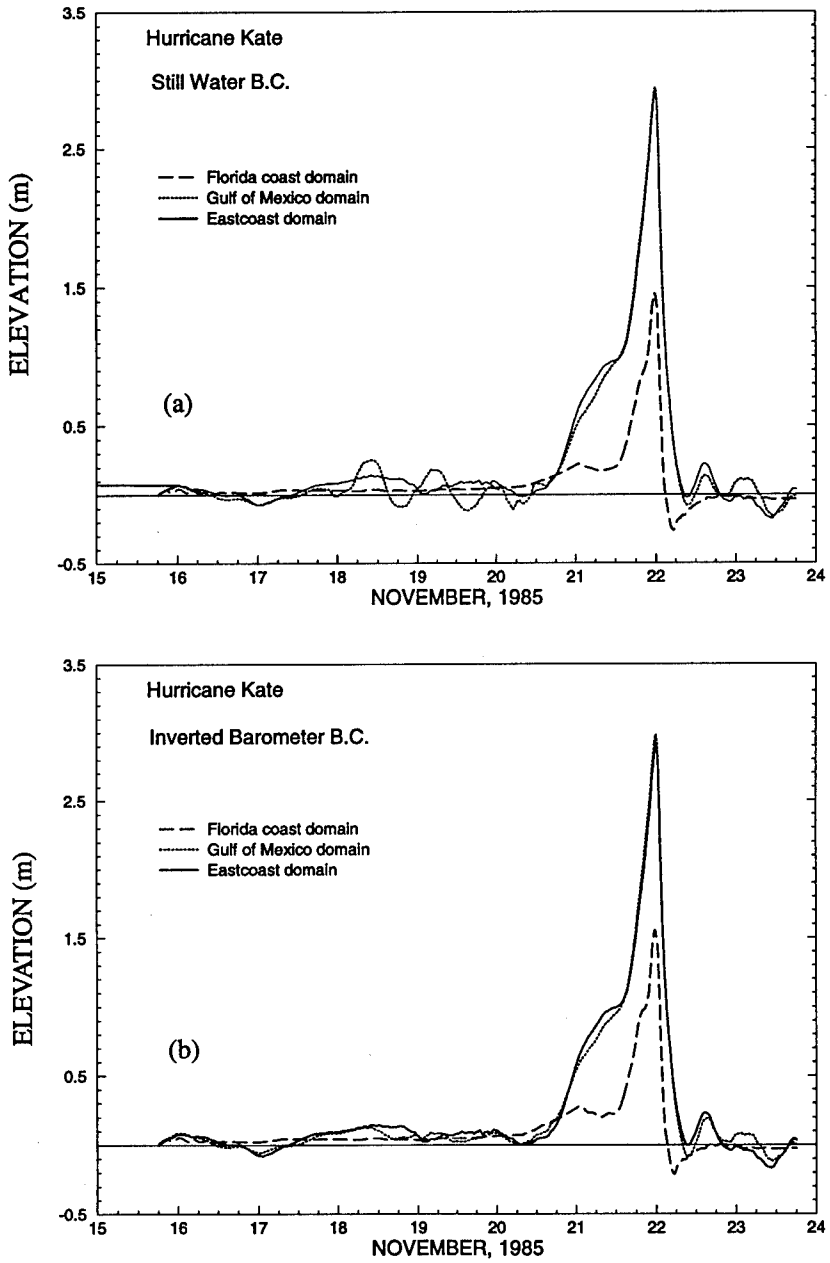

Figure 15. Computed storm surge from Hurricane Kate using (a) a still-water boundary condition, and (b) an inverted barometer boundary condition at Turkey Point, FL

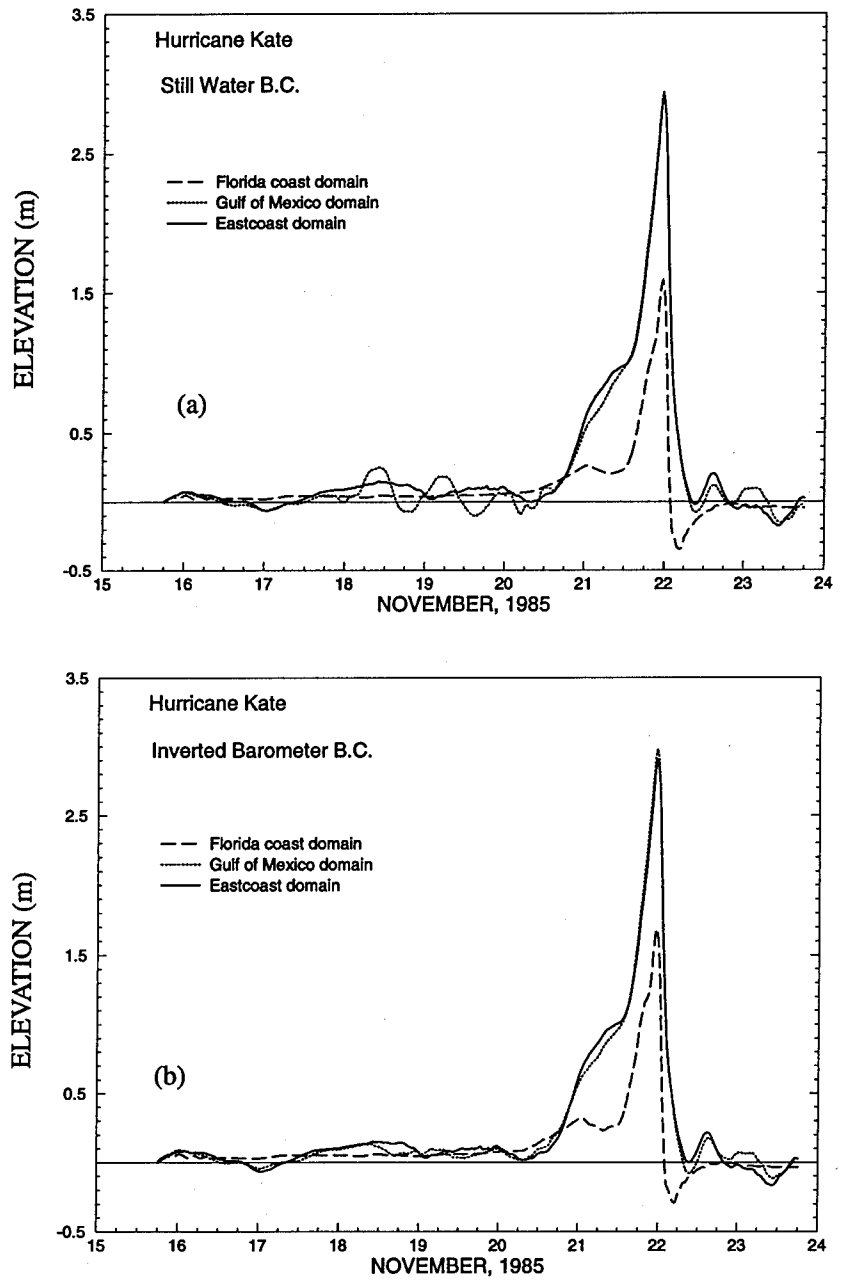

Figure 16. Computed storm surge from Hurricane Kate using (a) a still-water boundary condition, and (b) an inverted barometer boundary condition at Carrabelle, FL

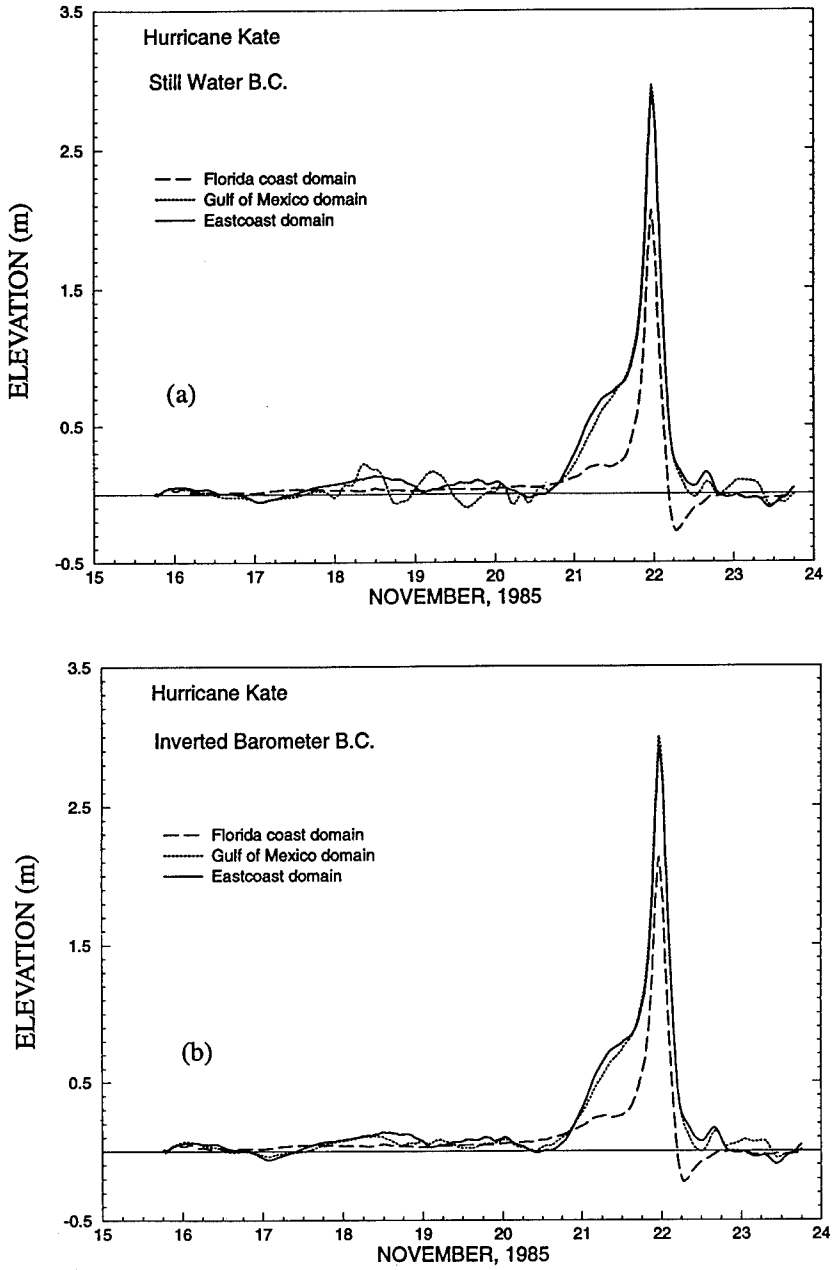

Figure 17. Computed storm surge from Hurricane Kate using (a) a still-water boundary condition, and (b) an inverted barometer boundary condition at Apalachicola, FL

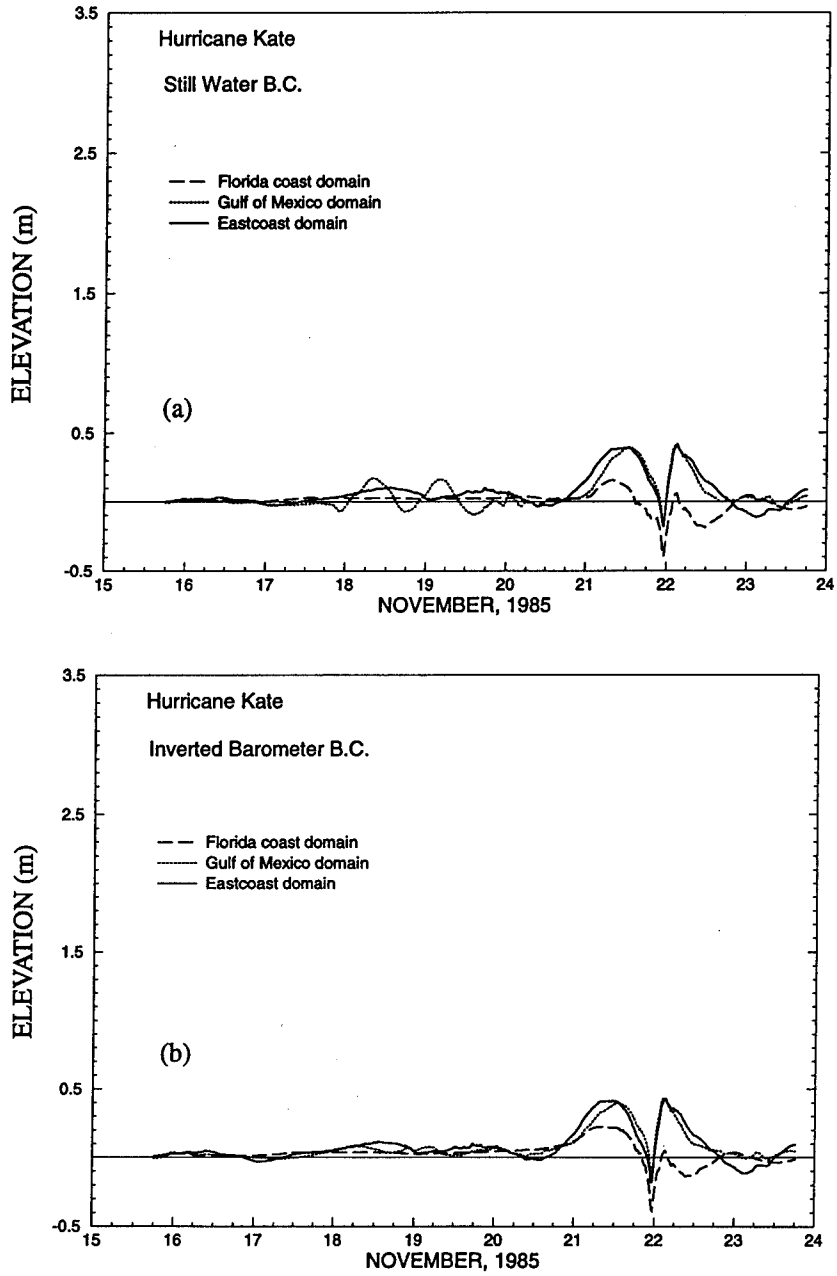

Figure 18. Computed storm surge from Hurricane Kate using (a) a still-water boundary condition, and (b) an inverted barometer boundary condition at Panama City, FL

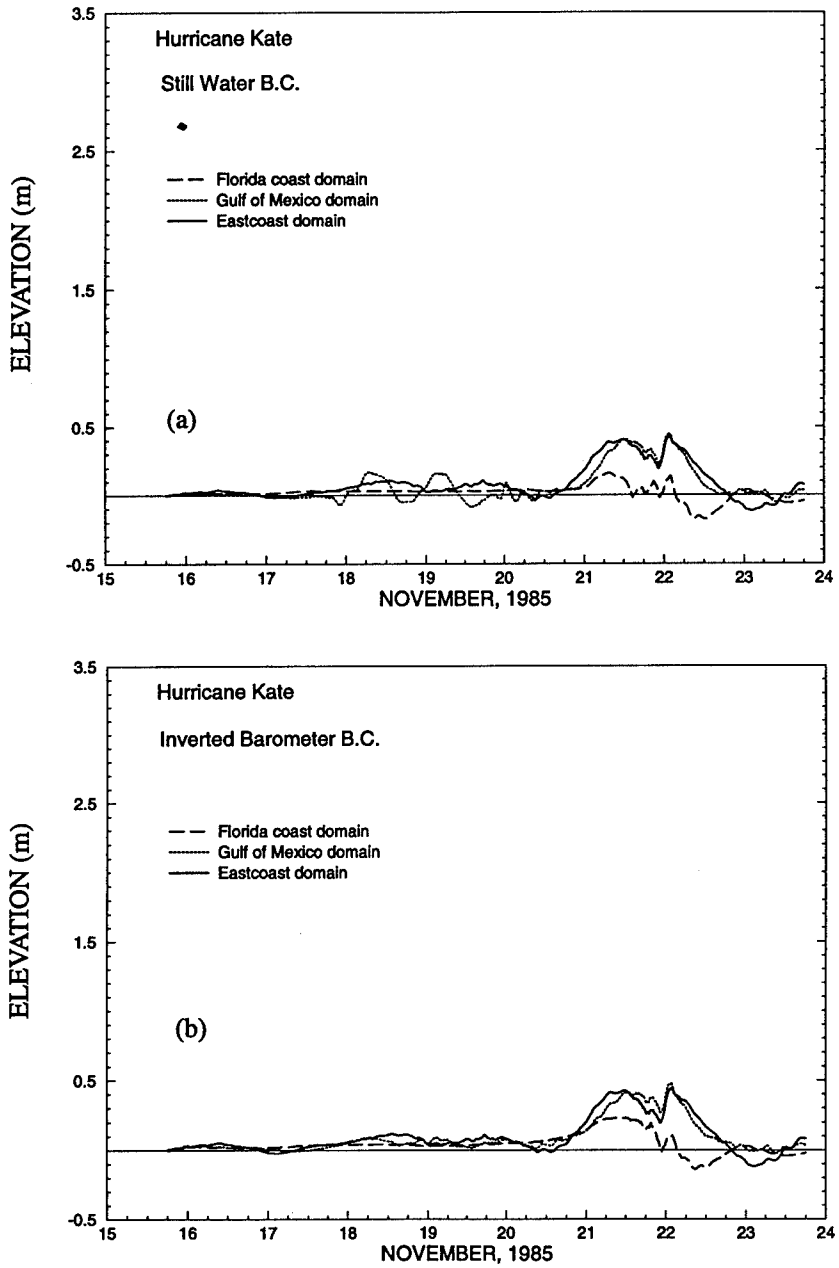

Figure 19. Computed storm surge from Hurricane Kate using (a) a still-water boundary condition, and (b) an inverted barometer boundary condition at Alligator Bayou, FL

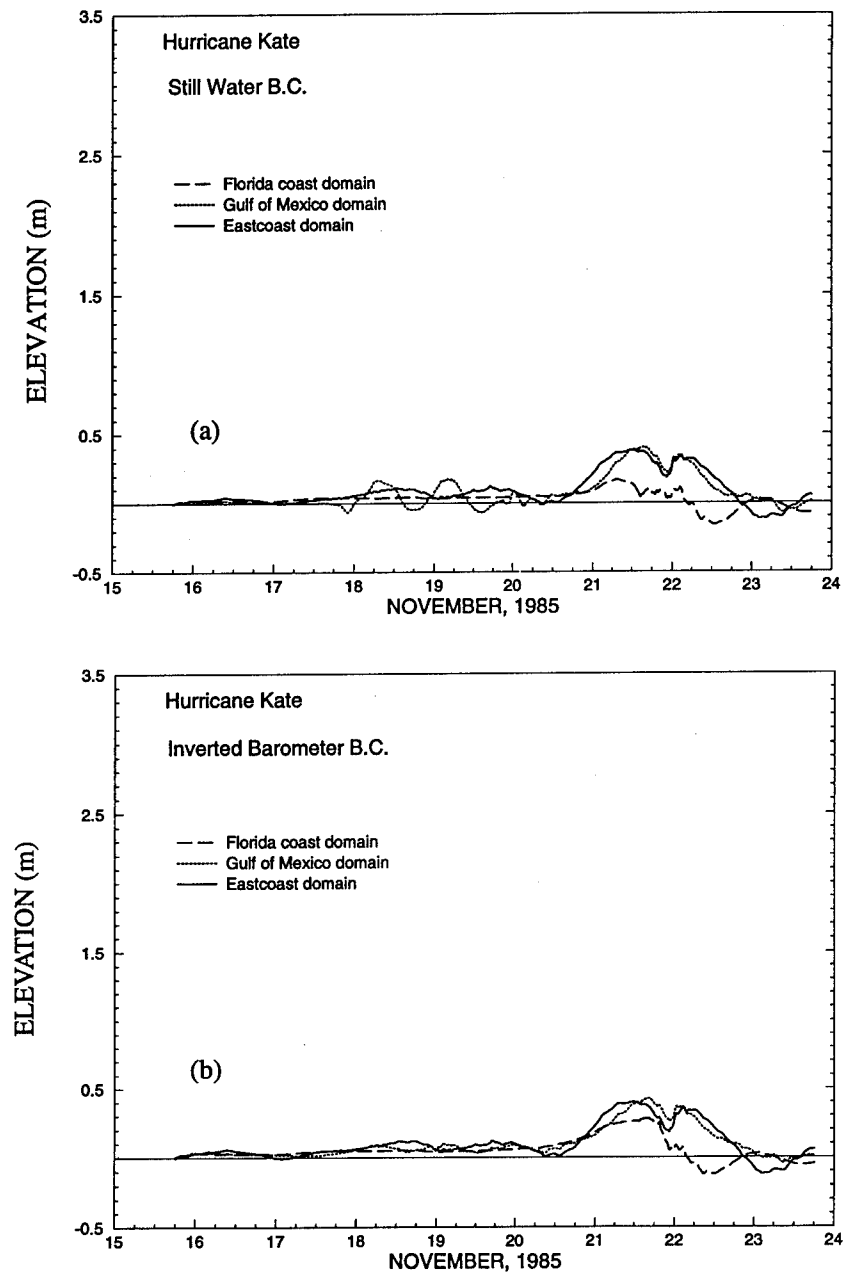

Figure 20. Computed storm surge from Hurricane Kate using (a) a still-water boundary condition, and (b) an inverted barometer boundary condition at Destin, FL

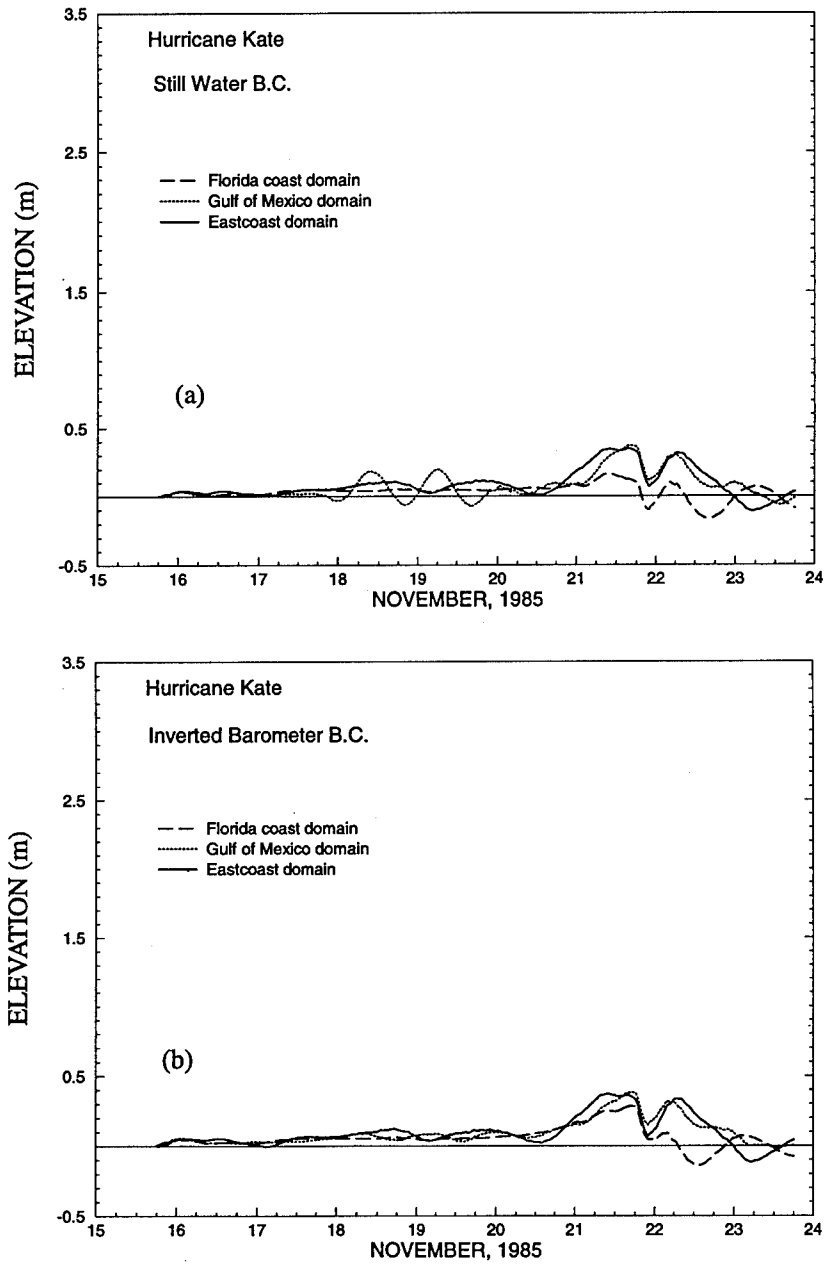

Figure 21. Computed storm surge from Hurricane Kate using (a) a still-water boundary condition, and (b) an inverted barometer boundary condition at Pensacola, FL

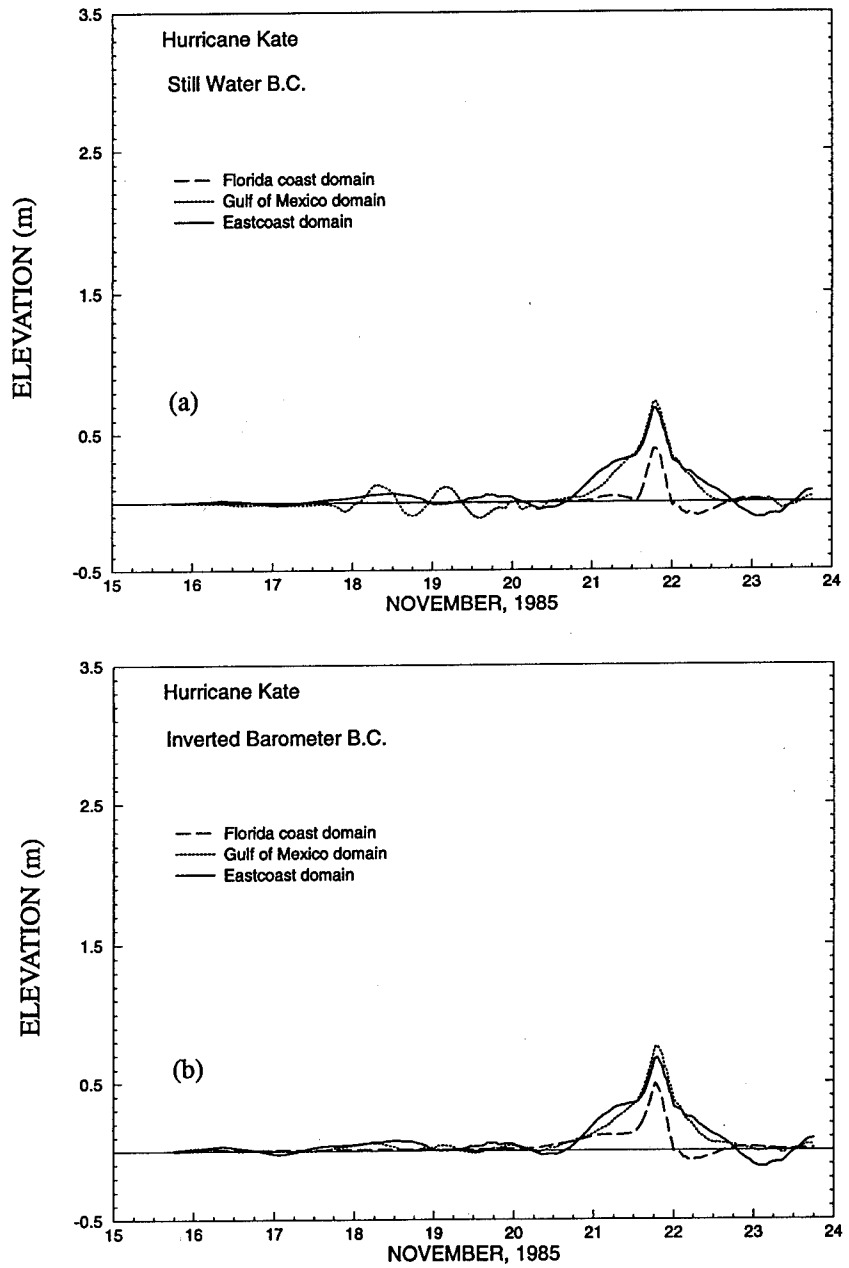

Figure 22. Computed storm surge from Hurricane Kate using (a) a still-water boundary condition, and (b) an inverted barometer boundary condition at Station T6.3

Pensacola (Figures 19-21) exhibit behavior characteristic of the left-hand side of the hurricane. The Panama City storm surge hydrograph (Figure 18) depicts water elevations at the point of landfall of Hurricane Kate. A representative storm surge profile on the shelf is shown in Figure 22 for Station T6.3 located on the continental shelf approximately 15 km from the shelf break at a depth of nearly 130 m.

In all of the storm surge hydrographs in Figures 13-22, the peak surge for the Gulf of Mexico and east coast domains closely correspond, whereas the elevation response computed over the Florida coast domain is significantly smaller, particularly on the right-hand side of the hurricane. For a given boundary condition specification, similar oscillatory patterns or modes are excited in the storm surge response at all 10 stations shown in Figures 13-22. However, in comparing the computed storm surge response between the east coast and Gulf of Mexico domains, different oscillatory behavior is evident. For the Gulf of Mexico domain, resonant modes are more pronounced when a still-water boundary condition is used (Figures 13a-22a) than when the inverted barometer boundary condition is implemented (Figures 13b-22b). The modes in the east coast domain solution in Figures 13-22 exhibit no sensitivity to boundary condition specification. Since all domains have identical discretizations over corresponding regions, and simulations were conducted using identical model parameters and wind and pressure forcing, differences between the model responses are due solely to the domain size and/or the boundary condition specification.

To investigate the origin of differences in the storm surge response over the three domains, elevation contours showing the progression of Hurricane Kate through the Gulf of Mexico toward Panama City, Florida, are shown in Figure 23 for successive time periods. At 20:00 GMT 20 November 1985 (Figure 23a), a widespread inverted barometer centered at the hurricane eye is evident. Already water is accumulating and elevation is increasing in the northeastern Gulf of Mexico, especially on the northeast Florida shelf. Ten hours later at 6:00 GMT 21 November 1985 (Figure 23b), as the eye of the hurricane approaches the Florida shelf, the inverted barometer effect has diminished and its structure is deteriorating. High water elevations on the shelf, particularly in shallow coastal areas, indicate that hurricane winds have pushed water up on the continental shelf. The last snapshot, shown in Figure 23c, is taken 8 hr prior to landfall of the hurricane at 18:00 GMT 21 November 1985. Hurricane Kate is now on the continental shelf and the surface elevation response no longer exhibits any inverted barometer structure. Water continues to pile up on the shelf in a pronounced way on the right-hand side of the hurricane.

The Florida coast domain is located almost entirely within the region of intense storm surge generation shown in Figure 23. In particular, the cross-shelf boundaries of the Florida coast domain are located in an area of significant surge where hurricane winds have driven water up onto the shelf. Even an inverted barometer forcing specified at these cross-shelf boundaries significantly underestimates the storm surge elevations that physically occur at these

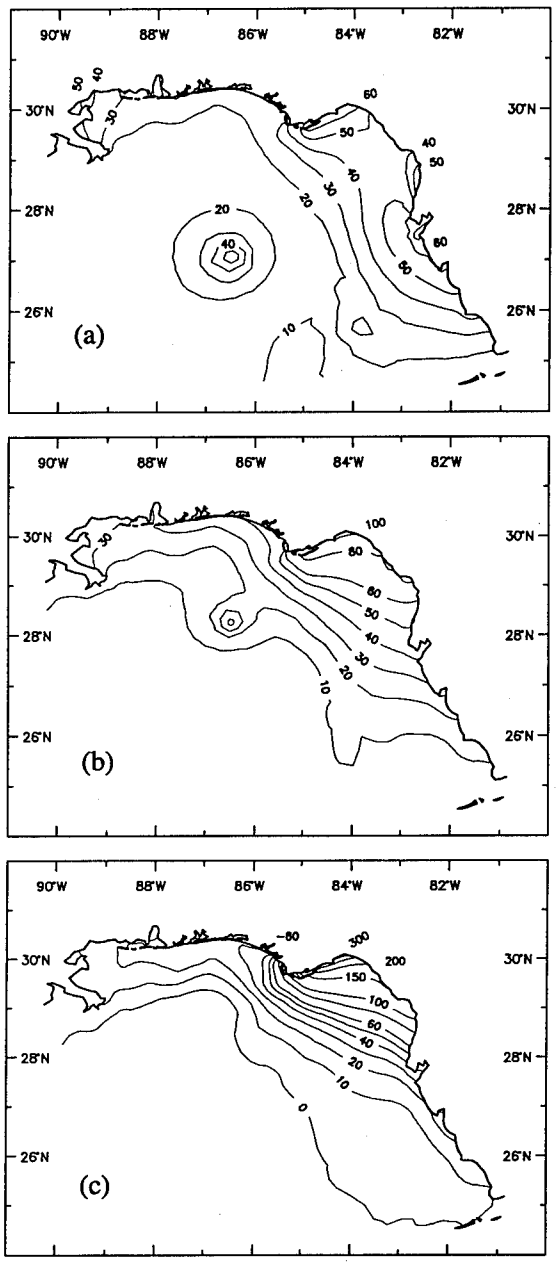

Figure 23. Storm surge elevations (in cm) in the northeast Gulf of Mexico due to Hurricane Kate on (a) 20:00 GMT 20 November 1985, (b) 6:00 GMT 21 November 1985, and (c) 18:00 GMT 21 November 1985

boundaries and are represented using the Gulf of Mexico and east coast domains. The storm surge hydrograph at Station T8.5 (Figure 24), which is located at the cross-shelf boundary of the Florida coast domain at a depth of approximately 80 m (262 ft), clearly demonstrates the inadequacy of the inverted barometer specified at these boundaries. The inverted barometer elevations are significantly less than storm surge elevations computed over the east coast and Gulf of Mexico domains at the same point. Since the storm surge generated on the shelf by hurricane winds is not known a priori, an appropriate elevation boundary condition cannot be specified at cross-shelf boundaries. Furthermore, these cross-shelf boundaries comprise nearly the entire open-ocean boundary of the small shelf domain. Consequently, a domain such as the Florida coast domain, which is small in size relative to the spatial scale of a hurricane and is located primarily on the continental shelf, cannot be used to obtain an accurate and physically relevant storm surge response.

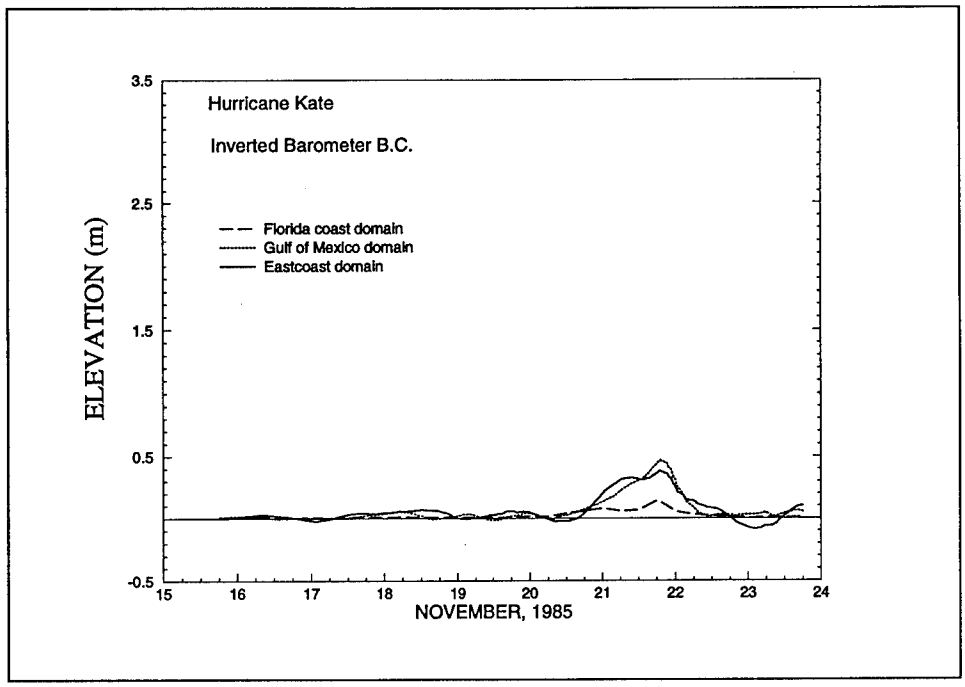

Figure 24. Computed storm surge from Hurricane Kate using an inverted barometer boundary condition at Station T8.5

The oscillatory behavior of the storm surge elevations or surge forerunner effect computed over the east coast and Gulf of Mexico domains exhibited in Figures 13-22 can be attributed to basin-wide resonant modes which exist in the Gulf of Mexico as documented by Platzman (1972); Reid and Whitaker (1981); and Bunpapong, Reid, and Whitaker (1985). These modes are not excited in the Florida coast domain due to the small size of the domain and the omission of the shelf from adjacent basin interaction in the specified boundary forcing. On the contrary, resonant modes are excited in the Gulf of Mexico domain. In fact, open boundary elevations specified at entrances to the Gulf of

Mexico significantly influence the setup of resonant modes in the Gulf. This is demonstrated in Figures 13-22 for the Gulf of Mexico domain, where oscillations in storm surge elevation are more pronounced when using a still-water boundary condition (Figures 13a-22a) as opposed to an inverted barometer boundary condition (Figures 13b-22b). Platzman (1972) and Reid and Whitaker (1981) also found that the frequency of modes in the Gulf of Mexico varied with the application of different boundary conditions. One concludes, then, that the resonant modes in the Gulf of Mexico may be difficult to model with the Gulf of Mexico domain due to the sensitivity of these modes to boundary condition specification and the associated shortcomings in the representation of basin-to-basin dynamics.

A comparison of water level response at all coastal stations using two different elevation conditions along the east coast domain open-ocean boundary (e.g. Figure 25 at Apalachicola, Florida) clearly demonstrates that the influence of boundary condition specification is minimized when using the east coast domain. This insensitivity to the specification of boundary conditions in the deep Atlantic as well as the fact that basin-to-basin interactions are more faithfully represented suggests that the flow physics at this boundary need not be precisely known and resonant modes in the Gulf of Mexico are properly set up in the east coast domain.

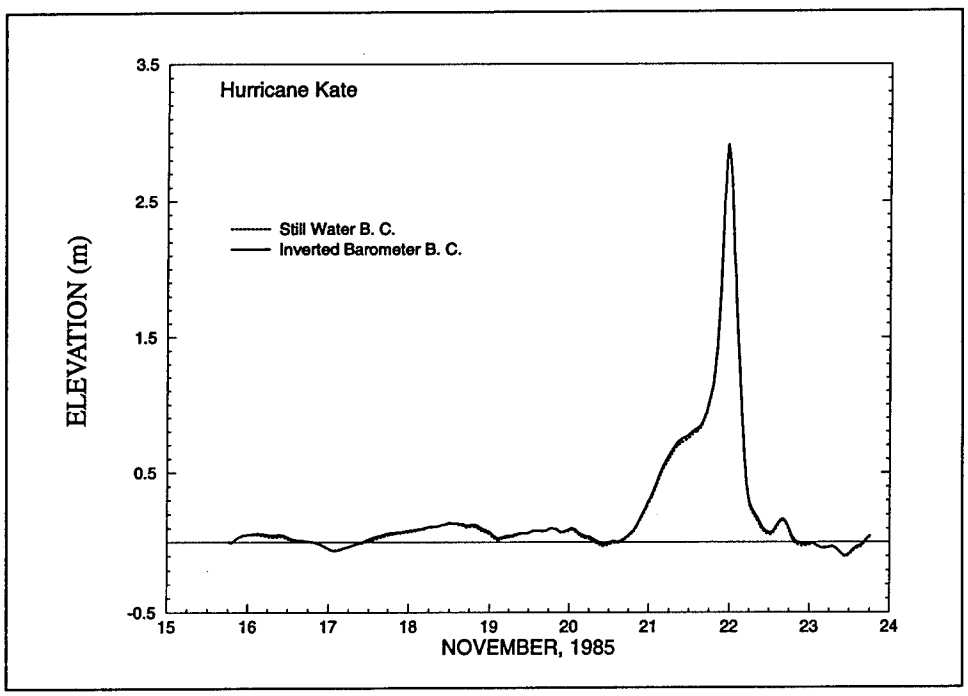

Figure 25. Comparison of storm surge computed over the east coast domain using both still-water boundary condition and an inverted barometer boundary condition at Apalachicola, FL

Thus, when using the east coast domain, hurricanes progress through the domain in a realistic fashion causing water to properly accumulate on the

continental shelf for the following three reasons: (a) factors affecting storm surge generation are more fully incorporated (i.e., bathymetry, shelf to adjacent basin interaction, basin- to-basin interaction), (b) resonant modes are more realistically excited without relying on the incorporation of this information into the boundary conditions, and (c) the influence of the boundary condition specification is generally minimized. This initial series of simulations clearly indicates that the east coast domain is optimal for both the representation of accurate primary storm surge and surge forerunner effects.

Comparison Between Observed and Computed Storm Surge Elevations Over the East Coast Domain

Uncalibrated, computed storm surge profiles at several elevation stations are now compared to measured storm surge data for verification of the model results. As a consequence of the analysis in the previous section, the east coast domain is utilized for this storm surge simulation. As in prior simulations, wind stress and pressure forcing from Hurricane Kate are applied throughout the domain. In addition, tidal potential forcing using five tidal constituents, K_1, O_1, P_1, M_2, and S_2, is specified on the interior of the domain. Table 3 details the frequencies, nodal factors, equilibrium arguments, and Earth elasticity factors used for each tidal constituent. The values of these tidal parameters are defined with reference to 0:00 GMT 19 November 1985. Along the open-ocean boundary, an inverted barometer boundary condition is applied in combination with tidal elevation forcing. The same five constituents, K_1, O_1, P_1, M_2, and S_2, are forced along the boundary with elevations obtained from the results of Schwiderski's global model (Schwiderski 1979, 1981a-d). However, the amplitude of the M_2 tide on the open-ocean boundary, as computed by Schwiderski, is reduced by 10 percent, a correction in accordance with the error analysis of tidal model computations over the western North Atlantic Ocean by Westerink, Luettich, and Muccino (1994a).

Table 3
Tidal Potential Constants Used for Storm Surge Simulations

Constituent	Period (hrs)	Potential Amplitude (m)	Earth Tide Reduction Factor	Nodal Factor	Equilibrium Argument (degrees)
K_1 luni-solar	23.934470	0.141565	0.736	1.086	321.3
O_1 principal lunar	25.819342	0.100514	0.695	1.140	271.35
P_1 principal solar	24.065890	0.046843	0.706	1.000	33.00
M_2 principal lunar	12.420601	0.242334	0.693	0.974	230.34
S_2 principal solar	12.000000	0.112841	0.693	1.000	0.00

Simulations used for verification of the computed storm surge predictions are conducted using a fully nonlinear model formulation with the exception of the finite amplitude terms. These terms are not included in the simulations because of instabilities caused by near drying elements in coastal areas. All other model parameters such as the bottom friction coefficient, the GWCE parameter, and the time-step remain as specified for the domain comparison simulations detailed in the previous section. Again, all parameters in both the hydrodynamic and wind models remain uncalibrated.

Verification of the tidal responses throughout the east coast domain is undertaken prior to simulation of the storm surge. Tides are computed for 45 days with a ramp-up period of 12 days. Tidal elevations are recorded after 30 days of computation to ensure dissipation of free modes within the Gulf of Mexico and Caribbean Sea as suggested by Westerink, Luettich, and Muccino (1994). At 77 stations placed throughout the east coast domain, computed tidal elevations are compared to measured water levels obtained at these same stations. Details regarding the location of all 77 stations and the source of measured tidal data are found in Westerink, Luettich, and Muccino (1994). Results are presented for a sampling of six tidal stations whose locations are given in Figures 11 and 12 (i.e., Key West, Cedar Key, St. Marks, Alligator Bayou, Southwest Pass, and the outer Florida shelf station). Tidal predictions shown in Figures 26-31 agree well with the measured data. The slight downward adjustment of the M_2 amplitude specified on the open-ocean boundary produces significantly improved tidal elevations at all stations as compared to those computed by Westerink, Luettich, and Muccino (1994).

Storm surge simulations are spun up from homogeneous initial conditions using a 1-day hyperbolic ramp in time. Actual simulations begin at 0:00 GMT 10 October 1985 and run a total of 45 days. During the first 36.75 days of simulation (including the 1-day ramp-up period), tidal forcing alone is applied before the hurricane enters the domain. After this period of pure tidal forcing, initial hurricane wind and pressure forcings are held stationary for a 6-hr ramp-up period. Thereafter, storm surge computations use the time-varying wind and pressure forcings and proceed for 8 days ending at 18:00 GMT 23 November 1985. Storm surge elevations are recorded every 3.75 min at eight elevation stations (shown in Figure 11) located along the Florida coastline where measured storm surge heights are also available.

Storm surge hydrographs, shown in Figures 32-39, compare computed numerical storm surge elevations with the measured water levels during Hurricane Kate. Conditions on the right-hand side of the hurricane, given by the computed storm surge profiles in Figures 32-36, correspond reasonably well to measured storm surge elevations. Deviations from the observed water levels include a premature and overpredicted peak surge and slight underprediction following the storm passage. At stations located at or left of the hurricane landfall position (Figures 37-39), computed storm surge hydrographs exhibit an enhanced and slightly elevated tidal cycle while actual elevations show a more pronounced surge which extends over about 1.5 days.

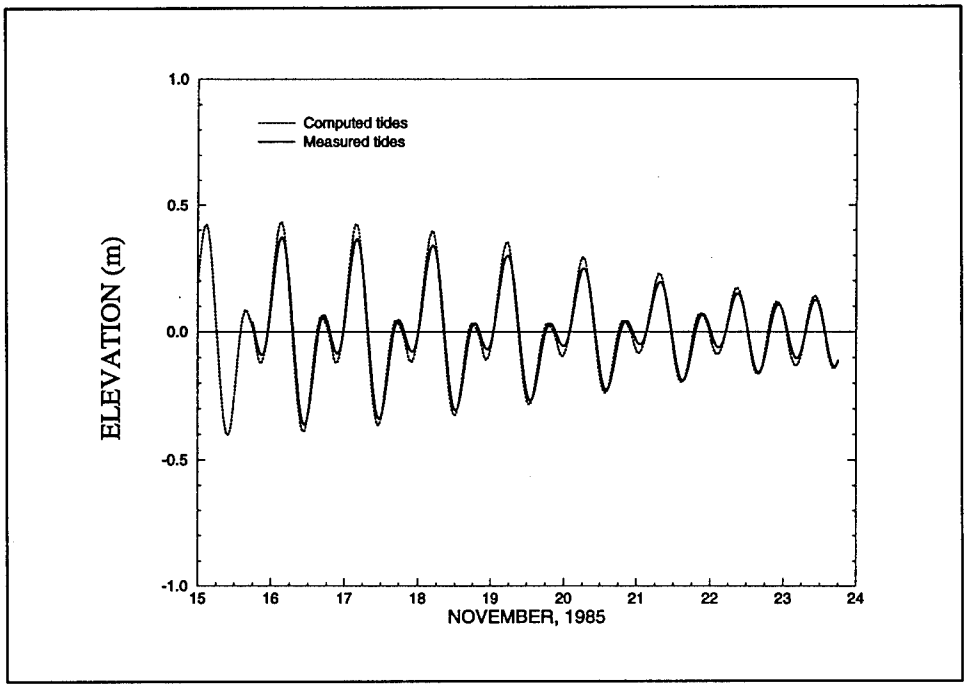

Figure 26. Comparison of computed and measured tidal elevations over the east coast domain at Key West, FL

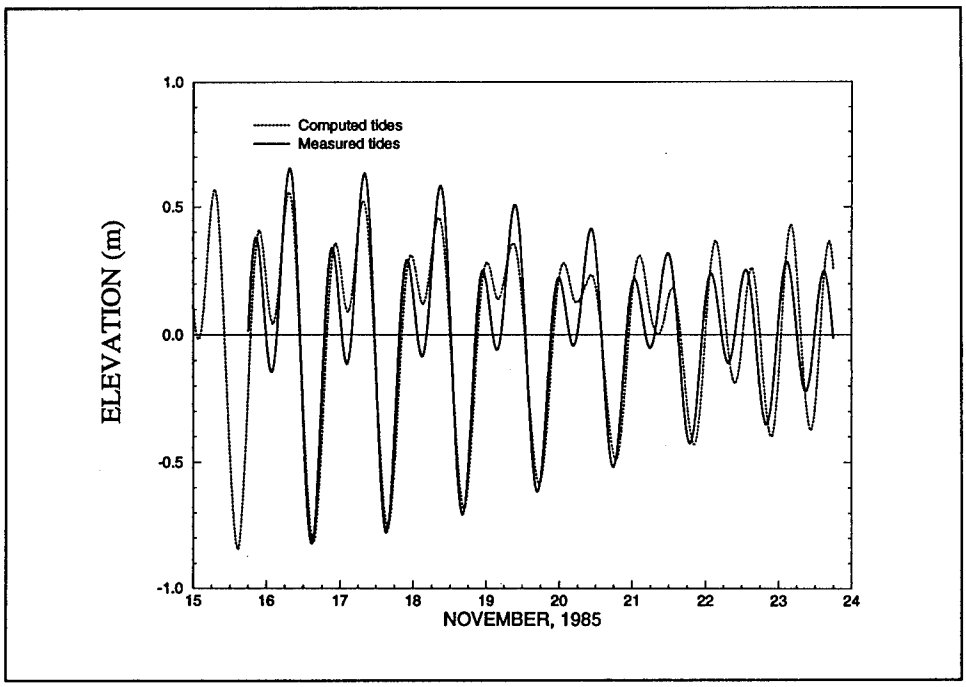

Figure 27. Comparison of computed and measured tidal elevations over the east coast domain at Cedar Key, FL

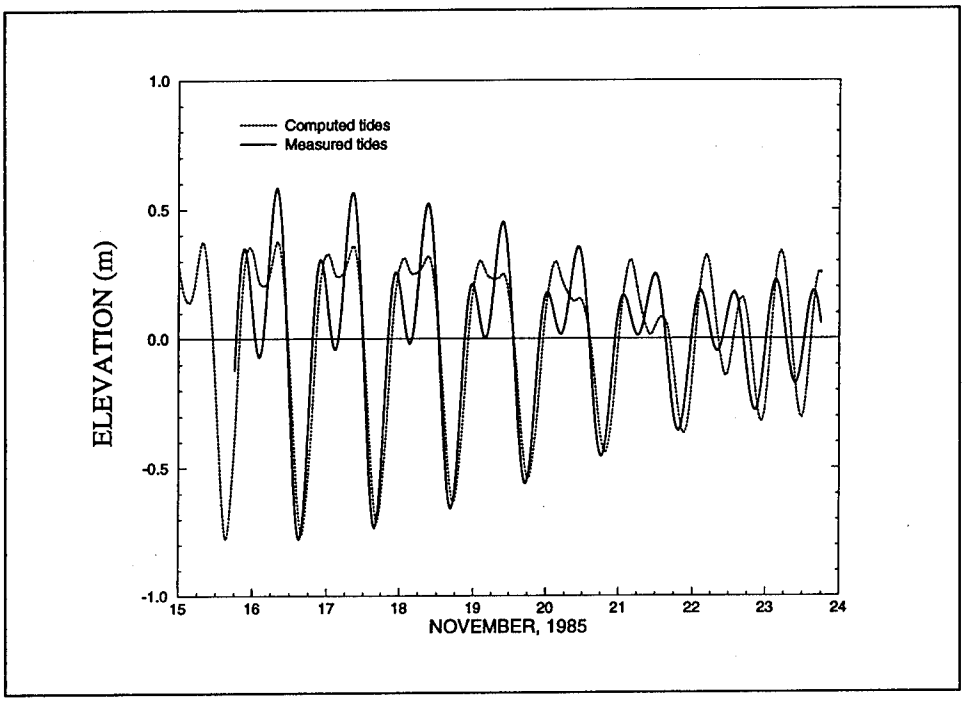

Figure 28. Comparison of computed and measured tidal elevations over the east coast domain at St. Marks, FL

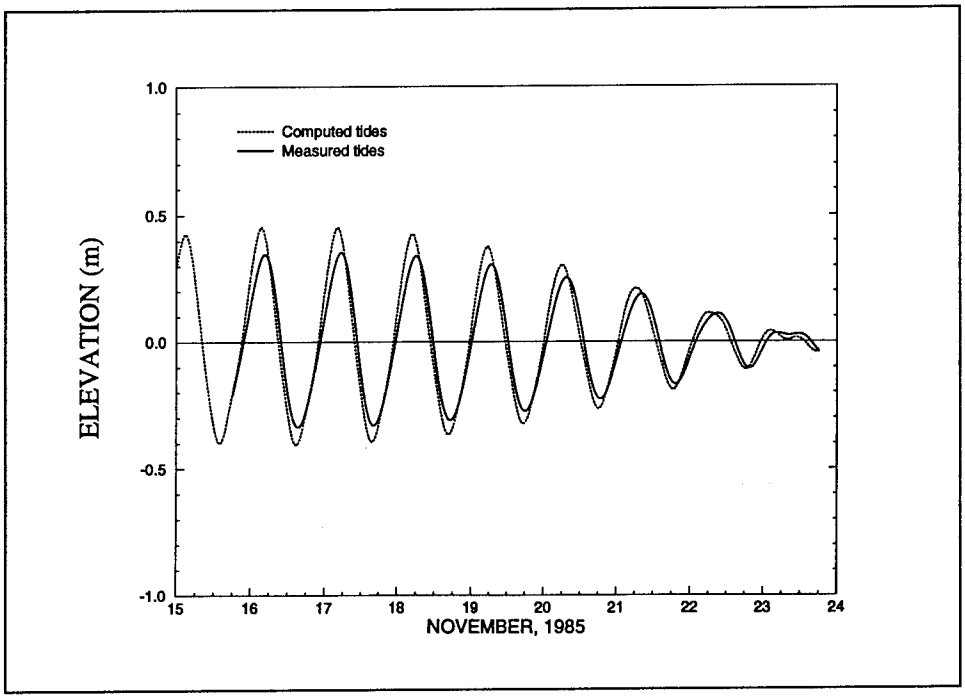

Figure 29. Comparison of computed and measured tidal elevations over the east coast domain at Alligator Bayou, FL

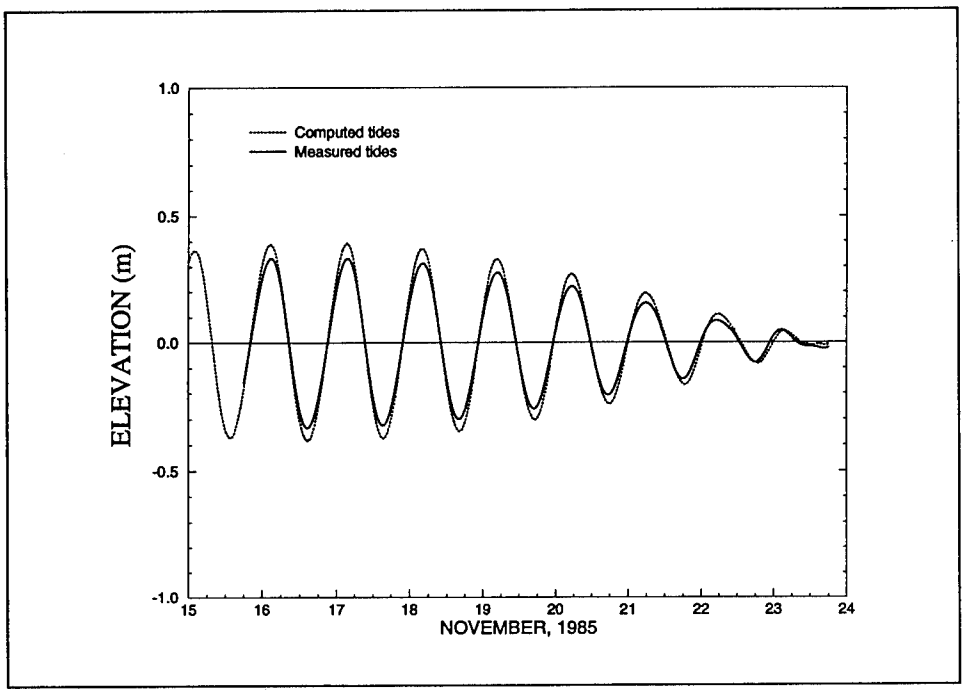

Figure 30. Comparison of computed and measured tidal elevations over the east coast domain at Southwest Pass, LA

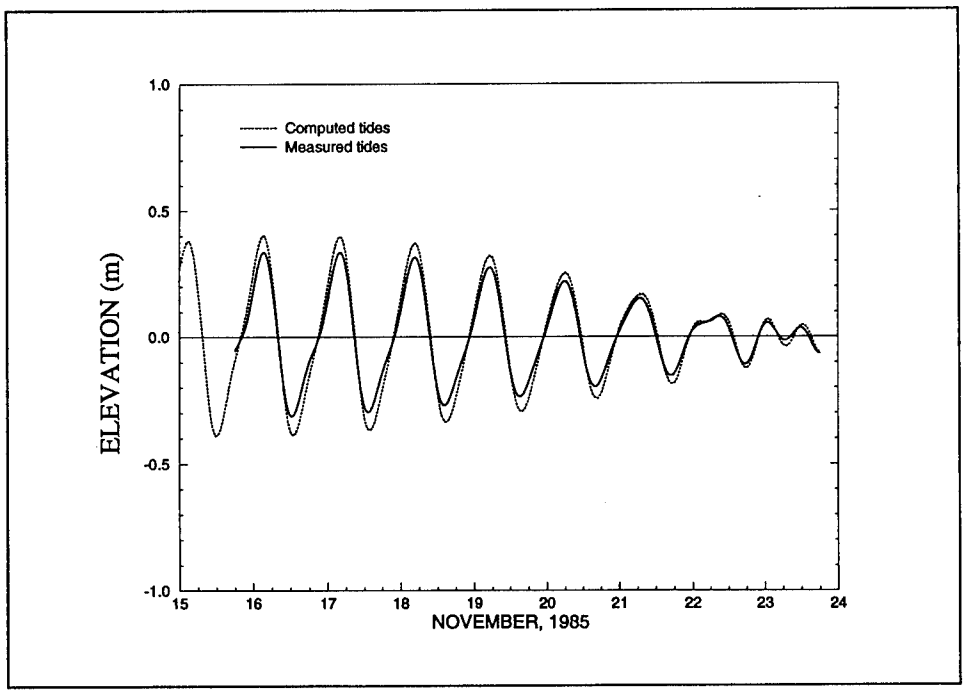

Figure 31. Comparison of computed and measured tidal elevations over the east coast domain at the outer Florida shelf station

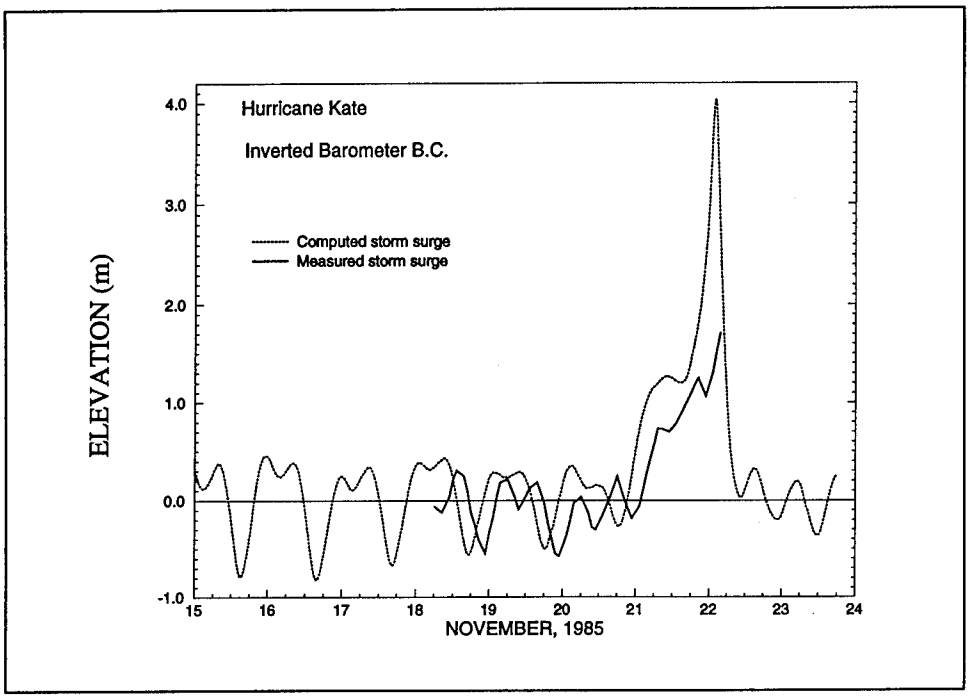

Figure 32. Comparison of computed and measured storm surge elevations for Hurricane Kate over the east coast domain at St. Marks, FL

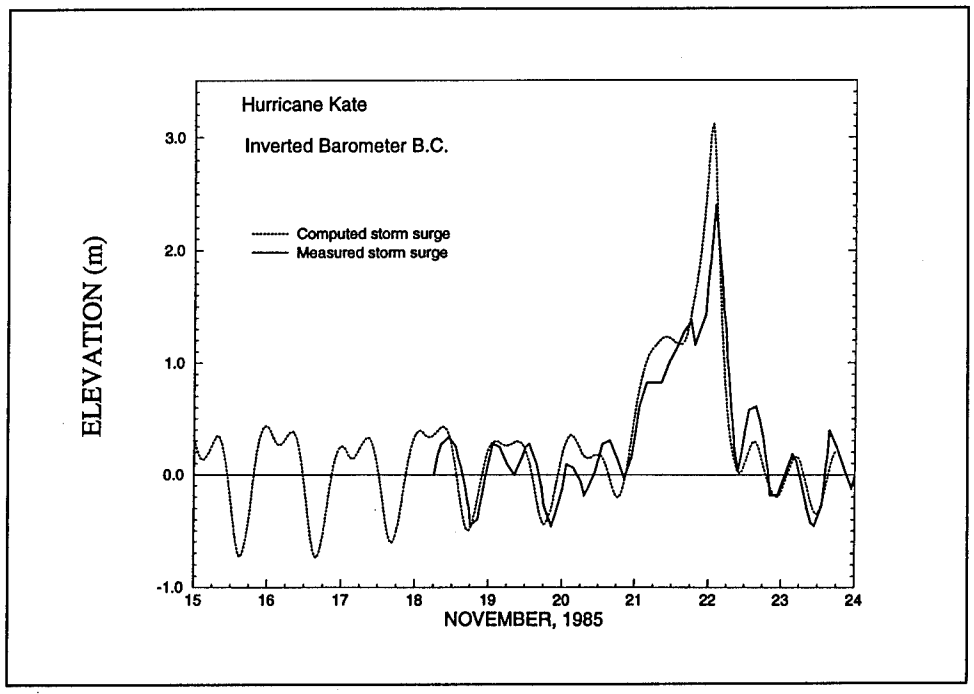

Figure 33. Comparison of computed and measured storm surge elevations for Hurricane Kate over the east coast domain at Shell Point, FL

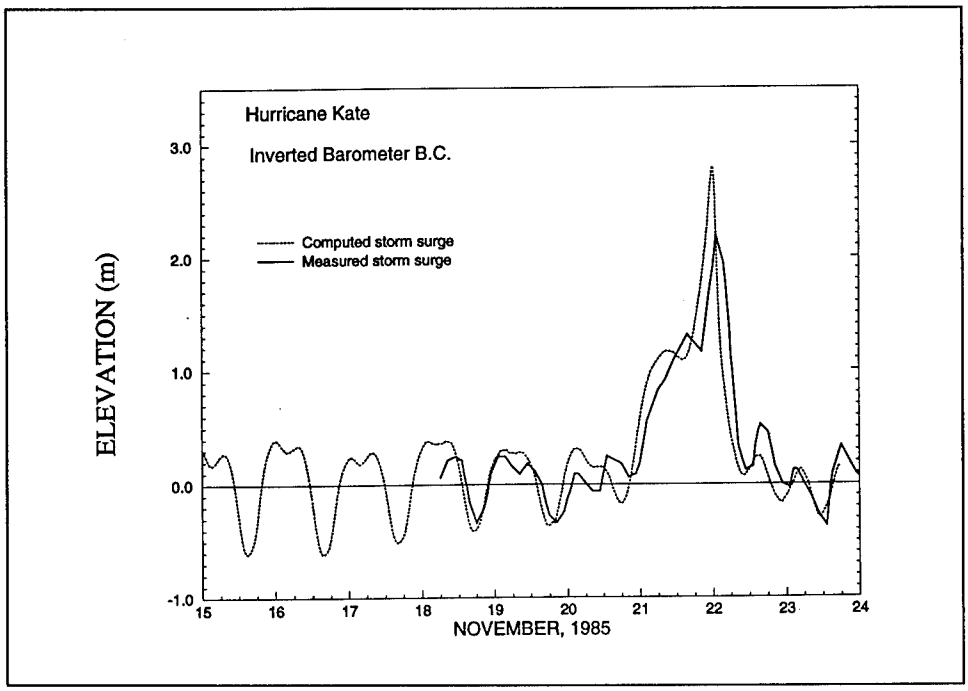

Figure 34. Comparison of computed and measured storm surge elevations for Hurricane Kate over the east coast domain at Turkey Point, FL

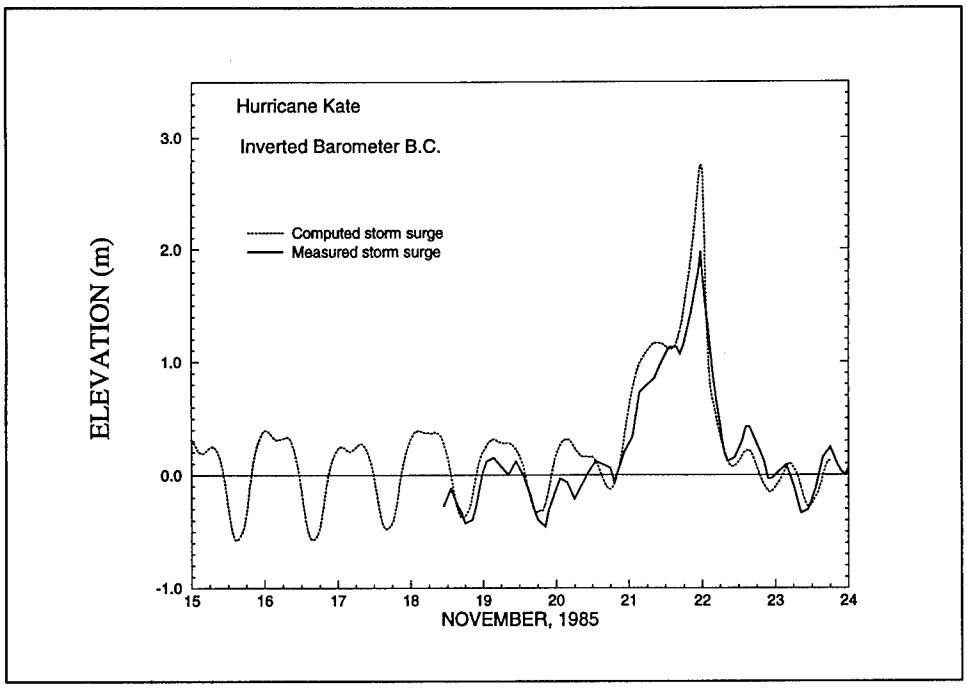

Figure 35. Comparison of computed and measured storm surge elevations for Hurricane Kate over the east coast domain at Carrabelle, FL

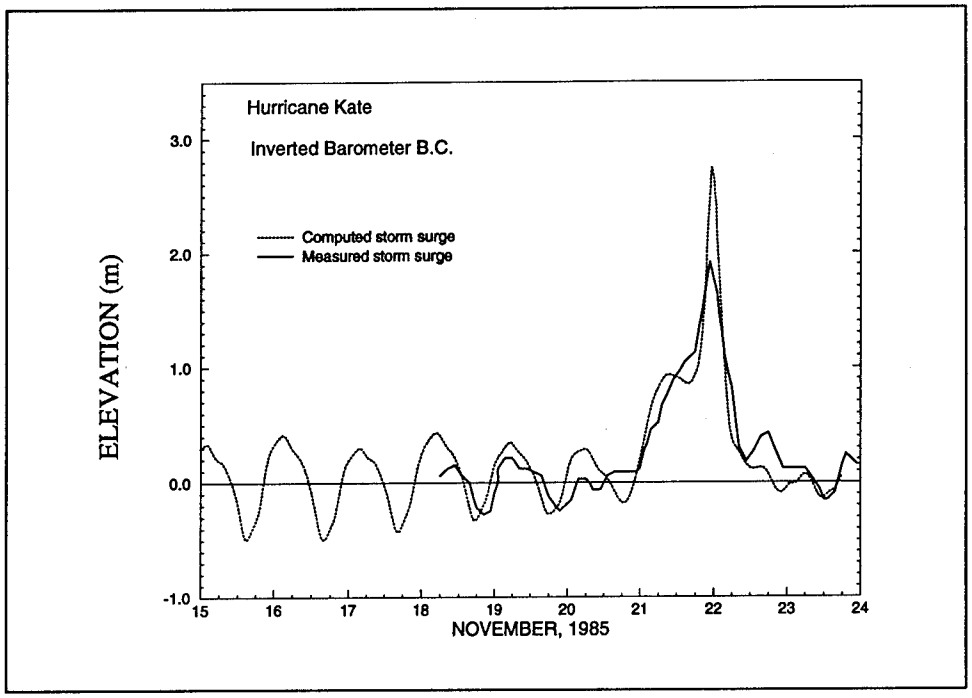

Figure 36. Comparison of computed and measured storm surge elevations for Hurricane Kate over the east coast domain at Apalachicola, FL

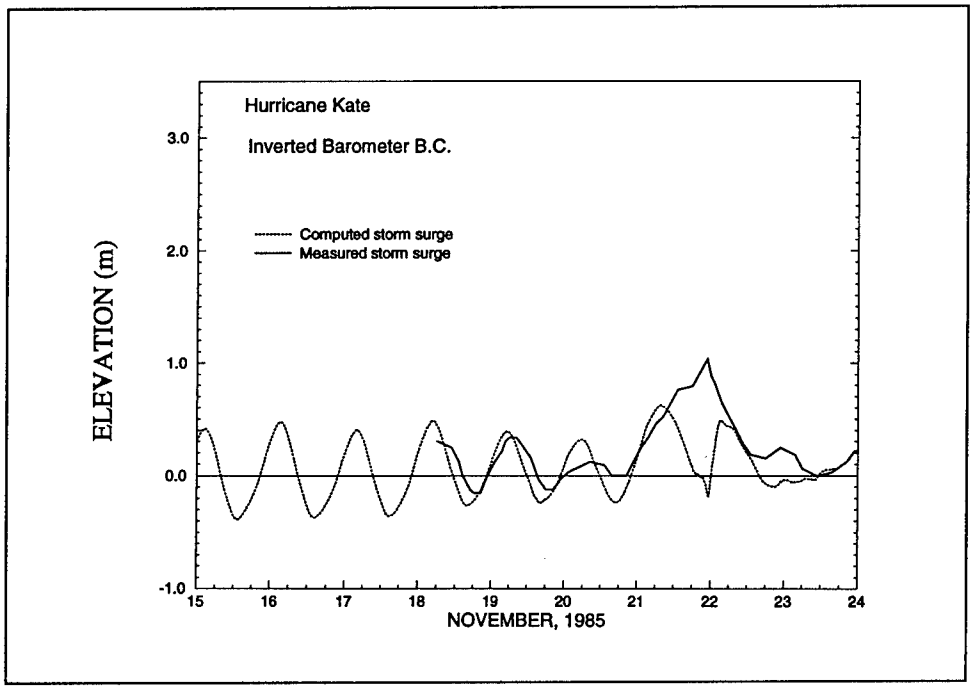

Figure 37. Comparison of computed and measured storm surge elevations for Hurricane Kate over the east coast domain at Panama City, FL

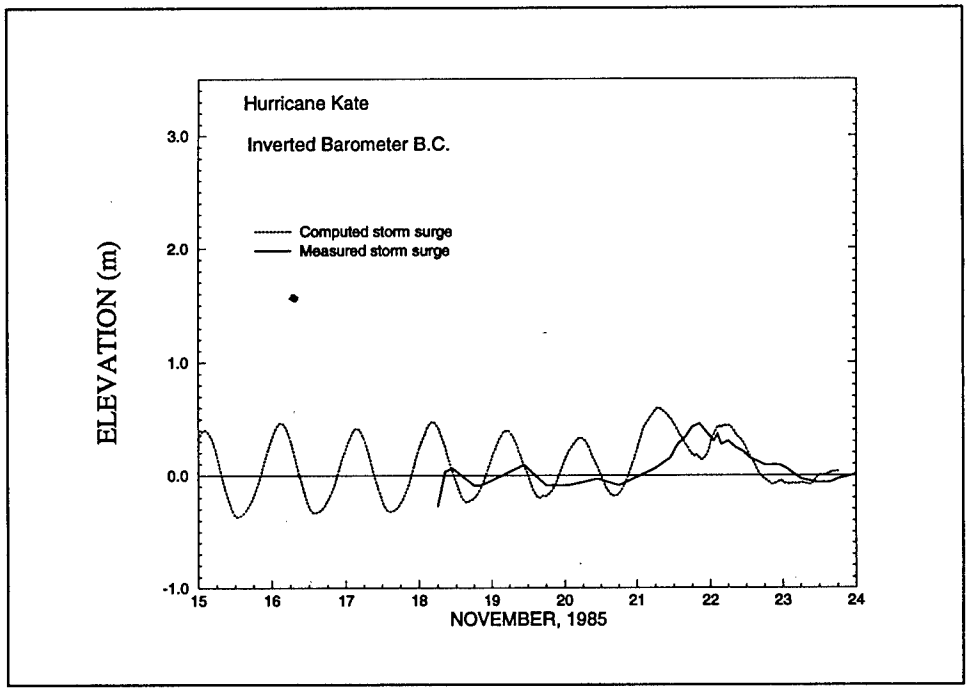

Figure 38. Comparison of computed and measured storm surge elevations for Hurricane Kate over the east coast domain at Destin, FL

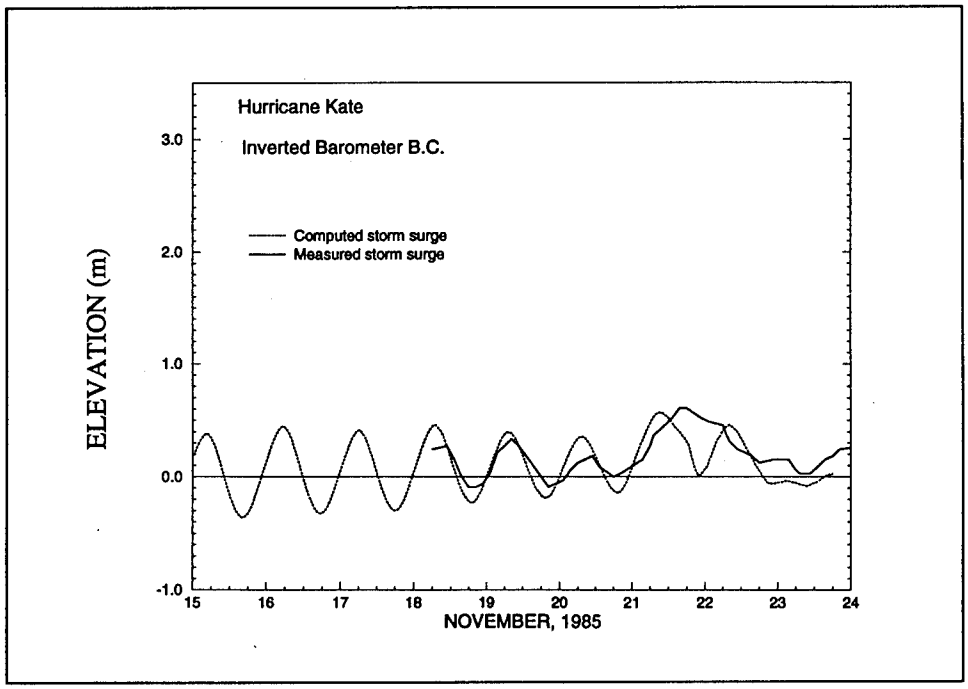

Figure 39. Comparison of computed and measured storm surge elevations for Hurricane Kate over the east coast domain at Pensacola, FL

Deviations from the observed storm surge, particularly the overprediction at stations east of Panama City, Florida, and the lack of a sustained surge at stations west of Panama City, Florida, may be indicative of an artificially high wind field forcing generated by the HURWIN wind model. A limitation of the HURWIN wind model as applied is its inability to account for frictional dissipation of the winds as a hurricane makes landfall. Prior to reaching the land, excessive wind speeds create an artificially high storm surge on the right-hand side of the hurricane causing overprediction by the model. As winds rotate overland without reduction in magnitude, a diminished surge occurs on the left-hand side of the hurricane. Despite the fact that wind stress values computed by the HURWIN model are generally too high in the region of hurricane landfall, the uncalibrated storm surge computations generated by the ADCIRC model are quite reasonable when computed over the east coast domain.

Conclusions

Previously, little effort has been made to understand the relationship between domain size, boundary conditions, and the resulting physics for hurricane storm surge modeling in continental margin waters. In this domain size sensitivity study, storm surge computations over three domain sizes subject to two different open ocean boundary forcings are compared to determine the influence of domain size on the computed response.

Results of this investigation clearly illustrate that storm surge model domains which are largely situated on the continental shelf and whose domain size is limited relative to the size of the storm significantly underestimate the primary storm surge response. Significant storm surge occurs in the vicinity of open ocean boundaries of such domains when water is pushed up on the shelf by hurricane winds. Therefore, appropriate boundary conditions are difficult, if not impossible, to specify for these domains which are small compared to the storm scale and which have large expanses of cross-shelf open ocean boundaries. Consequently, a significantly underestimated storm surge response results when using a small domain such as the Florida coast domain. Despite this, most storm surge modeling efforts to date have used similarly sized continental shelf domains, e.g. SLOSH model applications by the National Weather Service (Jarvinen and Lawrence 1985; Shaffer, Jelesnianski, and Chen 1986; Jelesnianski, Chen, and Shaffer 1992; Chen, Shaffer, and Kim 1993).

The computed storm surge response over a domain which encompasses the Gulf of Mexico exhibits oscillatory behavior due to the existence of resonant modes or surge forerunner in the Gulf of Mexico basin. These resonant modes in the Gulf of Mexico are well-documented and can be easily excited/influenced by a number of factors: numerical discretization, start-up conditions, interior domain forcing functions, and/or the boundary conditions. This study reinforces the findings of others that resonant modes within the Gulf of Mexico are quite sensitive to boundary forcing functions specified over the Gulf of Mexico domain. Consequently, the storm surge response computed

over the Gulf of Mexico domain may not capture the physics associated with the hurricane forerunner.

The east coast domain, which includes the western North Atlantic Ocean, the Gulf of Mexico, and the Caribbean Sea, leads to convergent predictions of both the primary storm surge and surge forerunner effect. A hurricane progresses through the domain generating and propagating storm surge in a natural and realistic fashion. The inclusion of contiguous basins allows proper setup of basin resonant modes and facilitates the realistic propagation of storm surge throughout the domain onto the continental shelf, where development of storm surge is most critical. The main advantage of the east coast domain is that the open boundaries lie within the deep Atlantic Ocean and are far from the intricate processes occurring on the continental shelf and within the Gulf of Mexico basin in response to the storm. As was demonstrated, sensitivity of the coastal response to open-ocean meteorological boundary forcing is minimal. Furthermore, tidal elevations appropriate at the deep Atlantic Ocean boundary in the east coast domain are readily extracted from global tidal models. Comparisons of storm surge elevations computed over the east coast domain to observed water levels verify that the model response is reliable. These comparisons also point out the importance of accurate meteorological forcing and possible shortcomings in the HURWIN wind model.

Response characteristics of a storm surge model of the continental margin are profoundly influenced by the domain size and the associated boundary conditions. The amplitude of the primary surge varied significantly over the three domains examined. Furthermore, entire flow phenomena may be mere model artifacts that appear and disappear. In fact, a significant Helmholtz mode could be easily excited in the Gulf of Mexico model domain while this is not the case in either of the other domains. Thus, in order to make meaningful statements about physics, the modeler should be reasonably certain about what level of convergence has been achieved relative to domain size.

5 Influence of Grid Structure

Discretization of the hydrodynamic domain is just as important as domain size selection in the formulation of a numerical storm surge model. The discrete form of the hydrodynamic model equations presented in Chapter 2 are applicable at individual points. Therefore, a discrete representation of the computational domain is constructed by dividing the domain into a mesh of nodal points to form a grid. Computed storm surge elevations and velocities are obtained at each nodal point within this grid upon solution of the model equations. The numerical solution procedure implemented at each grid node utilizes information from surrounding nodes. As a result, the degree of spatial resolution provided by a grid of discrete points significantly influences the computed storm surge response of the model.

Too often, grids are constructed using subjective criteria and their discretizations are based on computational constraints. Only recently have efforts been made to determine if such grids are convergent with respect to numerical model computations of tidal, wind-driven, and large-scale baroclinic circulation (Johns et al. 1983a,b; Le Provost and Vincent 1986; Bennett and Campbell 1987; Dietrich, Roache, and Marietta 1990; Lardner and Song 1992; Piacsek and Allard 1993; Dietrich 1993; Westerink, Luettich, and Muccino 1994; Westerink et al., in preparation (a); Luettich and Westerink 1994).

In most storm surge modeling applications, though, no rigorous studies of grid convergence are evident, though grid resolution is recognized as being important for accurate storm surge prediction. Recall that large domains extending into the deep ocean are desirable for accurate storm surge prediction. Such domains require variably spaced, and often unstructured, discretizations to meet computational constraints. Near coastal continuous grid compression (Dube, Sinha, and Roy 1986; Johns et al. 1983a) is one technique implemented to provide varying degrees of resolution throughout the model domain. However, restrictions on the skewness and maximum cell-to-cell size ratios severely limit the benefits of such an approach. The use of nested grids is a common way of handling resolution requirements (e.g. Flather (1984); Dendrou, Moore, and Myers (1985); Al-Rabeh, Eunay, and Cekirge (1990); Hubbert, Leslie, and Manton (1990)). In the nested grid approach, computations of storm surge over a large coarse grid are interpolated onto the boundaries of a local highly refined grid. Simulation of the storm surge then continues separately over the smaller grid. Nested grids are usually not coupled during a given simulation

and nodal spacing between nested grids generally differs by a factor of two to three with the minimum spacing in the finest grid ranging from 0.5 km (.3 s miles) to 10 km (6.2 s miles). A coupled, nested grid system would more closely approach the grid flexibility of the finite element method but may not be as convenient. Regardless of the gridding technique used, little has been done to determine if the spatial resolution provided by the grid discretization leads to accurate storm surge predictions.

The focus of this chapter is to systematically determine an optimal structure for the domain discretization which leads to accurate hurricane storm surge computations. The grid structure sought is one that provides only the spatial resolution necessary to capture pertinent storm surge physics and does not overdiscretize. This is particularly important if model efficiency is to be preserved when using large computational domains as suggested by the results of the domain size sensitivity study. Findings from the grid studies performed herein are applicable to any of the grid discretization strategies currently in use, though a variably spaced, unstructured grid is optimal when using very large domains.

For this study of grid structure, the placement of nodal points throughout the domain is examined with respect to the degree of spatial resolution required for accurate representation of storm surge generation. The affect of grid spacing and coastline resolution on hurricane storm surge calculations is also investigated. Errors in the primary surge computed over grids which have different nodal spacings and coastline resolutions are related to the grid spacing as well as bathymetric changes and characteristics of the hurricane forcing.

Investigation of grid discretization requirements for hurricane storm surge calculations involves the computation of storm surge elevations over an idealized domain using various regular and variably graded grid discretizations. Meteorological forcing is provided by four synthetic hurricanes. Results of this grid convergence study lead to guidelines for grid structure and discretization strategies when modeling hurricane storm surge generation.

Grid Descriptions

Domain and coastline definitions

A rectangular domain with dimensions of 2,500 by 3,000 km (8,200 by 9,840 miles) is constructed to correspond to the areal extent of the east coast domain used throughout Chapter 4. The rectangular domain defined does not include resonant basins such as the Gulf of Mexico or Caribbean Sea found within the east coast domain. Instead this domain more closely represents the Atlantic Ocean off the eastern shore of the United States. A land boundary representing the coastline lies along the left-most 3,000-km (9,840-mile) length of the rectangular domain and open ocean conditions apply at the remaining domain boundaries. A representative bathymetry profile, shown in Figure 40

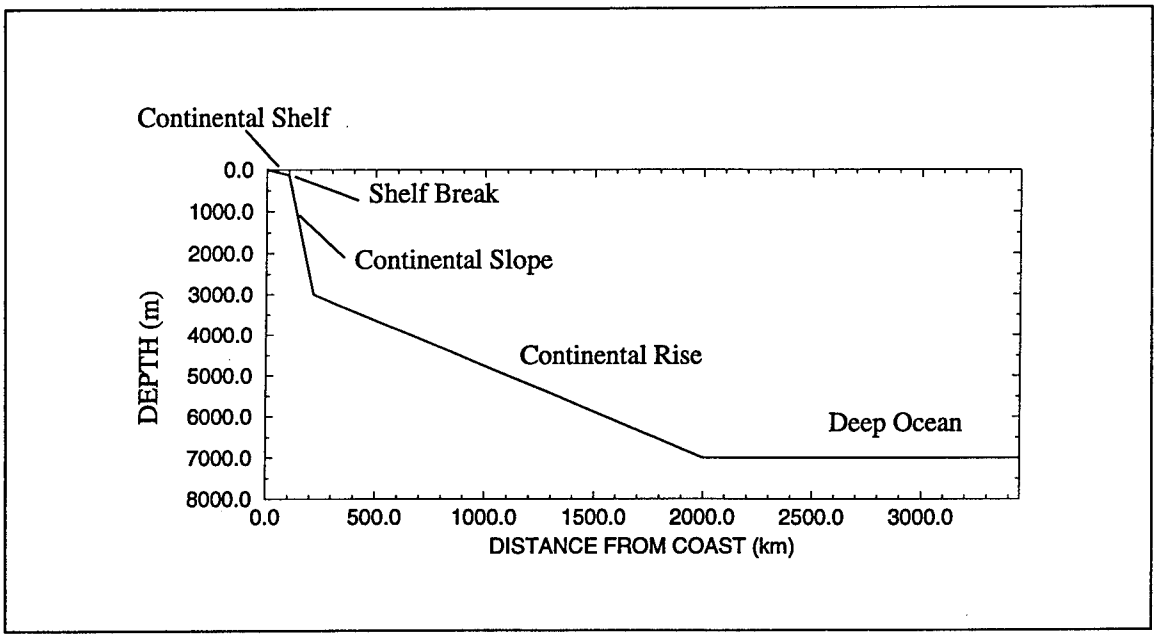

Figure 40. Bathymetry profile for the rectangular domain used in the study of grid structure relative to storm surge predictions

relative to the rectangular domain, is synthesized from ocean depth cross sections recorded off the coasts of Virginia and Florida in the western North Atlantic Ocean as well as average slopes and distances suggested in the literature for portions of the bathymetry profile (Weyl 1970; Weisberg and Parish 1974; Pickard and Emery 1982; Bearmad 1989; Thurman 1974).

Two different representations of the coastline are considered. The first is a simple straight-line coast. This particular land boundary eliminates the effect of coastline variability on storm surge generation. A second coastline is constructed using a sine wave variation, which has an amplitude of 30 km (18.6 statute miles) and a wavelength of 100 km (62.1 s miles) along the length of the shore and is given by:

$$x = 30\left[\frac{2\pi}{100}(y_o - y)\right] + x_o \tag{31}$$

where (x_o, y_o) are the coordinates, in kilometers, of the extreme northwest land boundary point in the domain, x is the horizontal coordinate of a point at the coast, and y is the distance, in kilometers, southward along the shoreline. The sinusoidal deviations of the coastline are intended to portray in an idealized way the highly irregular profile of the actual shoreline. For simulations over domains having this sinusoidal land boundary, the importance of spatial coastline variability on storm surge generation is examined.

Over domains having a sinusoidal coastline, the bathymetry profile taken from the land boundary is represented by the horizontal cross section shown in

Figure 40. This results in a north-south sinusoidal bathymetric variation due to the deviation of coastal node positions. In the ocean, the influence of shoreline bathymetric variations does not extend beyond the continental shelf. Thus, the north-south sinusoidal variation of bathymetry is attenuated over a distance equal to three times the amplitude of the sine wave variation at the coast (~ 90 km (55.9 miles)). This ensures that effects of coastline variation on the bathymetry profile remain on the continental shelf.

Discretizations

Six grid discretizations of the rectangular domain form the basis of this grid convergence study. Three uniform grids, designated as G01, G02, and G03 and shown in Figure 41 have regular nodal spacings of 50 km (31.1 statute miles), 25 km (15.5 statute miles, and 12.5 km (7.8 statute miles), respectively. Three variably graded grids, VG01, VG02, and VG03 (shown in Figure 42) have nodal spacings ranging between 12.5 km (7.8 miles) and 50 km (31.1 miles). Grid VG01 (Figure 42a) has the minimum nodal spacing of 12.5 km (7.8 miles) confined to a region near the coastline. The mesh spacing then rapidly increases to 50 km (31.1 miles) at a point approximately 50 km (31.1 miles) offshore. In grid VG02 (Figure 42b) refinement at the 12.5-km (7.8-mile) level extends from the shoreline to 25 km (15.5 miles) offshore and 25-km (15.5-mile) spacing covers the remainder of the continental shelf with 50-km (31.1-mile) spacing elsewhere. The final graded grid, VG03 (shown in Figure 42c), has extensive uniform resolution of 12.5 km (7.8 miles) over the entire continental shelf, shelf break, and portions of the continental slope out to a depth of approximately 1,000 m (3,280 ft). Spacing over the remainder of the deep ocean increases rapidly from 25 km to 50 km (15.5 to 31.1 miles).

Understanding the influence of coastline resolution is an important part of the study of domain discretization. Three coastline representations named C1, C2, and C3 and shown in Figure 43 have 5-, 9-, and 17-point-per-wavelength resolutions of the sinusoidally varying coastline, respectively. These three coastline discretizations are merged with the six grid discretizations previously described to form a total of fourteen grids. Table 4 summarizes the distinguishing features of the discretization associated with each of the fourteen grids.

Error Analysis

Grid comparisons

Four series of grid comparisons are defined using the fourteen grids outlined in Table 4. Each of these comparisons is designed to examine a particular aspect of the grid discretization in relation to its impact on storm surge predictions. Computations of storm surge over each grid within a series are compared to the storm surge elevations computed over a "truth" grid

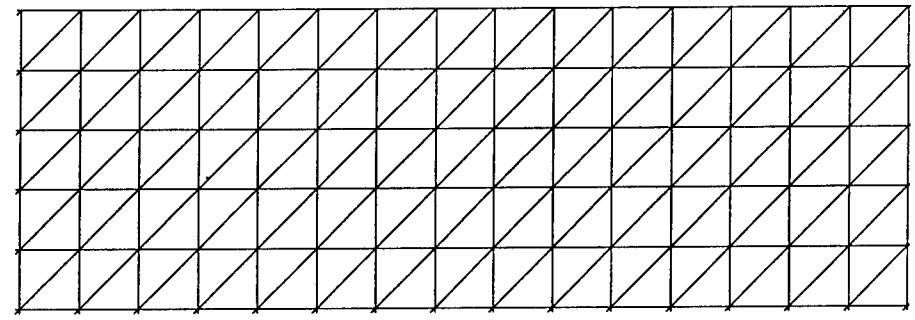

(a)

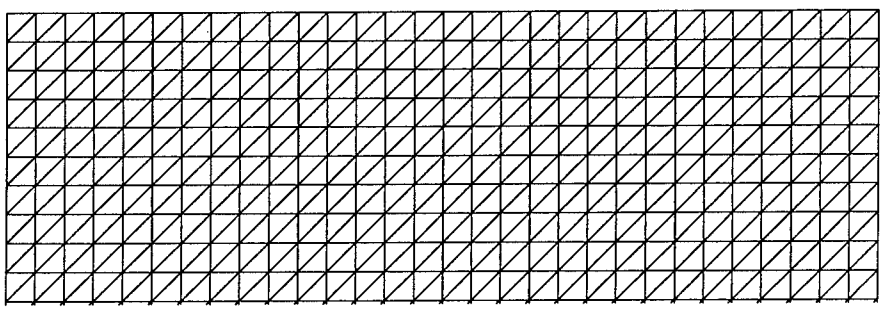

(b)

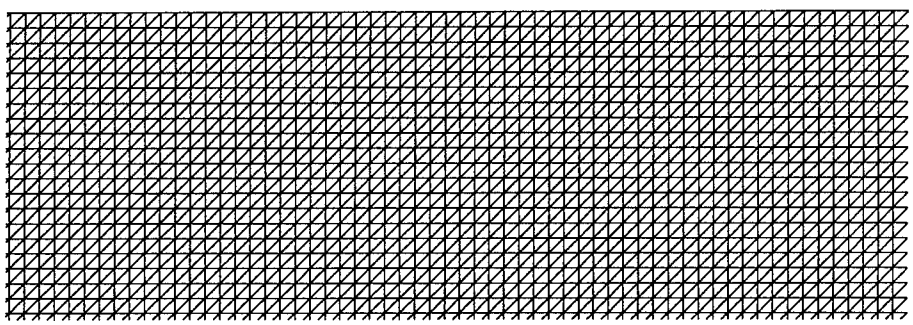

(c)

Figure 41. Enlargements of the (a) 50-km, (b) 25-km, and (c) 12.5-km uniform discretizations for grids G01, G02, and G03, respectively

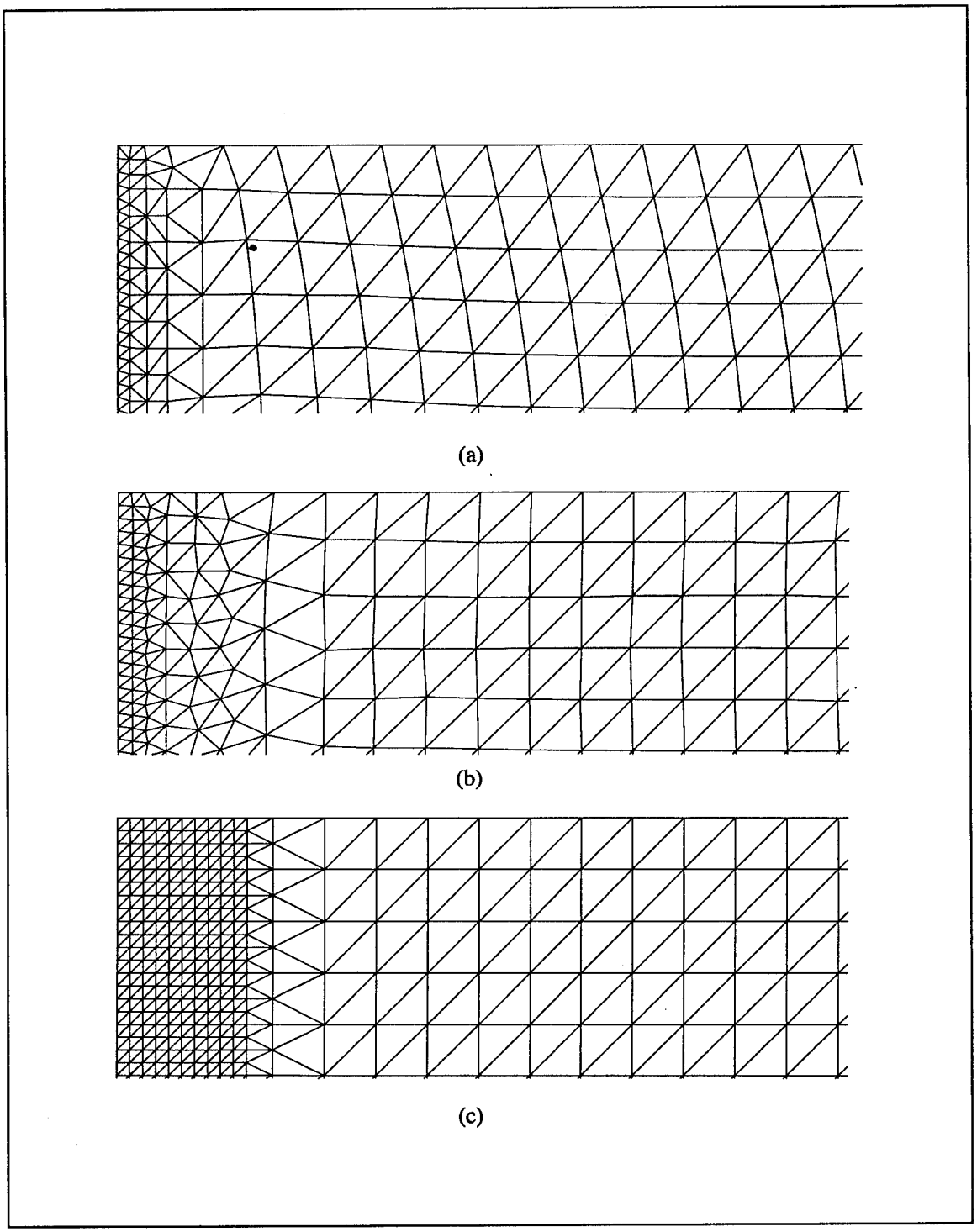

Figure 42. Enlargements of the variably graded discretizations for grids (a) VG01, (b) VG02, and (c) VG03, respectively

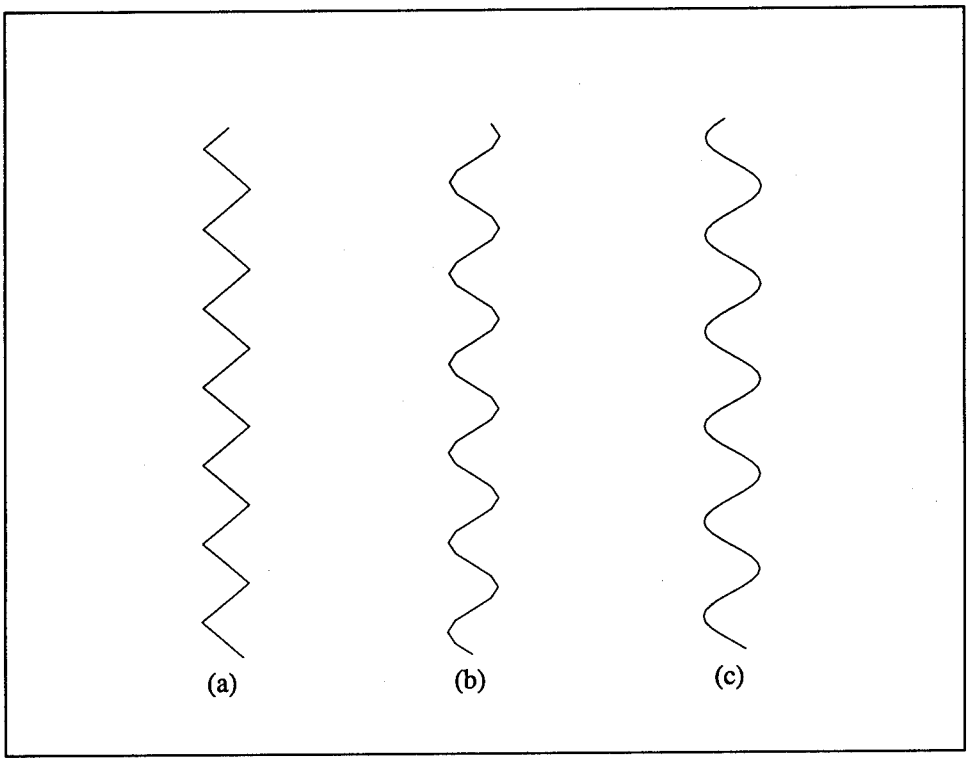

Figure 43. Sinusoidally varying coastlines (a) C1, (b) C2, and (c) C3, having resolutions of 5, 9, and 17 points per wavelength, respectively

Table 4
Characteristics of Rectangular Grid Discretizations

Name	Domain		Coastline		Number of Nodes
	Structure	Spacing	Type	Refinement	
G01	Regular	50 km	Straight	----	3,111
G02	Regular	25 km	Straight	----	12,221
G03	Regular	12.5 km	Straight	----	48,441
VG01	Graded	Variable	Straight	----	3,717
VG02	Graded	Variable	Straight	----	4,014
VG03	Graded	Variable	Straight	----	5,639
G01_C1	Regular	50 km	Sinusoidal	5 pts	3,171
G02_C1	Regular	25 km	Sinusoidal	5 pts	12,401
G03_C1	Regular	12.5 km	Sinusoidal	5 pts	48,920
G02_C2	Regular	25 km	Sinusoidal	9 pts	12,401
G03_C3	Regular	12.5 km	Sinusoidal	17 pts	49,040
VG01_C3	Graded	Variable	Sinusoidal	17 pts	4,136
VG02_C3	Graded	Variable	Sinusoidal	17 pts	4,374
VG03_C3	Graded	Variable	Sinusoidal	17 pts	5,910

designated within that series. The first series of grid comparisons investigates grid spacing effects without the influence of a spatially variable coastline. Thus, grids G01, G02, G03, VG01, VG02, and VG03, all of which have straight coastlines, make up the Series 1 grid comparisons. The "truth" grid solution for Series 1 is obtained using grid G03. A second series of grids, Series 2, which compares grids G01_C1 and G02_C1 to a "truth" grid solution over grid G03_C1, demonstrates the effect of a spatially varying shoreline. These grids all have uniform mesh spacings and a 5-point-per-wavelength representation of the sinusoidally varying coastline. Another set of grids, Series 3, compares grid G03_C1 to grid G03_C3 and grid G02_C1 to grid G02_C2, in order to assess the consequence of coastline refinement alone. A final series of comparisons, named Series 4, between grids G01_C1, G02_C2, VG01_C3, VG02_C3, and VG03_C3 with computations over grid G03_C3 designated as a "truth" solution, combines the influence of grid spacing and coastline resolution on storm surge computation. Table 5 summarizes the grid comparisons just outlined and notes the aspect of the grid discretization which is isolated by each grid comparison grouping. The truth grid designated within each series of grid comparisons is listed in boldface in Table 5.

Table 5
Definitions of Grid Comparisons

Series	Grids Compared	Objective
1	G01 G02 VG01 VG02 VG03 **G03**	Grid spacing
2	G01_C1 G02_C1 **G03_C1**	Coastline variation
3	G03_C1 **G03_C3**; G02_C1 **G02_C2**	Coastline refinement
4	G01_C1 G02_C2 VG01_C3 VG02_C3 VG03_C3 **G03_C3**	Combination

Storm surge computations

For the storm surge simulations pertinent to this grid convergence study, four synthetic hurricanes (H011, H012, H013, and H031) described in detail in Chapter 3 serve as the meteorological forcing over all fourteen grids. Important properties of these synthetic hurricanes are repeated in Table 6 for convenience. In the simulations of storm surge, wind stress and pressure forcing are applied on the interior of the domain and tidal forcing is neglected both on the interior and at the open ocean boundaries. Additionally, an inverted barometer condition is specified at the open ocean boundaries of the domain.

For this series of simulations, only the finite amplitude terms are not included in the governing equations due to instabilities caused by near drying elements. For consistency, model parameters are the same as those used in the domain comparison study (i.e., the bottom friction coefficient is constant and equal to 0.003 and the GWCE parameter τ_0 is defined equal to 0.001). In addition, model parameters are identical for all simulations in the grid

Table 6
Characteristics of Synthetic Hurricanes

Hurricane Name	R_{max} (km)	Velocity (km/hr)	Hurricane Path (Relative to the coast)	Length of Hurricane (days)	Time of Landfall (hrs)
H011	30	15	Perpendicular	8.75	192
H012	60	15	Perpendicular	8.75	192
H013	30	25	Perpendicular	6.00	126
H031	30	25	Parallel	20.50	----

convergence study so that comparisons between the computed storm surge for different grid discretizations are possible.

Simulations are spun up from homogeneous initial conditions using a 1-day ramp in time. An identical ramp function of 1 day length is applied to the wind and pressure forcing as well as the inverted barometer boundary condition. Actual simulation periods run 6 hr longer than the length of each hurricane listed in Table 6. This is due to a 6-hr ramp-up period at the start of simulation during which initial hurricane wind and pressure forcings are held stationary. Thereafter, storm surge computations use the time-varying wind and pressure fields. A time-step of 45 sec is used throughout the simulation period. No calibration or tuning of parameters is performed in either the weather model or in the hydrodynamic model.

Error measures

The objective of the error analysis is to determine the magnitude and location of errors in the predicted storm surge throughout the computational domain. Using this information, the level of resolution required to minimize these errors is determined. In general, this error analysis guides the placement of nodes throughout the domain such that the discretization of the domain uses a minimum number of points, yet yields an accurate representation of the storm surge generation in the coastal ocean.

Storm surge predictions computed over the most finely uniform discretized grid within each series of grid comparisons, shown in bold in Table 5, are considered "truth" solutions and are used to assess errors in the storm surge computations performed over the remaining grids within a series.

Maximum overprediction (positive) and underprediction (negative) errors in the storm surge are computed over each grid as a function of time. The absolute error is calculated simply as the difference between computed storm surge values and the "true" storm surge elevations at each point in time. The relative error normalizes the absolute error with respect to the highest surge elevation over the entire domain at the specific point in time being considered.

An inclusion of ocean bathymetry at each point in time considered indicates the location of the maximum over- and underprediction and helps identify where grid resolution is lacking.

Discussion of Results

For the discussion of storm surge prediction errors that follows, knowledge of the storm surge elevation profile for each hurricane is helpful in understanding the error patterns that develop. Figures 44a - 44d depict the maximum storm surge generated over the domain at a specific time and the depth at the location of maximum water elevation for meteorological forcing by Hurricanes H011, H012, H013, and H031. The surge profiles in Figures 44a - 44d are taken from computations over grid VG03 and will be referenced in discussing the storm surge prediction errors presented for each series of grid comparisons. Note the oscillatory behavior of the surge elevations in deep water. This is an artifact of the insufficient resolution provided over the deep ocean and will be discussed further in subsequent sections.

Series 1 Comparisons: G01, G02, VG01, VG02, VG03

For Hurricane H011, maximum overprediction and underprediction errors computed over uniform grids G01 and G02 are shown in Figures 45a and 45b, respectively. Up to about 174 hr, while the storm is predominately located in the deep ocean (Figure 44a), the oscillating error pattern seen in Figures 45a and 45b is associated with an insufficient resolution in deep water to capture the inverted barometer which forms (i.e., the pressure forcing function for Hurricane H011, which has a spatial scale of 30 km (18.6 s miles). This oscilllating error pattern is also insufficiently resolved over grids having uniform spacings of 50 km (31.1 statute miles) and 25 km (15.5 statute miles), and results in an aliased response which fluctuates depending on the position of the hurricane eye relative to the nearest node). This variably aliased behavior is also apparent in the storm surge elevation profile shown in Figure 44a while Hurricane H011 is in the deep ocean.

As the storm moves onto the continental shelf at about 180 hr, the absolute errors increase significantly. This error increase corresponds to the dramatic increase in storm surge as winds push water up onto the shelf against the coast. Also note the large increase in the relative error which coincides with a decreasing absolute error and a declining peak surge as the storm makes landfall. This behavior of the relative error indicates that processes which dissipate the peak surge are much more rapid than those which dissipate the errors in the storm surge. A comparison of the error magnitudes between Figures 45a and 45b demonstrates that halving the nodal spacing leads to a reduction of the error in deep waters by a factor of two and a threefold reduction of the errors generated on the continental shelf. Peak errors over grids G01 and G02 are concentrated on the continental shelf nearest the shoreline suggesting that a

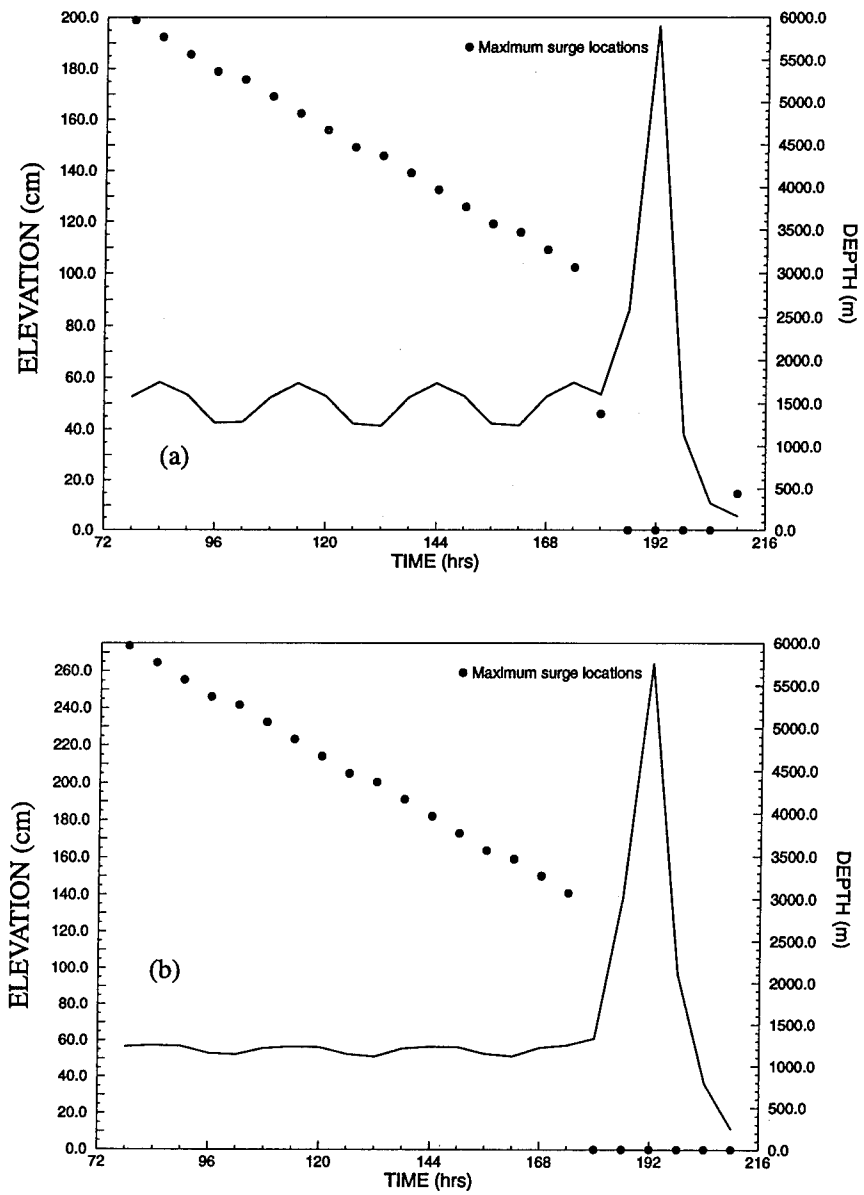

Figure 44. Maximum storm surge elevations over the domain and the depth at the location of maximum surge computed over grid VG03 for (a) Hurricane H011 and (b) Hurricane H012 forcing (Continued)

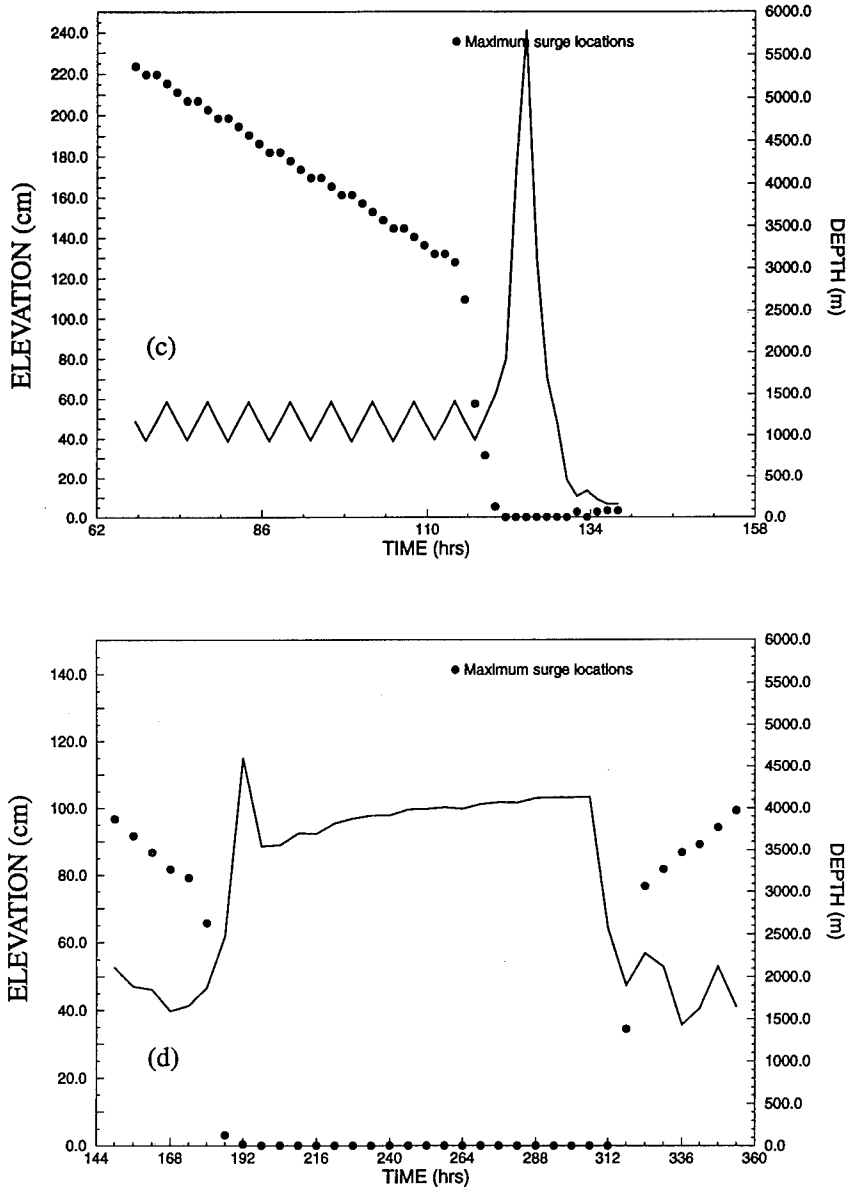

Figure 44. (Concluded)

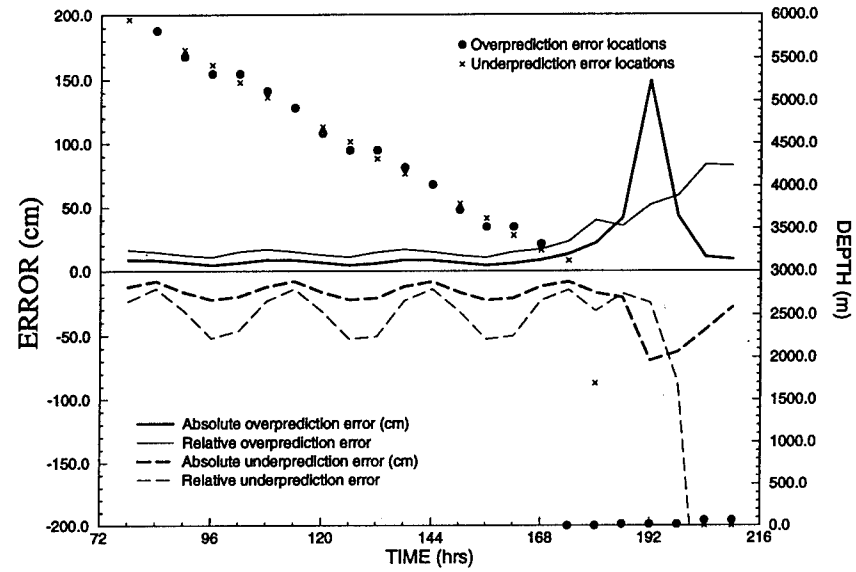

(a)

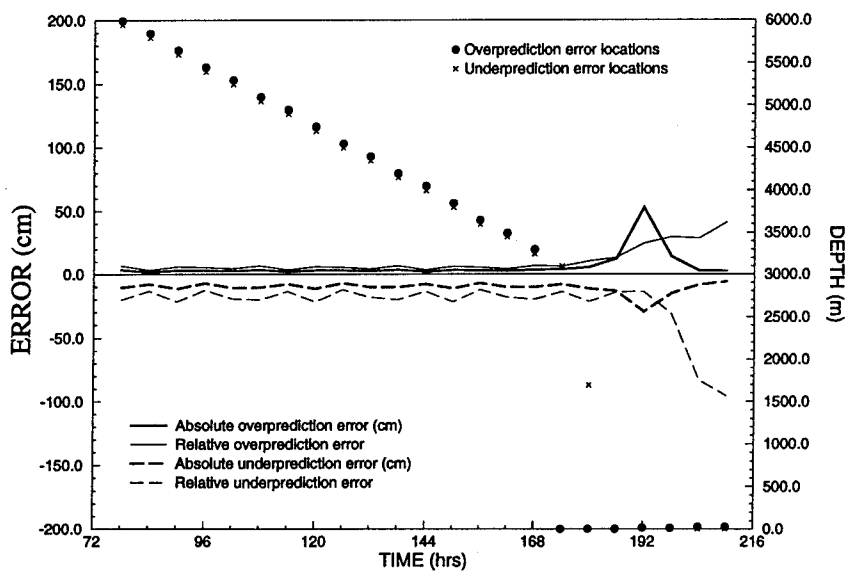

(b)

Figure 45. Maximum over- and underprediction errors of the storm surge generated by Hurricane H011 as computed over grids (a) G01, (b) G02, (c) VG01, (d) VG02, and (e) VG03 (Sheet 1 of 3)

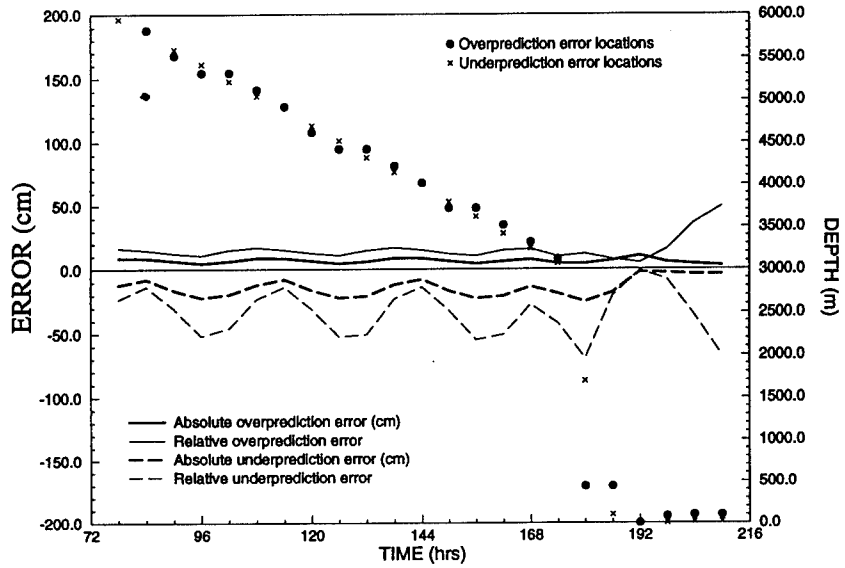

(c)

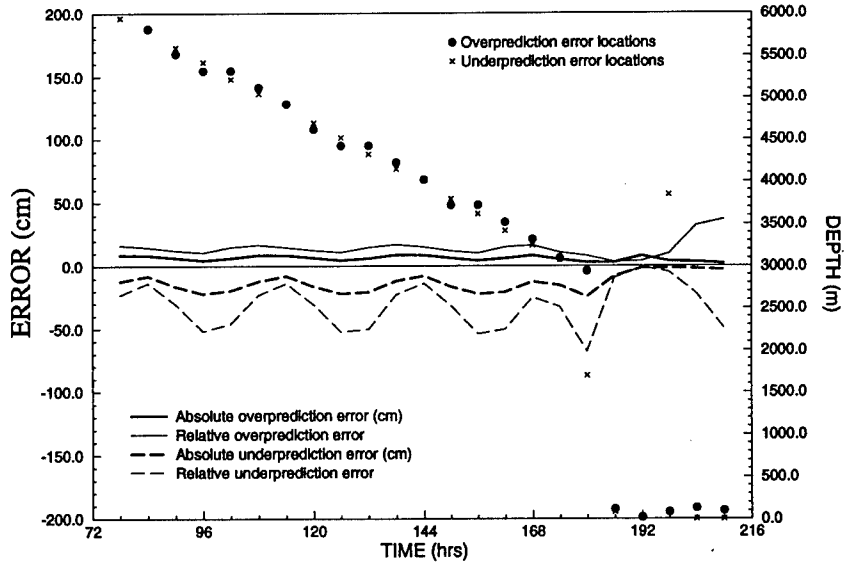

(d)

Figure 45. (Sheet 2 of 3)

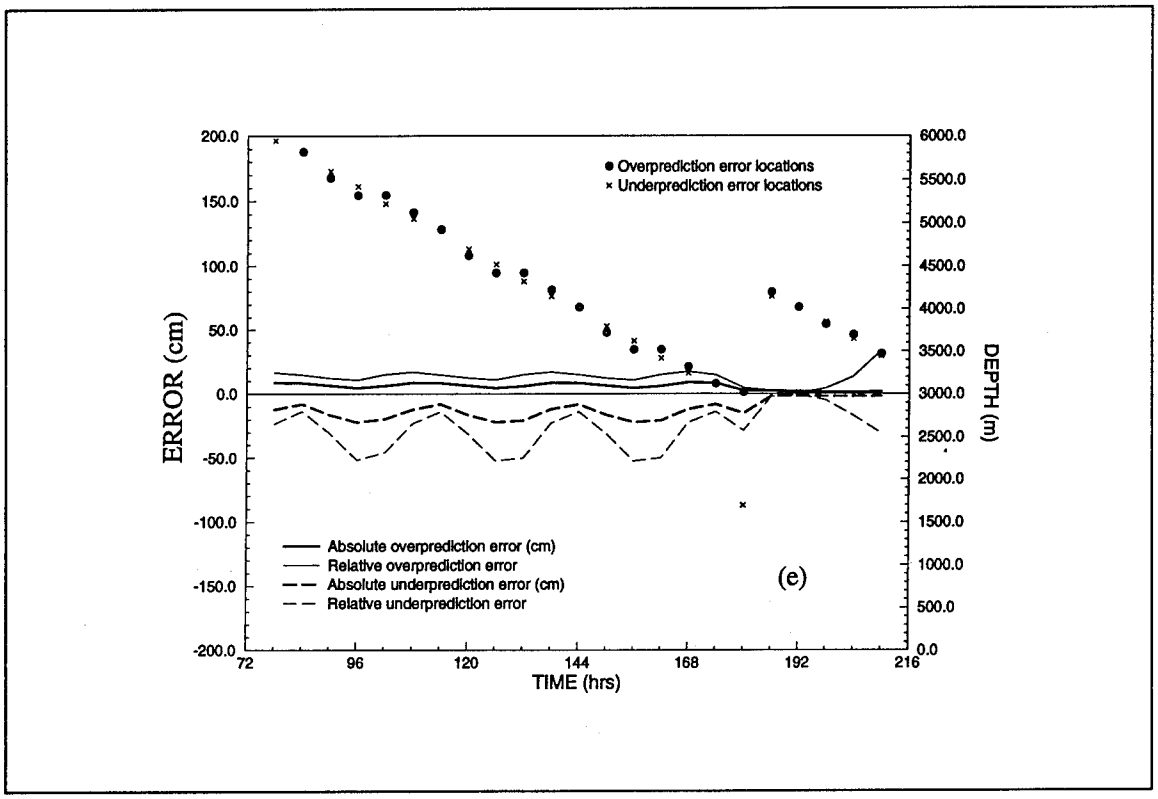

Figure 45. (Sheet 3 of 3)

variably graded grid may provide an optimal grid structure for minimization of the storm surge prediction errors.

For the three variably graded grids (VG01, VG02, and VG03) maximum storm surge prediction errors and depths at the location of the maximum errors for these grids are presented in Figures 45c - 45e relative to Hurricane H011 forcing. For each of the graded grids, errors in the storm surge computations over the deep ocean are the same as those computed over grid G01 due to an identical grid spacing of 50 km. As the storm moves onto the continental shelf at about 180 hr, the largest overprediction errors computed relative to grid VG01, seen in Figure 45c, initially occur over the continental slope, a shift from the predominate shoreline errors computed over grids G01 and G02 at the same times. The additional resolution provided at the coastline in grid VG01 improves storm surge predictions at the coast until the time of peak surge and hurricane landfall at 192 hr. Following the passage of Hurricane H011 onto land, maximum errors over grid VG01 remain on the continental shelf but are removed from the vicinity of the coastline. In comparison to grid G02, maximum errors over grid VG01 are reduced by a factor of four due to the additional refinement provided at the coastline. In general, the maximum errors computed over grid VG01 are relatively uniform in time and space and are significantly less than those computed over either grid G01 or G02.

Maximum error levels for graded grid VG02, presented in Figure 45d, indicate that the extreme errors are located on the continental shelf away from the coastline except at the time of peak surge when maximum errors remain at the shore. Increased shelf resolution over grid VG02 reduces error levels below that of grid VG01 but not significantly. Over VG03, which has extensive resolution over the continental shelf, shelf break, and slope, error reduction extends into deeper waters. Results from these error analyses indicate that storm surge calculations in nonresonant basins, where surge forerunners are not developed, do not require the same high level of grid resolution over the shelf break and slope as tidal computations (Westerink, Luettich, and Muccino 1994; Westerink et al., in preparation (b); Westerink, Luettich, and Hagen 1994).

Maximum over- and underprediction errors in the computed storm surge generated by forcing from Hurricane H012 are shown in Figures 46a - 46e for each grid in Series 1. Recall that Hurricane H012 has a spatial scale double that of Hurricane H011 (i.e., R_{max} is 60 km (32.4 n.m.)). Notice while the storm is in the deep ocean, at times less than 174 hr, the variably aliased error pattern is still evident over the uniform grid G01 but the magnitude of the errors is half of those associated with Hurricane H011 forcing during the same time period. Over grid G02, maximum errors computed in the deep ocean are negligible as seen in Figure 46b. Reduced deepwater errors computed over grids G01 and G02 are attributed to the larger spatial scale of Hurricane H012 (i.e., more nodal points are available to represent the features of a larger scale storm resulting in an increased resolution of the inverted barometer effect as well as wind forcing). For grid G02, the uniform spacing of 25 km is approximately one half the spatial scale of Hurricane H012.

Maximum overprediction errors over grid G01 occur at the coastline long before the storm reaches the continental shelf. As the storm progresses onto the continental shelf at about 180 hr, the magnitude of the absolute errors over grid G01 is somewhat higher than those computed for Hurricane H011 forcing, a consequence of the increased peak surge generated by the large-scale storm. However, when mesh spacing is halved as for grid G02, the same error trends are exhibited for Hurricane H012 forcing as were seen for forcing by Hurricane H011. Namely, a threefold reduction in error over the continental shelf is observed in comparing computed errors over grids G01 and G02 shown in Figures 46a and 46b. Maximum relative errors associated with Hurricane H012 forcing computed over all five grids in Series 1 are the same as or slightly less than those recorded for Hurricane H011 forcing. Generally, a large-scale storm has more nodal points available than a smaller scale storm to resolve the same features of the hurricane forcing. So naturally, for a given mesh spacing, more accurate predictions result for the larger storm event.

Relative to Hurricane H012 forcing, errors computed over grids VG01, VG02, and VG03 while the storm is in the deep ocean are the same as those computed over grid G01 due to the identical grid spacings of 50 km as seen in Figures 46c - 46e. Over grid VG01, maximum error values, shown in Figure 46c, remain in deeper waters until 12 hr prior to the time of landfall when

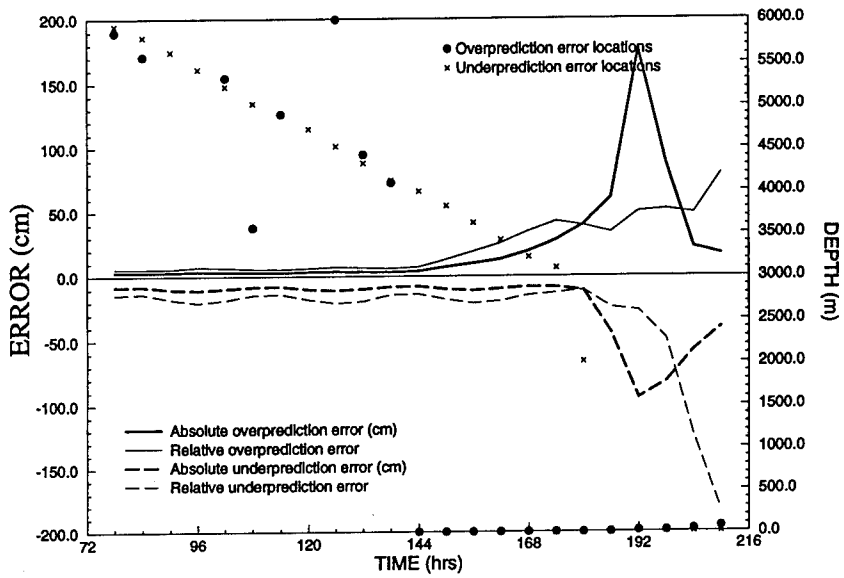

(a)

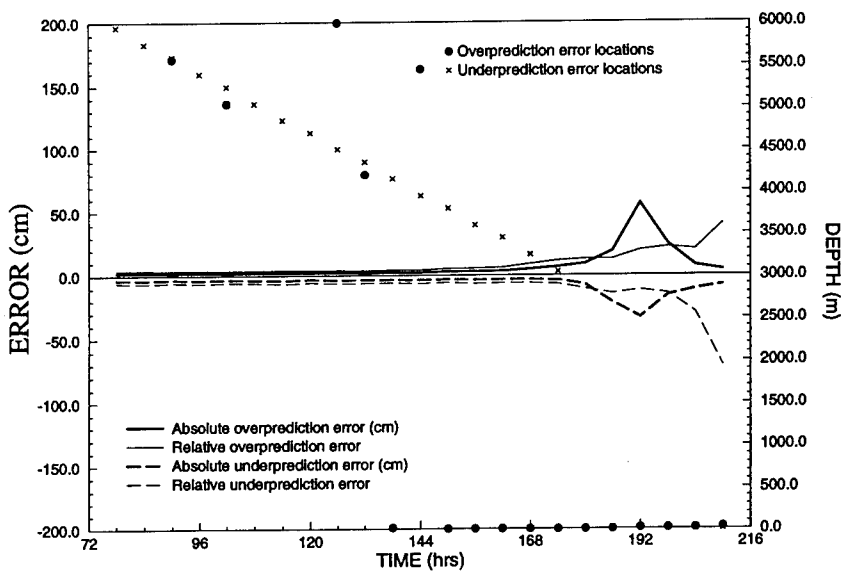

(b)

Figure 46. Maximum over- and underprediction errors of the storm surge generated by Hurricane H012 as computed over grids (a) G01, (b) G02, (c) VG01, (d) VG02, and (e) VG03 (Sheet 1 of 3)

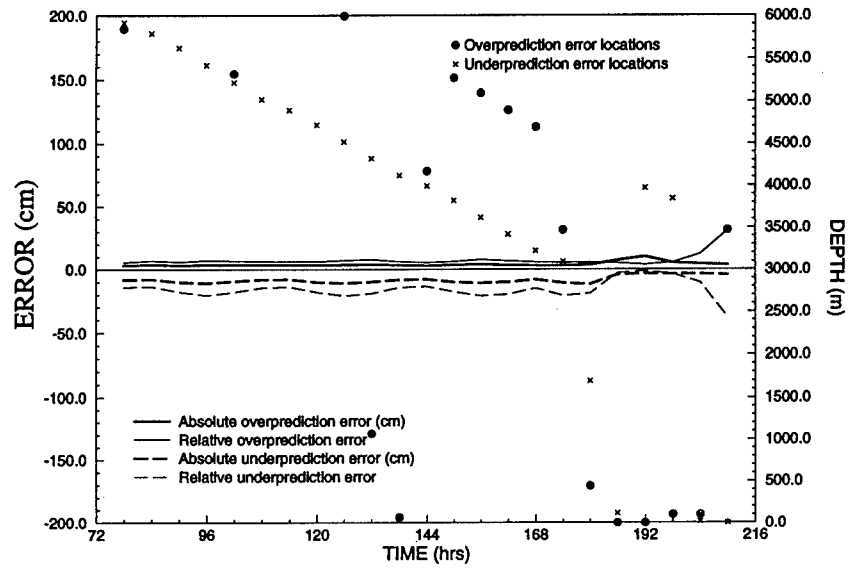

(c)

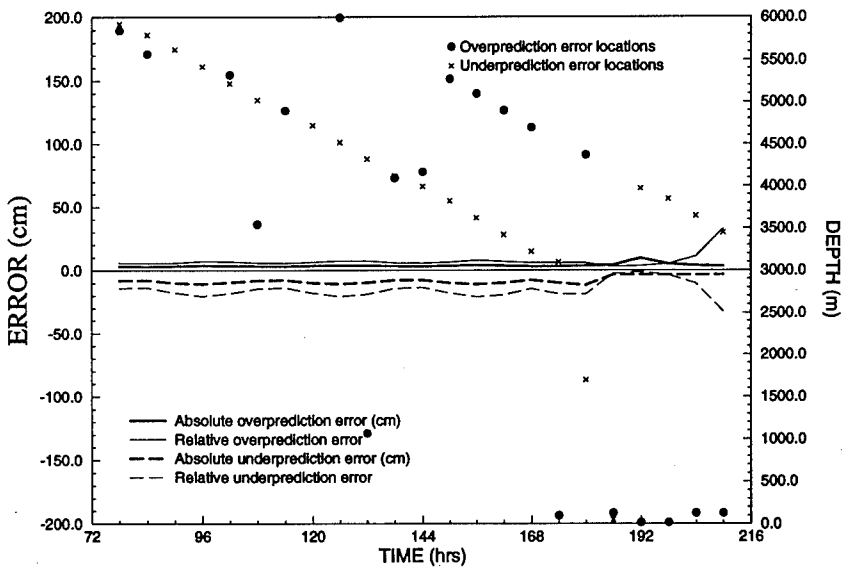

(d)

Figure 46. (Sheet 2 of 3)

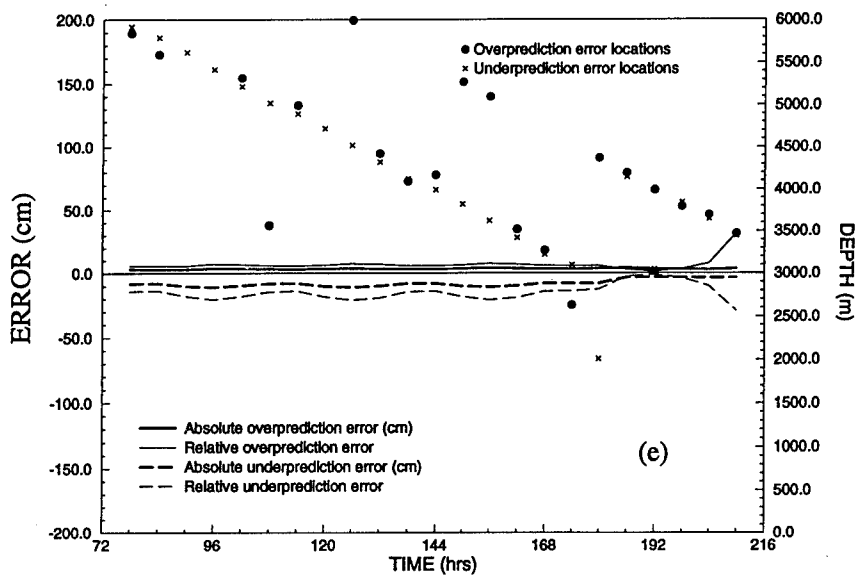

Figure 46. (Sheet 3 of 3)

maximum prediction errors shift to the continental slope. At the time of hurricane landfall, 192 hr, maximum errors move to the coastline. Unlike errors associated with grids G01 and G02, the increased refinement near the coastline in grid VG01 eliminates sizable errors at the coastline while the storm is over deeper waters. The resolution provided over graded grid VG01 reduces errors to an acceptable uniform level throughout the domain as seen in Figure 46c. Further discretization over the shelf leads to little change in the magnitude or location of prediction errors as seen in Figure 46d for grid VG02. Similar to the results presented for Hurricane H011 forcing, resolution over the entire shelf and beyond the shelf break shifts maximum errors back into the deep ocean as seen in Figure 46e for grid VG03. Error levels over grid VG03 during the 24-hr period surrounding the time of peak surge are reduced to magnitudes seen over deeper water.

Application of the meteorological forcing from Hurricane H013 over the Series 1 grid discretizations demonstrates the effect of an increased forward speed on grid resolution requirements. The forward speed of Hurricane H013 is approximately 1.5 times that of Hurricane H011. The storm surge hydrograph for Hurricane H013 in Figure 44c exhibits a peak surge which is much larger and occurs over a significantly shorter time period than the surge produced by Hurricane H011. As a result of the increased storm surge generation, the maximum over- and underprediction errors computed over each grid

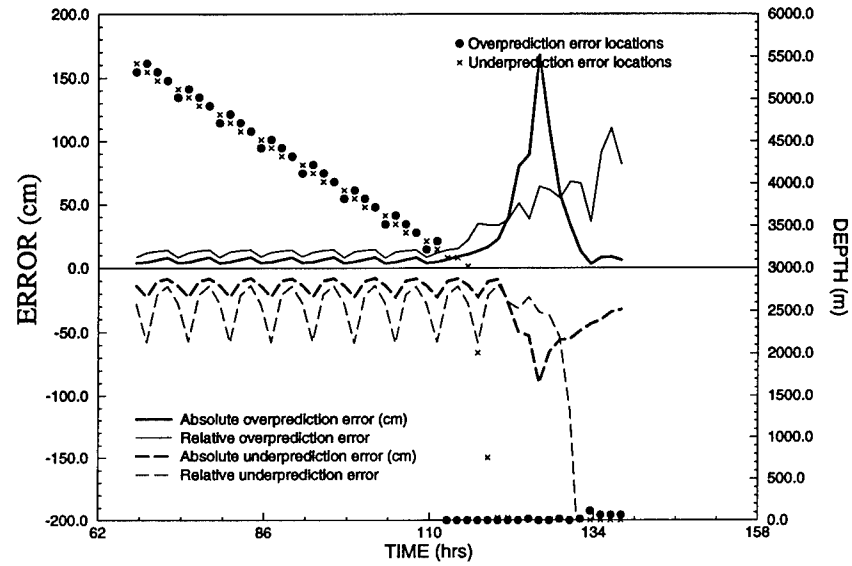

(a)

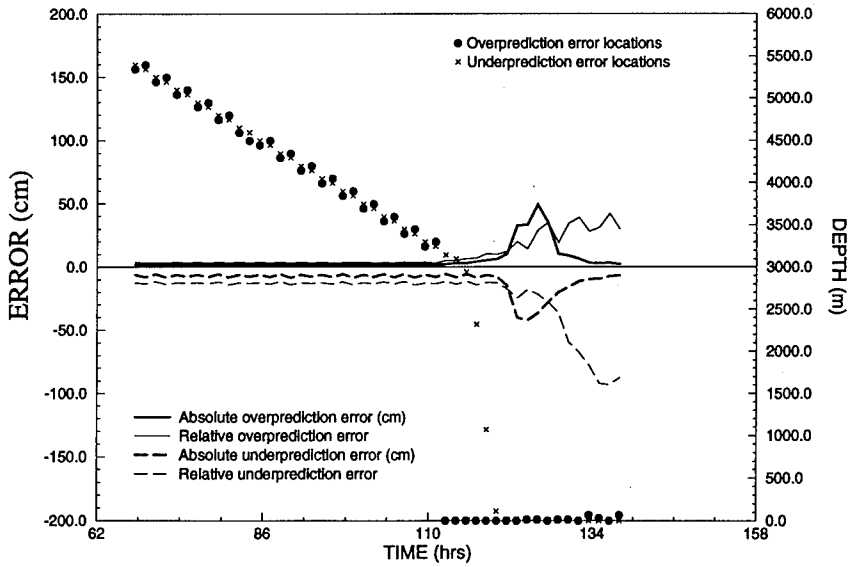

(b)

Figure 47. Maximum over-and underprediction errors of the storm surge generated by Hurricane H013 as computed over grids (a) G01, (b) G02, (c) VG01, (d) VG02, and (e) VG03 (Sheet 1 of 3)

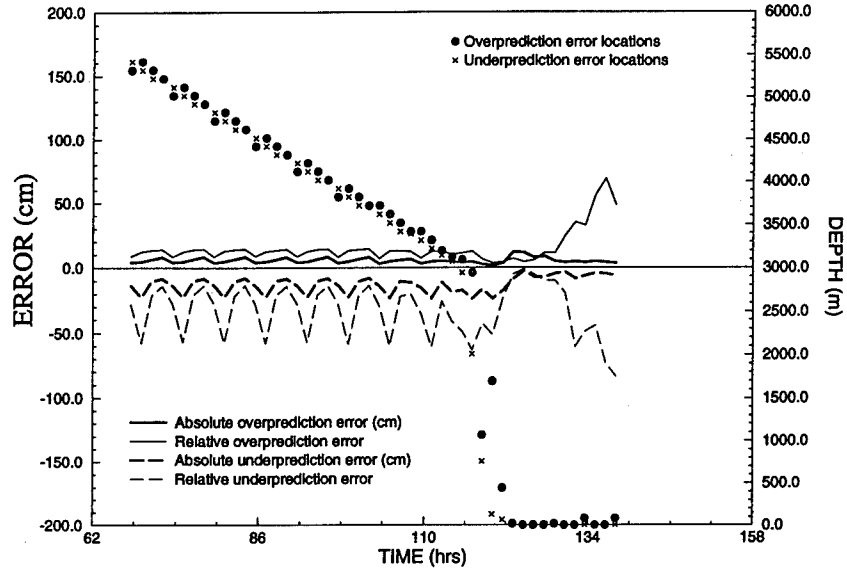

(c)

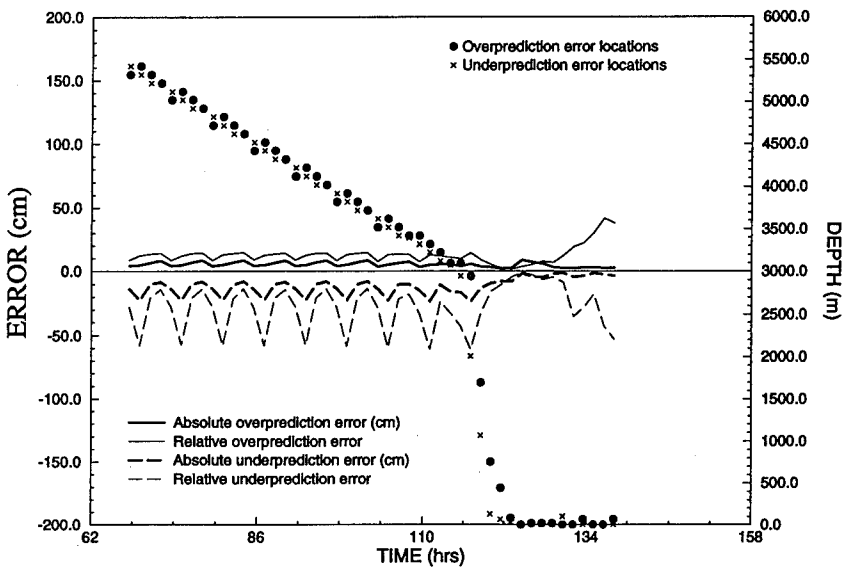

(d)

Figure 47. (Sheet 2 of 3)

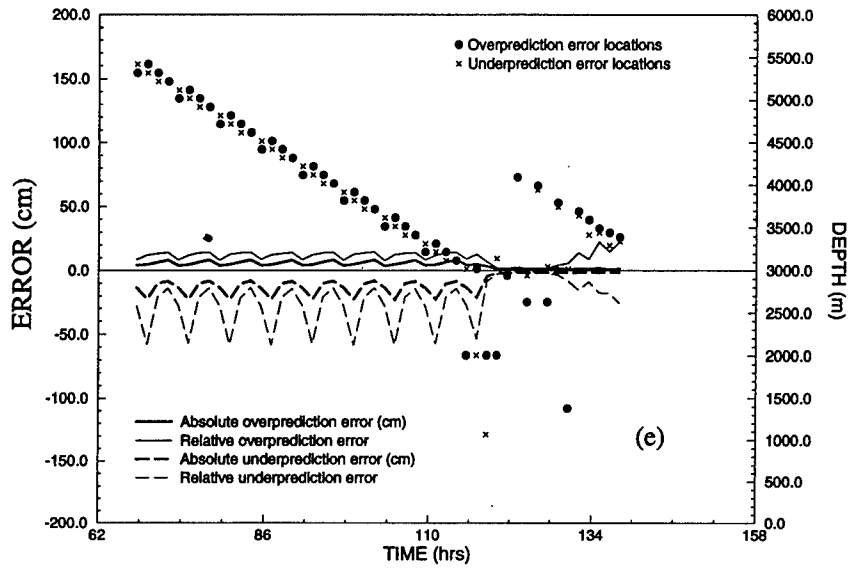

Figure 47. (Sheet 3 of 3)

in Series 1, shown in Figures 47a - 47e, deviate slightly upwards from the errors associated with Hurricane H011 over the same grids.

Since the spatial scale of Hurricane H013 is the same as that for Hurricane H011, errors occurring while the storm is in the deep ocean are similar to those reported for Hurricane H011 and indicate under-resolution of the inverted barometer effect in deep water. Maximum storm surge prediction errors over grids G01 and G02 occur at the shoreline 18 hr in advance of the storm entry onto the continental shelf at 128 hr. A reduction in grid spacing by a factor of 2 halves the errors in the deep ocean while on the continental shelf errors are diminished by a factor of 2 to 3 when comparing maximum errors relative to grids G01 and G02 shown in Figures 47a and 47b. Further reduction of the nodal spacing at the coastline in grid VG01 leads to errors which are diminished by more than a factor of 3 from those over grid G02 and the locations of these errors coincide with the path of the storm as it moves onto the continental shelf. Only minor differences are evident in a comparison of the magnitudes and locations of the maximum errors shown in Figures 47c and 47d for grids VG01 and VG02. The extension of maximum errors into deeper waters and the substantial reduction in the magnitude of the maximum error over grid VG03, shown in Figure 47e, indicate that errors over the continental slope may be more significant for the case of forcing by a relatively fast-moving hurricane.

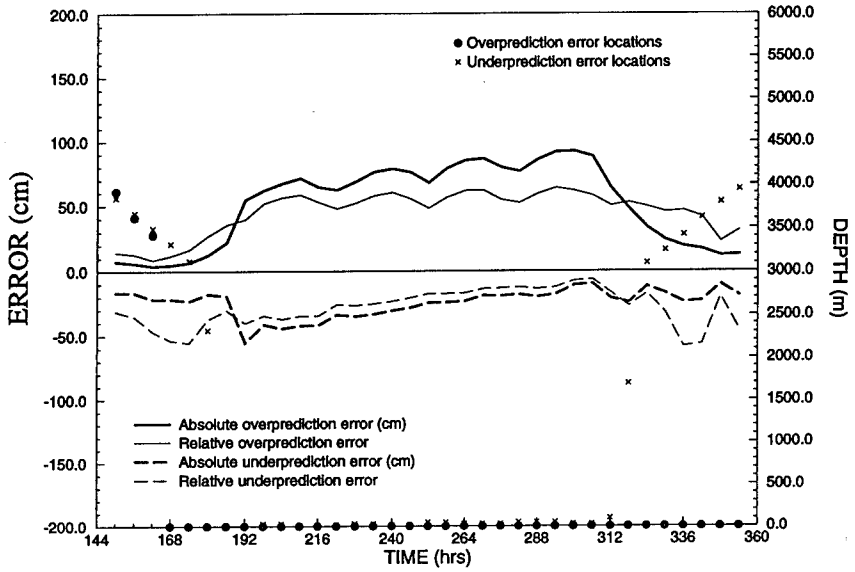

(a)

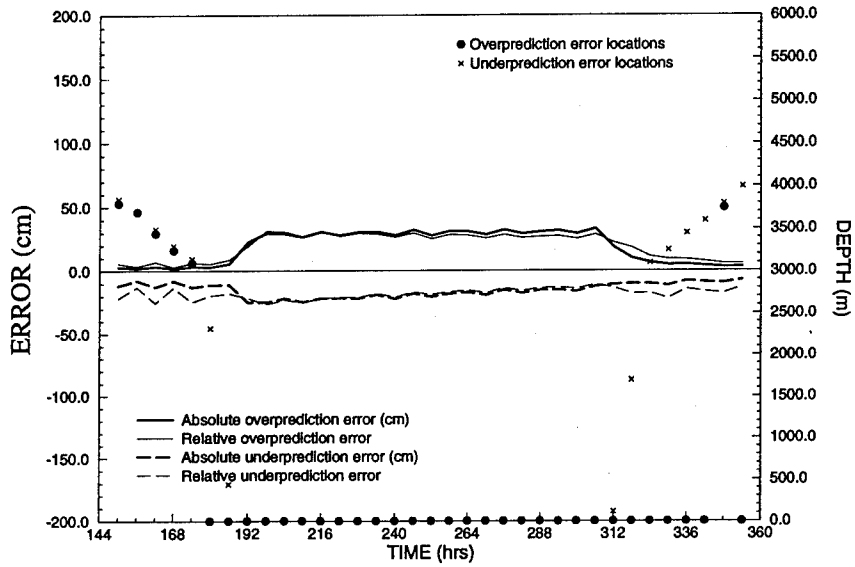

(b)

Figure 48. Maximum over- and underprediction errors of the storm surge generated by Hurricane H031 as computed over grids (a) G01, (b) G02, (c) VG01, (d) VG02, and (e) VG03 (Sheet 1 of 3)

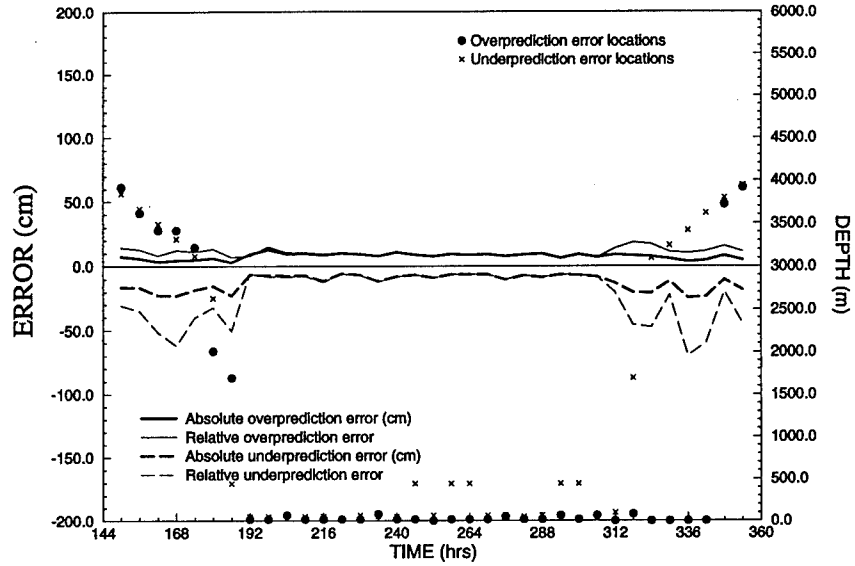

(c)

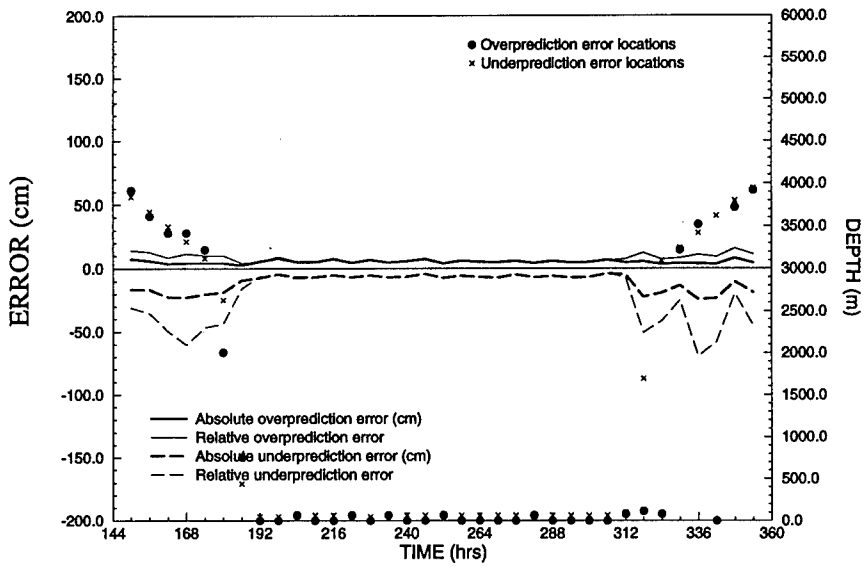

(d)

Figure 48. (Sheet 2 of 3)

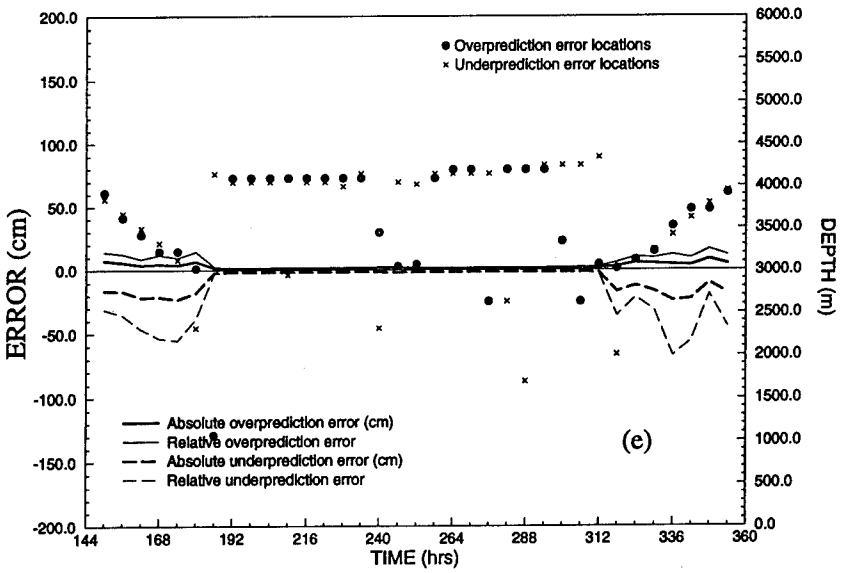

Figure 48. (Sheet 3 of 3)

Maximum errors computed over the grids in Series 1 for hurricane forcing which remains parallel to the coastline, Hurricane H031, are shown in Figures 48a - 48e. The maximum surge profile for Hurricane H031, depicted in Figure 44d, shows more sustained but reduced surge elevations. While the hurricane is in the deep ocean, errors computed over all grids are similar to those recorded for forcing by Hurricane H011. As seen in Figures 48a and 48b, which compare storm surge prediction errors over grids G01 and G02, the maximum error in deep waters decreases by a factor of 2 when grid spacing is halved. As the storm approaches the continental shelf, maximum errors over grids G01 and G02 are concentrated at the shoreline and remain there over 24 hr after the storm has returned to deeper waters. Generally, on the continental shelf absolute errors computed over the uniform grids G01 and G02 relative to H031 forcing are less than those experienced with respect to Hurricane H011 forcing. This observation is correlated to the decreased storm surge heights generated by Hurricane H031. Both the absolute and relative errors reduce threefold when nodal spacing is halved between grids G01 and G02.

Graded grid VG01, which has twice the resolution of grid G02 at the coastline, yields maximum prediction errors which are located primarily offshore as the storm moves parallel to the coastline as seen in Figure 48c. These errors have magnitudes which are one half the value of those computed over grid G02. While the storm is on the continental shelf, errors over grid VG02,

shown in Figure 48d, are essentially uniform and error magnitudes are reduced slightly from those associated with grid VG01. Additionally, the offshore locations of the maximum error are quite similar between grids VG01 and VG02. Upon finely resolving the entire shelf and slope, storm surge prediction errors are further reduced and their locations are shifted to the deep ocean as seen in Figure 48e for grid VG03. Generally, though, the level of resolution provided by grid VG02, which produces low uniform errors over the continental shelf, is satisfactory.

The maximum values of the computed errors over both the deep waters and continental shelf regions of the ocean are presented in Tables 7 - 10 for each grid in Series 1 relative to meteorological forcing from Hurricanes H011, H012, H013, and H031. The maximum error values recorded in Tables 7 - 10 relative to each hurricane forcing clearly exhibit the trends discussed previously when grid resolution is increased by a factor of two among grids G01, G02, and VG01. Over deep waters, a reduction of the grid spacing by half diminishes the error in the computed storm surge by a factor of two. On the continental shelf and in coastal regions, the error reduction is generally threefold. Maximum storm surge prediction errors computed over the variably graded grids are minimal and essentially uniform throughout the domain. Furthermore, differences in the errors associated with each of the graded grids VG01, VG02, and VG03 are often slight with regard to the error magnitudes.

Table 7
Maximum Errors Over Grid Series 1 for Hurricane H011

Grid	Overprediction				Underprediction			
	Absolute (cm)		Relative		Absolute (cm)		Relative	
	Deep	Shelf	Deep	Shelf	Deep	Shelf	Deep	Shelf
G01	4-9	153	10-18	59	8-22	68	12-51	61
G02	1-4	57	3-8	28	8-12	30	12-22	24
VG01	4-9	11	10-18	10	8-22	4	12-51	8
VG02	4-9	9	10-18	5	8-22	2	12-51	4
VG03	4-9	--	10-18	--	8-22	--	12-51	--

In comparing the errors among Tables 7 - 10 for different hurricane forcings, the relative improvement of the deep-ocean resolution for forcing by the more expansive storm, Hurricane H012, is evident. In Tables 8 and 9, the increased values of the maximum error associated with Hurricanes H012 and H013 are correlated to the significant storm surge generated by these hurricanes. Relative errors computed over each grid in Tables 7 - 10 are strikingly similar regardless of the hurricane forcing applied. This behavior of the relative error reinforces that resolution at the coastline, not the character of the hurricane forcing, is the predominate factor affecting the accurate prediction of hurricane storm surge.

Table 8
Maximum Errors Over Grid Series 1 for Hurricane H012

Grid	Overprediction				Underprediction			
	Absolute (cm)		Relative		Absolute (cm)		Relative	
	Deep	Shelf	Deep	Shelf	Deep	Shelf	Deep	Shelf
G01	2-4	179	6-8	52	8-11	94	12-21	122
G02	2	55	4	21	2-4	35	4-8	15
VG01	2-4	10	6-8	5	8-11	5	12-21	3
VG02	2-4	9	6-8	5	8-11	5	12-21	3
VG03	2-4	--	6-8	--	8-11	--	12-21	--

Table 9
Maximum Errors Over Grid Series 1 for Hurricane H013

Grid	Overprediction				Underprediction			
	Absolute (cm)		Relative		Absolute (cm)		Relative	
	Deep	Shelf	Deep	Shelf	Deep	Shelf	Deep	Shelf
G01	5-10	167	9-16	72	7-22	91	12-58	56
G02	2	52	4	37	4-9	41	10-12	28
VG01	5-10	11	9-16	9	7-22	9	12-58	60
VG02	5-10	9	9-16	8	7-22	9	12-58	6
VG03	5-10	--	9-16	--	7-22	--	12-58	--

Table 10
Maximum Errors Over Grid Series 1 for Hurricane H031

Grid	Overprediction				Underprediction			
	Absolute (cm)		Relative		Absolute (cm)		Relative	
	Deep	Shelf	Deep	Shelf	Deep	Shelf	Deep	Shelf
G01	4-8	95	9-15	65	23	57	58	40
G02	2-4	32	4-8	31	8-12	27	12-25	28
VG01	4-8	32	9-15	20	23	12	69	12
VG02	4-8	9	9-15	15	23	29	69	9
VG03	4-8	--	9-15	--	23	--	69	--

Series 2 Comparisons: G01_C1, G02_C1

The second series of grid comparisons examines the influence of a spatially varying shoreline. The two grids studied, G01_C1 and G02_C1, have uniform spacings of 50 km (31.1 statute miles) and 25 km (15.5 statute miles), respectively, and use a 5-point-per-wavelength representation of the sinusoidal coastline. Maximum overprediction and underprediction errors computed relative to forcing by Hurricane H011 are shown in Figures 49a and 49b. Errors computed while the storm is in the deep ocean are similar to those computed over grids using a straight-line coast indicating that the influence of the coastline does not extend past the continental shelf. At 156 hr, prior to the storm entry onto the shelf, the overprediction errors computed with respect to grid G01_C1 (Figure 49a) are already located at the coastline. Absolute error values computed over both grid G01_C1 and grid G02_C1 are nearly twice the value of those errors computed over grids having the same domain discretization but without spatial coastline variations; i.e., grids G01 and G02. The sinusoidally varying coastline magnifies the storm surge elevations generated at the shore. In comparing grid G01_C1 to grid G02_C1, a reduction in the grid spacing by a factor of 2 leads to a fourfold decrease in the absolute errors at the coastline. Relative errors are similar in magnitude to those computed over grids G01 and G02 in Series 1. Table 11 records the maximum overprediction and underprediction error values for the two grids in Series 2 subject to forcing by Hurricane H011.

Series 3 Comparisons: G03_C1, G02_C1

The impact of coastline resolution is examined by considering the storm surge errors produced when comparing a 5-point to a 17-point-per-wavelength resolution of the sinusoidally varying coastline (i.e., a comparison between grids G03_C1 and G03_C3) and by comparing a 5-point to a 9-point-per-wavelength resolution of the sinusoidally varying coastline (i.e., a comparison between grids G02_C1 and G02_C2). The applied meteorological forcing is from Hurricane H011. Since each of the grids compared has identical and fine discretizations everywhere except at the coastline, errors throughout the domain are negligible, as seen in Figures 50a and 50b. At the coastline, however, over- and underprediction errors have extreme magnitudes ranging from 20 cm to 40 cm, (0.6 ft to 1.3 ft), as seen in Table 12, which summarizes the maximum error values for the Series 3 grid comparisons. The discrepancy between storm surge predictions made using different coastline representations clearly illustrates the importance of coastline resolution in the accurate prediction of hurricane storm surge.

Series 4 Comparisons: G01_C1, G02_C2, VG01_C3, VG02_C3, VG03_C3

The Series 4 grid comparisons include the influences of grid spacing, spatial coastline variation, and coastline resolution on storm surge prediction. The

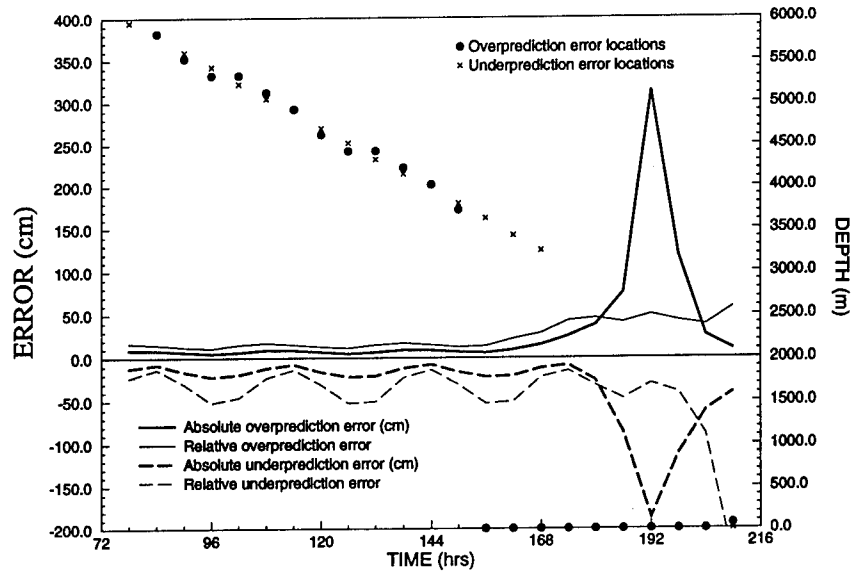

(a)

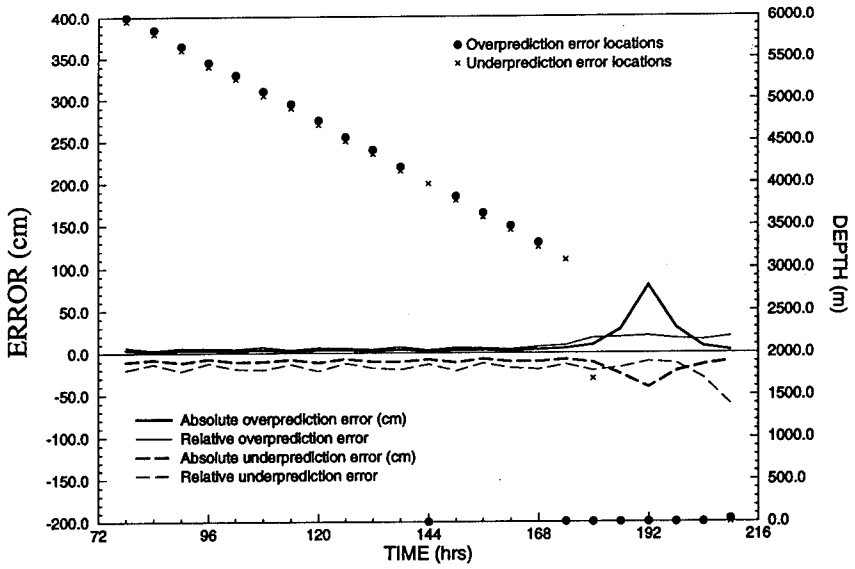

(b)

Figure 49. Maximum over- and underprediction errors of the storm surge generated by Hurricane H011 as computed over grids (a) G01_C1, and (b) G02_C1

Table 11
Maximum Errors Over Grid Series 2 for Hurricane H011

Grid	Overprediction				Underprediction			
	Absolute (cm)		Relative		Absolute (cm)		Relative	
	Deep	Shelf	Deep	Shelf	Deep	Shelf	Deep	Shelf
G01_C1	4-9	320	10-18	53	8-22	188	12-51	71
G02_C1	1-4	80	3-8	21	8-12	41	12-22	19

storm surge generated by each of the four synthetic hurricanes is simulated over all grids in Series 4. The maximum errors in computed storm surge are presented for Hurricane H011 forcing in Figures 51a - 51e, for Hurricane H012 forcing in Figures 52a - 52e, for Hurricane H013 forcing in Figures 53a - 53e, and for Hurricane H031 forcing in Figures 54a - 54e. Analysis of the overprediction and underprediction errors reconfirms the general observations noted in the grid comparisons for Series 1-3. Namely, while the storm is in the deep ocean, prediction errors exhibit a variably aliased behavior indicating under- resolution of the inverted barometer forcing as well as the wind forcing function. For the larger scale storm, Hurricane H012, the relative deep-ocean resolution is essentially halved in comparison to the size of the storm and consequently, errors are reduced twofold as seen in Figures 52a and 52b.

A sinusoidally varying coastline amplifies the absolute errors computed over the uniform grids G01_C1 and G02_C2 to at least twice the value of the errors computed over the straight-line coast grids G01 and G02 (see Figures 51a and 51b; 52a and 52b; 53a and 53b; 54a and 54b). As grid spacing over the uniform grids is cut by a factor of 2, the absolute and relative errors in computed storm surge are reduced twofold in the deep ocean and as much as three times over the continental shelf. Relative maximum errors remain similar in magnitude to those reported in the Series 1 grid comparisons as seen in Tables 13 - 16 which present the maximum error values for each grid in Series 4 subject to forcing from the four synthetic hurricanes. Generally, though, the magnitude of the errors for the Series 4 grid comparisons are somewhat elevated over the error magnitudes recorded for the Series 1 comparisons.

The effect of spatial variation at the shoreline is an increased generation and accumulation of water along the coast. The variably graded discretization of grid VG01_C3, which includes a highly resolved coastline, leads to a decrease in the magnitude of the prediction errors over the continental shelf by a factor of 2 to 3 as seen in Tables 13 - 16. This reduction in error is due to the combination of a finely discretized coastline and the doubling of resolution near the shore to 12.5 km (see Figures 51c, 52c, 53c, and 54c). Despite the diminished prediction errors, error magnitudes over grid VG01_C3 remain at unacceptable levels between 20 and 30 cm. Over graded

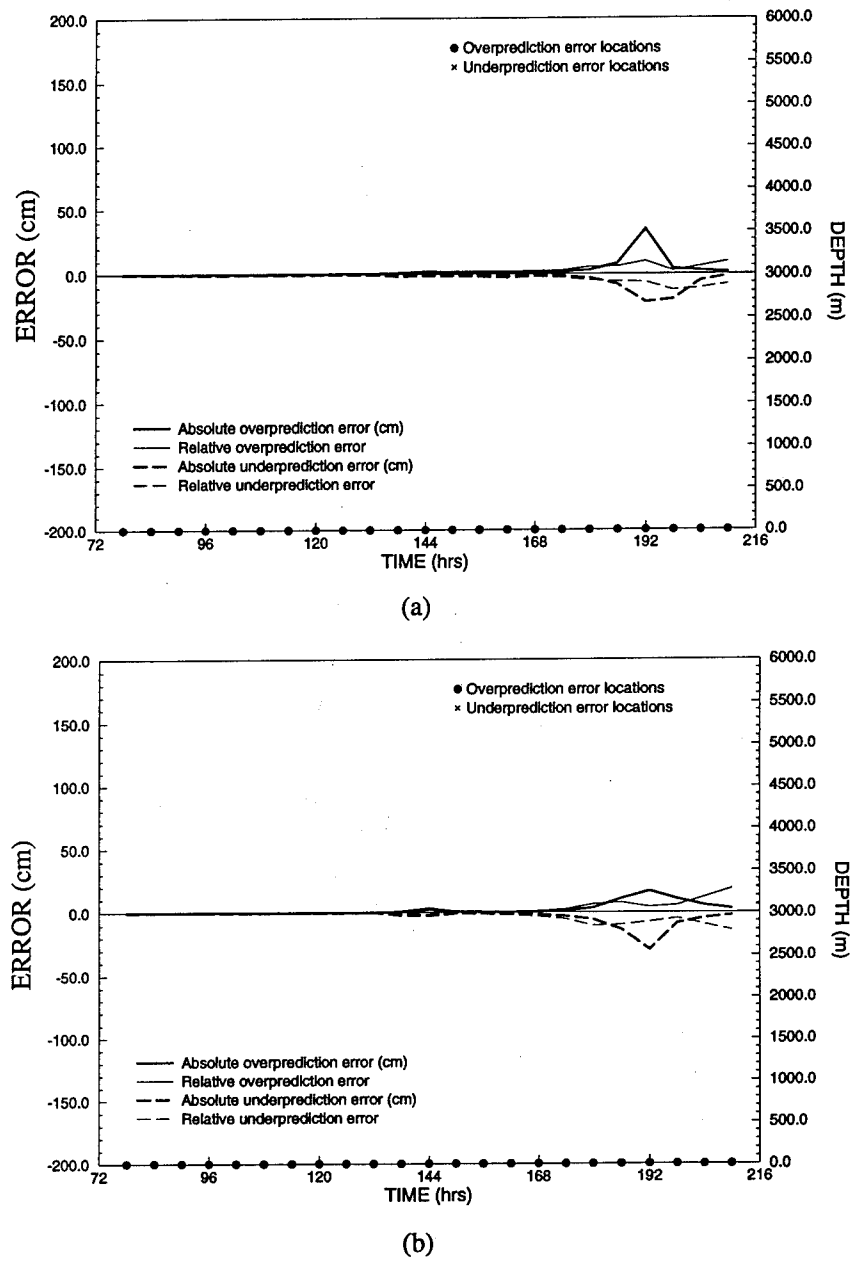

Figure 50. Maximum over- and underprediction errors of the storm surge generated by Hurricane H011 as computed over grids (a) G03_C1, and (b) G02_C1 when compared to grids G03_C3 and G02_C2, respectively

Table 12
Maximum Errors Over Grid Series 3 for Hurricane H011

Grid	Overprediction				Underprediction			
	Absolute (cm)		Relative		Absolute (cm)		Relative	
	Deep	Shelf	Deep	Shelf	Deep	Shelf	Deep	Shelf
G03_C1	--	38	--	11	--	21	--	12
G02_C1	--	18	--	8	--	30	--	10

grids VG02_C3 and VG03_C3, maximum prediction errors are further reduced from the levels computed over VG01_C3, but error magnitudes at the coastline remain significant. While the storms are on the continental shelf, computed errors over grid VG03_C3 persist at the coastline unlike the deepwater locations of the prediction errors computed relative to the straight coastline graded grid, VG03. Upon resolution of the shelf, shelf break, and portions of the continental slope, it has been previously shown that errors over grid VG03 shifted to deep waters, whereas errors over grid VG03_C3 remain predominately at the coastline. For each of the hurricane forcings applied in the Series 4 grid comparisons, storm surge prediction errors persist at the coastline regardless of the discretization strategy. Thus, the grid comparisons in Series 4 conclusively demonstrate that the spatial variation of the coastline dominates the generation of storm surge. Resolution of and around the shoreline is critical for accurate prediction of hurricane storm surge.

Conclusions

A study of the influence of grid structure on hurricane storm surge prediction demonstrates that discretization of the computational domain can significantly affect the storm surge elevation computed in the coastal region. A decrease in mesh spacing by a factor of 2 halves the errors over the deep ocean and results in a two- to threefold reduction of errors in the coastal region for the storms studied. This relationship between errors in the computed storm surge and mesh spacing is observed until error magnitudes stabilize and are relatively uniform throughout the domain. At this point, storm surge predictions over a particular grid discretization are considered acceptable within a defined error limit. Over the deep ocean, errors in the predicted storm surge are minimized by using a nodal spacing which is approximately one half the spatial scale of the hurricane. In coastal areas, significant refinement both of the coastline geometry and nearshore regions is necessary to eliminate excessive error in storm surge predictions. Determination of the exact grid spacing required in coastal areas depends primarily on the complexity of the coastline detail and the extent of very shallow waters.

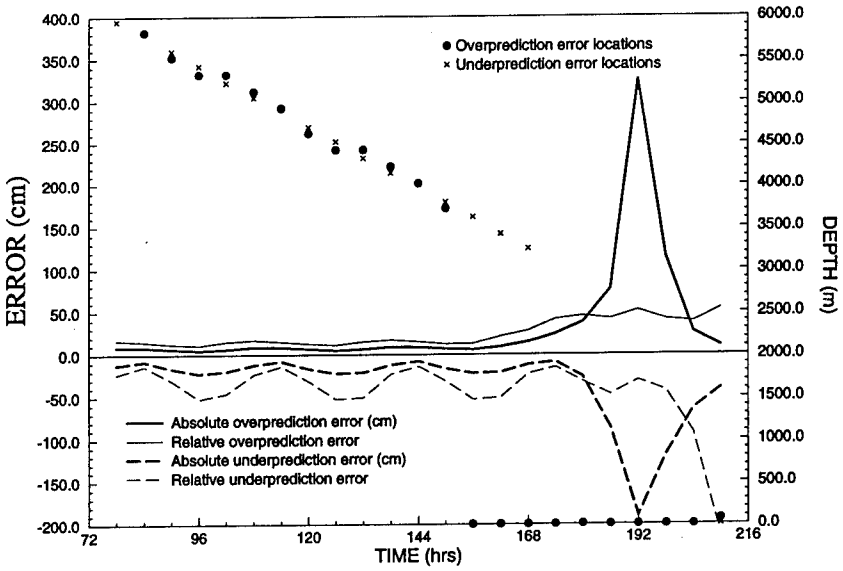

(a)

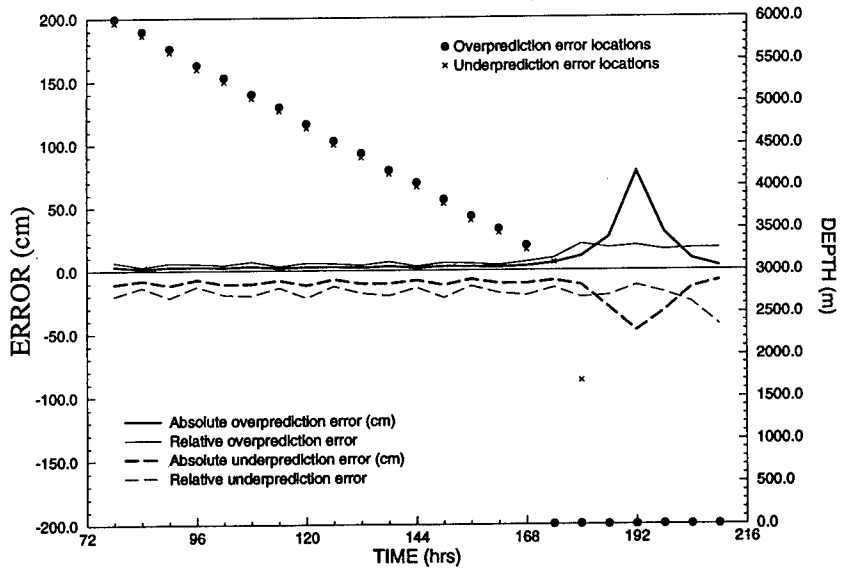

(b)

Figure 51. Maximum over- and underprediction errors of the storm surge generated by Hurricane H011 as computed over grids (a) G01_C1, (b) G02_C2, (c) VG01_C3, (d) VG02_C3, and (e) VG03_C3 (Sheet 1 of 3)

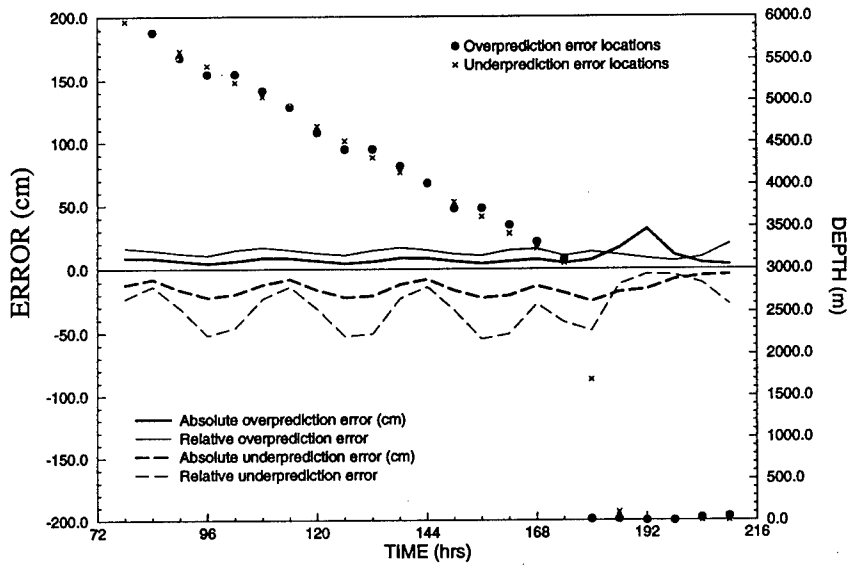

(c)

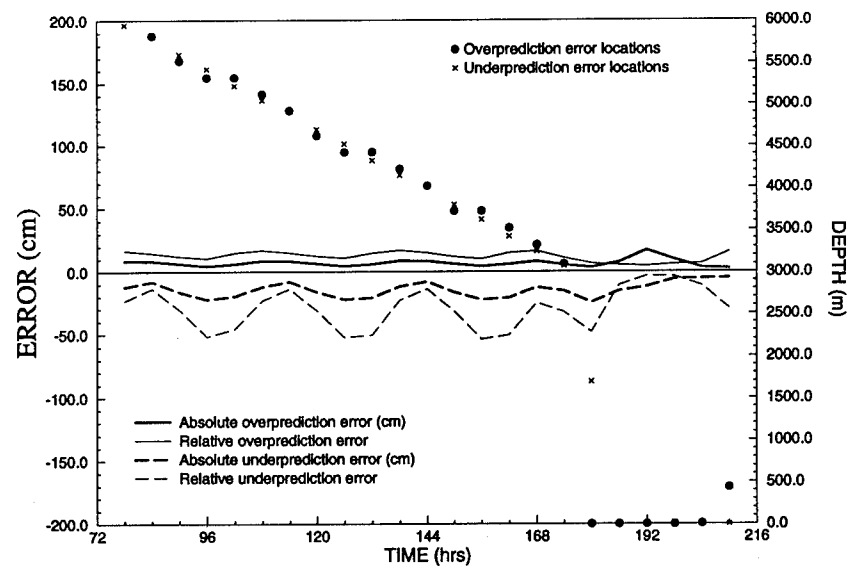

(d)

Figure 51. (Sheet 2 of 3)

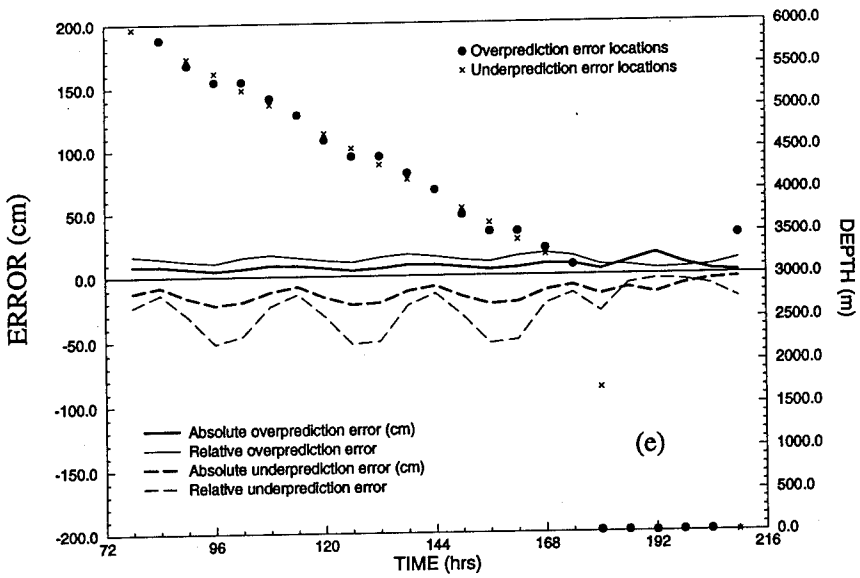

Figure 51. (Sheet 3 of 3)

High levels of resolution over the continental shelf break and slope do not appear to be necessary for the storm surge calculations performed in this nonresonant basin grid structure study. Rather, the finest level of resolution is needed adjacent to the coast in shallow waters. Furthermore, refinement of the coastline detail is shown to be very important for accurate prediction of storm surge elevations. Significant errors are recorded when coastline detail alone is under-resolved.

In relation to the parameters of hurricane forcing (i.e., path, forward velocity, and spatial scale) resolution near the coastline is still the most significant factor in storm surge computations. Faster moving and/or larger storms magnify the errors in under-resolved regions of the domain, particularly near the coast. One possible exception is for storms which track parallel to the coastline. In addition to the generation of storm surge at the coast, these storms produce significant surge elevations over the entire continental shelf and slope. As a result, higher resolution of the continental shelf break and slope may improve storm surge predictions for hurricanes approaching along a path parallel to the shoreline. The level of resolution required over the continental shelf and slope will depend on the areal extent of the storm and the relative position of the path to the shelf break.

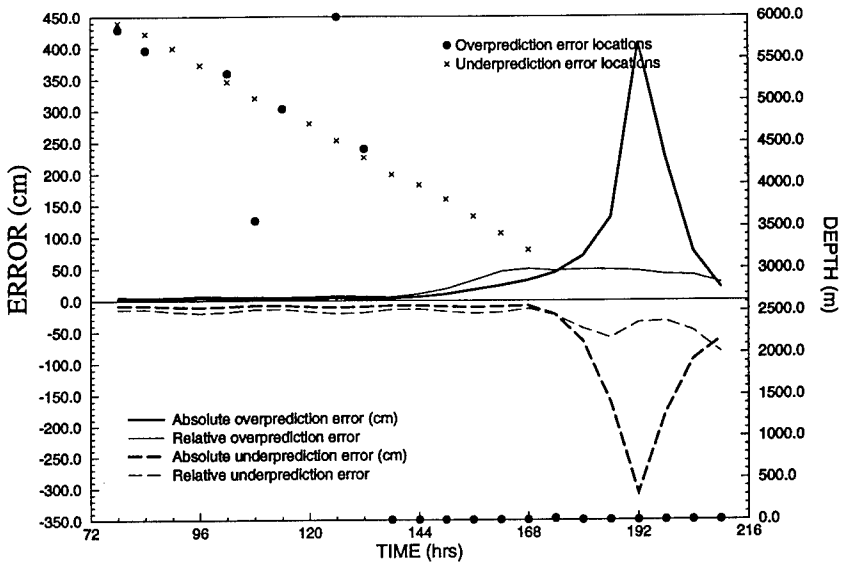

(a)

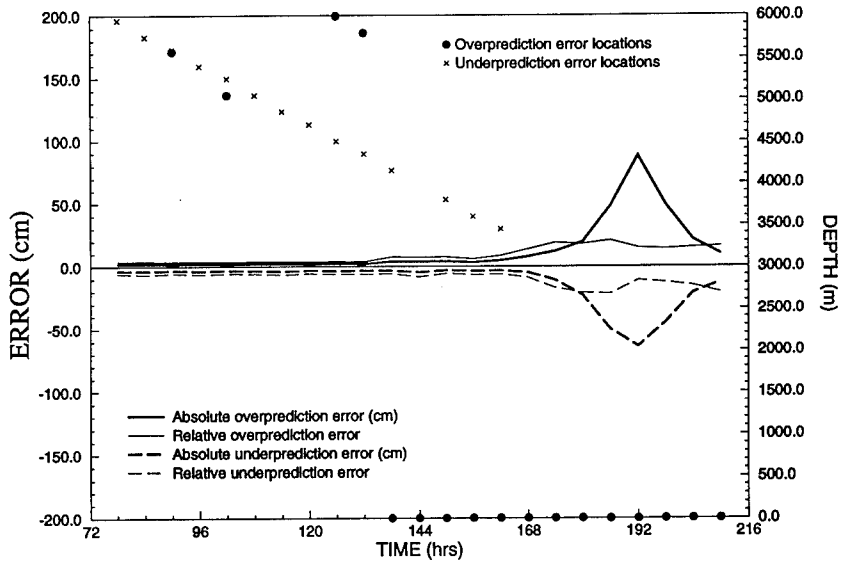

(b)

Figure 52. Maximum over- and underprediction errors of the storm surge generated by Hurricane H012 as computed over grids (a) G01_C1, (b) G02_C2, (c) VG01_C3, (d) VG02_C3, and (e) VG03_C3 (Sheet 1 of 3)

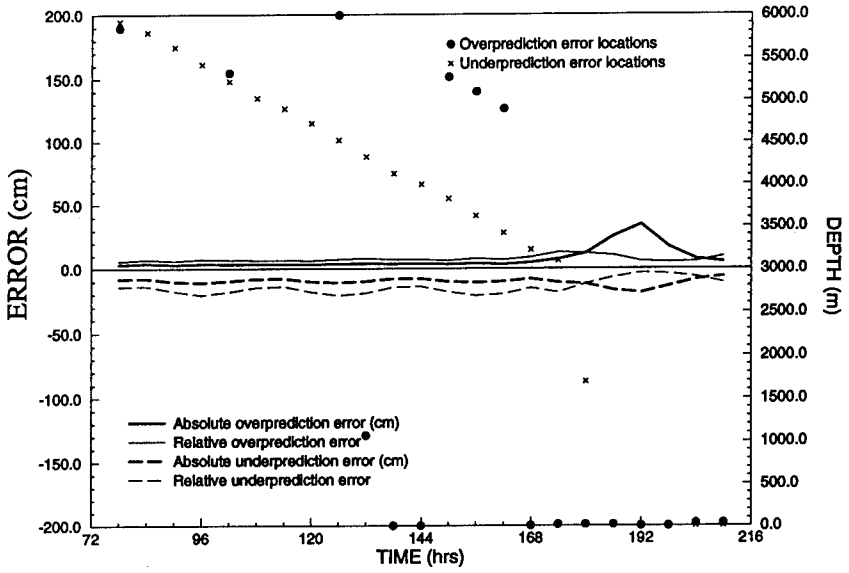

(c)

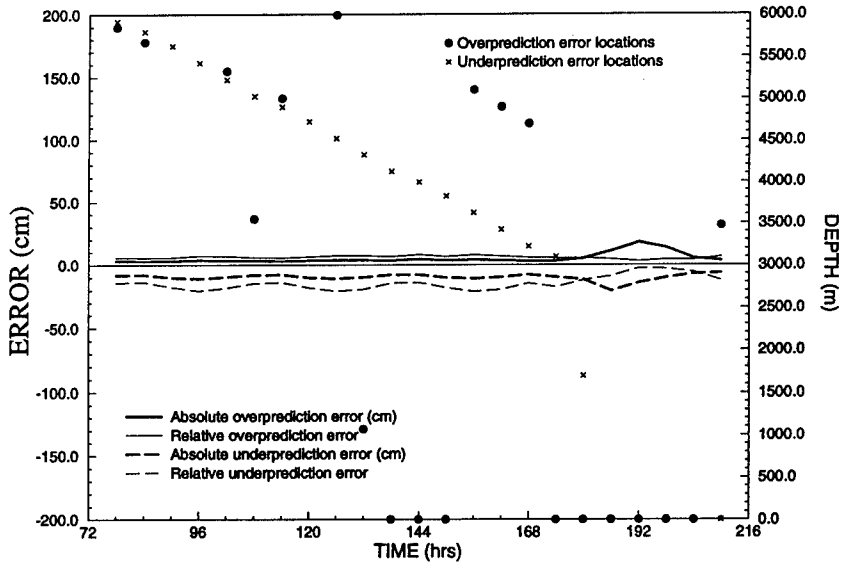

(d)

Figure 52. (Sheet 2 of 3)

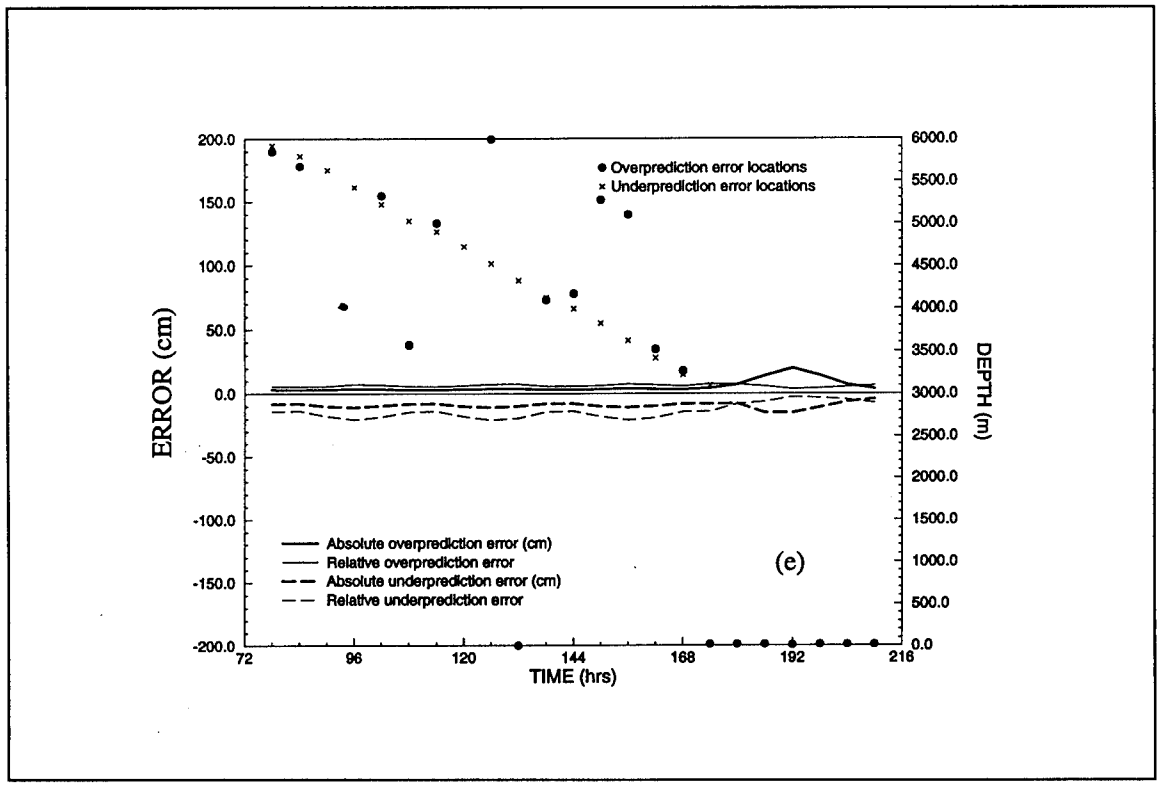

Figure 52. (Sheet 3 of 3)

The disparity between grid resolution requirements in the deep ocean and coastal regions suggests that a variably graded grid structure is most appropriate. For the grid study and error analyses conducted, a variable grid structure which has extensive refinement in the nearshore region leads to low uniform errors throughout the domain. Since discretization errors can never be completely eliminated, uniform errors over a grid are desired. Even more importantly, errors in the prediction of storm surge generation near the land and on the continental shelf must be minimized. An appropriate grid discretization is constructed by considering the phenomenon of interest (i.e., primary surge and/or resonant mode behavior), the accuracy constraints for storm surge predictions in the region of interest, desired error levels throughout the remainder of the domain, and computational effort.

In addition to providing low uniform errors over the domain, the variable grid structure requires minimum computational effort which is particularly noticeable when implemented in conjunction with large domains. The flexibility of the finite element approach used to discretize the grids within this study leads to easy incorporation of coastline detail and nodal densities which range over an order of magnitude. The variation in nodal density arises from the significant refinement provided in shallow coastal areas where storm surge generation is important and in regions of complex coastline detail and/or bathymetric change, in conjunction with the coarse discretizations over the deep ocean where processes occur more gradually and are of less interest.

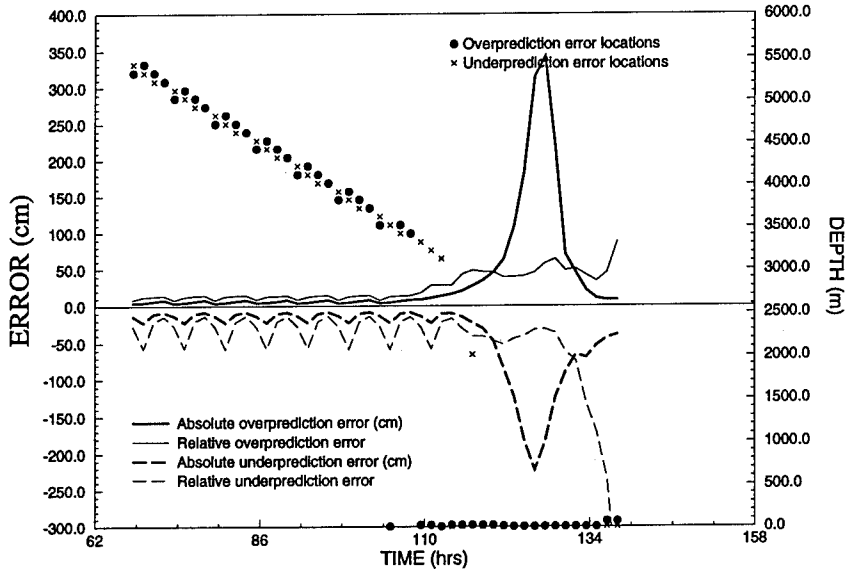

(a)

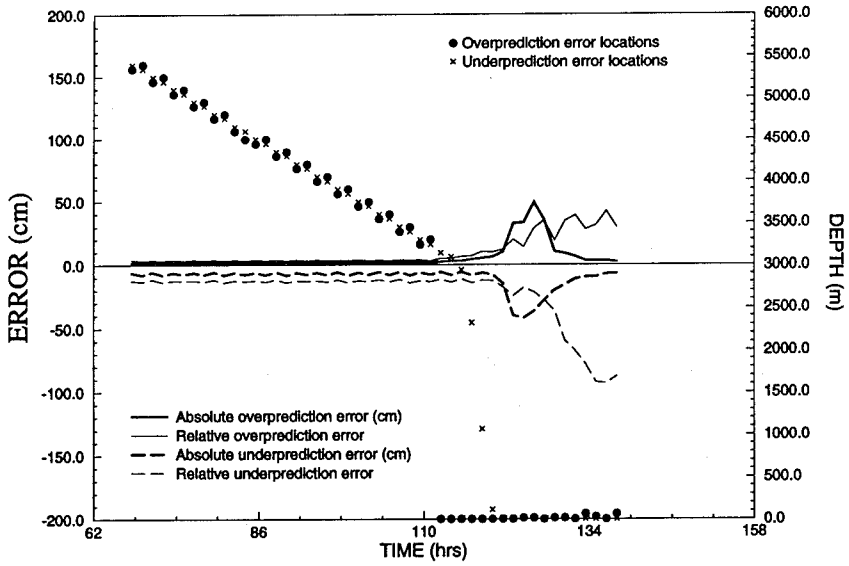

(b)

Figure 53. Maximum over- and underprediction errors of the storm surge generated by Hurricane H013 as computed over grids (a) G01_C1, (b) G02_C2, (c) VG01_C3, (d) VG02_C3, and (e) VG03_C3 (Sheet 1 of 3)

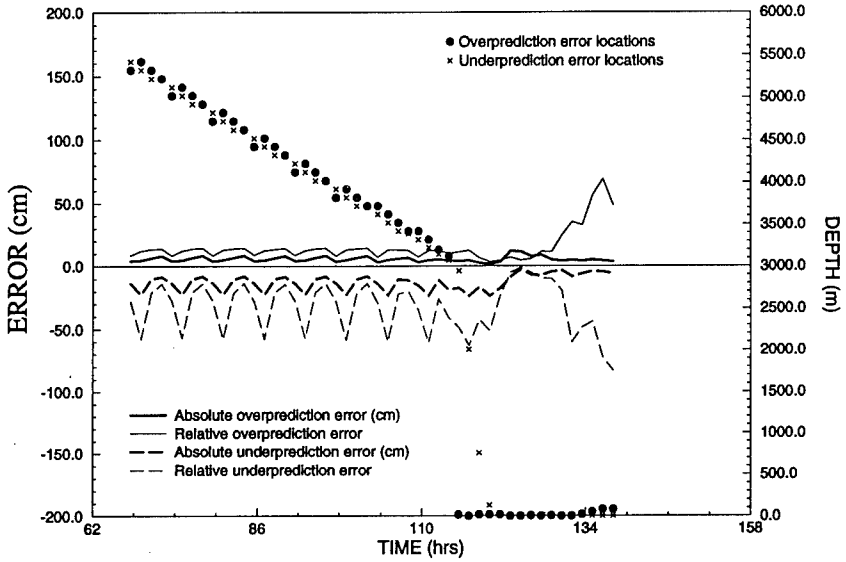

(c)

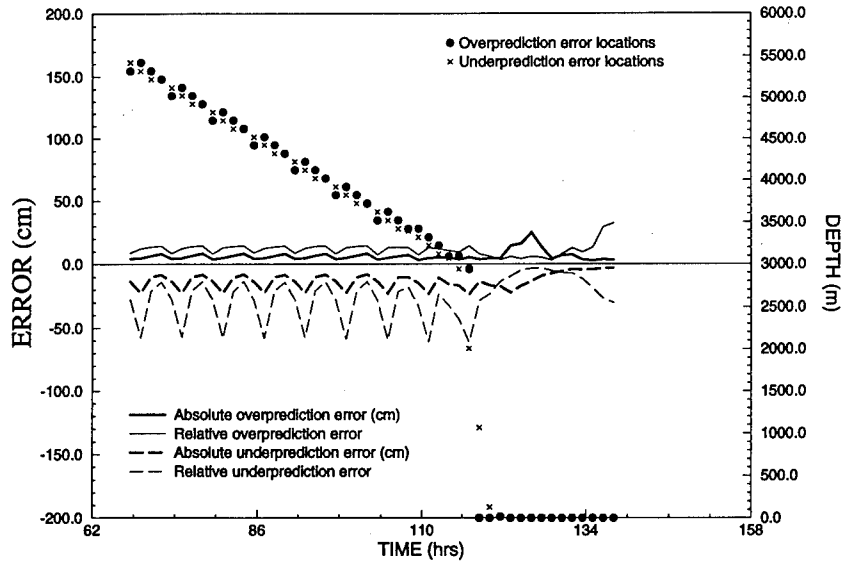

(d)

Figure 53. (Sheet 2 of 3)

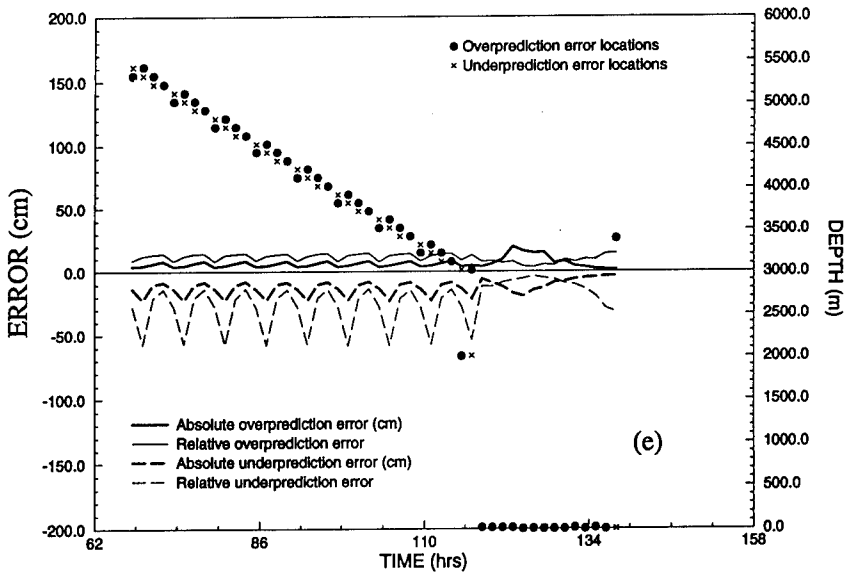

Figure 53. (Sheet 3 of 3)

Implementation of a graded grid discretization over large domains, coupled with the efficiency of the finite element method, leads to a discrete problem that remains well within computational limits.

Furthermore, the error analysis procedure implemented to assess the quality of predicted storm surge elevations offers a straightforward means to evaluate the performance of a particular grid discretization. The magnitude and location of errors in the computed storm surge are readily obtained and can assist in the construction of an optimal grid structure which yields accurate storm surge predictions.

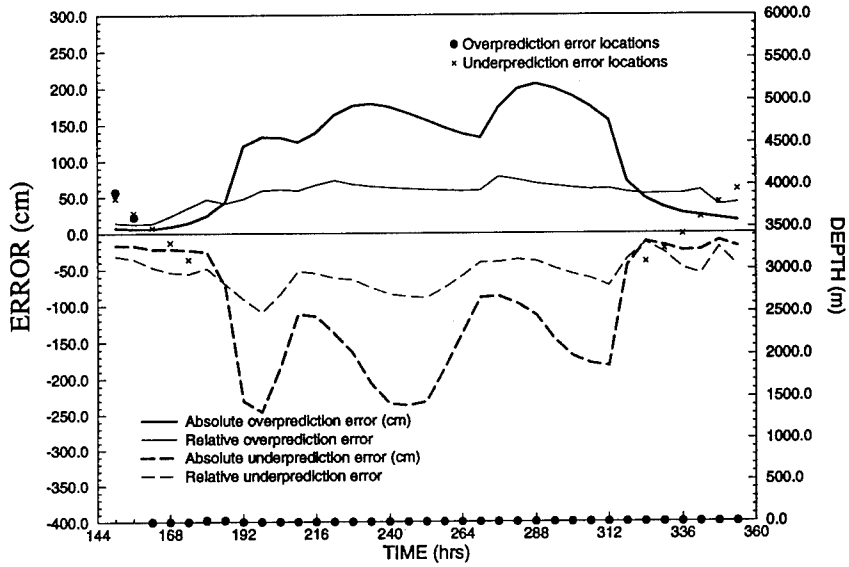

(a)

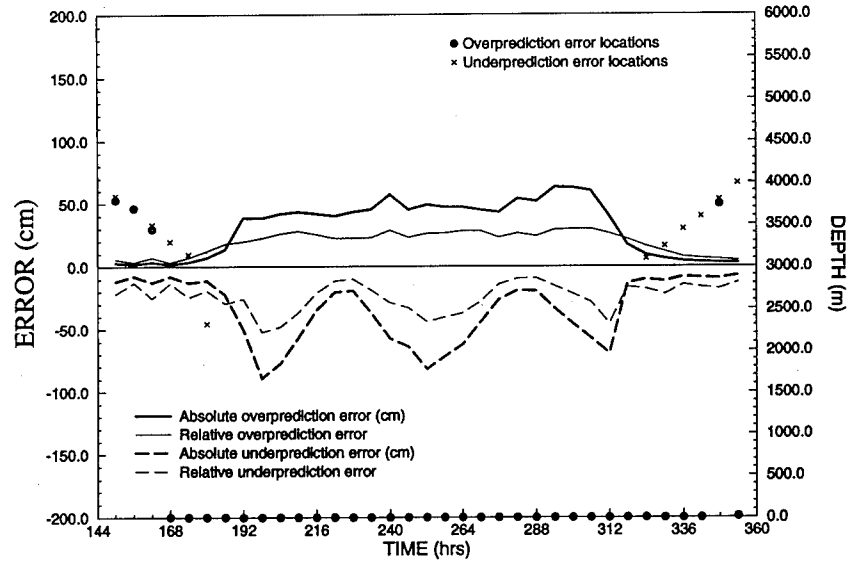

(b)

Figure 54. Maximum over- and underprediction errors of the storm surge generated by Hurricane H031 as computed over grids (a) G01_C1, (b) G02_C2, (c) VG01_C3, (d) VG02_C3, and (e) VG03_C3 (Sheet 1 of 3)

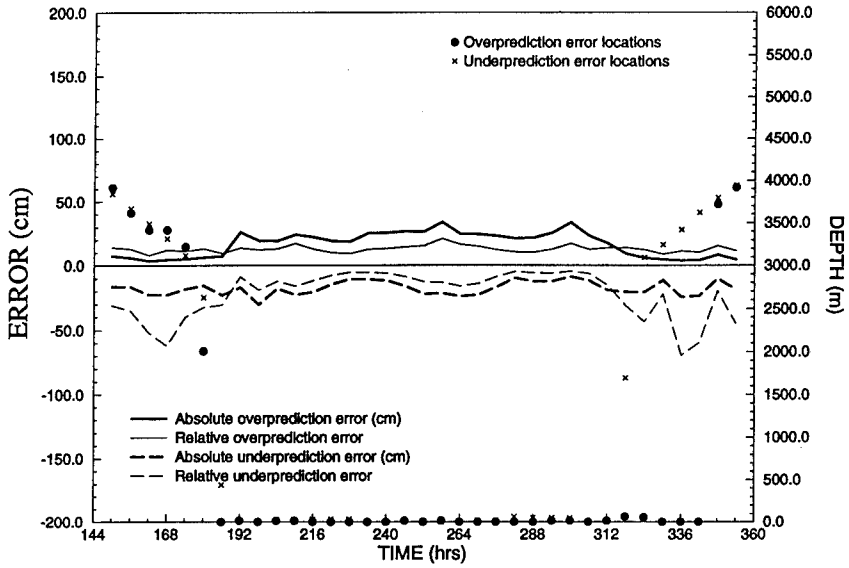

(c)

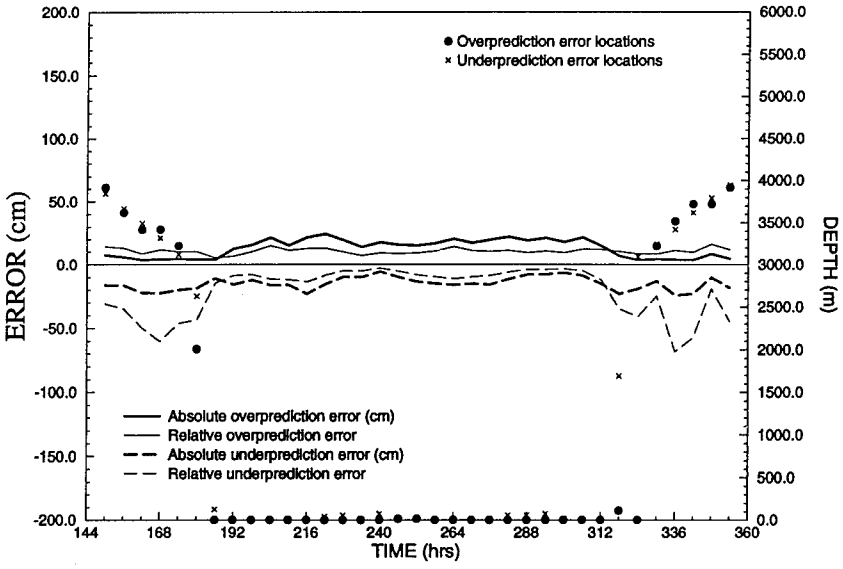

(d)

Figure 54. (Sheet 2 of 3)

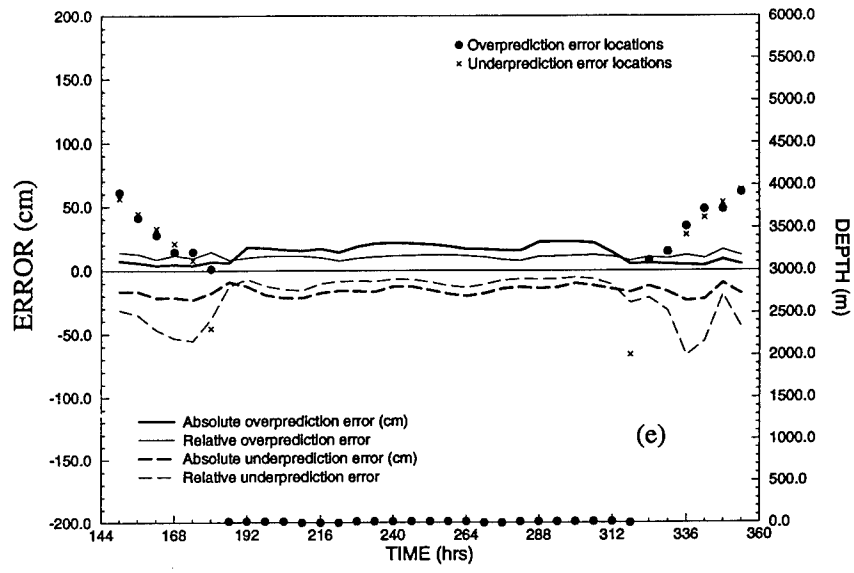

Figure 54. (Sheet 3 of 3)

Table 13
Maximum Errors Over Grid Series 4 for Hurricane H011

Grid	Overprediction				Underprediction			
	Absolute (cm)		Relative		Absolute (cm)		Relative	
	Deep	Shelf	Deep	Shelf	Deep	Shelf	Deep	Shelf
G01_C1	4-9	331	10-18	53	8-22	191	12-51	80
G02_C2	1-4	80	3-8	20	8-12	48	12-22	20
VG01_C3	4-9	32	10-18	21	8-22	20	12-51	11
VG02_C3	4-9	19	10-18	7	8-22	17	12-51	11
VG03_C3	4-9	19	10-18	7	8-22	14	12-51	6

Table 14
Maximum Errors Over Grid Series 4 for Hurricane H012

Grid	Overprediction				Underprediction			
	Absolute (cm)		Relative		Absolute (cm)		Relative	
	Deep	Shelf	Deep	Shelf	Deep	Shelf	Deep	Shelf
G01_C1	2-4	413	6-8	48	8-11	310	12-21	60
G02_C2	2	92	4	21	2-4	63	4-8	21
VG01_C3	2-4	34	6-8	12	8-11	19	12-21	7
VG02_C3	2-4	17	6-8	6	8-11	21	12-21	10
VG03_C3	2-4	20	6-8	8	8-11	16	12-21	7

Table 15
Maximum Errors Over Grid Series 4 for Hurricane H013

Grid	Overprediction				Underprediction			
	Absolute (cm)		Relative		Absolute (cm)		Relative	
	Deep	Shelf	Deep	Shelf	Deep	Shelf	Deep	Shelf
G01_C1	5-10	346	9-16	68	7-22	227	12-58	71
G02_C2	2	81	4	22	4-9	89	10-12	40
VG01_C3	5-10	40	9-16	16	7-22	21	12-58	8
VG02_C3	5-10	28	9-16	13	7-22	21	12-58	18
VG03_C3	5-10	21	9-16	11	7-22	20	12-58	10

Table 16
Maximum Errors Over Grid Series 4 for Hurricane H031

Grid	Overprediction				Underprediction			
	Absolute (cm)		Relative		Absolute (cm)		Relative	
	Deep	Shelf	Deep	Shelf	Deep	Shelf	Deep	Shelf
G01_C1	4-8	205	9-15	75	23	246	58	109
G02_C2	2-4	62	4-8	29	8-12	90	12-25	53
VG01_C3	4-8	34	9-15	21	23	31	69	20
VG02_C3	4-8	25	9-15	15	23	23	69	13
VG03_C3	4-8	22	9-15	12	23	21	69	17

6 Application of Domain Size and Gridding Strategy

The domain size sensitivity study and the investigation of grid resolution effects have established several guidelines for selection of a domain and construction of the domain discretization associated with a numerical storm surge model.

To properly represent the generation and propagation of storm surge into coastal areas, a very large domain is required. This domain includes the coastal region of interest, contiguous basins, and extends out of resonant basins into the deep open ocean. A domain of this size allows proper setup of resonant modes/surge forerunner. Furthermore, specification of elevations at the open ocean boundary is simplified and has little perceptible influence on the model response in coastal regions.

An optimal discretization of the domain assumes a graded structure with a high level of resolution provided in near coastal regions. Nodal spacing in the deep ocean is less dense and should approximate one half the spatial scale of the hurricane forcing. Significant coastline detail must be included in the discretization as well if accurate storm surge predictions are to result.

An application of the numerical modeling strategy just outlined with respect to domain size and grid structure is presented. Forcing from two historical hurricanes is applied over a large domain having a variably graded grid discretization. Errors in the storm surge predicted over this grid discretization are identified by comparison to a "truth" grid solution. The "truth" grid for these applications no longer has uniform mesh spacing but is a variably graded discretization, defined by a fourfold refinement of the resolution provided in the original study grid. Differences between storm surge elevations computed over the study grid and the "truth" grid are examined to determine the magnitude and location of the maximum storm surge prediction errors. Spatial distributions of prediction errors are also utilized to assess the performance of the study grid in accurately representing the storm surge response in coastal regions.

The applications presented demonstrate the utility of the large domain and graded grid structure advocated for use in conjunction with numerical storm

surge models. Furthermore, the procedure applied to assess the level of grid convergence with respect to storm surge computations is easily implemented and can be used effectively to assist in the construction of an optimal grid discretization.

Domain and Grid Construction

Two historical hurricanes, Kate (November 1985) and Camille (August 1969), will serve as the meteorological forcing for these storm surge model applications. Details regarding the paths and characteristics of Hurricanes Kate and Camille are specified in Chapter 3. Each of these hurricanes made landfall at points along the Gulf of Mexico coast in the United States (i.e., Hurricane Kate at Panama City, FL, and Hurricane Camille near Biloxi, MS).

An appropriate domain, then, is one that centers on regions surrounding Biloxi, MS, and Panama City, FL, but also includes the Gulf of Mexico basin and extends into the deep regions of the western North Atlantic Ocean. The domain selected is based on the east coast domain, which encompasses the western North Atlantic Ocean, the Caribbean Sea, and the Gulf of Mexico as described and used in Chapter 4. The inclusion of greater coastline detail in the region of Biloxi, MS, shown in Figure 55, (e.g. the addition of Lake Pontchartrain, Louisiana west of Biloxi, MS) is the only change made to the east coast domain. The deep Atlantic Ocean boundary remains along the 60 °W meridian and all other boundaries are defined by the eastern coastlines of North, Central, and South America. Topography within the domain is the same as that of the east coast domain except in the region surrounding Biloxi, MS. In this area, bathymetry has been updated using the National Oceanic and Atmospheric Administration Digital U.S. Coastal Hydrography sounding database. Recall from the description of the east coast domain that the continental shelf has depths ranging from an imposed minimum between 3 m (10 ft) and 7 m (23 ft) to 130 m (426 ft) at the shelf break, the continental slope has a typical depth range of 130 m to 3,000 m (426 ft to 9,840 ft), and depths of the continental rise and deep ocean increase upwards from 3,000 m (9,840 ft) to nearly 8,000 m (26,240 ft).

Having defined the model domain, a discrete representation of the domain, grid SG01, is constructed using 23,566 nodes and 43,238 elements. The variably graded structure of the SG01 grid discretization yields nodal spacings that range from a maximum of 98 km (60.9 statute miles) in the deep ocean to a minimum of 0.5 km (0.3 statute miles) near coastal areas. A map depicting the distribution of grid resolution provided throughout the domain of grid SG01 is shown in Figure 56. As demonstrated in the study of grid structure in Chapter 5, capturing the inverted barometer effect of the hurricane over deep waters requires a level of resolution which is at least one half the spatial scale of the hurricane. Throughout the period of simulation, Hurricane Camille maintains a large spatial scale of approximately 80 km (49.7 statute miles).

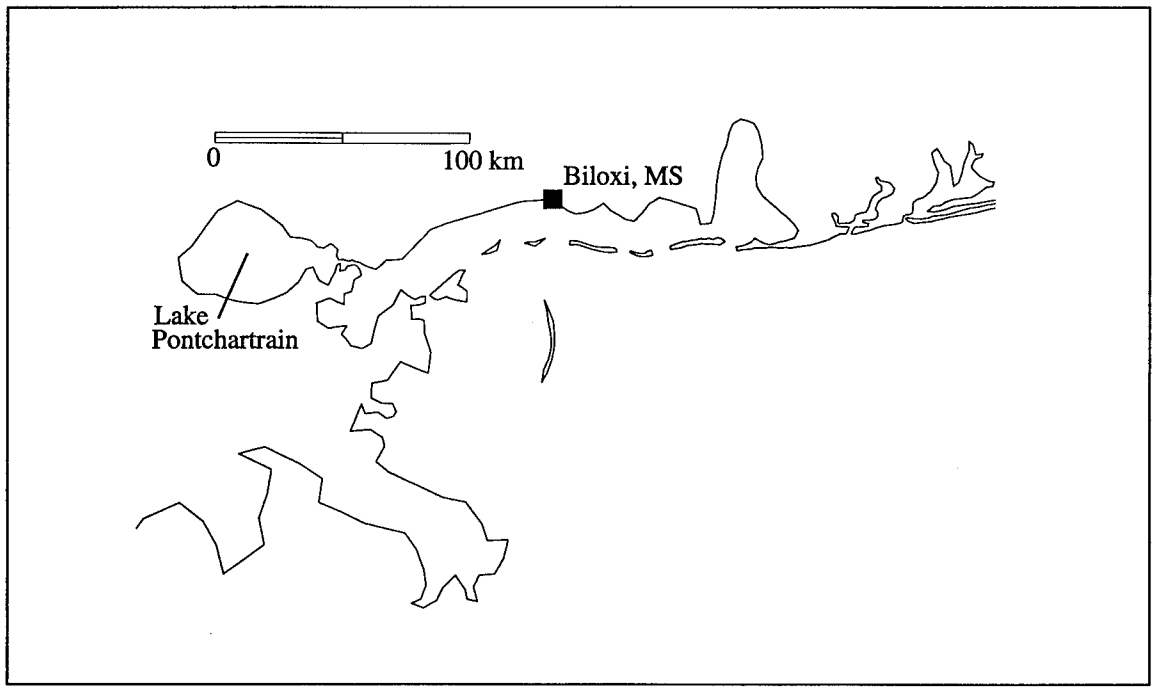

Figure 55. Region of coastline detail surrounding Biloxi, MS, which has been added to the east coast domain used throughout Chapter 4

The tracking of Hurricane Camille begins near Cuba and follows a path over the Gulf of Mexico where the maximum grid spacing is approximately 40 km (24.8 statute miles). Thus, over deep waters, the resolution provided for Hurricane Camille is indeed half the spatial scale of the hurricane.

For Hurricane Kate, the spatial scale of the storm over the deep ocean is highly variable and ranges from 20 km to 80 km (12.4 statute miles to 49.7 statute miles). During the initial 18 hr of Hurricane Kate over the deep western North Atlantic Ocean, grid spacing in the vicinity of the path of Hurricane Kate is between 50 km (31.1 statute miles) and 60 km (37.3 statute miles). Consequently, during this period, the inverted barometer effect associated with the pressure forcing of Hurricane Kate is under-resolved. However, as Hurricane Kate moves towards Cuba, grid spacing rapidly decreases to 30 km (18.6 statute miles) or less and at entrances to the Gulf of Mexico and Caribbean Sea (which are important for resonant mode set-up), the grid spacing drops to 15 km (9.3 statute miles) and below. Except for very deep portions of the western North Atlantic Ocean, the spatial scale of Hurricane Kate is generally well resolved using the discretization provided by grid SG01.

Another consideration in the construction of a grid is the representation of the coastline. Coastline detail plays an important role in the generation of storm surge. Results from the grid sensitivity study in Chapter 5 clearly demonstrate that representation of the shoreline contour is critical to achieving accurate computations of hurricane storm surge. Highly detailed shoreline

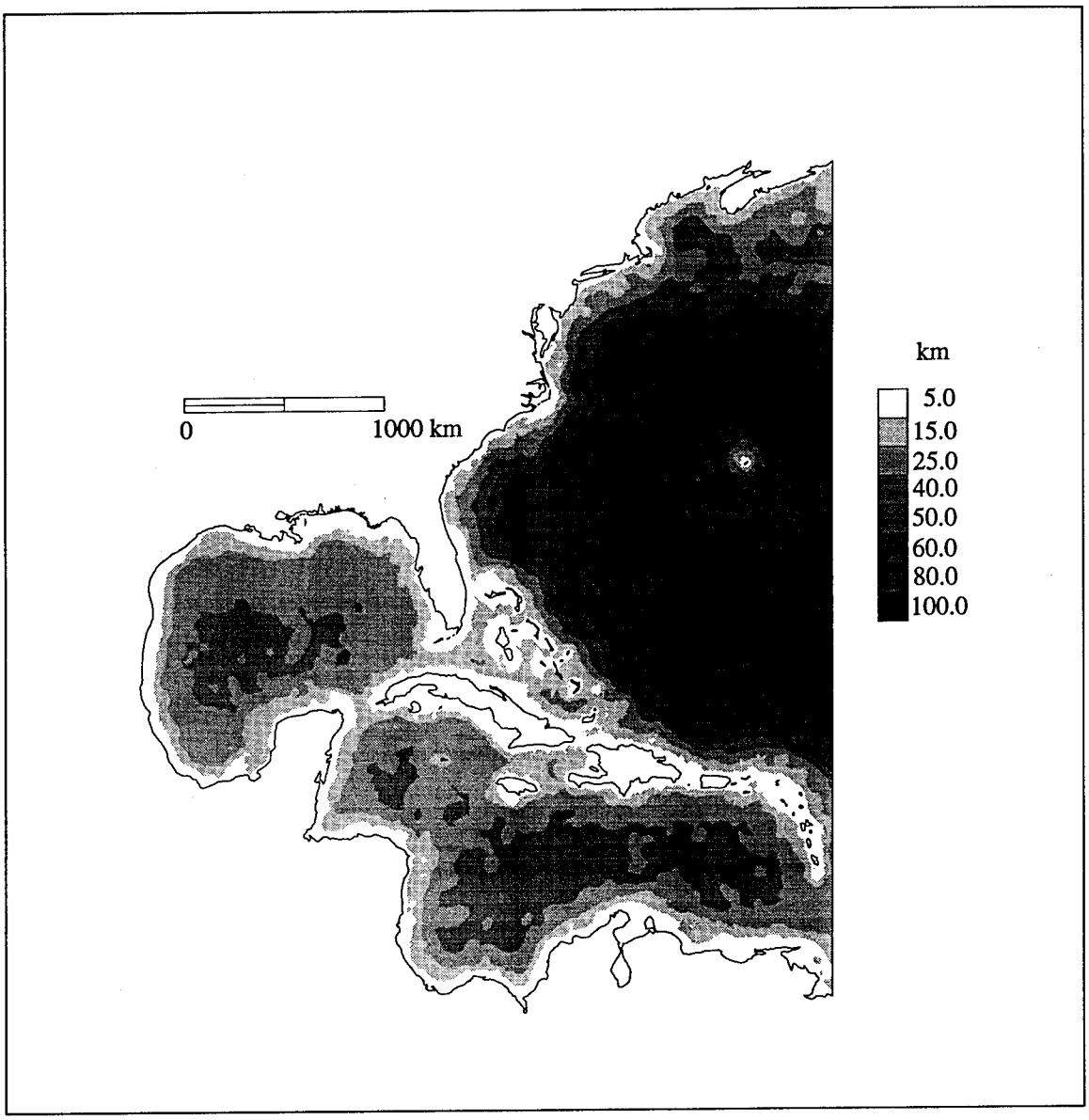

Figure 56. Distribution of nodal spacing, in kilometers, over grid SG01

coordinates obtained from the CIA database and NOAA bathymetric charts are used to define the shoreline profile of grid SG01 along the gulf coast. The representation of coastline detail and the discretization associated with grid SG01 in the gulf coast region near the vicinity of hurricane landfall locations are shown in Figure 57. A map of grid spacing for this same region is presented in Figure 58. In the near-shore regions of grid SG01, grid spacing ranges from 0.5 km (0.3 statute miles) to 2 km (1.2 statute miles). The finest resolution in Figure 58 is located at the entrances to inlets, where setup of exchange processes with the coastal ocean is important. Over a majority of the continental shelf, the grid resolution is less than 5 km (3.1 statute miles).

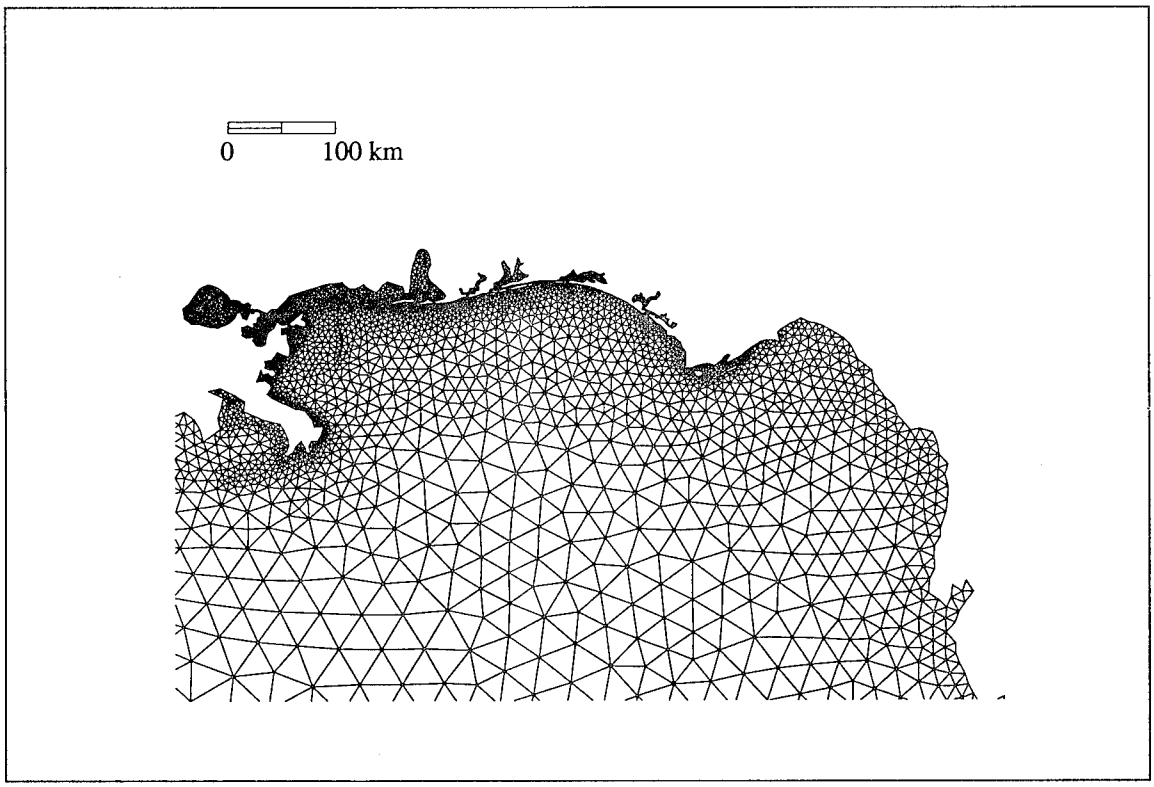

Figure 57. Coastline detail and discretization for gird SG01 in the northeast Gulf of Mexico

For the grid convergence analysis which follows, a highly refined "truth" grid (CG01) is also constructed. The discretization of grid CG01 is comprised of 90,435 nodes and 172,952 elements, exactly a fourfold increase of the grid resolution provided over grid SG01. Storm surge predictions over grid SG01 will be compared to computations over grid CG01 to determine the relative accuracy of storm surge elevations computed over grid SG01.

Storm Surge Simulations

A series of simulations were conducted to investigate the performance of the selected domain size and the grid discretization strategy implemented for the prediction of hurricane storm surge. Computations were made over grids SG01 and CG01, previously discussed. Hurricane Camille and Hurricane Kate are used separately as the wind and pressure forcing over the entire model domain. Along the open ocean boundary, an inverted barometer pressure forcing is applied. Simulations performed using Hurricane Kate as forcing implement a fully nonlinear model formulation with the exception of the finite amplitude terms. These terms are not included in the simulations because of instabilities caused by near-drying elements in coastal areas. For the case of Hurricane Camille, the model formulation eliminates all nonlinearities except the bottom friction terms. The magnitude of the surge generated by Hurricane Camille in conjunction with instabilities in the convective terms

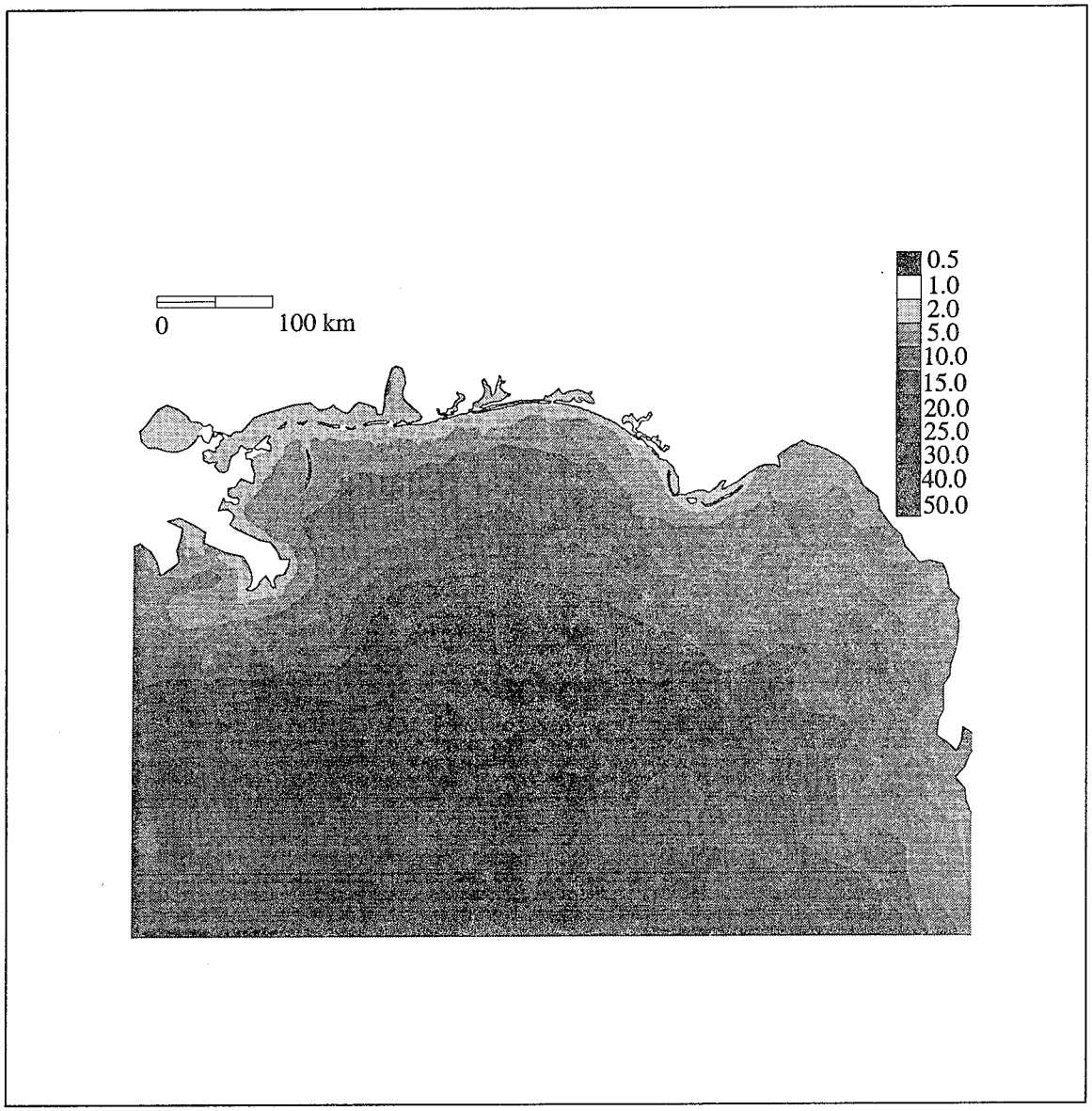

Figure 58. Distribution of nodal spacing in kilometers over grid SG01 in the northeast Gulf of Mexico

computed over grid CG01 have led to this formulation. As in prior simulations, model parameters are specified such that the bottom friction coefficient is constant and equal to 0.003 and the GWCE parameter τ_0 is defined equal to 0.001.

Simulations are spun up from homogeneous initial conditions using a 1-day ramp in time. Application of the hyperbolic ramp function reduces the excitation of nonphysical short wavelength frequencies. An identical ramp function of 1 day length is applied to the wind and pressure forcing as well as the inverted barometer boundary condition. Actual simulations for Hurricane Kate begin at 12:00 GMT 15 November 1985 and run over 8.25 days (including a

1-day ramp-up period). For Hurricane Camille, model computations begin at 12:00 GMT 14 August 1969 and run for 8.00 days (including the 1-day ramp-up period). During the first 6 hr of each simulation, the initial hurricane wind and pressure forcings are held stationary. Thereafter, storm surge computations use the time-varying wind and pressure fields. The time-step for simulations over grid SG01 is 45 sec. This time-step length is halved to 22.5 sec for simulations using grid CG01 so that the Courant number based on wave celerity is identical to that over grid SG01 and remains below 1.5 for accuracy considerations (Westerink et al. 1992b). All parameters in both the hydrodynamic and wind models remain uncalibrated.

Seventy-five elevation stations, shown in Figures 59 - 61, are placed along the eastern and gulf coasts of the United States, on the continental shelf, and at the shelf break in the northeastern portion of the Gulf of Mexico near the landfall regions of Hurricanes Kate and Camille. Comparisons between storm surge elevation solutions computed over grids SG01 and CG01 will be made at these stations.

Discussion of Convergence Analysis

Hurricane Camille

An evaluation of the storm surge predictions computed over grid SG01 begins with an examination of the maximum storm surge errors over the domain at specific points in time. The location and magnitude of the maximum overprediction and underprediction errors are shown in Figure 62. Absolute and relative error measures are the same as those prescribed in Chapter 5 with the "truth" solution now defined by storm surge elevations computed over grid CG01.

As seen in Figure 62, all maximum prediction errors occur at the coastline throughout the period of simulation. Furthermore, the maximum errors exhibit peaks in magnitude at several times. The first peak of the absolute overprediction error, approximately 110 cm, is seen at 84 hr, the time of peak surge and hurricane landfall. The second noticeable increase in the absolute overprediction error occurs after 138 hr as Hurricane Camille moves off land and returns to the coastal waters near Chesapeake Bay-Bridge, Virginia. Areas along the shoreline of the eastern United States are not under consideration and thus have not been discretized to the same levels found in the Gulf of Mexico. The increase in absolute error after 138 hr is a direct consequence of this under-resolution along the eastern coast of the United States.

Figure 62 exhibits relative errors that remain fairly uniform during the approach and landfall of Hurricane Camille within the Gulf of Mexico and on the Mississippi shelf. The extreme relative errors coincide with hurricane positions in deep waters or over land. At a time of 126 hr, the relative error maximum is due to a combination of residual errors at the coastline following

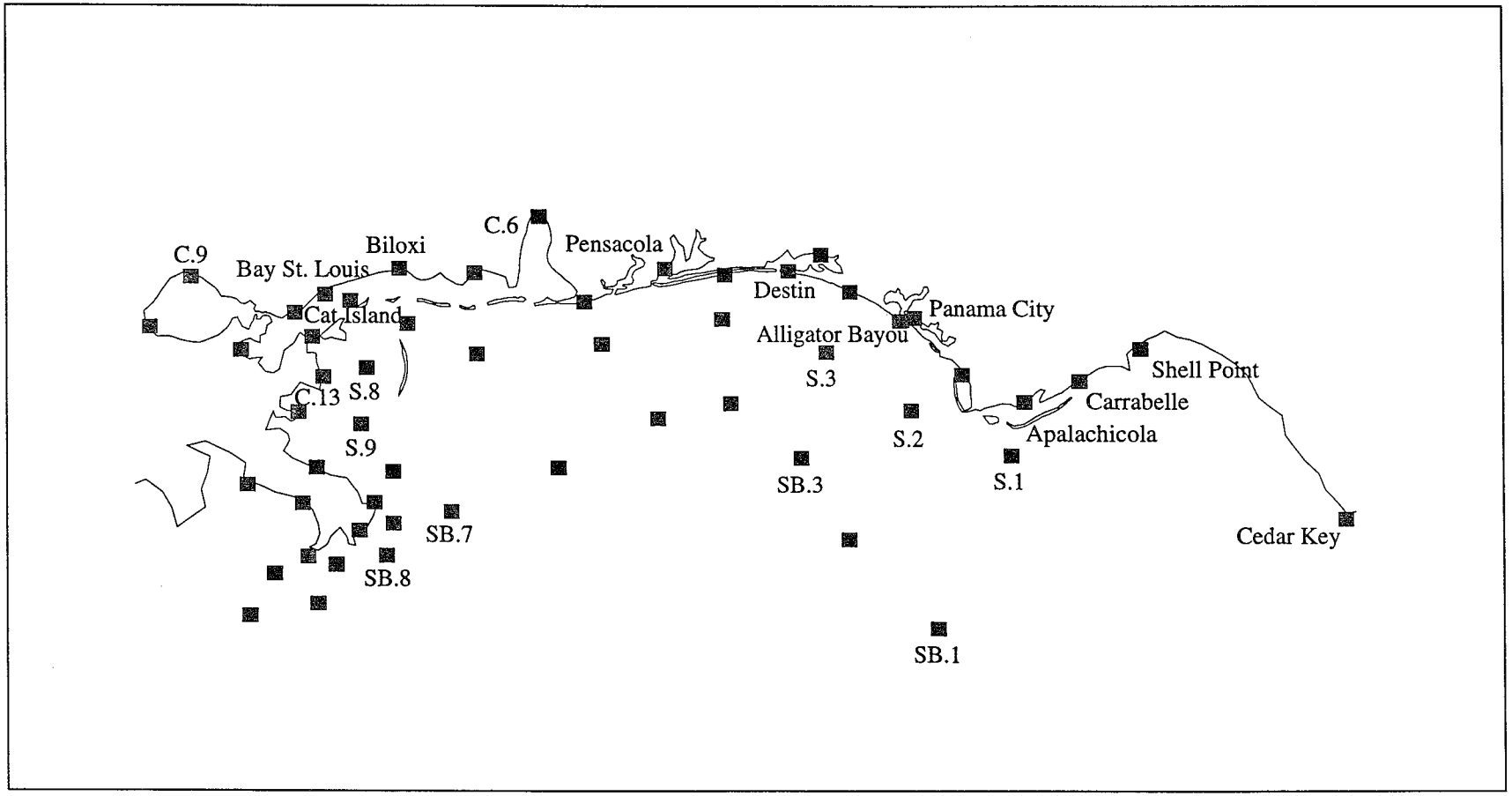

Figure 59. Storm surge elevation stations located throughout the northeast Gulf of Mexico

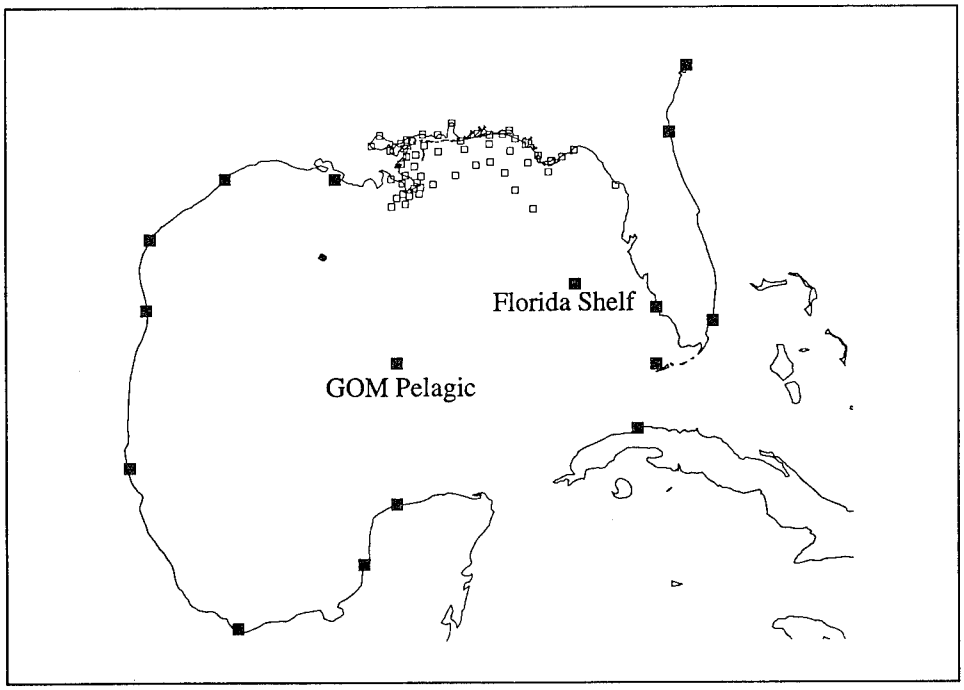

Figure 60. Additional storm surge elevation stations, shown as solid squares, in and around the Gulf of Mexico

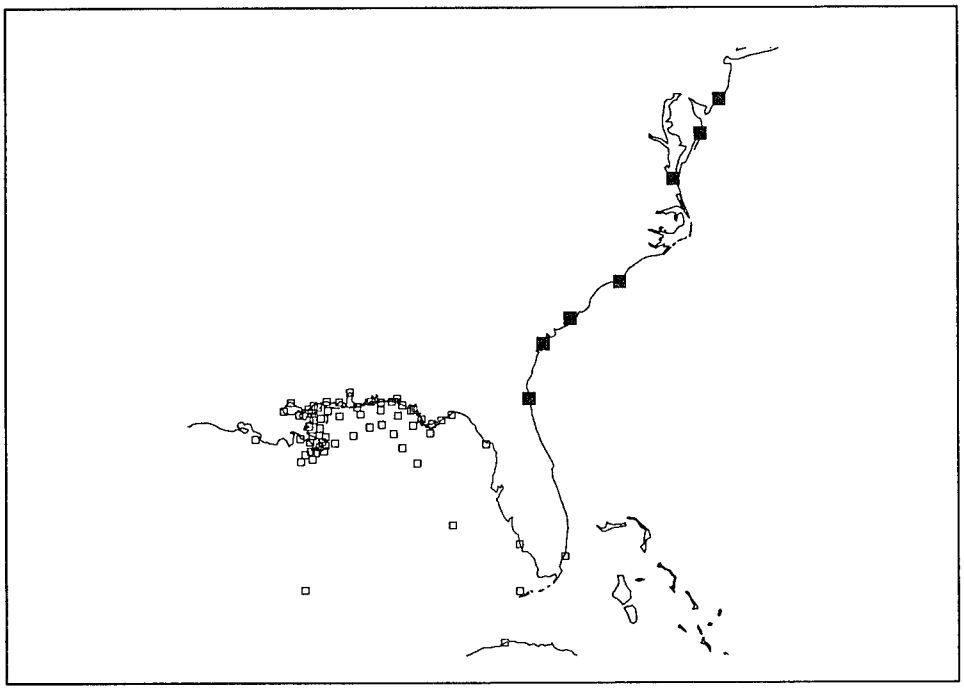

Figure 61. Seven storm surge elevation stations, shown as solid squares, along the eastern United States coastline

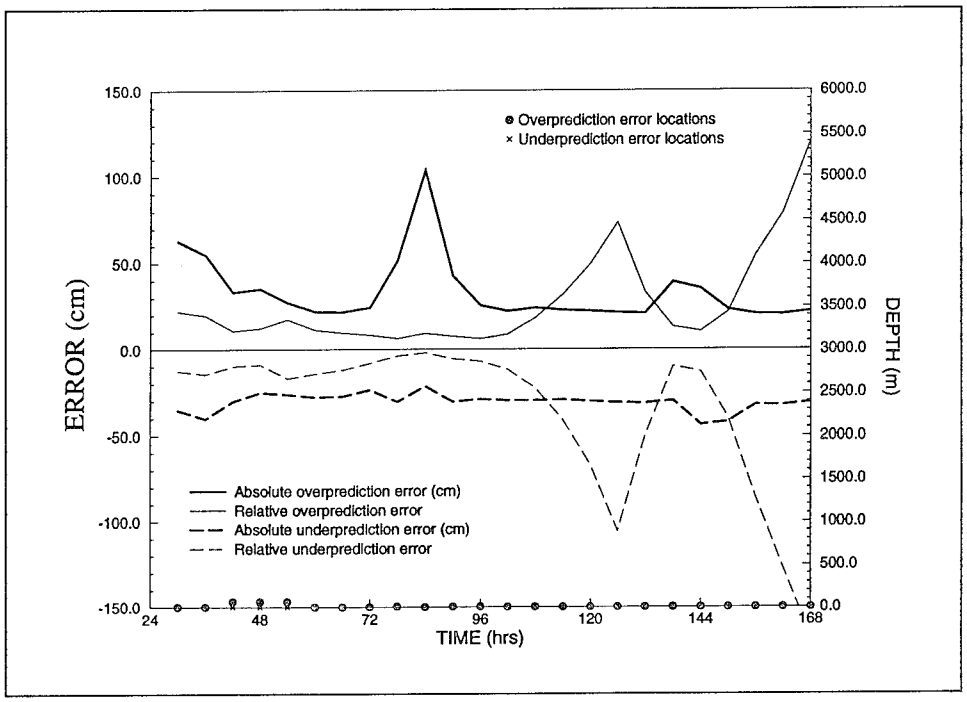

Figure 62. Maximum over- and underprediction errors in the storm surge generated by Hurricane Camille as computed over grid SG01

landfall of the hurricane and the presence of minimal surge elevations as the hurricane moves inland. Relative errors are at a minimum as Hurricane Camille approaches the coast and makes landfall. The uniform, low-magnitude profile of the relative prediction error for the simulation period corresponding to Hurricane Camille's movement through the Gulf of Mexico indicates the appropriateness of the variably graded discretization in grid SG01. However, high magnitudes of the absolute error at the time of peak surge warrant examination of the spatial distribution of storm surge prediction errors throughout the domain.

A series of snapshots taken at different times during the simulation and shown in Figure 63 depict the absolute overprediction (shown as shades of red) and underprediction (shown in shades of blue) errors of the storm surge calculated over grid SG01 as compared to computations made over grid CG01. As Hurricane Camille approaches land, errors increase over an 18-hr period surrounding the time of landfall but are confined to a limited region at the coast near Biloxi, MS. After 84 hr on 18 August 1969, errors build around an island directly in the path of Hurricane Camille as seen in Figure 63c. An enlargement of the discretization in this region, presented in Figure 64, shows relatively coarse resolution around the island, which would indeed cause larger storm surge prediction errors. Six hours later, overprediction of the storm surge reaches the 1-m level in a localized area between the coastline and the offshore barrier islands near Biloxi, MS, as seen in Figure 63d. As Camille moves onto land (Figures 63e and 63f), the error in computed storm surge shifts from overprediction to underprediction as winds come off the land. In

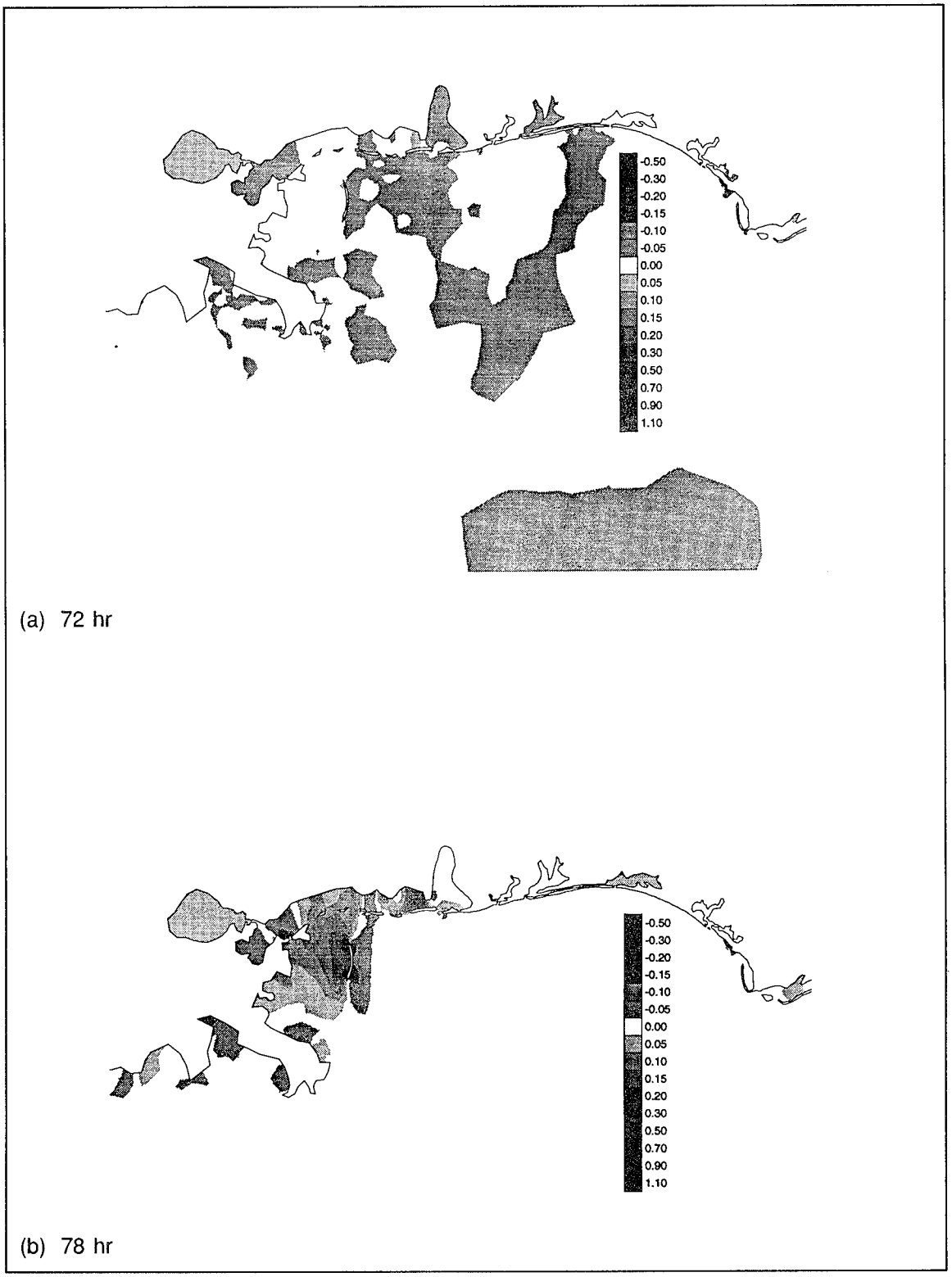

Figure 63. Contours of the absolute overprediction (reds) and underprediction (blues) errors in the storm surge computed over grid SG01 (Sheet 1 of 3)

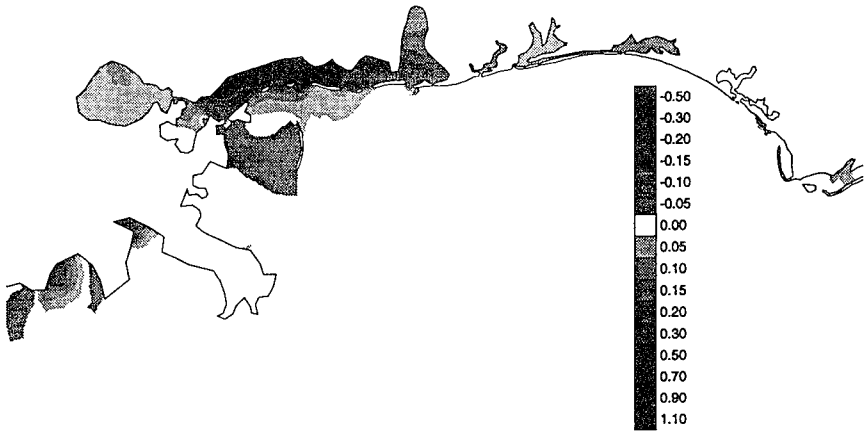

(c) 84 hr

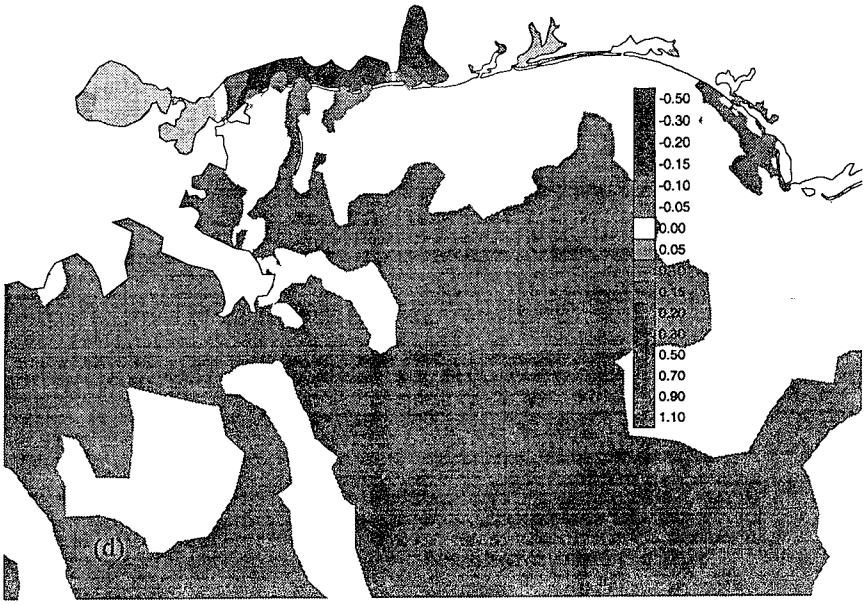

(d) 90 hr

Figure 63. (Sheet 2 of 3)

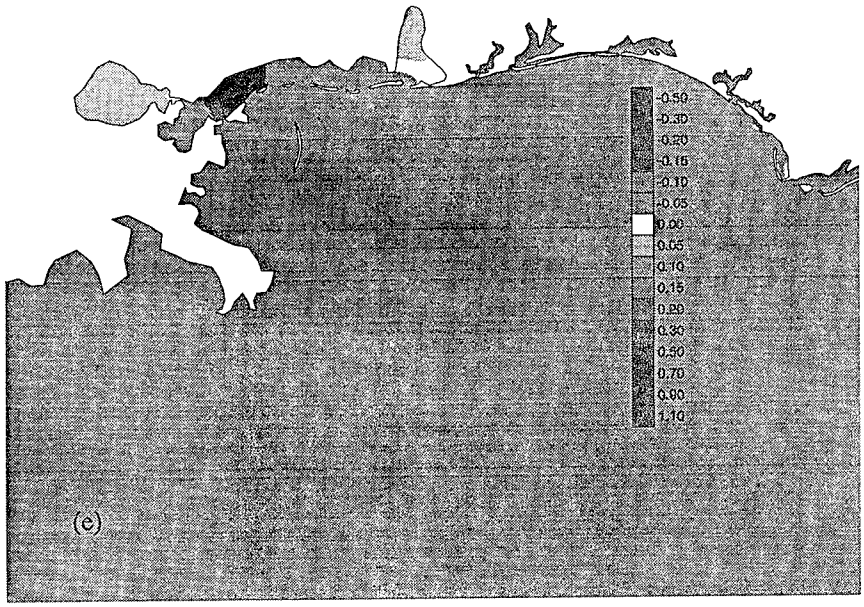

(e) 96 hr

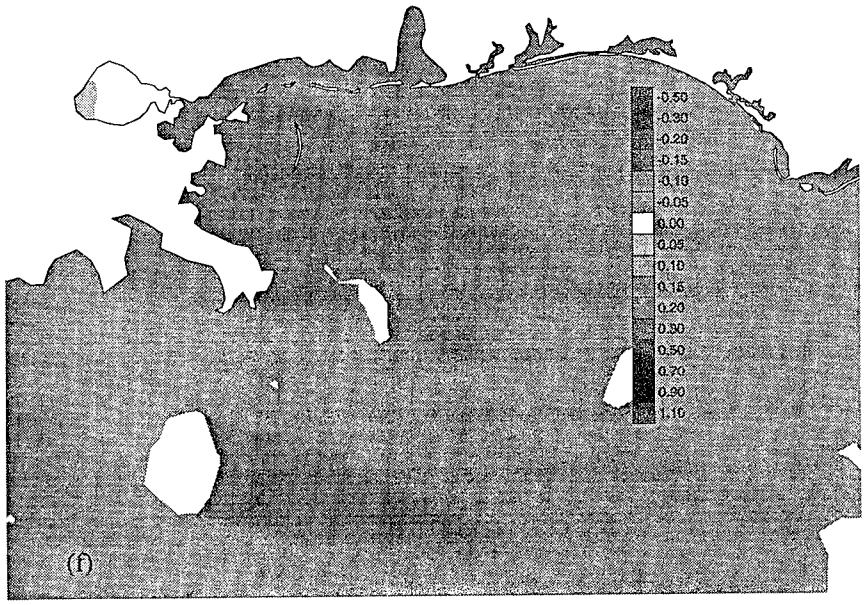

(f) 102 hr

Figure 63. (Sheet 3 of 3)

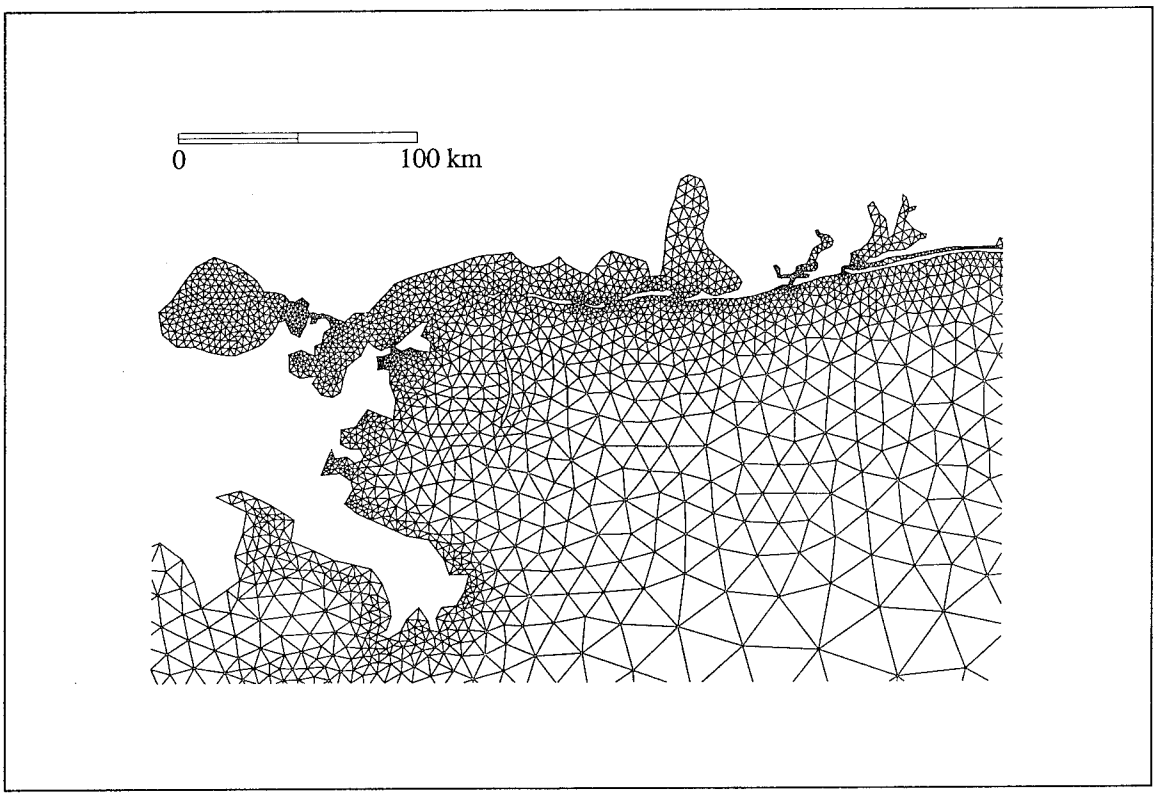

Figure 64. Enlargement of the resolution provided by grid SG01 in the landfall region of Hurricane Camille

general, the spatial distribution of the absolute error indicates that increased resolution around offshore islands and in coastal areas near the landfall point of Hurricane Camille may reduce the extreme error magnitudes observed in the storm surge prediction.

A sampling of 13 storm surge hydrographs taken at Alligator Bayou, Pensacola, Biloxi, Bay St. Louis, Cat Island, Stations C.6, C.9, and C.13 along the Gulf of Mexico coast, Stations S.8 and S.9 on the continental shelf, Stations SB.7 and SB.8 along the shelf break, and at the GOM Pelagic in the deep Gulf of Mexico are shown in Figures 65 - 77. Each hydrograph compares the storm surge elevations computed over grid SG01 to those computed over grid CG01. Generally, the peak storm surge is overpredicted with errors ranging from 5 cm at Pensacola, FL, to 70 cm at Biloxi, MS. On the right-hand side of the hurricane, overprediction of the storm surge increases as station location nears the proximity of the landfall location of Hurricane Camille. The hydrograph at Station C.9 exhibits drying in the form of negative surges which are associated with the left-hand side of the hurricane. At stations on the continental shelf and at the shelf break, seen in Figures 73 - 76, the peak surge is represented with considerably more accuracy. Overprediction errors are commonly less than 5 cm, with a maximum overprediction of 20 m seen at Station S.8 in Figure 73. Representation of the surge forerunner over

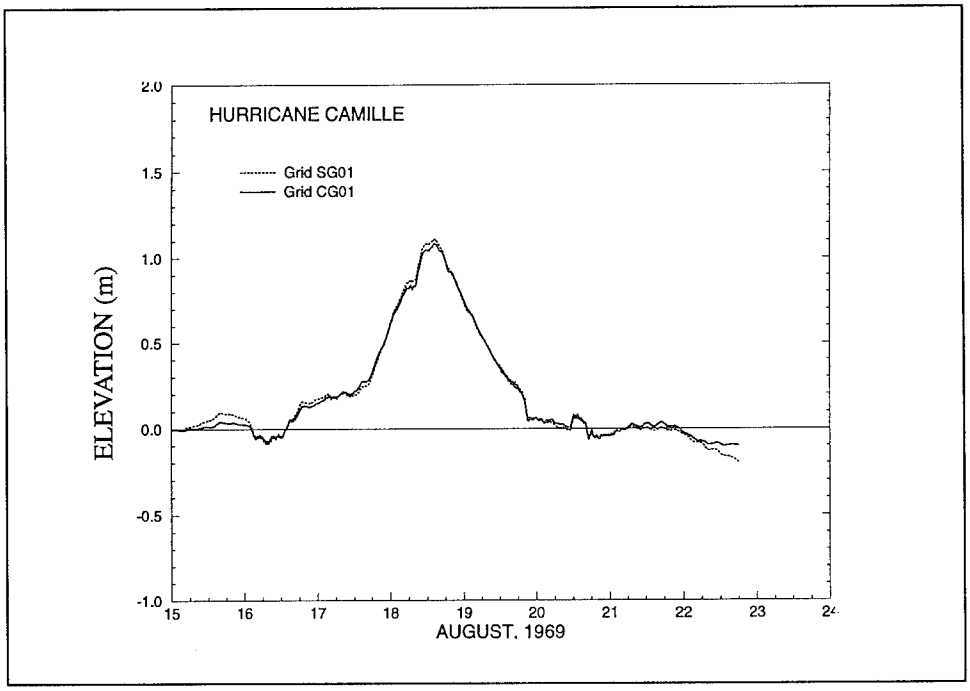

Figure 65. Storm surge hydrograph comparing computations over grids SG01 and CG01 at Alligator Bayou, FL

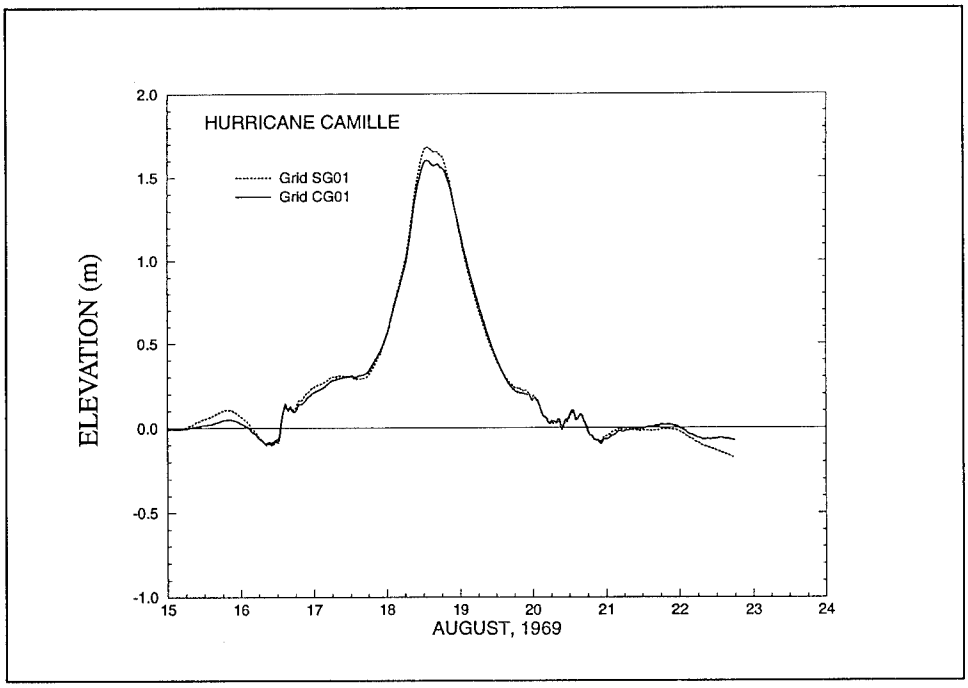

Figure 66. Storm surge hydrograph comparing computations over grids SG01 and CG01 at Pensacola, FL

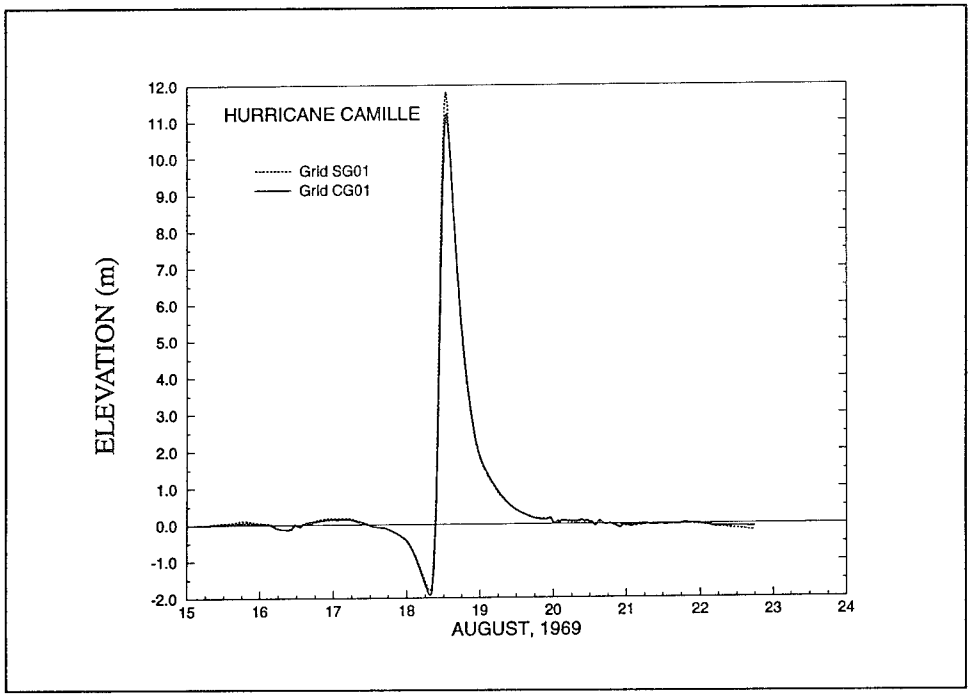

Figure 67. Storm surge hydrograph comparing computations over grids SG01 and CG01 at Biloxi, MS

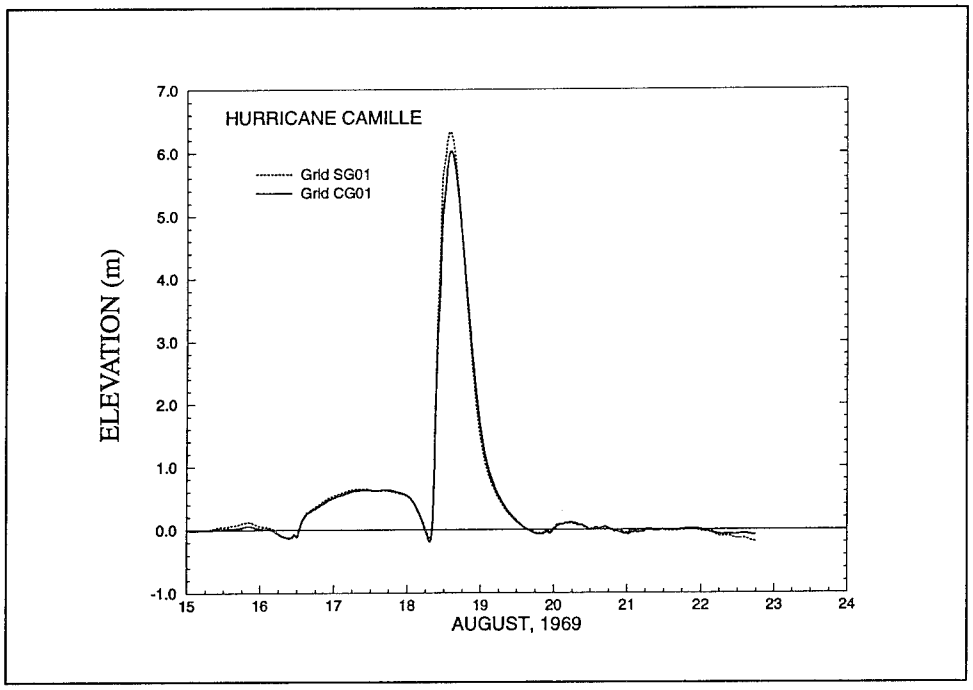

Figure 68. Storm surge hydrograph comparing computations over grids SG01 and CG01 at Bay St. Louis, MS

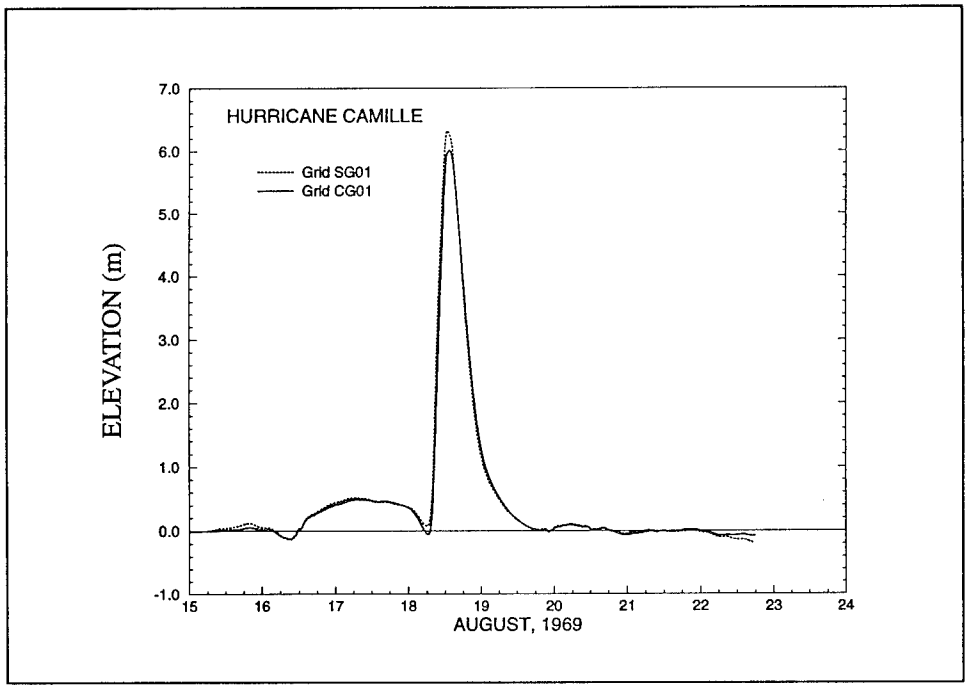

Figure 69. Storm surge hydrograph comparing computations over grids SG01 and CG01 at Cat Island, MS

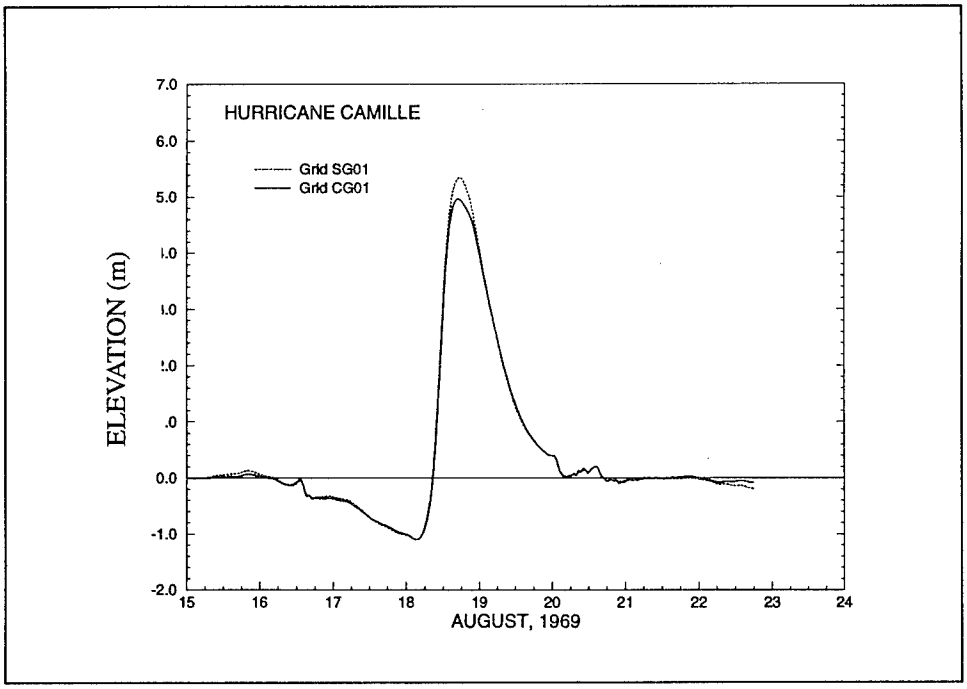

Figure 70. Storm surge hydrograph comparing computations over grids SG01 and CG01 at Station C.6

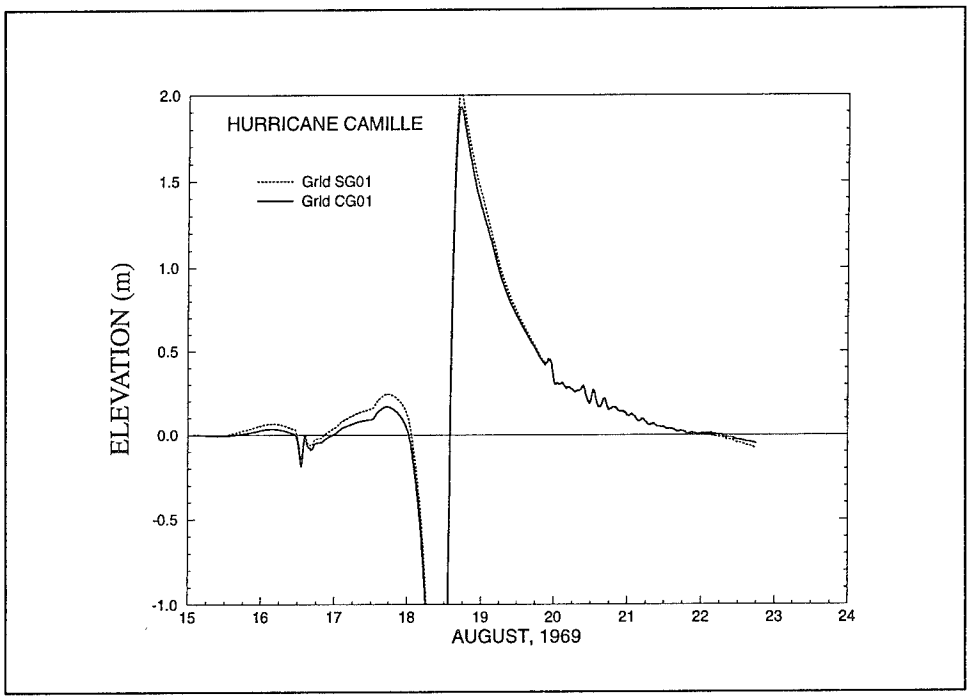

Figure 71. Storm surge hydrograph comparing computations over grids SG01 and CG01 at Station C.9

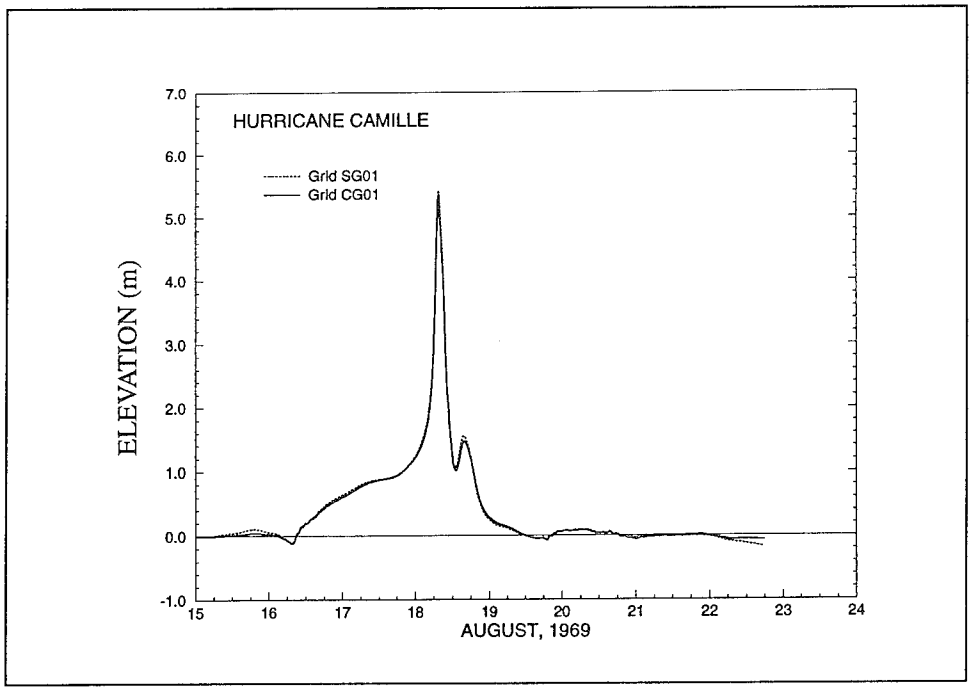

Figure 72. Storm surge hydrograph comparing computations over grids SG01 and CG01 at Station C.13

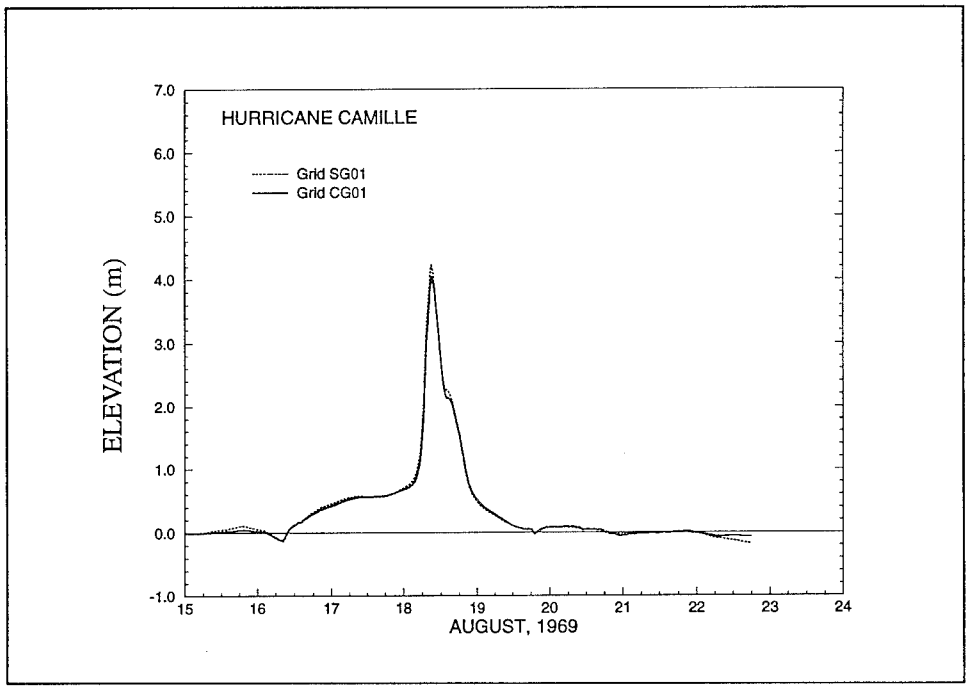

Figure 73. Storm surge hydrograph comparing computations over grids SG01 and CG01 at Station S.8

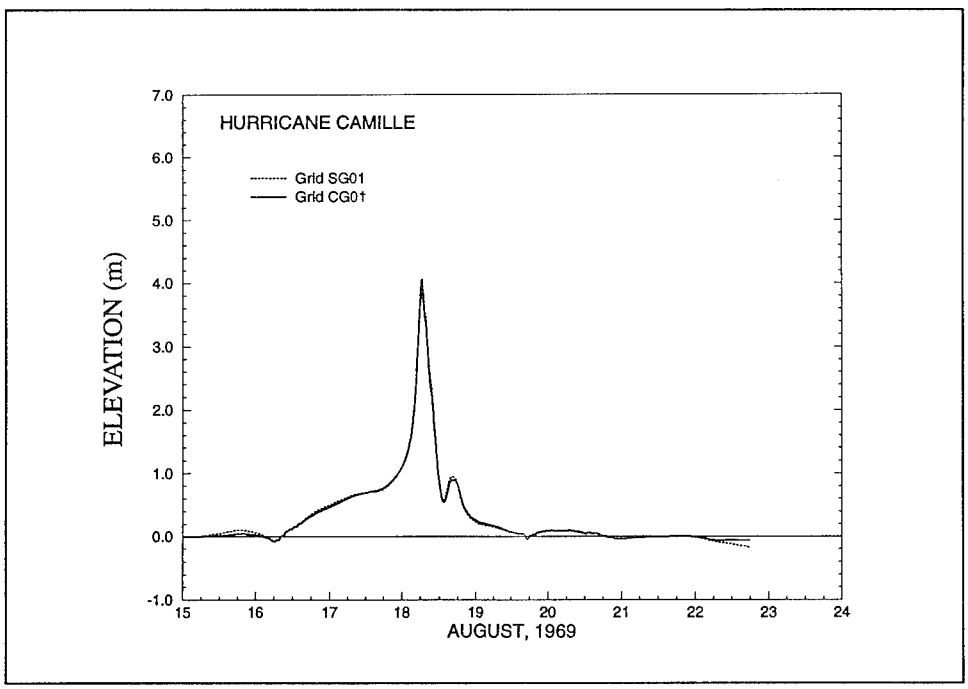

Figure 74. Storm surge hydrograph comparing computations over grids SG01 and CG01 at Station S.9

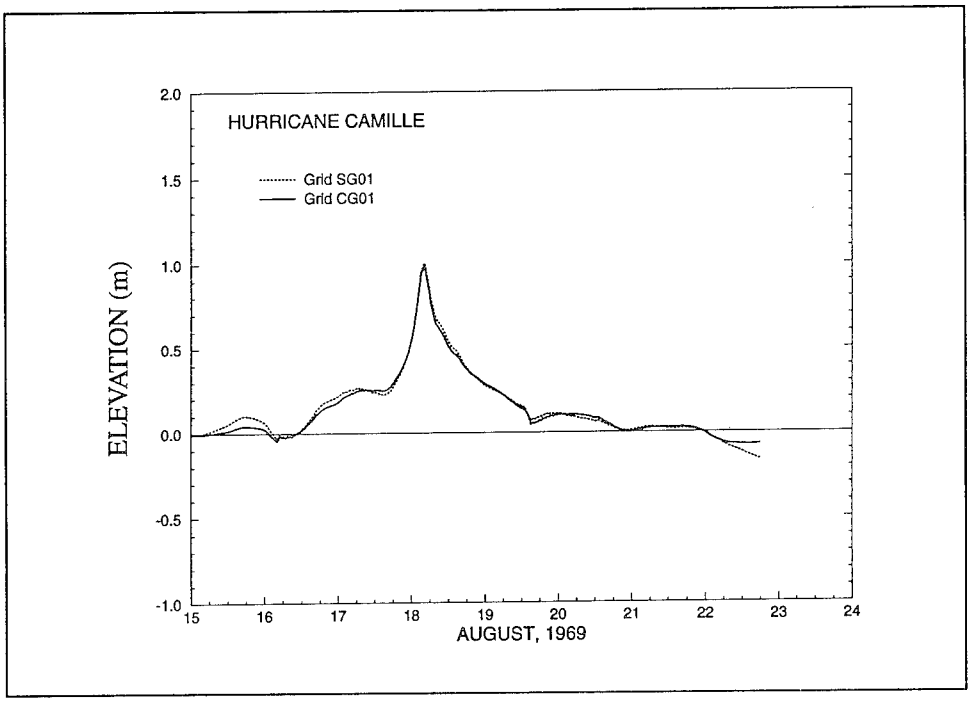

Figure 75. Storm surge hydrograph comparing computations over grids SG01 and CG01 at Station SB.7

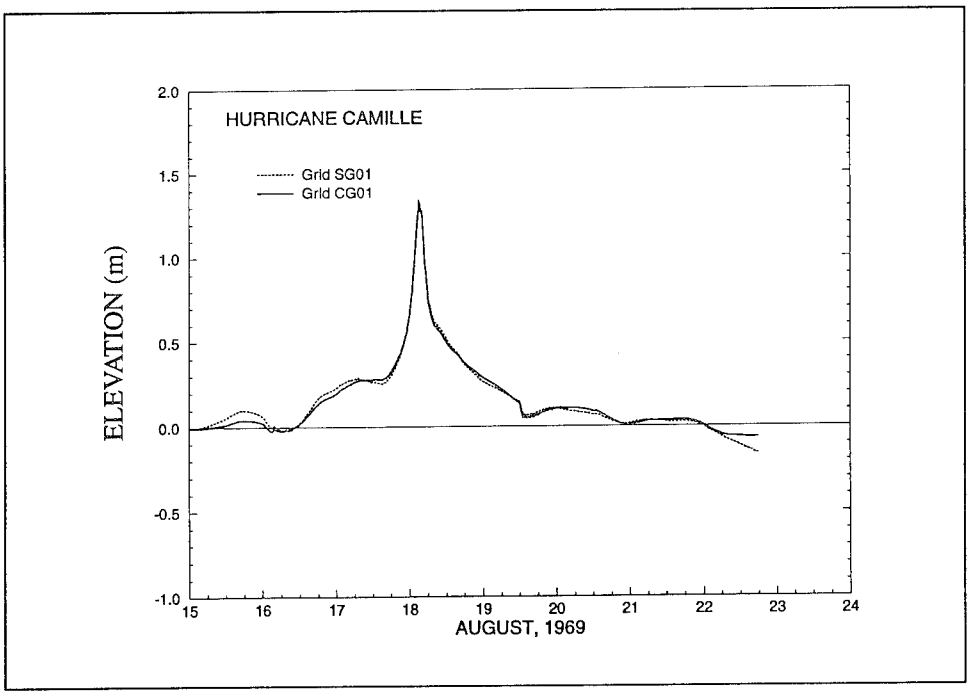

Figure 76. Storm surge hydrograph comparing computations over grids SG01 and CG01 at Station SB.8

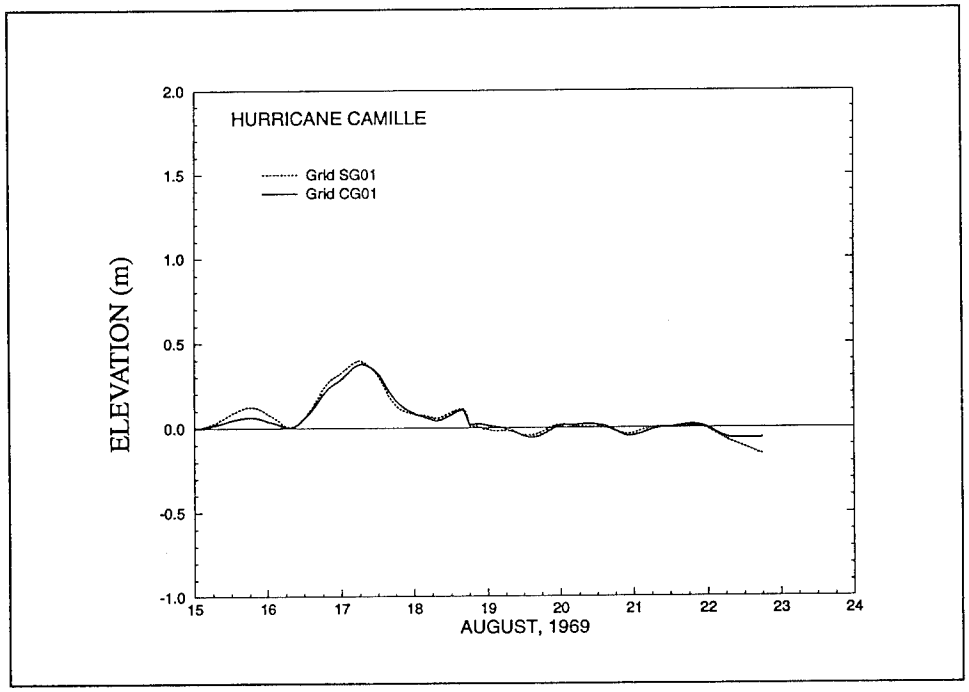

Figure 77. Storm surge hydrograph comparing computations over grids SG01 and CG01 at the GOM (Gulf of Mexico) Pelagic station

grid SG01 differs by less than 5 m with storm surge elevations computed over grid CG01.

As predicted by the study of grid structure in Chapter 5, the most significant errors are computed in regions where grid refinement is less and the detail of the shoreline is more complex. Overall, errors in the storm surge elevations computed over grid SG01 are uniform and minimized throughout the domain. Further refinement in coastal areas near Biloxi, MS, may improve representation of the peak surge as the hurricane makes landfall.

Hurricane Kate

Locations and magnitudes of the maximum storm surge prediction errors for Hurricane Kate computed over grid SG01 are presented in Figure 78. Similar to the analysis for Hurricane Camille forcing, a "truth" solution is defined as surge elevations computed over grid CG01. In Figure 78, the maximum absolute errors remain uniform throughout the simulation and range between 20 and 25 cm of overprediction and 25 and 30 cm of underprediction. The largest relative errors in Figure 78 are computed during the beginning of the simulation, while Hurricane Kate is in the deep ocean and are a result of an under-resolution of the spatial scale of Hurricane Kate over deep Atlantic waters. At 108 hr, a peak of the maximum relative error seen in Figure 78 coincides with resonant mode generation prior to the time of peak surge.

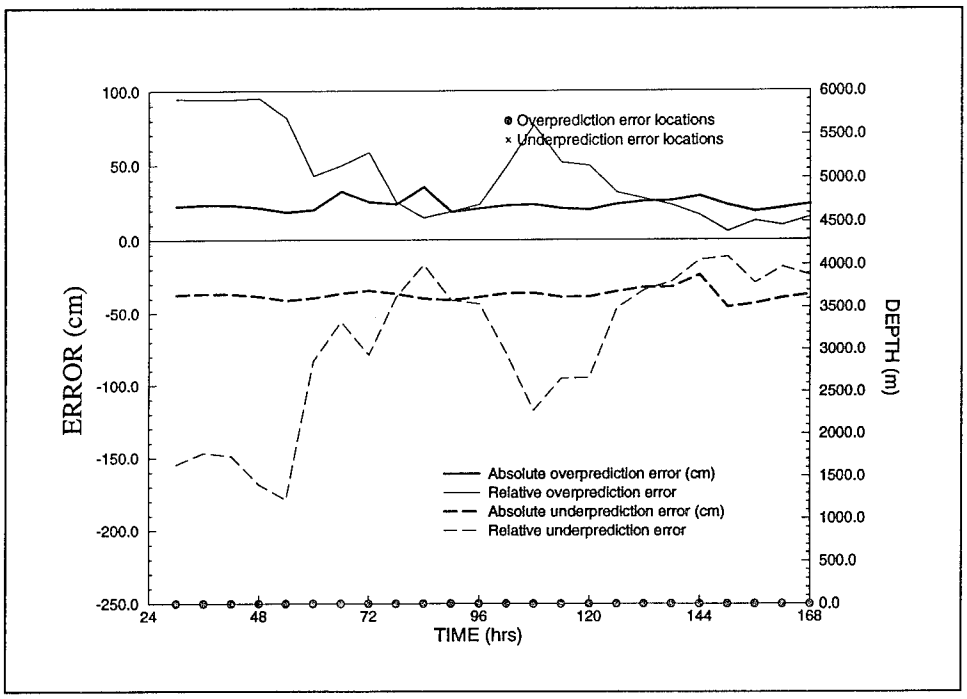

Figure 78. Maximum over- and underprediction errors in the storm surge generated by Hurricane Kate as computed over grid SG01

Spatial distributions of the absolute error associated with the storm surge calculated over grid SG01 and compared to computations over grid CG01 are presented at different times in Figures 79a - 79f. In Figure 79, the overprediction of storm surge is shown in shades of red and the underprediction in shades of blue. As Hurricane Kate moves into the northeast Gulf of Mexico, seen in Figures 79a and 79b, overprediction errors along the right- hand side of the hurricane are evident in regions where the discretization is relatively coarse. Under-resolved areas are evident upon examination of the grid discretization in the landfall region of Hurricane Kate shown in Figure 80. The extreme errors seen in Figure 79c occur near the islands offshore from Apalachicola, FL. At 150 hr, approximately the time of landfall of Hurricane Kate, errors in the predicted storm surge near the landfall location at Panama City, FL, shown in Figure 79d, are noticeable and localized errors around Apalachicola persist. Elsewhere the storm surge is underpredicted, particularly over the less resolved portions of the Gulf of Mexico away from the shoreline.

Following the time of peak surge, underprediction of the water elevation occurs in the northeast corner of the Gulf of Mexico (Figure 6.25e) where resolution is particularly coarse relative to the surrounding coastline. As the storm moves further inland and dissipates (Figure 6.25f), errors in the predicted storm surge return to levels of 1 to 2 cm (0.4-.8 in.). In general, errors in the storm surge predicted for Hurricane Kate forcing are quite low (i.e., less than 5 cm (2.0 in.)). Only errors in a few localized areas remain problematic.

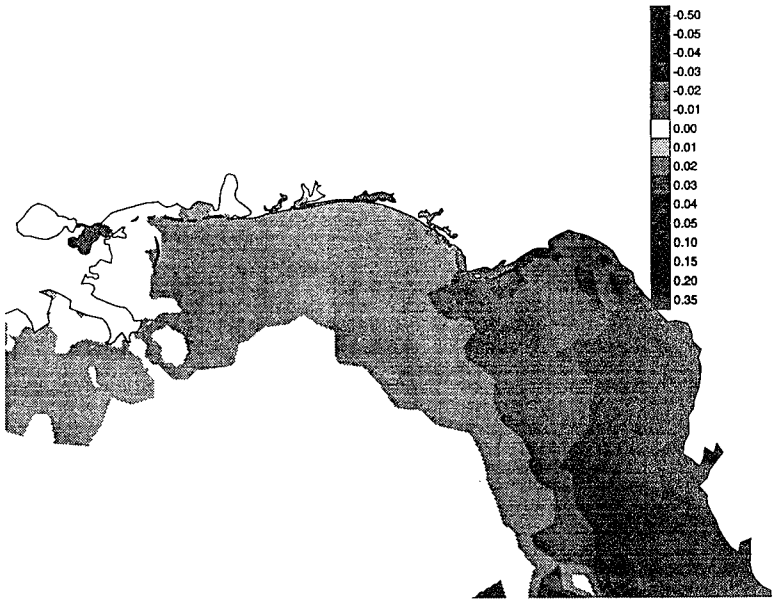

(a) 132 hr

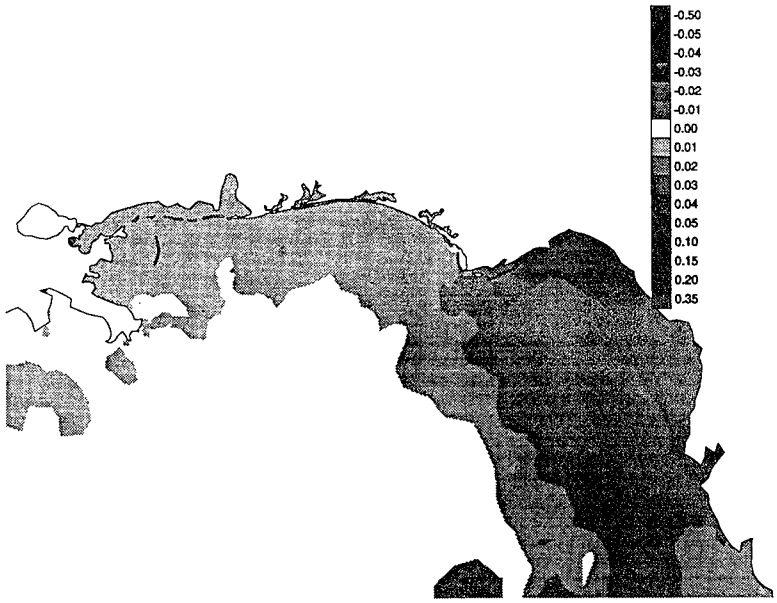

(b) 138 hr

Figure 79. Contours of the absolute overprediction (reds) and underprediction (blues) errors in the storm surge computed over grid SG01 (Sheet 1 of 3)

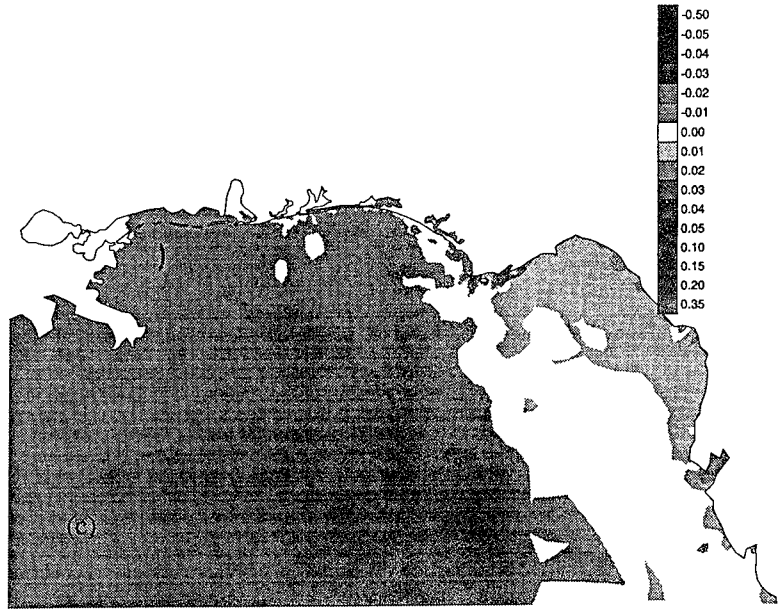

(c) 144 hr

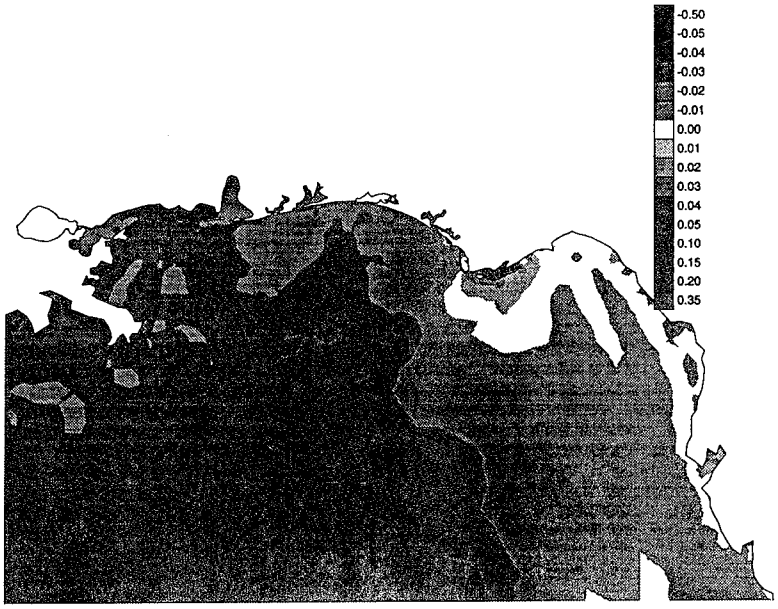

(d) 150 hr

Figure 79. (Sheet 2 of 3)

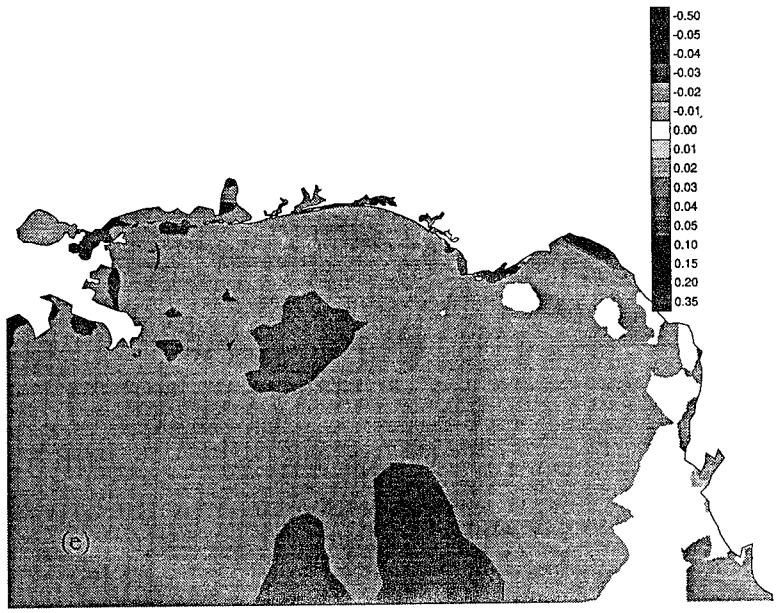

(e) 156 hr

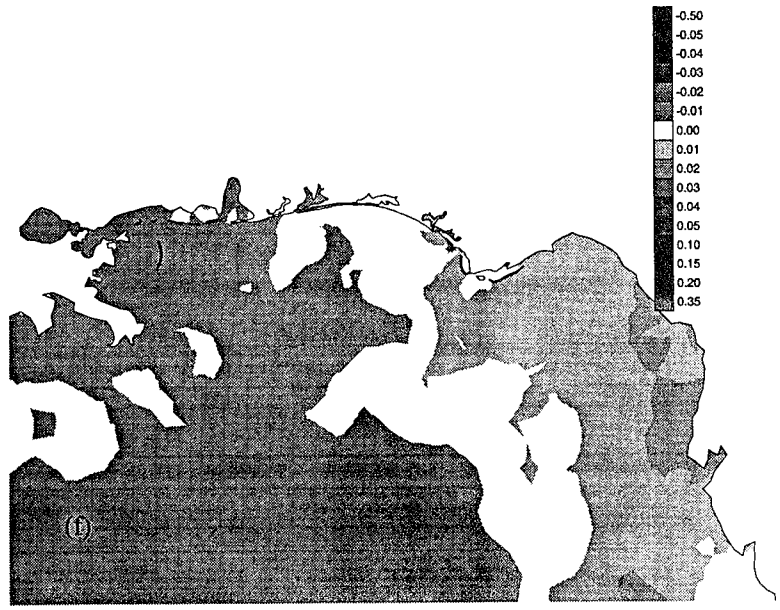

(f) 162 hr

Figure 79. (Sheet 3 of 3)

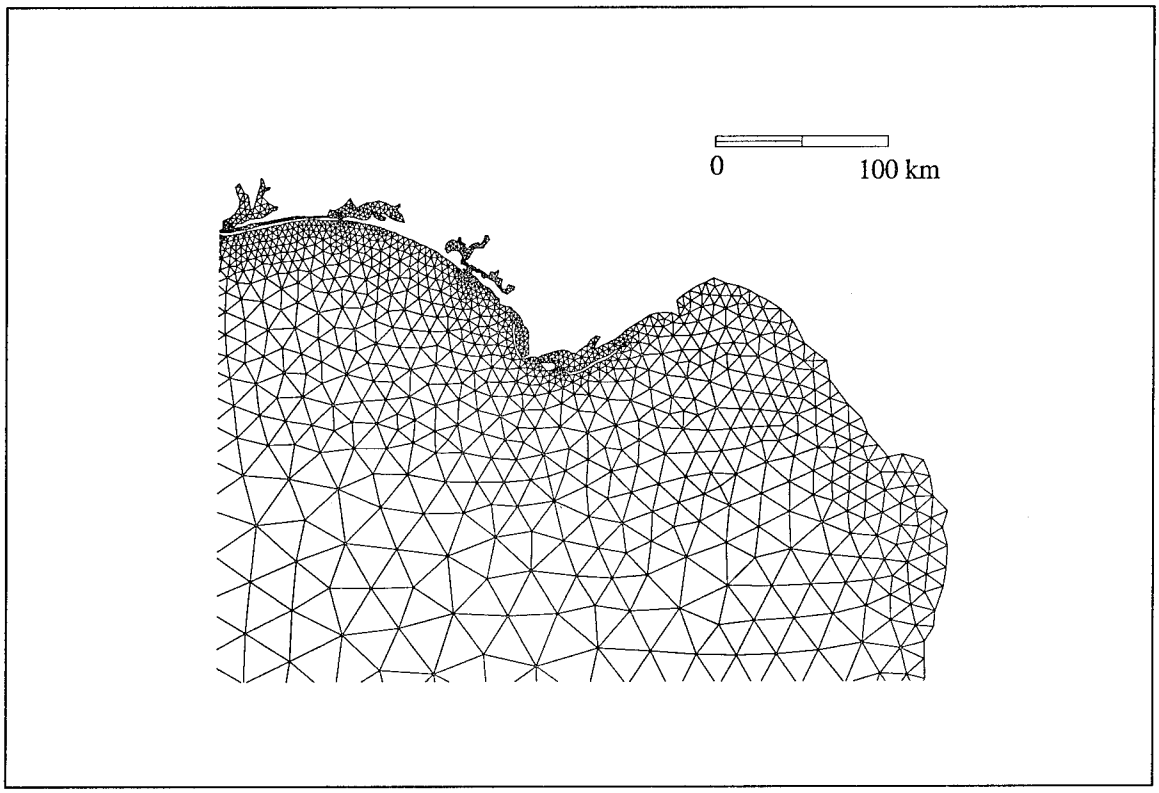

Figure 80. Enlargement of the resolution provided by grid SG01 in the landfall region of Hurricane Kate

A sampling of 13 storm surge hydrographs at Alligator Bayou, Destin, Panama City, Apalachicola, Carrabelle, Shell Point, and Cedar Key along the Gulf of Mexico coast, Stations S.1, S.2, S.3, and the outer Florida Shelf station on the continental shelf, and Stations SB.1 and SB.3 along the shelf break in the Gulf of Mexico are shown in Figures 81 - 93. Each hydrograph compares storm surge elevations computed over grid SG01 to those computed over grid CG01. The peak storm surge at all stations is well-predicted, having errors less than 4 cm (1.6 in.) at all stations except Apalachicola where errors of 10 cm (3.9 in.) are computed. A majority of the error in the computed storm surge for Hurricane Kate arises when representing the resonant modes, which are excited as Hurricane Kate enters and moves through the Gulf of Mexico. Note that while errors in the prediction of surge forerunner persist, error magnitudes are generally less than 5 cm (2.0 in.).

Storm surge heights computed over grid SG01 due to forcing from Hurricane Kate are well-represented when compared to the storm surge calculated for the over-refined "truth" grid, CG01. Errors in the computed storm surge relative to Hurricane Kate are similar to errors in the storm surge elevations predicted for Hurricane Camille in that they are confined to very localized areas where resolution is coarse and coastline detail is highly irregular.

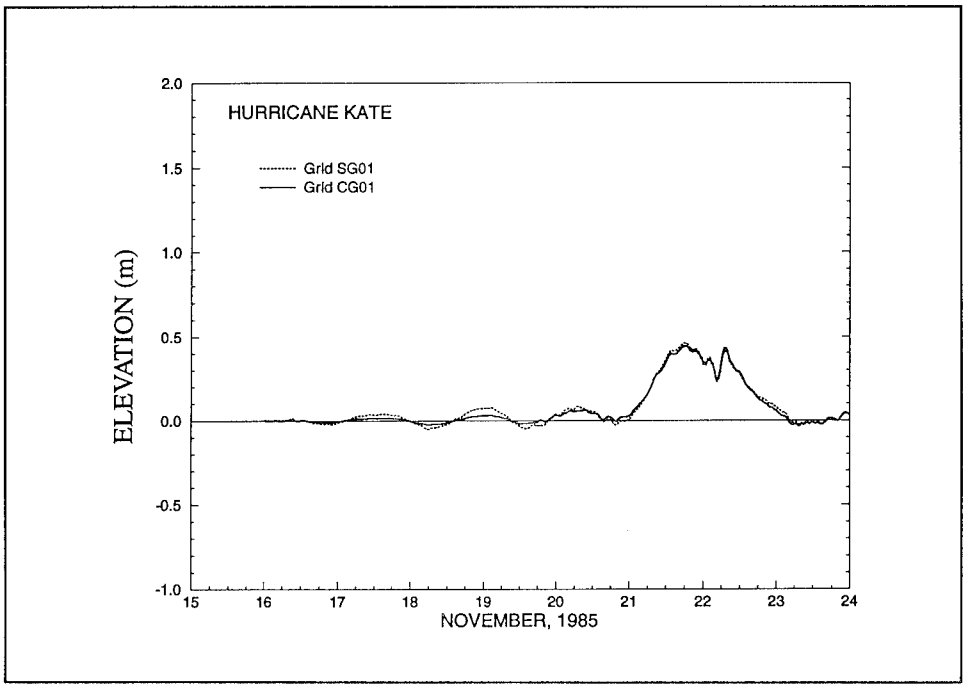

Figure 81. Storm surge hydrograph comparing computations over grids SG01 and CG01 at Alligator Bayou, FL

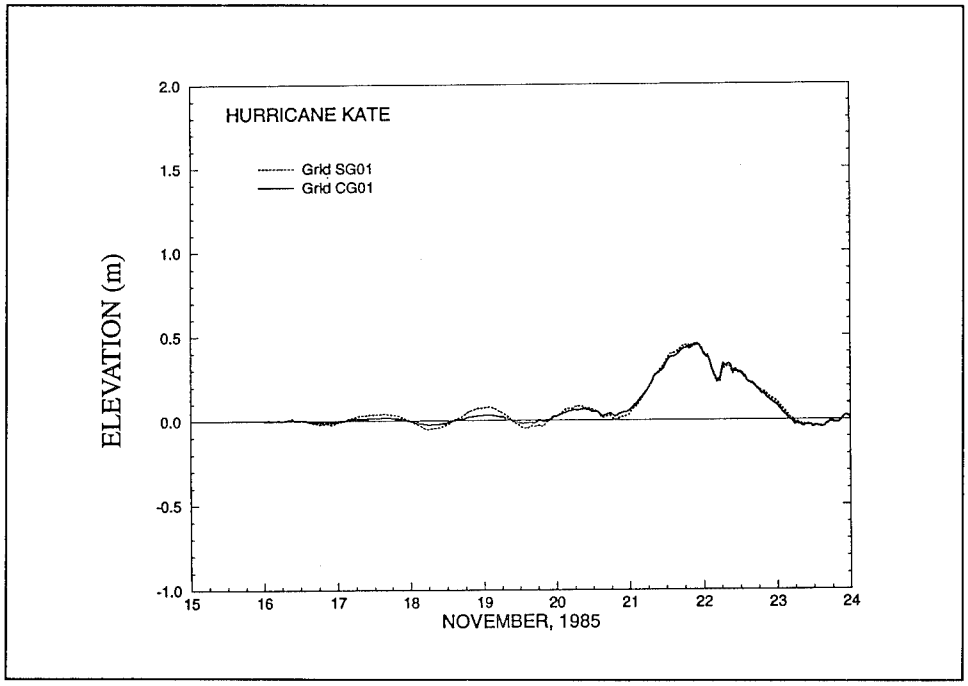

Figure 82. Storm surge hydrograph comparing computations over grids SG01 and CG01 at Destin, FL

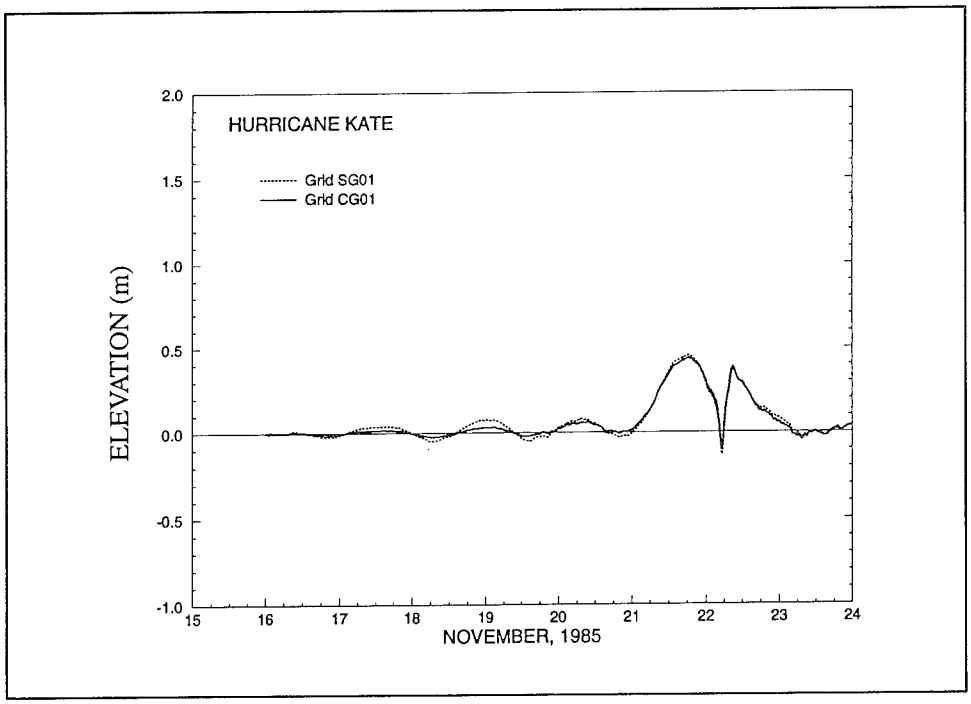

Figure 83. Storm surge hydrograph comparing computations over grids SG01 and CG01 at Panama City, FL

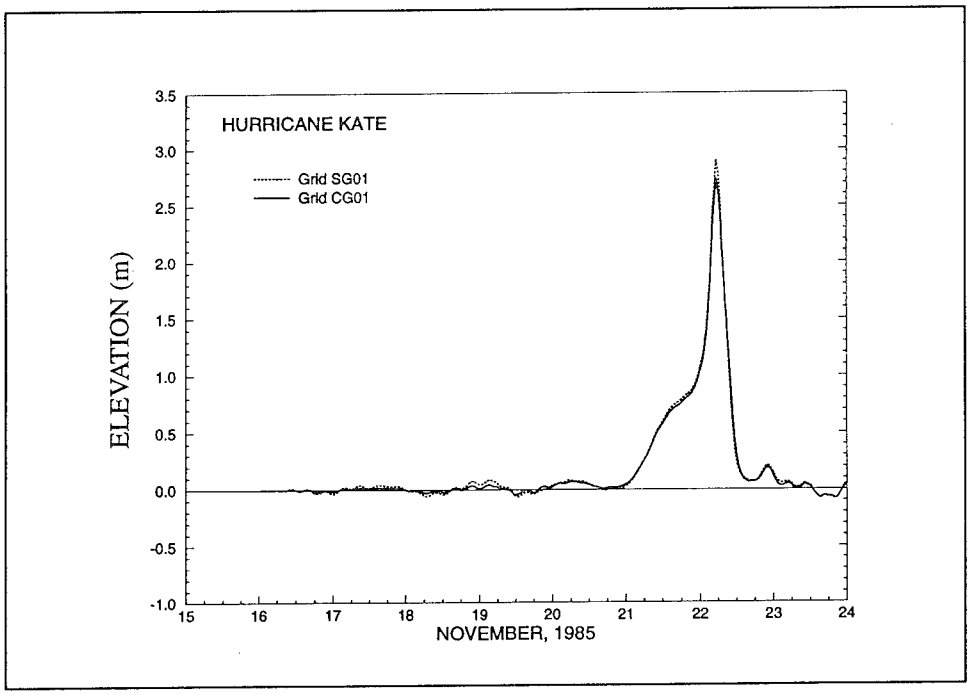

Figure 84. Storm surge hydrograph comparing computations over grids SG01 and CG01 at Apalachicola, FL

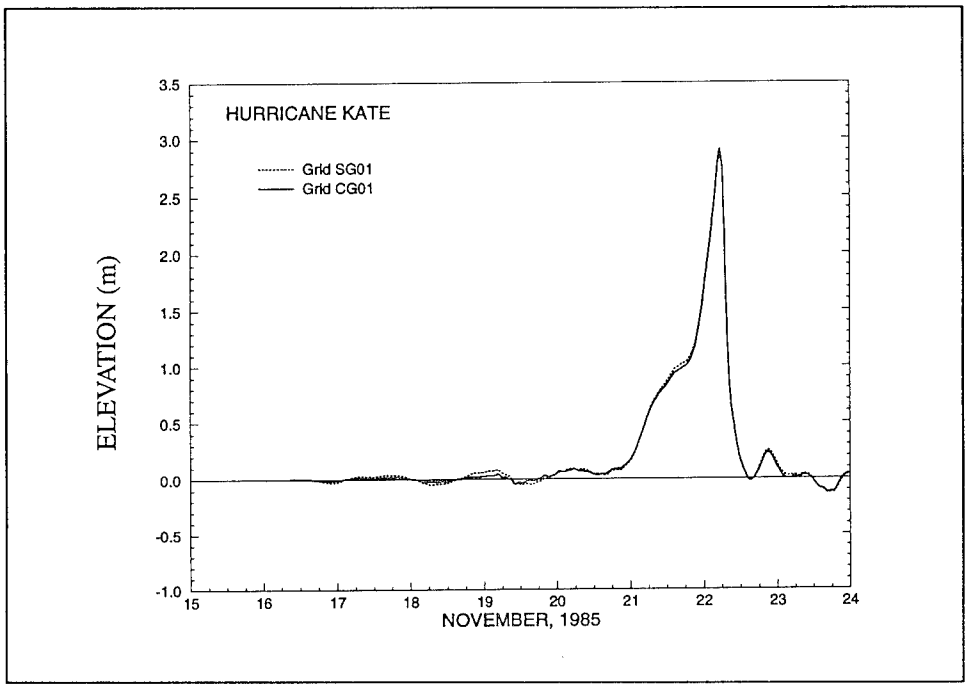

Figure 85. Storm surge hydrograph comparing computations over grids SG01 and CG01 at Carrabelle, FL

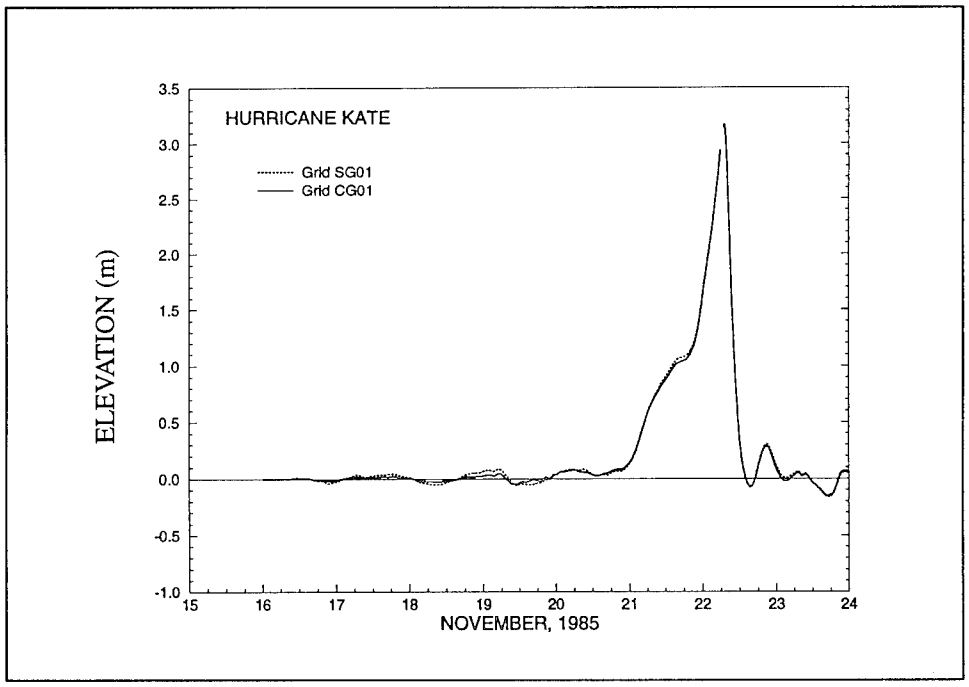

Figure 86. Storm surge hydrograph comparing computations over grids SG01 and CG01 at Shell Point, FL

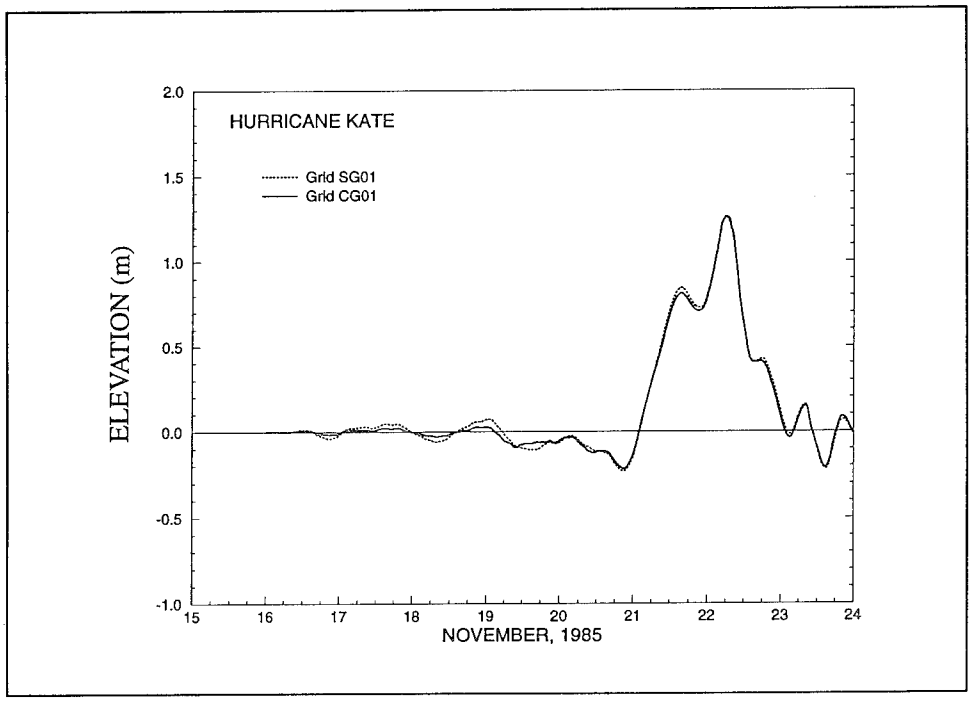

Figure 87. Storm surge hydrograph comparing computations over grids SG01 and CG01 at Cedar Key, FL

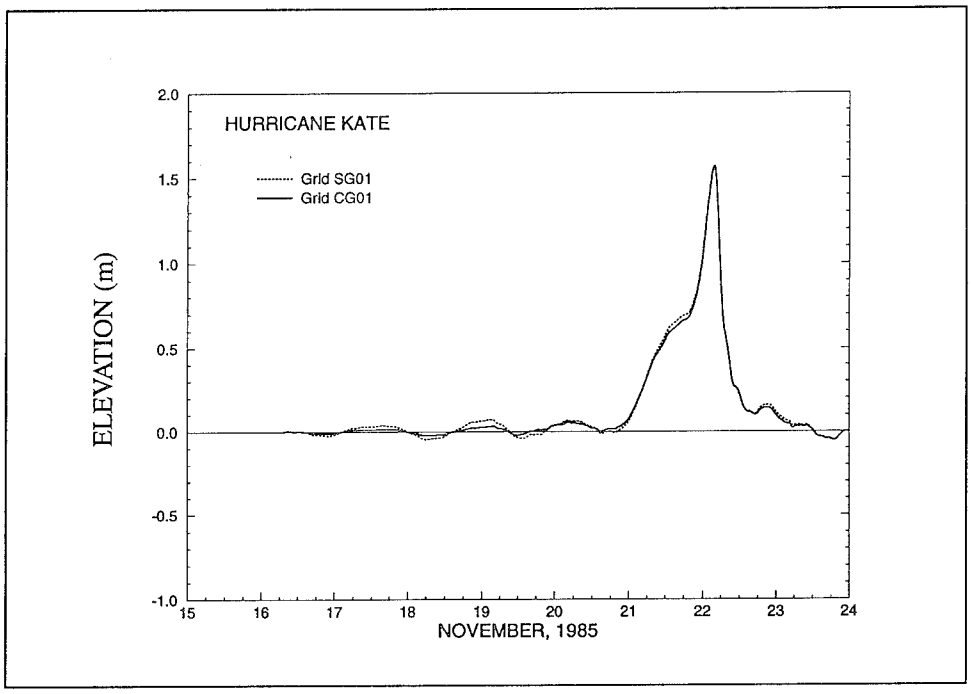

Figure 88. Storm surge hydrograph comparing computations over grids SG01 and CG01 at Station S.1

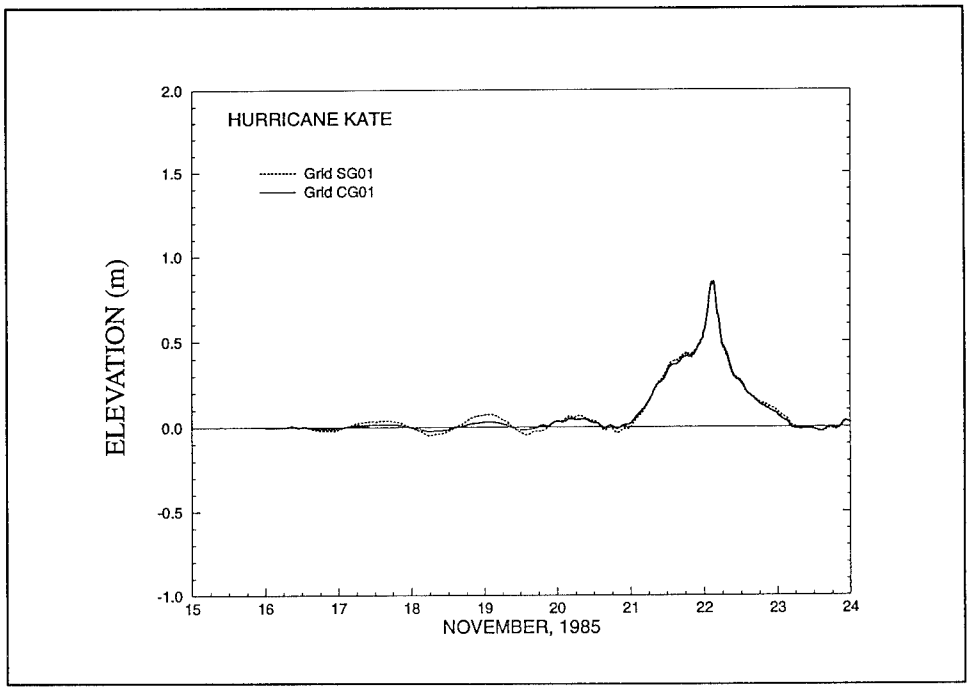

Figure 89. Storm surge hydrograph comparing computations over grids SG01 and CG01 at Station S.2

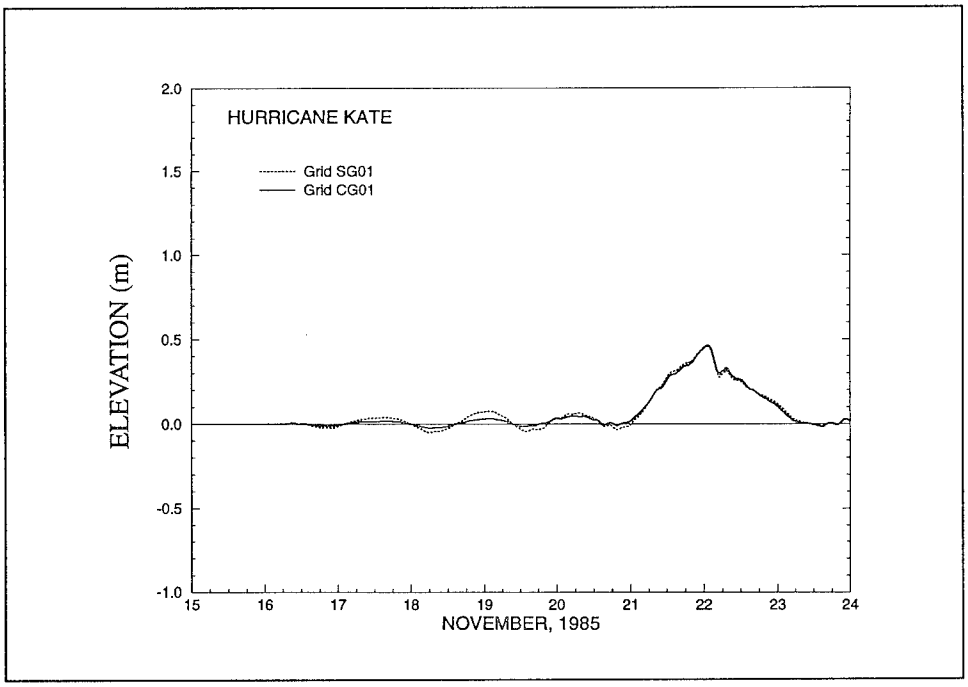

Figure 90. Storm surge hydrograph comparing computations over grids SG01 and CG01 at Station S.3

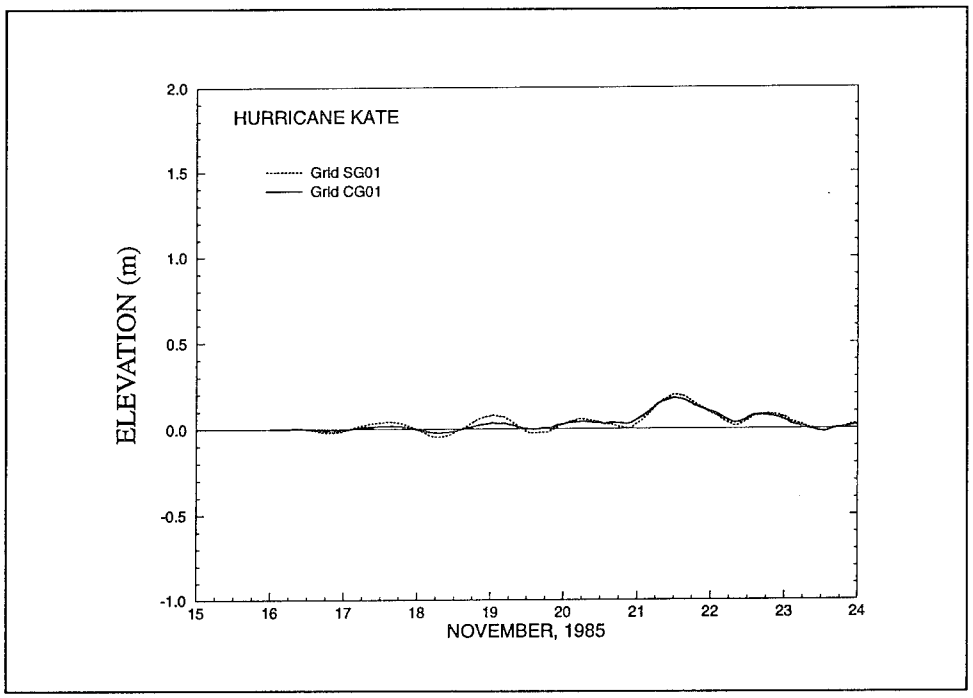

Figure 91. Storm surge hydrograph comparing computations over grids SG01 and CG01 at the outer Florida Shelf Station

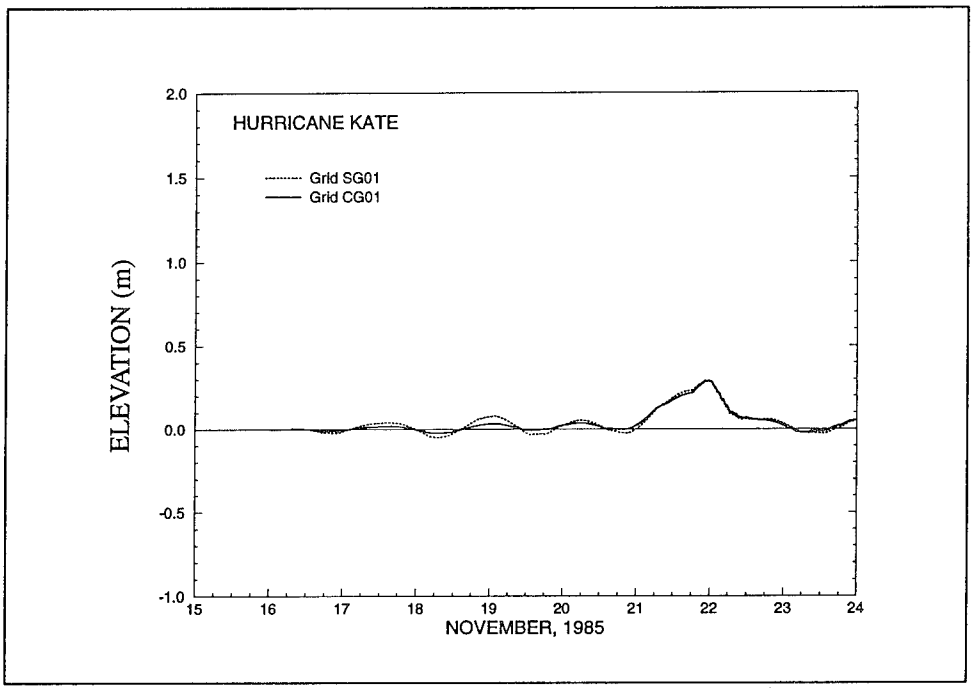

Figure 92. Storm surge hydrograph comparing computations over grids SG01 and CG01 at Station SB.1

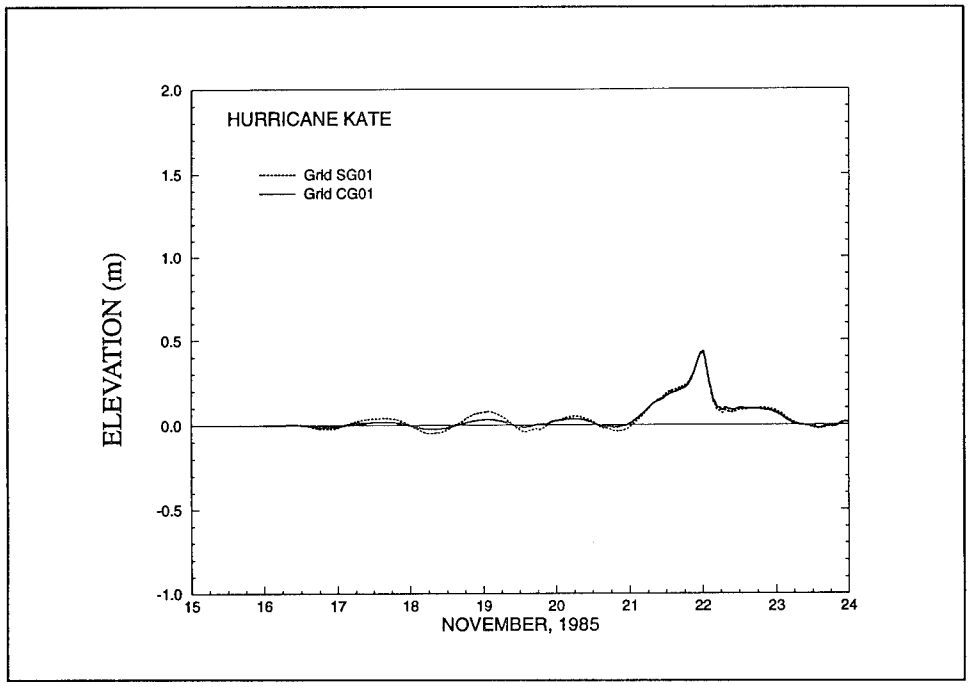

Figure 93. Storm surge hydrograph comparing computations over grids SG01 and CG01 at Station SB.3

Conclusions

A numerical storm surge model implementing a variably graded grid structure in combination with a large domain which extends from the coastal region to portions of the deep ocean (e.g. grid SG01) reproduces well the primary storm surge elevations generated by Hurricane Kate and Hurricane Camille. Errors in the predicted storm surge associated with each hurricane remain fairly uniform over the domain, which is essential to eliminating the influence of the discretization on storm surge computations. Resolution over the deep open ocean for forcing due to Hurricane Kate could be improved. However, along the path of Hurricane Kate at entrances to the Gulf of Mexico, where the setup of resonant modes is critical, mesh spacing is generally less than one half the spatial scale of the hurricane, meeting the guideline set forth to reduce storm surge prediction errors over deep water.

For both Hurricane Kate and Hurricane Camille, the largest storm surge prediction errors occur near the shore at the landfall point of the hurricane. For Hurricane Kate, errors are highly localized in the vicinity of the complex morphology associated with coastal inlets and islands. Errors in the predicted storm surge elevation relative to Hurricane Camille forcing are significantly larger in magnitude and extend over greater portions of the nearshore region than errors produced by Hurricane Kate forcing. However, the pattern of the prediction errors are similar to those seen relative to Hurricane Kate computations. Storm surge prediction errors associated with Hurricane Camille are

concentrated around the irregular shorelines of barrier islands off the Mississippi and Florida coasts and in and around coastal inlets. The increased speed of Hurricane Camille relative to Hurricane Kate may in fact amplify the errors in under-resolved regions.

The surge forerunner generated within the Gulf of Mexico is not well represented by the variably graded discretization associated with grid SG01. Meteorological forcing from Hurricane Kate produces noticeable oscillations of the storm surge elevation. The discretization provided by grid SG01 leads to 5-cm errors in the prediction of these resonant modes. The work of Westerink, Luettich, and Muccino (1994) and Luettich and Westerink (1994) has shown that accurate prediction of periodic forcing, such as that caused by tides, requires additional resolution over the continental shelf break. The discretization provided by grid SG01 concentrates refinement at the coastline, so periodic phenomena requiring substantial resolution at the shelf break would not be accurately captured.

The rectangular basins used for the grid structure study in Chapter 5 were not constructed to have resonant characteristics. Consequently, the need for resolution at the shelf break is not evident from the error analyses of storm surge predictions over the rectangular grids. Significant refinement at the coastline serves to accurately predict the primary surge but not surge forerunner effects.

In contrast to forcing by Hurricane Kate, the storm surge hydrographs associated with Hurricane Camille indicate that the generation of resonant modes is not as prevalent. This may be caused in part by the fact that Hurricane Camille enters the Gulf of Mexico, at least partially, from the Island of Cuba causing perhaps an incomplete excitation of resonant modes in the Yucatan Channel. Secondly, the rapid speed of Hurricane Camille may not allow proper setup of the resonant modes within the Gulf of Mexico.

One further point is that the grid convergence techniques used to evaluate errors in the computed storm surge relative to the grid discretization are easily implemented and readily identify regions within the grid discretization which may require additional refinement. The use of storm surge elevations computed over an over-refined "truth" grid which has a fourfold refinement of the study grid resolution is a convenient and tractable way of assessing errors in the predicted storm surge associated with a particular grid discretization. The error analysis procedure presented offers an efficient means of evaluating storm surge prediction errors and consequently assists in the construction of a grid discretization which is both computationally efficient and yields accurate predictions of hurricane storm surge in coastal regions.

7 Concluding Remarks

Numerical models of continental margin waters are a powerful tool when properly applied. Most coastal ocean problems of interest involve highly nonlinear hydrodynamic processes which occur over a wide range of scales. An accurate model must represent the complex coastal geometries along the shoreline and in and around inlets and embayments as well as incorporate the detailed bathymetric variations of the continental shelf and slope region. Realistic coastal ocean problems preclude solution by analytical means. As a result, numerical model computations assume a primary role in the study of the physics of continental margin waters.

The success of a numerical model depends on the formulation of each of its components including the governing equations, numerics, boundary conditions, grid discretization, and the computational domain. Convergence studies are undertaken to assess the performance of model components in simulating coastal ocean processes. Rigorous convergence testing leads to formulations of the model components which have a minimal impact on the computed solution. Furthermore, any remaining errors due to the discrete model form are quantified. Upon application of a numerical model which has been subjected to extensive convergence testing, computations can be interpreted with respect to the physical phenomena simulated and any numerical artifacts which may reside in the computed solution. Convergence properties of a numerical model must be well understood to obtain meaningful results from numerical model computations.

For the study of storm surge generation and propagation in the coastal ocean due to hurricane forcing, a numerical storm surge model is implemented. Convergence of numerical storm surge models with respect to the governing equations, numerics, and boundary condition formulations is well established. However, no previous efforts have been made to assess the effects of domain size and grid structure on numerical storm surge predictions. The work performed herein has quantified the influences of domain specification and grid discretization on the computation of storm surge elevation. As a consequence, a series of guidelines is set forth to direct the construction of the computational domain and its discretization so that accurate storm surge predictions result.

Development of a hydrodynamic model has not been the focus of the work presented, but the success of the storm surge convergence studies undertaken

does depend on selection of an accurate, efficient, and flexible numerical storm surge model. A finite element, two-dimensional hydrodynamic model, ADCIRC-2DDI, based on the generalized wave continuity formulation of the depth-averaged conservation equations fulfills the accuracy, efficiency, and grid flexibility requirements set forth and has provided an appropriate framework for modeling the storm surge response of the coastal ocean. Convergence of this model has already been proven with regard to the governing equations, numerics, and boundary condition formulation.

The domain size sensitivity study conducted establishes a relationship between domain size, boundary condition specification, and the resulting physics associated with hurricane storm surge generation in continental margin waters. Comparisons of storm surge computations over three domain sizes subject to two different open ocean boundary forcings form the core of this study.

Results clearly illustrate that a large storm surge model domain, which includes the western North Atlantic Ocean, the Gulf of Mexico, and the Caribbean Sea, leads to convergent predictions of both the primary storm surge and surge forerunner effects. The inclusion of contiguous basins within the large domain allows proper setup of basin resonant modes and facilitates the realistic propagation of storm surge onto the continental shelf where development of storm surge is most critical. The main advantage of the large domain is that open boundaries lie within the deep Atlantic Ocean and are far from the intricate processes occurring on and around the continental shelf.

Study of domain size demonstrates that the commonly used computational domain, one that is situated on the continental shelf and whose size is limited relative to the size of the storm, significantly underestimates the primary storm surge response. The large expanse of cross-shelf open ocean boundaries, located in the vicinity of significant storm surge generation, prevents accurate water elevation specifications at the open boundaries of this small domain. Furthermore, a domain encompassing a resonant basin, such as the Gulf of Mexico, which is quite sensitive to boundary forcing functions, may not capture the physics associated with the hurricane forerunner.

Having established the convergence of the storm surge model with respect to domain size, an investigation into the influence of the domain discretization on storm surge computations proceeds. Comparisons of storm surge elevations computed over 14 grids subject to 4 synthetic hurricane forcings substantiates the need for significant resolution in near-coastal regions and of the shoreline itself. For the hurricanes considered, storm surge generation is shown to intensify for storms of large spatial scale, those moving rapidly, and for storms which make landfall at the coast. Accurate prediction of the storm surge for hurricanes having these characteristics requires even higher levels of grid refinement in the near-shore region. Complex coastline geometries also increase storm surge generation and can lead to substantial error in predicted storm surge elevations when shoreline detail is misrepresented. In the deep ocean, the inverted barometer effect is captured by grid refinements of

approximately one half the spatial scale of the hurricane as measured by the radius to maximum wind. The disparity in discretization requirements over a large domain render the variably graded, unstructured discretization as optimal. The variably graded grid structure yields low uniform errors in the storm surge prediction throughout the domain and minimizes computational effort.

Application of the guidelines for domain size and grid discretization strategy to two historical hurricanes (Hurricane Camille (1969) and Hurricane Kate (1985)) reinforces the findings that high levels of resolution in the nearshore region and in areas of complex coastal geometry are important for accurate prediction of primary storm surge. This is particularly noticeable for storm surge generation associated with the intense hurricane forcing of Hurricane Camille. These applications indicate that the resolution provided at the coastline by the study grid is not sufficient for proper representation of hurricane forerunner/resonant mode behavior and that additional resolution over the continental shelf break may be necessary.

In the context of these applications, a procedure to assess the performance of a particular grid discretization is demonstrated. The analysis techniques implemented are easily applied and extremely effective in identifying portions of the grid discretization which may be under-resolved. The convergence analysis presented through these applications demonstrates the form of testing which should be conducted prior to any numerical storm surge modeling effort.

In summary, recall that hurricanes are large-scale phenomena whose winds cover significant areal regions. As such, a domain which has an areal extent much greater than the scale of the hurricane is likely to more realistically capture the physics associated with storm surge generation and propagation without requiring a detailed a priori knowledge of the hydrodynamics at the open ocean boundaries of the domain. Thus, the complex oceanic response generated by hurricane wind forcing is best represented when modeled near its inception in the deep Atlantic ocean and tracked naturally through contiguous basins, onto the continental shelf, and into shallow coastal regions. Furthermore, the range of grid spacings required to accurately represent the storm surge throughout the domain is best accommodated through the use of a variably graded grid structure. The graded grid discretization has significant refinement at the coastline and in nearshore regions and resolution to one half the spatial scale of the storm in the deep ocean. Using these guidelines for selection of a domain size and construction of a grid discretization, errors in the prediction of storm surge over the domain remain low and uniform. Finally, flexibility of the finite element method ensures that storm surge can be computed efficiently over large domains with grid spacings ranging over three to four orders of magnitude.

Aside from the reported findings of the storm surge convergence studies, several issues arise which require further investigation. Accurate representation of resonant modes generated by hurricane forcing is beyond the scope of the work presented but remains an important area of study. The work of Westerink, Luettich, and Muccino (1994) and Luettich and Westerink (in

preparation) demonstrates that additional resolution over the shelf break is necessary to properly represent tidal forcing. Refinement of the shelf break may also improve the accurate propagation of resonant modes onto the continental shelf. Furthermore, storm surge simulations of Hurricane Kate and Hurricane Camille have shown vastly different resonant characteristics, indicating a complex relationship between the influence of the basin and the hurricane forcing on the excitation of resonant modes. Resonant modes/surge forerunner are an important component of the overall storm surge elevation but their generation is not well understood.

All of the convergence studies presented are conducted relative to the prediction of water elevations. Clearly, analogous studies are also needed to examine the effects of domain size and, in particular, grid structure on velocity computations. Moreover, all computations were performed using two-dimensional, depth-averaged equations. Three-dimensional storm surge simulations are a logical progression to determine under what conditions use of the depth-averaged equations in storm surge prediction is inappropriate.

Finally, use of the HURWIN wind model for the generation of hurricane wind and pressure fields reinforces the sensitivity of the specification of meteorological forcing on the hydrodynamic model response. Sensitivity and verification studies undertaken with respect to the meteorological forcing are in order, as well as a quantification of resolution requirements for the wind forcing in relation to the hydrodynamic model grid discretization.

References

Al-Rabeh, A. H., Eunay, N., and Cekirge, H. M. (1990). "A hydrodynamic model for wind driven and tidal circulation in the Arabian Gulf." *Applied mathematical modelling*. 14, 410-19.

Baptista, A. M., Westerink, J. J., and Turner, P. J. (1989). "Tides in the English Channel and Southern North Sea - A frequency domain analysis using model TEA-NL," *Advances in Water Resources* 12, 166-83.

Bearmad, G. (ed.) (1989). *The ocean basins: Their structure and evolution.* Pergamon Press.

Becker, E. B., Carey, G. F., and Oden, J. T. (1981). *Finite elements, an introduction.* Vol 1, Prentice Hall, NJ.

Bender, M. A., Tuleya, R. E., and Kurihara, Y. (1984). "A numerical study of the effect of a mountain range on a landfalling tropical cyclone," *Mon. Wea. Rev.* 113, 567-82.

Bennett, J. R., and Campbell, J. E. (1987). "Accuracy of a finite-difference method for computing lake currents," *J. Comput. Phys.* 68, 262-71.

Blumberg, A. F., and Mellor, G. L. (1987). "A description of a three-dimensional coastal ocean circulation model," *Three-Dimensional Coastal Ocean Models.* N. S. Heaps, ed., AGU Press, 1-16.

Bunpapong, M., Reid, R. O., Whitaker, R. E. (1985). "An investigation of hurricane induced forerunner surge in the Gulf of Mexico," Technical Report CERC-85-5, U.S. Army Engineer Waterways Experiment Station, Vicksburg, MS.

Cardone, V. J., Greenwood, C. V., and Greenwood, J. A. (1992). "Unified program for the specification of hurricane boundary layer winds over surfaces of specified roughness," Contract Report CERC-92-1, U.S. Army Engineer Waterways Experiment Station, Vicksburg, MS.

Celia, M. A., and Gray, W. G. (1992). *Numerical methods for differential equations, fundamental concepts for scientific and engineering applications.* Prentice Hall, NJ.

Chen, J., Shaffer, W. A., and Kim, S. C. (1993). "A forecast model for extra-tropical storm surge," *Proceedings of the First International Conference on Hydro-Science and Engineering,* Washington, DC, Vol 1, Part B.

Chow, S. (1971). *A study of the wind field in the planetary boundary layer of a moving tropical cyclone,* M.S. thesis, New York University.

Cialone, M. A. (ed.) (1991). "Coastal Modeling System (CMS) user's manual," Instruction Report CERC-91-1, U.S. Army Engineer Waterways Experiment Station, Vicksburg, MS.

Cooper, C., and Thompson, J. D. (1989). "Hurricane generated currents on the outer continental shelf; 1, Model formulation and verification," *J. Geophys. Res.* 94 (C9), 12,513-39.

Dendrou, S. A., Moore, C. I., and Myers, V. A. (1985). "Application of storm surge modeling to coastal flood rate determinations," *Marine Science Technology Journal* 19, 42-49.

Dietrich, D. E. (1993). "A numerical study of small scale continental shelf features and their interactions with deep water flows," *SIAM conference on mathematical and computational issues in the geosciences,* April 19-21, Houston, TX.

Dietrich, D. E., Roache, P. J., and Marietta, M. G. (1990). "Convergence studies with the Sandia Ocean modeling system," *Int. J. Num. Meth. Fluids* 11, 127-50.

Dube, S. K., Sinha, P. C., and Roy, G. D. (1986). "Numerical simulation of storm surges in Bangladesh using a bay-river model," *Coastal Engineering* 10.

Dunn, G. E., and Miller, B. I. (1964). *Atlantic hurricanes.* Louisiana State University Press, Baton Rouge, LA.

Flather, R. A. (1984). "A numerical model investigation of the storm surge of 31 January and 1 February 1953 in the North Sea," *Quart. J. R. Met. Soc.* 110, 591-612.

_____. (1988). "A numerical model investigation of tides and diurnal-period continental shelf waves along Vancouver Island," *J. Phys. Ocea.* 18, 115-39.

Foreman, M. G. G. (1983). "An analysis of the wave equation model for finite element tidal comparisons," *J. Comput. Phys.* 52, 290-312.

Foreman, M. G. G. (1988). "A comparison of tidal models for the southwest coast of Vancouver Island," *Proceedings of the VII international conference on computational methods in water resources,* Cambridge, MA, Elsevier.

Garcia, A. W., and Hegge, W. S. (1987). "Hurricane Kate Storm Surge Data, Report 5," Technical Report CERC-87-12, U. S. Army Engineer Waterways Experiment Station, Vicksburg, MS.

Garratt, J. R. (1977). "Review of drag coefficients over oceans and continents," *Mon. Wea. Rev.* 105, 915-29.

Gray, W. G. (1982). "Some inadequacies of finite element models as simulators of two-dimensional circulation," *Advances in Water Resources* 5, 171-77.

_____. (1989). "A finite element study of tidal flow data for the North Sea and English Channel," *Advances in Water Resources* 12, 143-54.

Gray, W. G., and Kinnmark, I. P. E. (1983). "QUIET: A reduced noise finite element model for tidal circulation," *Advanced Engineering Software 5* (3), 130-136.

Gray, W. G., Leijnse, T., Kolar, R. L., and Blain, C. A. (1993). *Mathematical tools for changing scales in the analysis of physical systems.* CRC press, Ann Arbor, MI.

Heath, R. E., Johnson, B. H., and Kim, K. W. (1990). "Grid-induced errors in depth averaged flow fields," *Proc. of the ASCE Hydraulics Division Specialty Conf.,* San Diego, CA, ASCE.

Hearn, C. J., and Holloway, P. E. (1990). "A three-dimensional barotropic model of the response of the Australian north west shelf to tropical cyclones," *J. Phys. Ocea.* 20, 60-80.

Hendershott, M. C. (1981). "Long waves and ocean tides," *Evolution of physical oceanography.* B. A. Warren and C. Wunsch, eds., MIT Press, Cambridge, MA., 292-341.

Hubbert, G. D., Leslie, L. M., and Manton, M. J. (1990). "A storm surge model for the Australian region," *Quart. J. R. Met. Soc.* 116, 1,005-20.

Jarvinen, B. R., and Lawrence, M. B. (1985). "An evaluation of the SLOSH storm surge model," *Bull. Amer. Met. Soc.* 11, 1,408-11.

Jarvinen, B. R., Neumann, C. J., and Davis, M. A. S. (1984). "A tropical cyclone data tape for the North Atlantic Basin, 1886-1983: Contents, limitations, and uses," NOAA Technical Memorandum, NWS NHC22.

Jarvinen, B. R., Neumann, C. J., and Davis, M. A. S. (1993). "A tropical cyclone data tape for the North Atlantic Basin, 1886-1992," NOAA data tape.

Jelesnianski, C. P. (1979). "Tropical storm surge forecasting in the National Weather Service," *ASCE Proceedings of the Engineering Foundation Conference on Improved Hydrologic Forecasting, Why and How?*, March 25-30, Pacific Grove, CA, 65-75.

Jelesnianski, C. P., and Taylor, A. D. (1973). "A preliminary view of storm surges before and after storm modifications," *NOAA Tech. Memorandum ERL WMPO-3.*

Jelesnianski, C. P., Chen, J., and Shaffer, W. A. (1992). "SLOSH: Sea, lake, and overland surges from hurricanes," NOAA Technical Report NWS 48.

Johns, B., and Ali, M. A. "The numerical modeling of storm surges in the Bay of Bengal," *Quart. J. R. Met. Soc.* 106, 1-18.

Johns, B., Dube, S. K., Mohanty, U. C., and Rao, A. D. (1983a). "Simulation of storm surges using a three-dimensional numerical model: An application to the 1977 Andhra Cyclone," *Quart. J. R. Met. Soc.* 109, 211-24.

_____. (1983b). "On the effect of bathymetry in numerical storm surge simulation experiments," *Computers and Fluids,* 11, 161-74.

Jones, R. W. (1987). "Simulation of hurricane landfall with a numerical model featuring latent heating by the resolvable scales," *Mon. Wea. Rev.* 115, 2,279-97.

Kincaid, B., and Cheney, W. (1991). *Numerical analysis, mathematics of scientific computing.* Brooks/Cole Pub. Co., CA.

Kinnmark, I. P. E. (1984). *The shallow water wave equations: Formulation, analysis and application,* Ph.D. Diss., Department of Civil Engineering, Princeton University.

Kinnmark, I. P. E., and Gray, W. G. (1984). "A two-dimensional analysis of the wave equation model for the finite element tidal computations," *Int. J. Num. Methods,* 20, 369-83.

_____. (1985). "Stability and accuracy of spatial approximations for wave equation tidal models," *J. Comp. Phys.* 60, 447-66.

Kolar, R. L., Gray, W. G., Westerink, J. J., and Luettich, R. A. (1994a). "Shallow water modeling in spherical coordinates: Equation formulation, numerical implementation, and application," *J. Hydraul. Res.* 32, 3-24.

Kolar, R. L., Westerink, J. J., Cantekin, M. E., and Blain, C. A. (1994b). "Aspects of nonlinear simulations using shallow water models based on the wave continuity equation," *Computers and Fluids* 23, 523-38.

Kowalik, Z. (1984). "Storm surges in the Beaufort and Chukchi Seas," *J. Geophys. Res.* 89 (C6), 10,570-78.

Kurihara, Y., Bender, M. A., Tuleya, R. E., and Ross, R. J. (1990). "Prediction experiments of Hurricane Gloria (1985) using a multiply nested movable mesh model," *Mon. Weav. Rev.* 118, 2,185-98.

Lapidus, L., and Pinder, G. F. (1982). *Numerical solution of partial differential equations in science and engineering.* John Wiley and Sons, NY.

Lardner, R. W., and Cekirge, H. M. (1988). "A new algorithm for three-dimensional tidal and storm surge computations," *Applied mathematical modelling* 12, 471-81.

Lardner, R. W., and Song, Y. (1992). "A comparison of spatial grids for numerical modelling of flows in near-coastal seas," *Int. J. Num. Meth. Fl.* 14, 109-14.

Lee, J. K., and Froehlich, D. C. (1986). "Review of literature on the finite-element solution of the two-dimensional surface-water flow in the horizontal plane," *U.S. Geological Circular 1009*, U.S. Department of the Interior.

Leendertse, J. J. (1987). "Aspects of SIMSYS2D, A system for two-dimensional flow computation," *Rand Report R-3712-USGS.*

Le Mehaute, B. (1976). *An introduction to hydrodynamics and water waves.* Springer-Verlag, NY.

Le Provost, C., and Vincent, P. (1986). "Some tests of precision for a finite element model of ocean tides," *J. Comput. Phys.* 65, 273-91.

Luettich, R. A., and Westerink, J. J. "Continental shelf scale convergence studies with a barotropic tidal model," *Quantitative skill assessment for coastal ocean models.* D. R. Lynch and A. M. Davies, eds., AGU Press, in preparation.

Luettich, R. A., Westerink, J. J., and Scheffner, N. W. (1992). "ADCIRC: An advanced three-dimensional circulation model for shelves, coasts, and estuaries; Report 1, Theory and methodology of ADCIRC-2DDI and ADCIRC-3DL," Technical Report DRP-92-6, U.S. Army Engineer Waterways Experiment Station, Vicksburg, MS.

Lynch, D. R. (1983). "Progress in hydrodynamic modeling, review of U.S. Contributions 1979-1982," *Rev. Geophys. Space Phys.* 21 (3), 741-54.

Lynch, D. R., and Gray, W. G. (1979). "A wave equation model for finite element tidal computations," *Comp. Fluids* 7, 207-28.

Lynch, D. R., and Werner, F. E. (1991). "Three-dimensional hydrodynamics in finite elements; Part II: Nonlinear timestepping," *Int. J. Numer. Methods Fl.* 12, 507-33.

Lynch, D. R., Werner, F. E., Cantos-Figuerola, A., and Parilla, G. (1988). "Finite element modeling of reduced-gravity flow in the Alboran Sea; Sensitivity studies," *Seminario sobre oceanografia fiscia del Estrecho de Gibraltar*, Madrid, Spain, 283-95.

Murty, T. S., Flather, R. A., and Henry, R. F. (1986). "The storm surge problem in the Bay of Bengal," *Prog. Oceanog.* 16, 195-233.

Pearson, F. (1990). *Map projections: Theory and applications.* CRC Press, Inc., Boca Raton, FL.

Piacsek, S., and Allard, R. (1993). "The importance of horizontal resolution in coupled ice/ocean models of the Arctic," *SIAM conference on mathematical and computational issues in the geosciences*, April 19-21, Houston, TX.

Pickard, G. L., and Emery, W. J. (1982). *Descriptive physical oceanography, an introduction.* Pergamon Press, NY.

Platzman, G. W. (1972). "Two dimensional free oscillations in natural basins," *J. Phys. Ocea.* 2 (2), 117-30.

_____. (1981). "Some response characteristics of finite element tidal models," *J. Comput. Phys.* 40, 36-63.

Powell, M. D. (1982). "The transition of the Hurricane Frederic boundary-layer wind field from the open Gulf of Mexico to landfall," *Mon. Wea. Rev.* 110, 1,912-32.

Press, W. H., Flannery, B. P., Tuekolsky, S. A., and Vetterling, W. T., (eds.) (1986). *Numerical recipes, the art of scientific computing.* Cambridge University Press, NY.

Reid, R. O. (1990). "Waterlevel changes," *Handbook of coastal and ocean engineering.* J. Herbich, ed., Gulf Publishing, Houston, TX.

Reid, R. O., and Whitaker, R. E. (1981). "Numerical model for astronomical tides in the Gulf of Mexico: Volume I, Theory and application," *Coastal Engineering Research Center*, U.S. Army Engineer Waterways Experiment Station, Vicksburg, MS.

Scheffner, N. W., Mark, D. J., Blain, C. A., Westerink, J. J., and Luettich, R. A., Jr. (1994). "ADCIRC: An advanced three-dimensional circulation model for shelves, coasts, and estuaries; Report 5, A tropical storm database for the east and Gulf of Mexico coasts of the United States," Technical Report DRP-92-6, U.S. Army Engineer Waterways Experiment Station, Vicksburg, MS.

Schwiderski, E. W. (1979). "Global ocean tides; Part II: The semidiurnal principle lunar tide (M_2)," *Atlas of tidal charts and maps*, NSWC TR 79-414.

_____. (1980). "On charting global ocean tides," *Rev. Geophys. Space Phys.* 18, 243-68.

_____. (1981a). "Global ocean tides; Part III: The semidiurnal principle solar tide (S_2)," *Atlas of tidal charts and maps*, NSWC TR 81-122.

_____. (1981b). "Global ocean tides; Part IV: The diurnal luni-solar declination tide (K_1)," *Atlas of tidal charts and maps*, NSWC TR 81-142.

_____. (1981c.). "Global ocean tides; Part V: The diurnal principle lunar tide (O_1)," *Atlas of tidal charts and maps*, NSWC TR 81-144.

_____. (1981d.). "Global ocean tides; Part VII: The diurnal principle solar tide (P_1)," *Atlas of tidal charts and maps*, NSWC TR 81-220.

Shaffer, W. A., Jelesnianski, C. P., and Chen, J. (1986). "Hurricane storm surge forecasting," Preprints *Oceans 86*, Sep 23-26, Washington, DC, 1,379-85.

Signorini, S. R., and Miller, C. D. (1992). "Hurricane induced surge and currents on the Texas-Louisiana Shelf," *J. Geophys. Res.* 97, (C2), 2,227-44.

Simpson, R. H., and Riehl, H. (1981). *The hurricane and its impact.* Louisiana State University Press, Baton Rouge, LA.

Stubbs, S. A. (ed.) (1986). *Proceedings of the American Society for Oceanography Hurricane Symposium*, October 10-11, Houston, TX.

Thurman, H. V. (1974). *Introductory oceanography.* Macmillian Publishing Co., NY.

Vincent, P., and Le Provost, C. (1988). "Semidiurnal tides in the northeast Atlantic from a finite element numerical model," *J. Geophys. Res.* 93 (C1), 543-55.

Wahr, J. M. (1981). "Body tides on an elliptical, rotating, elastic and oceanless earth," *Geophys. J. R. Astr. Soc.* 64, 677-703.

Walters, R. A. (1988). "A finite element model for tides and currents with field applications," *Comm. Applied Numerical Methods* 4, 401-11.

Walters, R. A., and Carey, G. F. "Analysis for spurious oscillation modes for the shallow water and Navier Stokes equation," *Computers and Fluids* 2, 51-68.

Walters, R. A., and Werner, F. E. (1989). "Comparison of two finite element models of tidal hydrodynamics using a North Sea data set," *Advances in Water Resources* 12 (4), 84-193.

Wang, J. D. (1987). "Hurricane effects on the surface gulf stream currents," *Ocean Engng.* 14 (3), 165-80.

Weisberg, J., and Parish, H. (1974). *Introductory oceanography*. McGraw Hill, NY.

Werner, F. E., and Lynch, D. R. (1989). "Harmonic structure of English Channel/Southern Bight tides from a wave equation simulation," *Adv. Water Resour.* 12, 121-42.

Westerink, J. J., and Gray, W. G. (1991). "Progress in surface water modeling," *Rev. Geophys.* 29, April Supplement, 210-17.

Westerink, J. J., Luettich, R. A., and Hagen, S. C. (1994). "Meshing Requirements for Large Scale Coastal Ocean Tidal Models," *Numerical Methods in Water Resources*, A. Peters, G. Wittum, B. Herrling, and U. Meissner, eds., Kluwer Academic Publishers, The Netherlands.

Westerink, J. J., Luettich, R. A., and Muccino, J. C. (1994). "Modeling tides in western North Atlantic using unstructured graded grids," *Tellus* 46A, 178-99.

Westerink, J. J., Luettich, R. A., Baptista, A. M., Scheffner, N. W., and Farrar, P. (1992a). "Tide and storm surge predictions using a finite element model," *J. Hydraul. Eng.* 118, 1,373-90.

Westerink, J. J., Luettich, R. A., Blain, C. A., and Hagen, S. C. "The utility of the finite element method in computing surface elevation and circulation in continental margin waters," *Finite element modeling of environmental problems*. G. F. Carey, ed., in preparation (a).

Westerink, J. J., Luettich, R. A., Blain, C. A., and Scheffner, N. W. (1992b). "ADCIRC: An advanced three-dimensional circulation model for shelves, coasts, and estuaries; Report 2, User's manual for ADCIRC-SDDI," Technical Report DRP-92-6, U.S. Army Engineer Waterways Experiment Station, Vicksburg, MS.

Westerink, J. J., Luettich, R. A., Wu, J. K., and Kolar, R. L. "The influence of normal flow boundary conditions on spurious modes in finite element solutions to the shallow water equations," *Int. J. Num. Meth. Fl.*, in preparation (b).

Westerink, J. J., Stolzenback, K. D., and Connor, J. J. (1989). "General spectral computations of the nonlinear shallow water tidal interactions within the Bight of Abaco," *J. Phys. Ocea.* 19, 1,350-73.

Weyl, P. K. (1970). *Oceanography: An introduction to the marine environment.* John Wiley and Sons, NY.

Woodworth, P. L. (1990). "Summary of recommendations to the UK Earth Observation Data Centre (UK-EODC) by the Proudman Oceanographic Laboratory (POL) for tide model corrections on ERS-1 geophysical data records," Proudman Oceanographic Laboratory Communication.

REPORT DOCUMENTATION PAGE

Form Approved
OMB No. 0704-0188

Public reporting burden for this collection of information is estimated to average 1 hour per response, including the time for reviewing instructions, searching existing data sources, gathering and maintaining the data needed, and completing and reviewing the collection of information. Send comments regarding this burden estimate or any other aspect of this collection of information, including suggestions for reducing this burden, to Washington Headquarters Services, Directorate for Information Operations and Reports, 1215 Jefferson Davis Highway, Suite 1204, Arlington, VA 22202-4302, and to the Office of Management and Budget, Paperwork Reduction Project (0704-0188), Washington, DC 20503.

1. AGENCY USE ONLY *(Leave blank)*

2. REPORT DATE
March 1995

3. REPORT TYPE AND DATES COVERED
Final report

4. TITLE AND SUBTITLE
Influence of Domain Size and Grid Structure on the Response Characteristics of a Hurricane Storm Surge Model

5. FUNDING NUMBERS
WU 32466

6. AUTHOR(S)
C. A. Blain, J. J. Westerink, R. A. Luettich, Jr., Norman W. Scheffner

7. PERFORMING ORGANIZATION NAME(S) AND ADDRESS(ES)
University of Notre Dame, Notre Dame, IN 46556;
University of North Carolina at Chapel Hill, Morehead City, NC 28557;
U.S. Army Engineer Waterways Experiment Station, Coastal Engineering Research Center, 3909 Halls Ferry Road, Vicksburg, MS 39180-6199

8. PERFORMING ORGANIZATION REPORT NUMBER
Technical Report DRP-95-4

9. SPONSORING/MONITORING AGENCY NAME(S) AND ADDRESS(ES)
U.S. Army Corps of Engineers
Washington, DC 20314-1000

10. SPONSORING/MONITORING AGENCY REPORT NUMBER

11. SUPPLEMENTARY NOTES
Available from National Technical Information Service, 5285 Port Royal Road, Springfield, VA 22161.

12a. DISTRIBUTION/AVAILABILITY STATEMENT
Approved for public release; distribution is unlimited.

12b. DISTRIBUTION CODE

13. ABSTRACT *(Maximum 200 words)*

Formulation of a numerical storm surge model directly affects the physical content of the predicted storm surge response. The influence of domain size and grid structure on computations of storm surge generation in the coastal region are studied.

Storm surge response along the Florida shelf in the Gulf of Mexico due to Hurricane Kate is examined over three domains using two different open ocean boundary forcing functions. The computed storm surge response indicates that a small domain situated primarily on the continental shelf is inadequate since cross shelf boundaries are in regions of significant storm surge generation where surge and therefore boundary conditions are not known a priori. A second domain including the entire Gulf of Mexico basin captures the primary storm surge well but may not correctly model resonant modes. The dependence of these modes on interactions with contiguous basins makes accurate setup by the boundary condition specification difficult. The primary storm surge response as well as resonant modes excited by the storm are best represented using the largest domain, which encompasses the western North Atlantic ocean, the Caribbean Sea, and the Gulf of Mexico. This domain with deep Atlantic ocean boundaries facilitates simple boundary condition specification and minimizes the influence of boundary conditions on storm surge generation in the coastal region. Basin resonant modes and basin interactions are also captured.

(Continued)

14. SUBJECT TERMS

Circulation Model	Finite element model	Storm surge model
Computational domain size	Grid analysis	Tropical storm simulation
Computational grid resolution	Hydrodynamic model	Two-dimensional model

15. NUMBER OF PAGES
174

16. PRICE CODE

17. SECURITY CLASSIFICATION OF REPORT
UNCLASSIFIED

18. SECURITY CLASSIFICATION OF THIS PAGE
UNCLASSIFIED

19. SECURITY CLASSIFICATION OF ABSTRACT

20. LIMITATION OF ABSTRACT

13. (Concluded).

Comparisons between storm surge elevations computed over fourteen grid discretizations subject to four synthetic hurricane forcings indicate that accurate predictions of storm surge result when significant refinement of shoreline geometry and nearshore regions is provided along with resolution to one half the spatial scale of the storm over deep waters. These grid discretization requirements are best met using a graded grid structure which yields low uniform prediction errors throughout the domain and minimizes computational effort.

Application of the guidelines for specification of domain size and grid structure to Hurricanes Kate and Camille reinforces the necessity of using a large domain, which has high levels of resolution in nearshore regions and areas of complex coastal geometry, for accurate prediction of primary storm surge.